71-27,606

CRITES, Thomas Richard, 1942-
BACKSCATTER OF NORMALLY INCIDENT INTERMEDIATE ENERGY BREMSSTRAHLUNG FROM SEMI-INFINITE MEDIA OF VARYING ATOMIC NUMBER.

The University of Oklahoma, Ph.D., 1971
Engineering, nuclear

University Microfilms, A XEROX Company, Ann Arbor, Michigan

THIS DISSERTATION HAS BEEN MICROFILMED EXACTLY AS RECEIVED

Downloaded from SHAREOK. Persistent Handle URL: https://hdl.handle.net/11244/3042

THE UNIVERSITY OF OKLAHOMA

GRADUATE COLLEGE

# BACKSCATTER OF NORMALLY INCIDENT INTERMEDIATE ENERGY BREMSSTRAHLUNG FROM SEMI-INFINITE MEDIA OF VARYING ATOMIC NUMBER

A DISSERTATION

SUBMITTED TO THE GRADUATE FACULTY

in partial fulfillment of the requirements for the degree of

DOCTOR OF PHILOSOPHY

BY

THOMAS RY CRITES

Norman, Oklahoma

1970

PLEASE NOTE:

Some pages have light
and indistinct print.
Filmed as received.

UNIVERSITY MICROFILMS.

BACKSCATTER OF NORMALLY INCIDENT INTERMEDIATE ENERGY BREMSSTRAHLUNG FROM SEMI-INFINITE MEDIA OF VARYING ATOMIC NUMBER

APPROVED BY

Robert J. Nelson

H. J. Fischbach

Larry Cantlon

William S. Emmett

James M. Peterson

DISSERTATION COMMITTEE

## ACKNOWLEDGMENTS

The author expresses his sincere appreciation to Dr. Robert Y. Nelson, dissertation advisor, and William D. Burnett, research advisor, for their valuable guidance, suggestions, and review throughout this research, which could not have been meaningfully completed without their assistance.

The author is very grateful to his wife, Frances, for the great personal efforts she has made in seeing this work through, and her excellent support in typing and proofreading.

The author is deeply indebted to William H. Kingsley and Harold L. Rarrick for their efforts in making possible the work arrangement under which the dissertation was completed.

Gratitude is extended to the many Sandia Corporation personnel who aided in this project, in particular: Bill L. O'Neal and Donald E. Amos for many fruitful discussions; James H. Renken, Joann H. Flinchum and Kenneth G. Adams for the great amount of work they did in making possible the computer comparisons; Lawrence D. Posey, Jesse

E. Harness, and Dan D. Craig for their support in obtaining data on the 3.5 and 10.5 MeV flash x-ray machine; Robert W. Mottern and S. A. Ravenbyrne at the Van de Graaff facility; and Alvie A. Barrett for his able shop assistance.

Financial aid for this portion of the requirements for the Doctor of Philosophy Degree at the University of Oklahoma was furnished in part by a United States Public Health Service Grant and in major by a United States Atomic Energy Commission prime contractor, Sandia Laboratories, Albuquerque New Mexico.

TABLE OF CONTENTS


| | | Page |
|---|---|---|
| ACKNOWLEDGMENTS | | iii |
| TABLE OF CONTENTS | | v |
| LIST OF TABLES | | viii |
| LIST OF ILLUSTRATIONS | | x |
| Section | | |
| 1. | INTRODUCTION | 1 |
| 2. | HISTORICAL REVIEW | 4 |
| | 2.1 Experimental | 4 |
| | 2.2 Numerical Studies | 13 |
| | 2.3 Summary | 19 |
| 3. | THEORETICAL CONSIDERATION | 20 |
| | 3.1 Introduction | 20 |
| | 3.2 Photon Interactions | 23 |
| | 3.2.1 Photoelectric Absorption | 23 |
| | 3.2.2 Compton Scattering | 28 |
| | 3.2.3 Pair Production | 39 |
| | 3.2.4 Rayleigh Scattering and Photonuclear Interactions | 45 |
| | 3.2.5 Summary | 49 |
| | 3.3 Detection Instrumentation | 50 |
| | 3.3.1 Scintillation Spectrometer | 50 |
| | 3.3.2 Thermoluminescent Detectors | 51 |

Page

3.3.3 Attenuation Methods of Spectral Determination 53

4. NUMERICAL ANALYSIS METHODS..... 57

4.1 Empirical Methods 57
4.2 Monte Carlo Methods 62
4.3 Method of Discrete Ordinates 64

5. EXPERIMENTAL DESIGN..... 66

5.1 Backscatter Materials 66

5.1.1 Introduction 66
5.1.2 Lead 68
5.1.3 Iron 68
5.1.4 Concrete 69

5.2 Photon Sources 72

5.2.1 Van de Graaff 72
5.2.2 Flash X-ray Devices 73

5.2.2.1 3.5 MeV Generator 74
5.2.2.2 7.0 MeV Generator 78
5.2.2.3 10.5 MeV Generator 80

5.3 Backscatter Surface, Collimator, and Detector Positions 83

6. EXPERIMENTAL RESULTS..... 86

6.1 Data Analysis 86
6.2 Presentation of Results 92
6.3 Discussion of Results 108

7. CONCLUSIONS AND RECOMMENDATIONS..... 112

8. BIBLIOGRAPHY..... 115

9. APPENDIX A: NOMENCLATURE..... 128

10. APPENDIX B: VIEWED AREA CONSIDERATIONS..... 132

| | | | Page |
|---|---|---|---|
| 11. | APPENDIX C: | COLLIMATOR EFFECTS..... | 153 |
| 12. | APPENDIX D: | SPECTRAL DATA..... | 156 |
| 13. | APPENDIX E: | LiF ENERGY DEPENDENCY..... | 205 |
| 14. | APPENDIX F: | THERMOLUMINESCENT DOSIMETER READ-OUT AND ANNEALING PROCEDURES..... | 208 |
| 15. | APPENDIX G: | INFINITE SLAB SIZE MEASUREMENTS. | 213 |
| 16. | APPENDIX H: | BEAM DIVERGENCE..... | 219 |
| 17. | APPENDIX I: | THERMOLUMINESCENT DOSIMETER EXPERIMENTAL DATA..... | 230 |
| 18. | APPENDIX J: | ERROR ANALYSIS..... | 390 |
| 19. | APPENDIX K: | MONTE CARLO PROGRAM..... | 401 |
| 20. | APPENDIX L: | DTF PROGRAM..... | 407 |
| 21. | APPENDIX M: | A COMPARISON OF MONTE CARLO AND DTF RESULTS TO PREVIOUSLY PUBLISHED EXPERIMENTAL DATA..... | 413 |
| 22. | APPENDIX N: | RESULTS OF THE CHILTON-HUDDLESTON EQUATIONS APPLIED TO THE "EFFECTIVE" ENERGIES OF THE PRESENT WORK..... | 416 |
| 23. | APPENDIX O: | 20 - 60 MeV BACKSCATTER..... | 424 |

LIST OF TABLES


| Table | | Page |
|---|---|---|
| 1. | Concrete Compositions | 70 |
| 2. | REBA Shot Characteristics | 76 |
| 3. | $\alpha_{D3(H_2O)} \times 10^3$ | 104 |
| 4. | Detector Collimator Correction | 155 |
| 5. | 2.0 MeV Measured Spectra (99, 100) | 159 |
| 6. | 3.5 MeV Measured Spectra (102) | 160 |
| 7. | 2.0 MeV Empirical Spectra | 165 |
| 8. | 3.5 MeV Empirical Spectra | 166 |
| 9. | 7.0 MeV Measured Spectra (105) | 169 |
| 10. | 7.0 MeV Empirical Spectra | 170 |
| 11. | 10.5 MeV Measured Spectra (110) | 171 |
| 12. | 10.5 MeV Empirical Spectra | 173 |
| 13. | 10.5 MeV Spectra | 179 |
| 14. | TLD Annealing Procedures | 210 |
| 15. | TLD Annealing Procedure Summary | 211 |
| 16. | Iron Reflector Ratios ($\times 10^5$) | 214 |
| 17. | Concrete Reflector Ratios ($\times 10^5$) | 214 |

LIST OF TABLES (cont'd)

18. Chilton-Huddleston Parameters..... 420

19. Klein-Nishina Cross-sections..... 421

20. Chilton-Huddleston Albedo Values..... 422

21. Differential Dose Flux Albedo..... 426

## LIST OF ILLUSTRATIONS


| Figure | | Page |
|---|---|---|
| 1. | Relative position of detector, source, and scattering medium, Hine and McCall.... | 5 |
| 2. | Experimental arrangement used by Clarke and Batten..... | 9 |
| 3. | Experimental arrangement used by Pruitt... | 12 |
| 4. | Experimental arrangement used by Sugiyama and Tomimasu..... | 13 |
| 5. | Relative position of source, detector, and scatterer for the Chilton-Huddleston development..... | 16 |
| 6. | Compton scattering..... | 30 |
| 7. | Multiple Compton scattering..... | 37 |
| 8. | Attenuation extractions..... | 54 |
| 9. | Geometry of the Chilton-Huddleston derivation..... | 57 |
| 10. | Albedo dependence on concrete composition for 2.0 MeV bremsstrahlung..... | 71 |
| 11. | REBA..... | 77 |
| 12. | Pulserad 1590..... | 79 |
| 13. | HERMES II..... | 81 |
| 14. | HERMES II..... | 82 |

LIST OF ILLUSTRATIONS, (cont'd)


| Figure | | Page |
|---|---|---|
| 15. | Experimental configuration..... | 83 |
| 16. | Detector collimator..... | 85 |
| 17. | 2.0 MeV lead scatterer $\alpha_{D1}$ vs Angle.... | 93 |
| 18. | 2.0 MeV iron scatterer $\alpha_{D1}$ vs Angle.... | 94 |
| 19. | 2.0 MeV concrete scatterer $\alpha_{D1}$ vs Angle | 95 |
| 20. | 3.5 MeV lead scatterer $\alpha_{D1}$ vs Angle.... | 96 |
| 21. | 3.5 MeV iron scatterer $\alpha_{D1}$ vs Angle.... | 97 |
| 22. | 3.5 MeV concrete scatterer $\alpha_{D1}$ vs Angle | 98 |
| 23. | 7.0 MeV lead reflector $\alpha_{D1}$ vs Angle.... | 99 |
| 24. | 7.0 MeV iron reflector $\alpha_{D1}$ vs Angle.... | 100 |
| 25. | 10.5 MeV lead scatterer $\alpha_{D1}$ vs Angle... | 101 |
| 26. | 10.5 MeV iron scatterer $\alpha_{D1}$ vs Angle... | 102 |
| 27. | 10.5 MeV concrete scatterer $\alpha_{D1}$ vs Angle | 103 |
| 28. | $A_{D1(H_2O)}$ vs $E_{max}$..... | 106 |
| 29. | $A_{D1(H_2O)}$ vs Atomic Number..... | 107 |
| 30. | Viewed area geometry..... | 133 |
| 31. | Crystal geometry considerations..... | 136 |
| 32. | Edge generated envelope..... | 137 |
| 33. | Envelope generated by two edges..... | 138 |
| 34. | Total viewed area..... | 139 |
| 35. | Umbral area..... | 139 |

LIST OF ILLUSTRATIONS, (cont'd)


| Figure | | Page |
|---|---|---|
| 36. | Total enclosed area..... | 145 |
| 37. | Point detector viewed area..... | 149 |
| 38. | Collimator detail..... | 154 |
| 39. | Copper absorption 2.0 MeV..... | 157 |
| 40. | 2.0 MeV iron scatterer (DTF)..... | 158 |
| 41. | 3.5 MeV copper absorption..... | 161 |
| 42. | DTF 3.5 MeV iron scatterer..... | 162 |
| 43. | Various 3.5 MeV input spectra..... | 164 |
| 44. | DTF 7.0 MeV lead scatterer..... | 167 |
| 45. | DTF 10.5 MeV lead scatterer..... | 168 |
| 46. | 10.5 MeV copper absorption..... | 175 |
| 47. | 10.5 MeV copper absorption..... | 176 |
| 48. | DTF 10.5 MeV iron scatterer..... | 178 |
| 49. | 10.5 MeV Spectra I..... | 180 |
| 50. | 10.5 MeV Spectra II..... | 181 |
| 51. | DTF Various $E_{max}$ concrete scatterers... | 183 |
| 52. | 2.0 MeV measured $60^{o}$ concrete scatterer | 185 |
| 53. | 2.0 MeV measured $30^{o}$ lead scatterer.... | 186 |
| 54. | DTF 2.0 MeV concrete scatterer..... | 187 |
| 55. | DTF 2.0 MeV iron scatterer..... | 188 |
| 56. | DTF 2.0 MeV lead scatterer..... | 189 |

LIST OF ILLUSTRATIONS, (cont'd)


| Figure | | Page |
|---|---|---|
| 57. | Monte Carlo 2.0 MeV aluminum scatterer | 190 |
| 58. | Monte Carlo 2.0 MeV lead scatterer.... | 191 |
| 59. | DTF 3.5 MeV concrete scatterer..... | 192 |
| 60. | DTF 3.5 MeV iron scatterer..... | 193 |
| 61. | DTF 3.5 MeV lead scatterer..... | 194 |
| 62. | Monte Carlo 3.5 MeV iron scatterer.... | 195 |
| 63. | DTF 7.0 MeV concrete scatterer..... | 196 |
| 64. | DTF 7.0 MeV iron scatterer..... | 197 |
| 65. | DTF 7.0 MeV lead scatterer..... | 198 |
| 66. | Monte Carlo 7.0 MeV lead scatterer.... | 199 |
| 67. | DTF 10.0 MeV concrete scatterer..... | 200 |
| 68. | DTF 10.5 MeV iron scatterer..... | 201 |
| 69. | DTF 10.5 MeV lead scatterer..... | 202 |
| 70. | Monte Carlo 10.5 MeV iron scatterer... | 203 |
| 71. | Monte Carlo 10.5 MeV lead scatterer... | 204 |
| 72. | TLD Energy response per R (81)..... | 206 |
| 73. | TLD Energy response per Rad($H_2O$)(123). | 206 |
| 74. | 2.0 MeV lead surface area effects..... | 215 |
| 75. | 2.0 MeV lead thickness effects..... | 216 |
| 76. | 60 MeV lead surface area effects..... | 217 |
| 77. | 60 MeV lead thickness effects..... | 218 |

LIST OF ILLUSTRATIONS, (cont'd)


| Figure | | Page |
|---|---|---|
| 78. | 2.0 MeV horizontal beam divergence.... | 220 |
| 79. | 2.0 MeV vertical beam divergence..... | 221 |
| 80. | 3.5 MeV vertical beam divergence..... | 222 |
| 81. | 3.5 MeV horizontal beam divergence.... | 223 |
| 82. | 7.0 MeV horizontal beam divergence.... | 224 |
| 83. | 7.0 MeV vertical beam divergence..... | 225 |
| 84. | 2.0 MeV beam divergence.............. | 226 |
| 85. | 3.5 MeV beam divergence.............. | 227 |
| 86. | 7.0 MeV beam divergence.............. | 228 |
| 87. | Charged particle equilibrium........ | 399 |
| 88. | $\alpha_{E1}$ vs Angle for Cs-137 lead scatterer | 414 |
| 89. | $\alpha_{E1}$ vs Angle for Co-60 iron scatterer | 415 |
| 90. | Lead C and C' vs Energy.............. | 417 |
| 91. | Iron C and C' vs Energy.............. | 418 |
| 92. | Concrete C and C' vs Energy.......... | 419 |

# 1. INTRODUCTION

The development of x-ray machines of greater output and the extension of accelerators for use outside experimental laboratories, require an accurate knowledge of the surrounding radiation fields. The radiation field about these facilities consists of two sources: transmitted and scattered radiation. Transmission and forward scattering (i.e. build-up) are fairly well documented in low to intermediate energy range photons.

Less well established is scattering in a backward direction, or backscattering. Though very little experimental data exist on the backscattering of bremsstrahlung sources (1), the backscattering of gamma rays from radioisotopes has been studied for a great many sources and scattering materials, and these efforts will be reviewed in Section 2.

The term "albedo" is generally accepted in the study of backscatter as the ratio of the radiation fluence reflected from a surface to the fluence incident on that surface. Unlike the reflection of light (where the term

albedo arises) which can be considered a surface phenomenon, photons of MeV energies are much more penetrating. The albedo considered in radiation research takes into account photons that are scattered back out of the medium from several mean free paths below the surface. The albedo determined in the present research effort is an "effective" albedo, consisting of characteristic x-rays, singly scattered and multi-scattered photons, and bremsstrahlung and annihilation radiation from pair production interactions. No attempt has been made to differentiate the contributions of each method, but rather the effort was to determine the overall fluence to obtain the differential albedo from the surface of the backscattering material.

The dissertation investigation studied the angular dependency of backscatter of normally incident broad beam bremsstrahlung of varying energies reflecting from surfaces of varying atomic number. The bremsstrahlung source machines used are discussed in Section 5.2. The reflected fluence was measured by LiF crystal thermoluminescent dosimeters, placed in highly collimated, copper-lined, lead shields to monitor the angular distribution. The scattering media used are common shielding materials of sufficient size to represent semi-infinite bodies, meaning that any increase in slab area or thickness will not result in a change in albedo. The

materials used in this work are concrete, steel, and lead.

An extensive comparison of experimental results with results obtained by other methods is made. Computer methods have primarily been used to estimate the extent of backscatter, particularly when complicated incident spectra are involved. Two different computer methods, a discrete ordinates solution to the photon transport equations and Monte Carlo, are used for comparison to the experimental data obtained. As the two computer methods approach the backscatter problem very differently, their results predictably differ somewhat from each other and from the data obtained. These differences are examined in the dissertation.

Nomenclature used in this dissertation is based on the International Commission of Radiological Units and Measurements recommendations in general (2) and the Oak Ridge National Laboratory Neutron and Gamma-Ray Albedos Report (1) in particular.

## 2. HISTORICAL REVIEW

As forward scattering is well considered elsewhere (3, 4, 5, 6, 7, 8, 9, 10, 11), the following discussion will consider only those experiments which center on backscatter.

### 2.1 EXPERIMENTAL

The first studies of backscatter gamma-rays were probably made by Imbert and Bertin-Sans in 1896 (12). This and other studies led to the famous work by Compton (13) in 1923 from which he developed his quantum theory of x-ray scattering. Klein and Nishina (14) in 1929 obtained a general expression for the Compton differential scattering and collision cross-sections for initially unbound and stationary electrons. It was not until the development of more sensitive detection equipment and larger sources in the nineteen-fifties, that gamma-ray scattering was studied experimentally in greater depth.

In 1954 Hayward and Hubbell (15), using a collimated cobalt-60 source, studied the energy and scattering angle distribution from wood and steel wool with a collimated

scintillation detector. Also in that year, Hine and McCall (16) studied the backscatter of gamma rays from lead, iron, aluminum, wood, and water using mercury-203, cesium-137, and cobalt-60 point sources in contact with the backscattering material. A scintillation gamma-ray spectrometer was again used to investigate the intensity and energy of the back-scattered radiation. These experiments demonstrated the

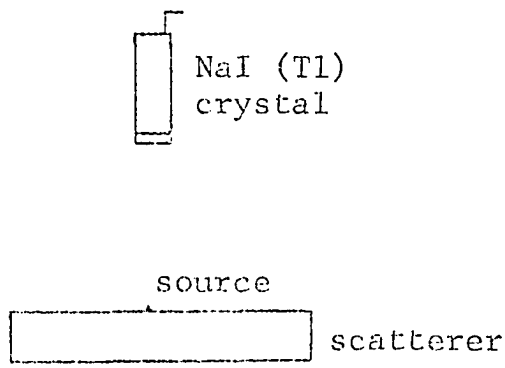


Figure 1. Relative position of detector, source, and scattering medium, Hine and McCall.

anistropy of single-scattering and the isotropy of multi-scattering; the significance of fluorescent radiation for matter of high atomic number, such as lead; and the dependence on incident energy and angle. By varying the thickness of backscatter material, Hine and McCall observed a variation in the amount of radiation scattered.

Bulatov and Garusov (17) in 1958 studied a very wide

range of backscattering materials using cobalt-60 and gold-198 sources of gamma-rays located some distance from the scattering media. By collimating the beam they were able to vary the angle of incidence of the gamma-rays and study this effect upon backscatter intensity. They, as did Hine and McCall, varied the thickness of the back-scatterer and then expressed the dependence of the energy albedo on scatterer thickness as

$$\eta(d) = \eta(\infty)(1 - e^{-d/a}) \qquad \text{Eq. 2.1}$$

where:

$\eta(d)$ = the value of the albedo for a scatter thickness, d

$\eta(\infty)$ = the limiting value of the albedo for "infinite" scatterer thickness

d = the scatterer thickness in $gm/cm^2$

a = a constant

From their work, Bulatov and Garusov formed an empirical relation to describe the variance of the albedo as a function of the primary beam energy, E; the angle of incidence at the surface of the scatterer, $\alpha$; the effective atomic number, Z, of the scatterer material; and its density, $\rho$,

$$\eta(E,\alpha,Z,\rho) = 3.2\,\frac{1}{E}\,\frac{1}{\cos\alpha}\,\frac{\rho}{Z^2} \pm 20\% \quad \text{Eq. 2.2}$$

Hyodo (18), in 1962, extended the work of Hine and McCall. He measured the spectra of backscattered radiation from semi-infinite slabs by means of a scintillation spectrometer as a function of the measuring angle. His sources were cobalt-60 and cesium-137 in close contact to slabs of paraffin, aluminum, iron, tin, and lead. Hyodo's work gives a comprehensive study of the energy and number albedos, the angular distributions of scattered energy and number of photons, and the energy distributions for the combinations of the gamma sources and scatterer materials used. Hyodo also studied the effect of thickness of scatterer material upon his results and, because of his geometry, arrived at a slightly lower value for "infinitely thick" than did Bulatov and Garusov. Hyodo's later work with Fujita et al. (19) and Nakamura (20) studied in greater detail the effect of scatterer thickness using iron as a backscatterer and cobalt-60 as a source in close contact with the iron. They arrived at the empirical relationship

$$A(\theta,x) = A(\theta,\infty)(1 - e^{-cx}) \quad \text{Eq. 2.3}$$

where:

$A(\theta,x)$ = the fraction of photons emergent at angle $\theta$ per steradian for one primary photon incident to the scatterer of thickness x

x = the slab thickness

Their value for "c" differs from that of $\frac{"1"}{a}$ in the Bulatov-Garusov development by about a factor of two. This study of the effect of thickness on backscattering was extended in 1967 by Hyodo, Matsumoto, and Mizukami (21) to cover polyethylene, aluminum, and lead, still using the point cobalt-60 source in contact with the slab. A least squares fit of their data against

$$A(x) - b = [A(\infty) - b](1 - e^{-cx}) \qquad \text{Eq. 2.4}$$

was made with good result. The terms here are the same as in Eq. 2.3, with "c" and "b" constants dependent upon experiment design. Their work, along with that of Bulatov and Garusov indicated that a thickness of material greater than two mean free paths of the source radiation would constitute an "infinite" thickness.

The first detailed backscatter work done with concrete as the scatter material was carried out in 1963 by Clarke

and Batten (22). They used uncollimated point sources of cobalt-60 and iridium-192 at varying heights above a concrete slab. An uncollimated ionization chamber detector was placed at various distances from the source and the concrete to determine the effect of concrete on the dose measured. This work was extended by Hendee and Ellis (23) in 1965,

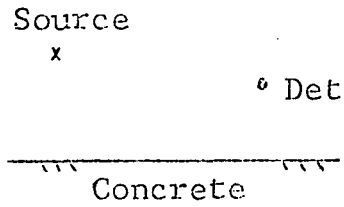


Figure 2. Experimental arrangement used by Clarke and Batten

using uncollimated cobalt-60 and cesium-137 sources scattered from semi-infinite slabs of concrete, lead, and water.

Jones, et al., (24, 25), in 1964, using cobalt-60 and cesium-137 as plane-parallel beam sources, studied the backscatter from concrete, aluminum, and steel as a function of the incident and the reflected angle with a scintillation detector. From their results, Jones, et al., developed the empirical formula

$$A_d(\Omega) = c \exp(-m\theta_s) + b' \qquad \text{Eq. 2.5}$$

where:

$A_d(\Omega)$ = the differential dose-rate ratio

$$A_d(\Omega) = \frac{D}{D_o} \qquad \text{Eq. 2.6}$$

with:

$D$ = the reflected dose per unit solid angle at d

$D_o$ = the incident dose rate at the center of the slab's surface

"c", "m", and "b" in Eq. 2.5 are constants which they determined for each source, backscatterer, and incident angle. $\theta_s$ was the Compton scattering angle. Steyn and Andrews (26) in their experiments of 1967, did a very complete study, extending this work using gold-198, cesium-137, and cobalt-60 point sources one meter from graphite, aluminum, high density concrete, iron, nickel, tin, lead, and uranium. A highly collimated scintillation spectrometer was used as the detector to determine angular and energy dependence of the backscattered photons. The expression chosen by Steyn to best fit his data is

$$d\,A_D = a_o + a_1 x + a_2 x^2 \qquad \text{Eq. 2.7}$$

where:

$d A_D$ = the differential dose albedo;

$x = 1 + \cos \theta_s$ Eq. 2.8

$\theta_s$ = scattering angle as in Figure 5.

"$a_o$", "$a_1$", and "$a_2$" are constants dependent upon the conditions of the experiment.

The integrated dose albedo empirical expression is represented by

$$\alpha_D = 3a_o + a_1 + \frac{a_2}{2} \qquad \text{Eq. 2.9}$$

where the constants have the same values as in Eq. 2.7. Both equations 2.7 and 2.9 neglect fluorescent x-ray dose contributions.

Data in the literature concerning the backscatter of x-rays in the source energy regions covered by the above papers show similar results (27, 28, 29, 30, 31, 32, 33).

The backscatter of high energy bremsstrahlung was first studied by Kruglov and Lopatin (34) in 1959, when they were concerned about energy losses in using absorption calorimetry for calibrating the beam output of an 85-MeV accelerator.

Pruitt (35) in 1964 was the first to consider backscatter from megavolt photons in the albedo sense. Using a scintillation spectrometer as a detector and backscatter media of carbon, magnesium, copper, tin, and lead, he determined the energy albedo for normally incident bremsstrahlung with a maximum photon energy of 90 MeV, and for lead at 25, 50, and 170 MeV maximum.

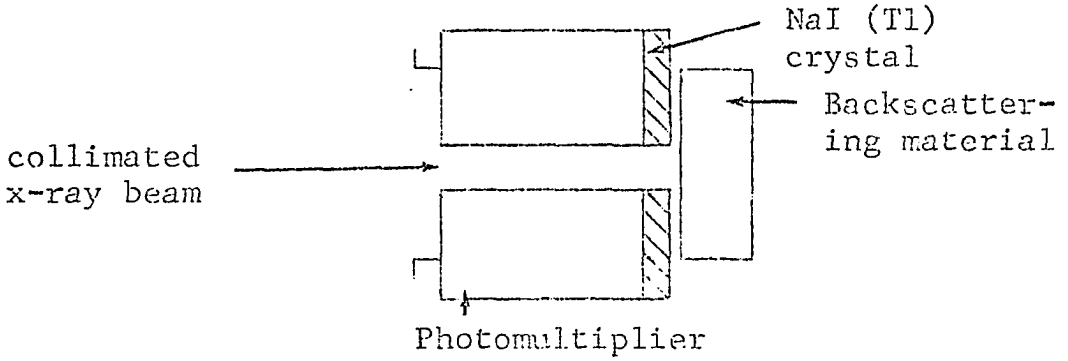


Figure 3. Experimental arrangement used by Pruitt.

In 1967, Sugiyama and Tomimasu (36), using lower energy (11.3 to 23.2 MeV maximum) bremsstrahlung, studied the angular distribution of the energy albedo from lead, copper, and Duralumin.

Karzmark and Capone (37), in 1968, performed a cursory look at radiation scattered from concrete by a 6 MeV linear accelerator.

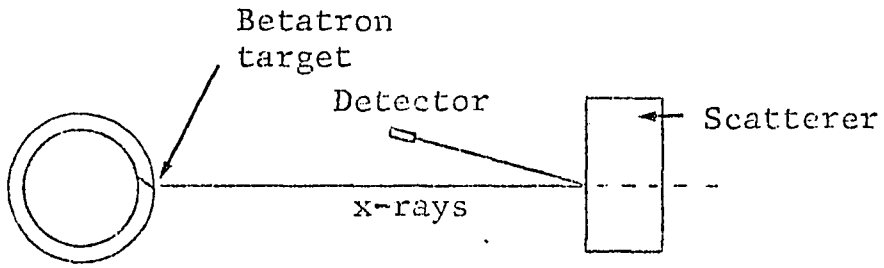


Figure 4. Experimental arrangement used by Sugiyama and Tomimasu.

## 2.2 NUMERICAL

The development of numerical estimates of albedo followed the gathering of experimental data. After the work of Compton (13) and Klein and Nishina (14) which described the basic scattering interaction, several years passed until sufficient data was collected to formulate empirical estimates. During this period the Monte Carlo technique of random sampling and high speed computers were developed, presenting another method of numerically estimating the photon backscatter from a surface. Hayward and Hubbell (38) were among the first to employ the Monte Carlo technique; using a desk calculator they estimated the albedo of various materials for 1 MeV photons in 1954. The next year, Perkins (39) with an IBM computer repeated their process with normally incident photons of 1 MeV on concrete. Berger's

(40) Monte Carlo calculations in 1957 were based on an experimental design (Figure 2) to be tested eight years later by Clarke and Batten (21).

Wells (41) in 1959, developed, by Monte Carlo techniques, a very complete study of the angular distribution and energy spectra of gamma-ray scatter from concrete. He postulated source energies of 0.6 MeV to 7.0 MeV incident at five different angles to the slab. His calculations include the effects of single and multiple scatter interactions, the photoelectric effect, and pair production reactions. As the cross-section data have since been largely revised (42), Wells repeated his analysis in 1964 (43). In 1962, Davisson and Beach (44) extended this type of calculation to include water, iron, and lead as backscatter media. In 1963, two studies were made which probably represent the best Monte Carlo examinations of photon backscatter from concrete available to date. Raso (45) and Leimdorfer (46) each worked on the reflection of photons from concrete in the energy range 1 to 10 MeV. While Raso allowed the angle of incident to vary and studied that effect, Leimdorfer used normal incidence and studied the variance of reflector thickness on albedo. Both considered photoabsorption, Compton interactions, and pair production. Their works are considered as standards against which experimental results

are often compared. Each of the above works considered only monoenergetic photons.

Bulatov and Leipunski (47) in 1961 were among the earliest to formulate quantitative expressions for albedo from experimental data. Based on experimental information gathered earlier by Bulatov (17), they expressed number and energy albedo as a function of build-up and build-up as a function of media thickness. Later in 1966, Bulatov (48) developed engineering formulas and nomograms for determining quantities of scattered gamma-radiation. These were based on three geometries: a narrow beam striking a scattering material, an isotropic source in contact with a surface, and a plane unidirectional flow of gamma quanta. Values are given primarily for cobalt-60 and gold-198 sources scattered from lead, iron, and aluminum. Some values for carbon and concrete are included.

In 1963, Chilton and Huddleston (49) developed a semi-empirical formula for the differential dose albedo from gamma-rays incident on concrete, which has been very useful in this field. The energy ranges covered are from 0.2 to 10 MeV in a geometry as shown in Figure 5.

Their development considers single scattering as expressed by the Klein-Nishina representation and pair production annihilation and multiple scattering components

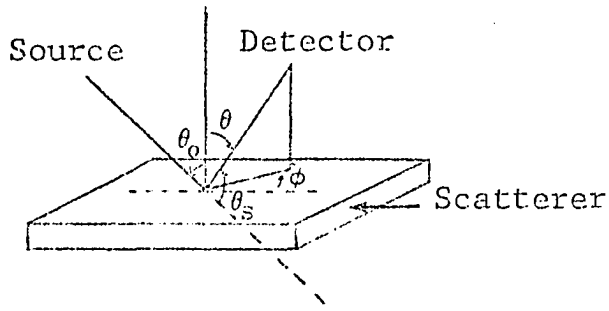


Figure 5. Relative position of source, detector, and scatterer for the Chilton-Huddleston development.

as isotropic sources at the surface of the backscatterer.

The relationship they derived is given by

$$a_d(\theta_o, \theta, \phi) = \frac{C\, K(\theta_s)\, .10^{26} + C'}{1 + \cos\, \theta_o \sec\, \theta} \qquad \text{Eq. 2.10}$$

where:

$a_d(\theta_o, \theta, \phi)$ = the differential dose albedo

C and C' = parameters to be adjusted for each incident energy

$K(\theta_s)$ = the Klein-Nishina value of the energy scattering cross-section per electron

$\cos\, \theta_s = \sin\, \theta_o \sin\, \theta \cos\, \phi - \cos\, \theta_o \cos\, \theta$

Values for C and C' are given in their report. A number of comparisons are made with the results of this equation and results from Monte Carlo estimates and existing experimental data. Chilton (50) extended this work in 1965 to calculate the total albedo. Also in 1965, Chilton and Davisson (51) published values for the constants in Equation 2.10 for concrete, water, iron, and lead.

Huddleston (52) in 1964 updated some of the original Chilton-Huddleston values and examined more closely those values near gold-198, cesium-137, cobalt-60, and sodium-24 gamma energies. With Shoemaker, he (53) set up a series of isoalbedo contours for engineering applications. In 1966, due to more accurate Monte Carlo information, Chilton (54) revised their formula to more closely represent available data. The new formula is

$$\alpha(\theta_o,\theta,\phi) = F(\theta_o,\theta,\phi)\,\frac{C.10^{26}K_e(E_o,\theta_s) + C'}{1+\cos\theta_o \sec\theta\left[1+2E_o(1-\cos\theta_s)\right]^{\frac{1}{2}}}$$

Eq. 2.11

where

$$F(\theta_o,\theta,\phi) = A_1 + A_2(1-\cos\theta_o)^2 + A^3(1-\cos\theta)^2$$

$$+ A_4(1-\cos\theta_o)^2(1-\cos\theta)^2 + A_5(1-\cos\theta_o)(1-\cos\theta)(1-\cos\phi)$$

Eq. 2.12

and the other parameters are as defined for the original equation 2.10. Thus far, only values for the constants with cesium-137 and cobalt-60 sources have been established. In 1967 Chilton (55) revised these particular numbers.

Recently several other techniques have been developed to estimate albedo (56, 57, 58, 59) and the method of discrete ordinates (as developed by Carlson [60]) deserves special mention. For some time neutron distributions have been calculated by discrete ordinates methods, while photon distributions had been calculated by Monte Carlo methods. In 1965 Lathrop (61) investigated the possibility of using the faster (computer time-wise) discrete ordinates method for photon distribution calculations. His investigation showed excellent agreement with Monte Carlo methods and pointed the way for further development of the discrete ordinates method. Renken and Adams (62) in 1967 expanded

Lathrop's work on photon scatter. Multiple scattering and fluorescence are extensively covered.

Pair production annihilation contributions were written into the program two years later (63). Their program (DTF) allows a rapid calculation of photon densities as a function of angle, radius, and energy. Input parameters may be widely varied with little resultant run-time penalty.

## 2.3 SUMMARY

Except for the few examples discussed, backscatter of bremsstrahlung above a few MeV has not been investigated experimentally. The experimental configuration used by Pruitt did not allow the investigation of angular distribution. Both works were somewhat limited as to the energy range studied and choice of backscatterer materials. The present research provides information on energy regions not yet studied, and develops a method for determining albedo dose and angular distributions from pulse-type bremsstrahlung sources.

The notation used in this section is in each case that of the author discussed and definitions are given at that point.

# 3. THEORETICAL CONSIDERATIONS

## 3.1 INTRODUCTION

As the research topic deals with a continuous spectrum bremsstrahlung having a leading spectrum edge of intermediate energy (1 to 10 MeV), all the familiar photon interactions are of interest.

In the lower energy regions of the bremsstrahlung spectrum, photoelectric absorption is the predominant interaction. Electrons released by the photoelectric effect are of low energy and are not considered further. (Their ionization losses far outweigh their radiation loss.) In filling the K- and L- orbital vacancies left by photoelectric absorption, K- and L- x-rays, respectively, are given off. These x-rays are given off isotropically from the point they arise.

Characteristically a sharp drop occurs in the absorption cross-section of the material at energies just below the capture edge. The x-rays generated fall in this "depressed" cross-section region and consequently contribute significantly to backscatter yields.

Compton interactions are highly anisotropic, with angle and energy distributions calculated by Klein-Nishina formulas. In high energy Compton scattering events, the scattered photon distribution is largely in the forward direction. However, multiple Compton scattering events occur to create an isotropic photon fluence from this source. Large energy transfers can occur to create Compton electrons. These electrons can then give up their energy through bremsstrahlung which will add to the photon fluence in the backscatter media.

Photons of energies greater than a few MeV can react in the field of a nucleus or an electron to create an electron-positron pair. The cross-section for these reactions increases with incident photon energies and increasing target mass number. The energy of the photon (in excess of that required for formation of the electron-positron pair) goes into kinetic energy of the created pair (or triplet if in the field of an electron). The angular distribution of the positron and negatron is mainly forward for incident photons of high energy. Each gives up its kinetic energy by ionization, excitation, and bremsstrahlung. As the positron slows down it will recombine with an electron giving rise to two 0.511 MeV annihilation photons at that point. The bremsstrahlung and annihilation radiation will contribute

isotropically to the backscatter fluence.

Coherent, or Rayleigh, scattering occurs in the energy regions where atomic electron binding effects must be considered in Compton scattering. The photon does not transfer energy to the atom while it is interacting. In the high energy regions where Rayleigh scattering need be considered (around 1 MeV) the majority of the photons are scattered by less than $5^{o}$ and in the lower energy regions the cross-section for photoelectric absorption greatly overshadows the coherent scattering effect.

The energy region employed for this study encompasses the photonuclear absorption resonance regions. However, the photonuclear cross-sections of the backscatter materials studied are small and the resultant photoneutron fluence would be quite small relative to the photon fluence. The effect of the photoneutron fluence on the detectors used will be discussed later in this section.

Other photon interactions of minor importance, resonance scattering and Thomson scattering by the nucleus, Compton scattering by nucleons, meson production, resonance scattering associated with meson production, Delbruck scattering, and nucleon-antinucleon production, will not be considered (3, 64).

The detection instruments used in this work are thermoluminescent crystals and a scintillation spectrometer. Each is differential with respect to angular distribution; i.e. neither covers the entire emission field in the experimental set-up chosen, and the spectrometer is differential also with respect to energy. Methods of using the output of these detectors in a manner suitable for comparison with prior numerical estimates will be discussed in greater depth.

Each of these topics will now be reviewed in depth to assess their contribution to albedo as considered in this study. It is not the purpose of the following sections to derive a rigorous theoretical solution to the backscattering of intermediate energy bremsstrahlung, but rather they are given in an effort to point out sources of photons which contribute to the backscatter field and consider their relative importance.

## 3.2 PHOTON INTERACTIONS

### 3.2.1 Photoelectric Absorption (3, 11)

As pointed out in the introduction, photoelectric absorption is the predominant interaction for photons of low energy. The cross-section for this reaction is heavily Z dependent. For high Z target nuclei, photoelectric absorption may remain the predominant interaction to about

900 KeV. Although no longer the predominant interaction, a cross-section does continue to exist for photoelectric absorption to high photon energies ($1.41 \times 10^{-2}$ barn/atom at 100 MeV in Pb [65]). This reaction will occur primarily with the low energy region of the incident bremsstrahlung and with photons being scattered back from some depth in the backscatter medium.

The photoelectric effect is not easily treated theoretically due to bound electron considerations and outer orbital shielding effects. Estimates have been made for cross-sections in the energy range 0.2 MeV to 100 MeV using

$$\tau_K \approx Z^5 \sum_{N=1}^{4} \frac{a_n + b_n Z}{1 + c_n Z} E_o^{-p_n} \quad \text{barn/atom} \quad \text{Eq. 3.1}$$

where:

$\tau_K$ = the K-shell photoelectric cross-section in barns per atom

$Z$ = the atomic number of the target nuclei

$a_n$, $b_n$, $c_n$, $p_n$ = constants chosen for an empirical fit

To add in the effect of other orbital electron interactions

$$\frac{\tau_{pe}}{\tau_K} \approx 1 + 0.01481\ \ln^2 Z - 0.000788\ \ln^3 Z \quad \text{Eq. 3.2}$$

is used where:

$\tau_{pe}$ = the total photoelectric cross-section in barns per atoms

In lower energy ranges absorption edges vary the cross-section greatly. At these edges the cross-section shows discontinuous jumps because the photon energy becomes smaller than the binding energy of some of the electrons. At this point the number of electrons which the photon is energetically capable of ejecting is suddenly decreased.

The photoelectrons resulting from this interaction tend to be ejected at right angles to the incident photon path, showing preference for the forward direction with increasing photon energy.

After the ejection of an orbital electron, a vacancy exists which must be filled. Generally an electron in a higher orbit gives up energy to drop into the deficient orbit. The energy given up is in the form of characteristic x-rays and can be estimated by

$$h\nu = 13.6\ Z^2 \left[\frac{1}{n_1^2} - \frac{1}{n_2^2}\right] \text{ eV} \qquad \text{Eq. 3.3}$$

where:

$h\nu$ = the emitted photon energy in eV

$n_1$ and $n_2$ are the principle quantum numbers for the initial and final electron vacancies. This radiation is given off in a truly isotropic distribution. The number of emitted photons by this process is dependent upon incident photon energy and the target material; the energy of each photon is dependent only upon the material. This energy range is such that the primary interactions these x-rays will undergo is photoelectric absorption. They are thus attenuated approximately exponentially from the point they arise until they exit from the surface of the backscatter media.

From these considerations, one can now derive an expression for the contribution to the backscatter fluence due to the photoelectric effect

$$ {}_{pe}\phi_N(\phi_o, E_o, Z, r) = \frac{\rho N.Z}{4\pi r^2 M} \int_d \int_A \left\{ \phi_o \exp[-\mu_t(E_o Z)d] \, \tau_{pe}(E_o Z) \right. $$

$$ \left. + \phi_c(d) \, \tau_{pe}(E_c Z) + \phi_{pp}(d) \, \tau_{pe}(0.511, Z) \right\} $$

$$ \left[ \exp[-\mu_t(E_{pe}, Z) d(\sec \theta_s)] \right] dd \, dA \qquad \text{Eq. 3.4} $$

where:

${}_{pe}\phi_N(\phi_o, E_o, Z, r)$ = the number fluence from the photoelectric effect at some point r from the surface of a backscatter material with atomic number Z

$\phi_o$ = the incident fluence of photons at energy $E_o$

$\tau_{pe}(E_o, Z)$ = the photoelectric microscopic cross-section of the incident bremsstrahlung fluence

$\tau_{pe}(E_c, Z)$ = the photoelectric microscopic cross-section of photons having undergone Compton scattering interactions

$\tau_{pe}(0.511, Z)$ = the photoelectric cross-section of photons created by pair production

$d$ = the depth in the backscatter media being considered

$\mu_t(E_o, Z)$ = the total attenuation coefficient for the incident bremsstrahlung fluence

$\phi_c(d)$ = the fluence due to Compton scattered photons at a depth d

$\phi_{pp}(d)$ = the fluence due to pair production at d

A = incident beam area

r is assumed much greater than the beam radius at the surface of the backscatterer.

The energy fluence under the same conditions is found to be

$$_{pe}\phi_N(\phi_o, E_o, Z, r) = {}_{pe}\phi_N \sum_n h\nu \qquad \text{Eq. 3.5}$$

where: $_{pe}\phi_N$ is given by Eq. 3.4 and $h\nu$ by Eq. 3.3

Using a detection system which is capable of differentiating energies, one would expect to observe an energy grouping due to these characteristic x-rays.

Fink, et al. (66) list extensive experimental results on fluorescence yields and energies.

3.2.3 Compton Scattering (3,11)

In the energy region approximately 0.5 to 5 MeV the dominant photon interaction is incoherent scattering from electrons, the Compton effect (67). Over this energy range

the cross-section for the Compton effect is given by the Klein-Nishina equation

$$e^{\sigma} = \frac{2\pi e^4}{m_o^2 c^4} \left\{ \frac{1+a}{d^2} \frac{2(1+a)}{1+2a} - \frac{1}{a} \ln(1+2a) \right.$$

$$\left. + \frac{1}{2a} \ln(1+2a) - \frac{1+3a}{(1+2a)^2} \right\} \frac{cm^2}{electron} \qquad \text{Eq. 3.6}$$

where:

$e^{\sigma}$ = the probability of removal of a photon from a collimated beam while passing through an absorber containing one electron/$cm^2$

$e$ = the electronic charge ($4.8 \times 10^{-10}$ statcoulomb)

$m_o$ = the electron mass ($9.1083 \times 10^{-28}$ gm)

$c$ = the velocity of light ($2.998 \times 10^{10}$ cm/sec)

and $$a = \frac{E_o}{m_o c^2} \qquad \text{Eq. 3.7}$$

where $E_o$ is the incident photon energy. This equation is based on interaction with an unbound electron. In those cases where the photon energy is comparable with the binding energy of the atomic electrons, the photoelectric

cross-section usually greatly exceeds the Compton scattering cross-section (11) which is given by

$$e\sigma_s = \frac{2\pi e^4}{m_o^2 c^4}\left[\frac{4a^2}{3(1+2a)^3} - \frac{(1+a)}{a^2(1+2a)^2}(1+2a-2a^2) + \frac{1}{2a^3}\ln(1+2a)\right] \qquad \text{Eq. 3.8}$$

with terms as defined in Eq. 3.7.

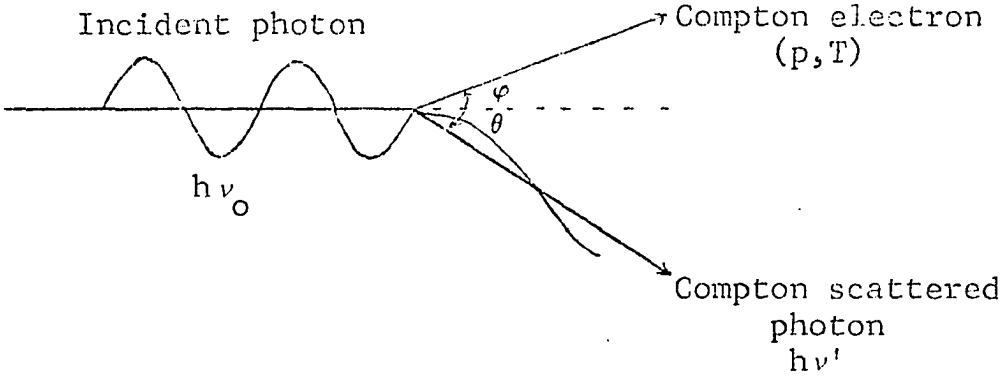


Figure 6. Compton Scattering

The energy of the incident photon will be shared after the collision by a scattered photon and the struck electron. The energy of the scattered photon is given by

$$h\nu' = \frac{m_o c^2}{1 - \cos\theta + \left(\frac{1}{a}\right)} \qquad \text{Eq. 3.9}$$

and the kinetic energy of the struck electron

$$T = h\nu_o \frac{2a\cos^2\varphi}{(1+a)^2 - a\cos\varphi} \qquad \text{Eq. 3.10}$$

The direction of the scattered photon is given by

$$\frac{d({}_e\sigma)}{d\theta} = \frac{d({}_e\sigma)}{d\Omega}\, 2\pi \sin\theta \, \frac{cm^2}{\text{electron}} \qquad \text{Eq. 3.11}$$

where:

$\frac{d({}_e\sigma)}{d\theta}$ = the number of photons scattered at angle $\theta$ per electron per $cm^2$ per incident $h\nu$

$\frac{d({}_e\sigma)}{d\Omega}$ = the number of scattered photons per unit solid angle given by

$$\frac{d({}_e\sigma)}{d\Omega} = \frac{e^4}{m_o^2 c^4}\left(\frac{h\nu'}{h\nu_o}\right)^2\left(\frac{h\nu_o}{h\nu'} + \frac{h\nu'}{h\nu_o} - \sin^2\theta\right) \qquad \text{Eq. 3.12}$$

with terms as defined before. Inspection of graphs of these functions by Evans (11) shows that as incident photon energy increases, scattering becomes greater in the forward direction.

The direction of the Compton electron is given by

$$\frac{d({}_e\sigma)}{d\varphi} = \frac{d({}_e\sigma)}{d\Omega'} \; 2\pi \sin\varphi \qquad \text{Eq. 3.13}$$

where:

$$\frac{d({}_e\sigma)}{d\Omega'} = \frac{d({}_e\sigma)}{d\Omega} \frac{\sin\theta \; d\theta}{\sin\varphi \; d\varphi} \qquad \text{Eq. 3.14}$$

The distribution of struck electrons also shows peaking in the forward direction with increased incident photon energy.

The number-energy distribution of the Compton electrons can be represented as

$$\frac{d({}_e\sigma)}{dT} = \frac{d({}_e\sigma)}{d\Omega} \frac{2\pi}{a^2 m_o c^2} \left[ \frac{(1+a)^2 - a^2 \cos^2\varphi}{(1+a)^2 - a(2+a)\cos^2\varphi} \right]^2 \qquad \text{Eq. 3.15}$$

From applying the conservation of momentum and energy in the Compton interaction one may write

$$\frac{1}{h\nu'} - \frac{1}{h\nu_o} = \frac{1}{m_o c^2}(1 - \cos\theta) \qquad \text{Eq. 3.16}$$

From an examination of Eq. 3.16 it follows that, for a given scatter angle, higher energy incident photons suffer a greater energy change than do lower energy incident photons. Since the energy gained by the struck electron is

$$T = h\nu_o - h\nu' \qquad \text{Eq. 3.17}$$

Compton scattering favors energy transfer to electrons in the higher energy ranges. However, since the Compton process only predominates through about 5 MeV, the bremsstrahlung from these electrons will be of moderate energy and will be emitted isotropically. The ratio of energy lost by these electrons by bremsstrahlung to energy lost by ionization is approximated by

$$\frac{\left(\frac{dT}{ds}\right)_{rad}}{\left(\frac{dT}{ds}\right)_{ion}} \approx Z\left(\frac{m_o}{M_o}\right)^2\left(\frac{T}{1400\ m_o c^2}\right) \qquad \text{Eq. 3.18}$$

where $M_o$ is the rest mass of the particle near which the energy loss occurs and the other terms are as previously defined. For this radiation to then be contributed to the backscatter fluence, it must pass through some thickness, d, from the point of origin to the surface of the backscatter medium.

The degraded photon can then undergo further Compton scatter to be emitted at the surface also. Previous experiments (16, 23) using monoenergetic photon sources have been able to differentiate between these multiply scattered photons and those singly scattered. Since the sources used for this research were bremsstrahlung spectra, this differentiation was not possible.

The contributions to backscatter fluence due to Compton interaction will be then

$$ {}_{C}\phi_N(\phi_o, E_o, Z, r) = {}_{SC}\phi_N + {}_{MC}\phi_N + {}_{BC}\phi_N \qquad \text{Eq. 3.19} $$

where:

$_{SC}\phi_N(\phi_o, E_o, Z, r)$ = the number fluence due to singly Compton scattered photons at some point, r, from the surface of a backscattering medium with atomic number Z when exposed to a photon fluence $\phi_o$ of energy $E_o$, given by

$$ {}_{SC}\phi_N\ (\phi_o, E_o, Z, r) = \int_d \int_A \frac{\phi_o(E_o)\ \exp[-\mu_t(E_o, Z)d]}{r^2} $$

$$ \frac{d({}_e\sigma_s)}{d\Omega}\ \frac{\rho N_o Z}{M}\ \exp[-\mu_t(E_c, Z)d(\sec\ \theta_s)]\ dd\ dA $$

Eq. 3.20

where:

$\phi_o(E_o)$ = the incident photon fluence

$\mu_t(E_o, Z)$ = the total attenuation coefficient to the incident photons

$d$ = the depth in the backscatterer being considered

$\frac{d({}_e\sigma_s)}{d\Omega}$ = the number of photons being scattered into the solid angle of concern

$\mu_t(E_c, Z)$ = the total attenuation coefficient to the scattered photons

${}_{MC}\phi_N(\phi_o, E_o, Z, r)$ is the number fluence contribution due to multiply Compton scattered photons at some point, r, given here for twice Compton scattered:

$$_{MC}\phi_N(\phi_o, E_o, Z, r) =$$

$$\int_A \int_{(t,\alpha,\beta)} \int_d \int_{d'} \phi_o(E_o) \exp[-\mu_t(E_o,Z)d'] \; {}_e\sigma_s(E_o) \frac{\rho N.Z}{M}$$

$$\exp[-\mu_t(E_c,Z)t] \frac{1}{4\Pi t^2} \frac{d({}_e\sigma_s)}{d\Omega}(E_c) \frac{\rho N.Z}{M}$$

$$\frac{\exp[-\mu_t(E_{DC},Z)d \sec \theta_s]}{r^2} \; dd' \; dd \; td\alpha t \sin\alpha \, d\beta \, dt$$

Eq. 3.21

where:

$d'$ = the depth into the backscatter medium until the first Compton interaction

${}_e\sigma_s(E_o)$ = the Compton microscopic scattering cross-section for the incident photons

$\mu_t(E_o Z)$ = the total attenuation coefficient to the once Compton scattered photons

$t$ = the distance between the first and second Compton scatter events

$\frac{d({}_e\sigma_s)}{d\Omega}(E_c)$ = the number of photons being scattered into the solid angle of concern dependent upon the energy of the once Compton scattered photons

$\mu_t(E_{DC},Z)$ = the total attenuation coefficient for the double Compton scattered photons

d = the depth in the backscatter medium to the second Compton event

$(\alpha,\beta)$ = angles defining the direction of first Compton scattering

and the rest of the terms are as previously defined. Higher order scattering would be handled similarly.

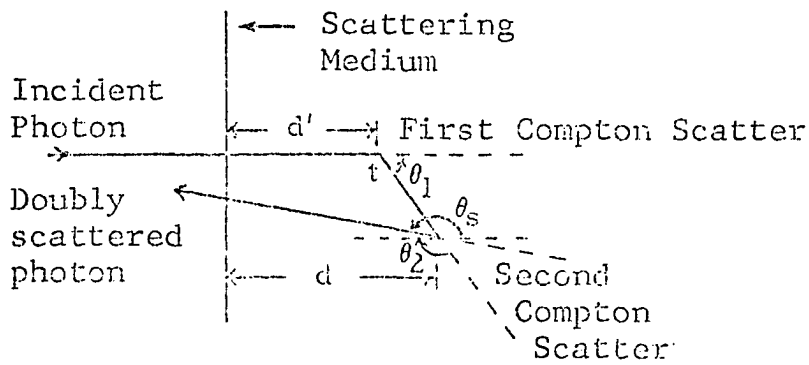


Figure 7. Multiple Compton Scattering

Finally, ${}_{BC}\phi_N$, the number fluence contribution due to bremsstrahlung produced by Compton scattered electrons, can more easily be represented by ${}_{BC}\phi_E$, the energy of photons contributed to the backscatter fluence by the bremsstrahlung of Compton electrons, which can be given by

$$ {}_{BC}\phi_E(\phi_o, E_o, Z, r) = \int_d \int_{d'} \int_A \int_{E_B} \phi_o(E_o) \exp[-\mu_t(E_o, Z)d'] $$

$$ e^{\sigma \frac{\rho N_o Z}{M}} \frac{\left(\frac{dT}{ds}\right)_{rad}}{\left(\frac{dT}{ds}\right)_{rad} + \left(\frac{dT}{ds}\right)_{ion}} $$

$$ \frac{\exp[-\mu_t(E_B, Z)d \sec \theta_s]}{4\pi r^2} \, dE_B \, dA \, dd' \, dd \qquad \text{Eq. 3.22} $$

where:

${}_{BC}\phi_E$ = the energy contributed to the backscatter fluence by the bremsstrahlung of Compton electrons at the point r

$\mu_t(E_B, Z)$ = the total attenuation coefficient to the bremsstrahlung radiation

and the rest of the terms are as previously defined.

The highest energy photon one might see emergent from the scattering surface due to Compton interaction, with the sources used in this dissertation, would be that due to a large number of Compton scatter events resulting in a photon emerging at $90^o$ to the incident beam. The larger the number of scatterings required the lower the probability of the

photon surviving. A 10 MeV photon undergoing three Compton scatterings of $30^{o}$ each would emerge with an energy of 1.13 MeV.

3.2.3 Pair Production (3, 11)

In the energy region of 5 MeV for high Z materials and 10 MeV for intermediate Z materials, the cross-section for pair production interactions becomes important. The energy threshold for pair production is 1.022 MeV in the field of a nucleus and 2.044 MeV in the field of an electron.

The cross-section for this interaction in the field of a nucleus is estimated by

$$K_n = \left[K_n(\text{Born, unscreened}) - S^{HFS}\right]\left[1 + \Delta(\text{rad. corr.})\right] - \Delta(\text{empirical}) \cdot \Delta K_n^{DBM} \qquad \text{Eq. 3.23}$$

where: $K_n$(Born, unscreened) is an approximation represented by

$$K_n(\text{Born}) \approx \frac{4Z^2 r_e^2}{137} \ln\left(183\, Z^{-1/3}\right)$$

$$\left[\left(1-\frac{2}{k}\right)\left(1+\frac{K}{k}\right) - \frac{\mu}{6} - \frac{2}{k} + \frac{\mu}{k^2} - \frac{2\mu}{3k^3} - \frac{2K}{k}\frac{\left(1+\frac{\mu K}{k}\right)}{\sqrt{1+\frac{4K}{k}}} \ln \frac{\sqrt{1+\frac{4K}{k}} + 1 - \frac{2}{k}}{\sqrt{1+\frac{4K}{k}} - 1 + \frac{2}{k}}\right]$$

Eq. 3.24

with

$$r_e = \frac{e^2}{m_o c^2} \qquad \text{Eq. 3.25}$$

$$k = \frac{E_\gamma}{0.511} \qquad \text{Eq. 3.26}$$

$$\mu = \frac{4}{3} + \left[9 \ln\left(183\, Z^{-1/3}\right)\right]^{-1} \qquad \text{Eq. 3.27}$$

and

$$K = \frac{255\, Z^{-1/3}}{(15.6 - 4/3 \ln Z)} \qquad \text{Eq. 3.28}$$

in Eq. 3.23.

$S^{HFS}$ = the Sorenssen screening correction

$1 + \Delta(\text{rad. corr.})$ = the Mork-Olsen radiative correction factor

$\Delta(\text{empirical})$ = a correction factor for high-energy Coulomb effects as is $\Delta k_n^{DBM}$

Values for each of these are found in the literature (3).

The cross-section for pair production in the field of an electron is estimated by

$$K_e = \frac{r_o^2}{137}\left\{\frac{28}{9}\ln(2k) - \frac{218}{27} - \frac{1}{k}\left[\frac{4}{3}\ln^3(2k) - 3\ln^2(2k) + 6.84\ln(2k) - 21.51\right]\right\}$$

Eq. 3.29

with terms as defined above. The energy of the incident photon is shared by the electron-positron pair.

$$h\nu = (T_- + m_o c^2) + (T_+ + m_o c^2) \qquad \text{Eq. 3.30}$$

where $T_-$ and $T_+$ are the kinetic energy of the electron and positron respectively. The kinetic energy of the positron is slightly greater than that of the electron when they are created in the field of a nucleus. This difference being, at most, about

$$T_+ - T_- = \frac{2\ Ze^2}{(h/2\pi m_o c^2)} = 0.0075\ Z \quad \text{Eq. 3.31}$$

The angular distribution of the pair peaks in the forward direction for high energy incident photons (68).

For pair production in the field of an electron the photon's energy is divided among three particles (the created positron and electron and the electron involved in the interaction).

All particles here lose energy by radiation, ionization, and excitation. The contribution of the bremsstrahlung can be considered in the same manner as described for the Compton electrons previously. As the positron slows down it will combine with an electron to create two annihilation photons of 0.511 MeV, which are emitted isotropically. This radiation is expected to comprise the major portion of the backscatter fluence due to pair production interactions (46,

69, 70).

The fluence contribution, due to pair production interactions, at some point, r, can then be represented by

$$_{PP}\phi_N\ (\phi_o, E_o, Z, r) = {}_{BPP}\phi_N + {}_A\phi_N \qquad \text{Eq. 3.32}$$

where $_{BPP}\phi_N$ is the number fluence due to bremsstrahlung of the electrons and positrons and is to be represented in the same manner as $_{BC}\phi_N$.

$_A\phi_N$ is the number fluence contribution due to annihilation radiation, expressed here as

$$_A\phi_N\ (\phi_o, E_o, Z, r) = \int_d \int_{d'} \int_A \phi_o(E_o)\ \frac{\exp[-\mu_t(E_o, Z)d']}{4\pi r^2}$$

$$2\ \tau_K\ \frac{\rho N_\cdot Z}{M}\ \exp[-\mu_t(0.511, Z)d \sec\theta_s]\ dA\ dd'\ dd$$

Eq. 3.33

where:

$\phi_o(E_o)$ = the incident fluence

$\mu_t(E_o,Z)$ = the total attenuation coefficient to the initial fluence in the backscatterer of atomic number Z

$d'$ = the distance from the surface to the pair production interaction

$\mu_t(0.511,Z)$ = the total attenuation coefficient to the annihilation radiation

$d$ = the distance from the point of positron annihilation to the surface of the backscatterer

$k_T$ = the pair production microscopic cross-section

$A$ = area of incident beam

The rest of the terms are as previously defined.

To obtain an idea of the photon energy to emerge under this interaction one can consider bremsstrahlung from the most probable electron energy to be produced in the pair production interaction

$$E_{e^-} = \frac{1}{2}(h\nu - 1.022) \text{ MeV} \qquad \text{Eq. 3.34}$$

Bremsstrahlung resulting from this electron will have a maximum leading edge equal to the energy of the electron. With the sources used, a photon energy of 4.64 MeV might be observed from the 10.5 MeV machine.

### 3.2.4 Rayleigh Scattering and Photonuclear Interactions

Although Rayleigh (coherent) scattering may be of some consequence in scattering radiation from a beam for transmission measurements, the angle of deflection is always (11) small, and can be estimated by

$$\theta_c = 2 \arcsin \frac{0.0133\ Z^{1/3}}{E_o(\text{MeV})} \qquad \text{Eq. 3.25}$$

where $\theta_c$ is the opening half angle of a cone containing at least 75% of the coherent-scattered photons. The number of Rayleigh scattering events necessary to reflect a photon reduces the probability of this contribution below the level to be considered here. Rayleigh scattered photons might well undergo further reactions to send them back out of the reflector, but since the total distance traveled by the photon will be nearly the same as the distance into the medium and nearly no energy is lost in the Rayleigh scattering process, for purposes of this report coherent scattering will not be considered further.

Although the photonuclear giant resonance peaks occur in the energy region of interest, their cross-sections are small (5% to 10%) compared to those for the Compton effect

and for absorption by nuclear pair production. The most probable result of photonuclear absorption is the emission of a neutron. At present only experimental data is available for determining cross-sections.

Considering the materials chosen for this work:

-- Lead has a photonuclear threshold of about 6.8 MeV and reaches its resonance peak at 13.7 MeV. The cross-section at this peak is 0.81 barns/atom.

-- Iron has a photonuclear threshold of 11.2 MeV and resonance peak at 18.0 MeV, with a cross-section of 0.075 barns/atom at that energy (71).

-- The principle components of concrete, oxygen and silicon, being of lower Z have higher threshold energies, and cross-sections at their resonance peaks are considerably smaller (0.02 - 0.03 barns/atom). (72)

Since the photonuclear cross-sections are a couple of orders of magnitude below the cross-section for pair production at the same energy, the decrease to the photon fluence due to photonuclear absorption will not be considered. However, it is necessary to consider the neutron fluence which arises. The number of neutrons arising can be calculated as

$$N_n = \int_{B_n}^{E_m} \int_{a} \sigma_{(\gamma,n)}(E,ZA)\left(\frac{\rho N_o}{M}\right)\phi_N(E)\, da\, dE \quad \text{Eq. 3.36}$$

where:

$\sigma_{(\gamma,n)}(E,ZA)$ = the photonuclear cross-section at energy E in a material of atomic number Z and atomic mass A

$\phi_N(E)$ = the photon number fluence at the point of interest

$B_n$ = the threshold energy

$E_m$ = the maximum energy at which nuclear capture occurs or the maximum energy of the incident beam, whichever is smaller

$a$ = incident beam area

The neutron number fluence at a point of interest, r, can be calculated

$$ {}_n\phi_N(\phi_o,E_o,r,ZA) = \int_d \int_{B_n}^{E_m} \int_A \frac{\phi_o(E_o)}{4\Pi r^2} \exp[-\mu_t(E_o,Z)d] \sigma_{(\gamma,n)}(E,ZA) \frac{\rho N_o}{M} \exp[-\Sigma_r(E,ZA)d]\, dA\, dE\, dd $$

Eq. 3.37

where:

$\phi_o(E_o)$ = the incident photon fluence

$\mu_t(E_o,Z)$ = the total attenuation coefficient to the incident fluence

d = the distance from the surface of the backscatter medium to the point of nuclear absorption

$\Sigma_r(E,ZA)$ = the removal cross-section to the emitted neutrons

and the other terms are as previously defined. Photons having undergone one of the interactions previously discussed will not have sufficient energy for photonuclear capture and their fluence is not added in this calculation.

For the materials and energies used in this dissertation,

$$ {}_n\phi_N(\phi_o,E_o,r,ZA) \ll {}_{pp}\phi_N + {}_C\phi_N + {}_{pe}\phi_N \qquad \text{Eq. 3.38} $$

where:

${}_{pe}\phi_N$ is given by Eq. 3.4

${}_C\phi_N$ is given by Eq. 3.19

${}_{pp}\phi_N$ is given by Eq. 3.32

Therefore no neutron response correction will be made for the TLD readings obtained.

Photofission is not considered for the materials chosen at the energies used for this research (73, 74).

3.2.5 Summary

The total energy fluence at some point, r, can then be represented as the sum of the previously calculated fluence.

$$\phi_E = {}_{pe}\phi_N \sum_n h\nu + F(E_c)\ {}_c\phi_N + 0.511\ {}_{pp}\phi_N \qquad \text{Eq. 3.39}$$

where:

${}_{pe}\phi_N \sum_n h\nu$ is given in Eq. 3.5

${}_c\phi_N$ is given by Eq. 3.19 and $F(E_c)$ is the distribution of the Compton scattered photons, and

${}_{pp}\phi_N$ is given by Eq. 3.32

The exposure-dose distribution may be determined from the energy distribution above by

$$D = \int \left(\frac{\mu(E)}{\rho}\right) \phi_E \, dE \qquad \text{Eq. 3.40}$$

where $\left(\frac{\mu(E)}{\rho}\right)$ is the energy mass absorption coefficient for water (since water is often used as a dose standard, any material could, of course, be chosen).

## 3.3 DETECTION INSTRUMENTATION

### 3.3.1 Scintillation Spectrometer

The scintillation detector used in this research was a 5" D x 3" right cylindrical NaI (Tl) crystal of Isotopes Inc. production with its photomultiplier package. A Nuclear Data 512 channel instrument was used as the multi-channel pulse height analyzer and data display device. The analyzer used has a "dead" time of (5 + 0.25N) $\mu$sec, where N is the channel number, and an internal delay time of 2 $\mu$sec. A detailed discussion of the operation of a scintillation spectrometer may be found in references 75 and 76.

Due to system "dead" time, the scintillation spectrometer could not be used in the experiments with the flash x-ray devices.

It was not possible to sufficiently "detune" the 2.0 MeV Van de Graaff to make a measurement of the beam spectrum. Even at the maximum distance allowed by the radiographic bay and with a very small opening collimator, the detector system was swamped out. Some measurements were made of the reflected spectra and these results are found in Appendix D for comparison with spectra generated by the two computer programs used.

Spectral data are given in Appendix D.

### 3.3.2 Thermoluminescent Detectors

The thermoluminescent detectors used in this research were Harshaw produced LiF crystals. Two sizes (1/8" x 1/8" x 0.035" and 6mm x 1mm x 0.9mm) were used to check for systematic errors arising from crystal size considerations.

Particular characteristics of the LiF thermoluminescent detector are:

-- a very linear response over a wide energy range (77) though with some under-response at low energies (40 KeV) to be discussed in greater detail in Appendix E;

-- fading of the "glow curve" is less than 5% per year (78) after an initial stabilizing period of a few hours;

-- linear response (±3%) to accumulated doses of about 700 R (79) and doesn't saturate until doses of about $10^5$ R (77);

-- lower limits of detection (with the detectors used) of approximately 5 MR (80);

-- and dose rate independence in response to rates up to $2 \times 10^{11}$ rad/sec ±10% (81, 82).

These characteristics make the LiF thermoluminescent detectors nearly ideal for the research undertaken, and certainly better than other, existing, passive detectors (83, 84).

The detectors used have some neutron response. TLD-100 (Harshaw manufactured LiF) shows a response of

about 1:37::thermal neutron:gamma exposure. The response to fast neutrons is much less (85, 86).

By placing these small detectors at various points from the surface of the backscattering material, one can determine the angular dependency of the scattered photons. Due to the integrating nature of the detector, they do not readily lend themselves to a determination of the energy of the backscattered fluence.

Much work has been done on various methods of obtaining data from TLD's. A variety of annealing and read-out procedures have been proposed (87, 88, 89, 90, 91), to accomplish greater statistical accuracy, reproducibility, handling convenience, etc. In the present research an Eberline TLD Reader Model TLR-5 was employed with the LiF crystals previously discussed. The reader allows the operator to control the time (0 - 60 seconds) and temperature (0 - 400$^{o}$C) of both a "pre-heat" cycle and an "integrate" cycle. Nitrogen is purged through the chamber at one liter per minute during read-out to lower the instrument background. A modification of the reader was made by connecting an additional variable rheostat in series with the photo-multiplier gain adjust to allow greater accuracy in setting the gain to a desired level. Appendix F discusses the method by which the read-out and annealing

procedures were chosen.

The theory of thermoluminescent dosimetry is well documented elsewhere (92, 93).

### 3.3.3 Attenuation Methods of Spectral Determination

Various methods have been used to attempt to gain information about the spectral distribution of x-rays (94). The method to be discussed here is that of graphically fitting three exponentials to an attenuation curve. It is felt that three extractions are all that can be made from a single attenuation curve with accuracy (95).

The clearest use of the attenuation curve comes from plotting the logarithm of the fraction transmitted (ordinate) verses the depth in the attenuating material (abscissa). If the absorber material is thick enough, the attenuation curve will approach a straight line at greater depths in the material. Extrapolation of this portion of the curve back to zero absorber thickness and subtraction from the original attenuation curve removes the high energy component of the incident fluence. The intercept of this portion of the curve on the ordinate axis gives the fraction of incident radiation contributed by the high energy component. This extraction procedure can then be repeated

as diagramed below.

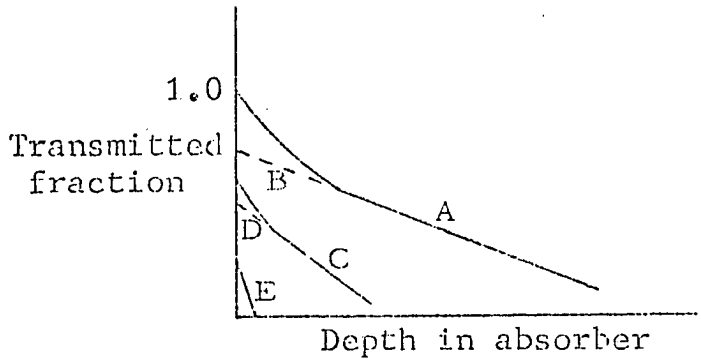


Figure 8. Attenuation extractions

Curve A is the original attenuation information, curve B the high energy component extracted, curve C that portion remaining after removal of the high energy contribution, curve D the intermediate energy extraction, and curve E is the remaining low energy component (after Greening - 94). Using the slopes of the linear curves, one can determine the linear attenuation coefficients of the various energy components in the particular absorber material used. From this an energy assignment can be made from values such as given in Attix, et al. (42). Having the energy and the fraction of the incident flux contributed by that energy, one can generally characterize the beam in a three-energy representation. Greening (96) also

discusses a method of incident energy spectrum determination from absorption data using Laplace transforms. A recent attempt has been made to computerize absorption data in an effort to obtain better energy representations (97).

Several difficulties arise in applying this method to determining the spectral output and reflected spectra for the machines used. The reflected intensity is so low as to be near the limit for statistically reliable measurement with TLD's. Any method which requires the attenuation of this intensity through several half values is impractical. The focal point for the electron beam striking an x-ray target is not precisely controlled on flash x-ray devices. It is therefore necessary to make a very large number of measurements with well collimated detectors to gain a meaningful absorption curve. This curve will then represent an average for the particular machine and not precisely represent any one shot. The spectral unfold for absorption data generated by bremsstrahlung spectra of the energy span covered in this dissertation becomes quite severe. A number of extensive measurements of spectra have been published (98, 99, 100, 101, 102, 103, 104, 105). These spectra represent a compilation of information gathered from Compton scatter devices, absorption data,

electron spectra-target codes, etc. In general previously published spectra are used in this report for computer program inputs. Appendix D discusses the spectra information generated in this work compared to previously published work. Sample albedo results with each are given to study the effect of different spectra inputs.

# 4. NUMERICAL ANALYSIS METHODS

## 4.1 EMPIRICAL METHODS

Of the empirical methods for calculating albedo, only the Chilton-Huddleston (49) development attempts to go beyond a few MeV. For that reason, theirs will be the only one discussed in this section. The initial development was limited to scatter from concrete.

The geometry of the Chilton-Huddleston (C-H) derivation is given in Figure 9.

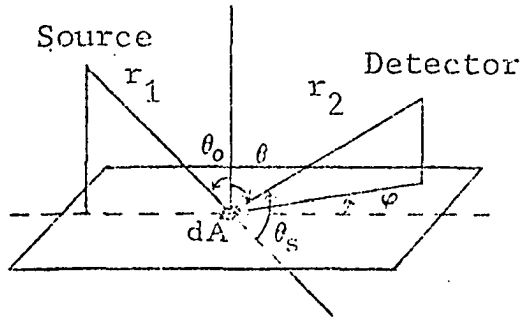


Figure 9. Geometry of the Chilton-Huddleston derivation

Starting with the formula for differential dose at a point, from single scattering

$$dD = \frac{D_1 \, \alpha_d \cos \theta_o \, dA}{r_1^2 r_2^2} \qquad \text{Eq. 4.1}$$

where:

$dD$ = the differential dose at point of measurement

$D_1$ = dose at reference point one unit distance from point source

$\alpha_d$ = dose albedo

$\theta_o$ = polar angle of incidence radiation

$dA$ = differential area of reflecting surface

$r_1$ = distance from source to differential area

$r_2$ = distance from differential area to detector.

They develop a representation of single scattering dose albedo

$$\alpha_{dS} = \frac{B \, K(\theta_s)}{\bar{\mu}_1 + \bar{\mu}_2 \cos \theta_o \sec \theta} \qquad \text{Eq. 4.2}$$

where:

$a_{dS}$ = the single scattering dose albedo

B = a collection of factors which depend only on the reflecting material or are constant

$K(\theta_s)$ = the Klein-Nishina value of the energy scattering cross-section per elcctron

$\bar{\mu}_1$ and $\bar{\mu}_2$ = the mass absorption coefficient for the gamma radiation before and after scattering, respectively.

Their representation of the contribution by annihilation radiation is of similar form but without the Klein-Nishina factor, since annihilation radiation is produced isotropically.

$$a_{di} = \frac{B_1'}{\bar{\mu}_1 + \bar{\mu}_2' \cos \theta_o \sec \theta} \qquad \text{Eq. 4.3}$$

where:

$a_{di}$ = annihilation dose albedo

$B_1'$ = a collection of factors which depend only on the reflecting material or are constant

$\bar{\mu}_2'$ = the energy absorption coefficient at the average energy of the isotropically produced radiation

Neglecting other contributions as being below the level of influence in this approximation, the over-all differential albedo is given as the sum of 4.2 and 4.3 with appropriate changes in the constants.

$$a_d(\theta_o, \theta, \phi) = \frac{B_3 K(\theta_s)}{\bar{\mu}_1 + \bar{\mu}_2 \cos \theta_o \sec \theta} + \frac{B_2'}{\bar{\mu}_1 + \bar{\mu}_2' \cos \theta_o \sec \theta}$$

Eq. 4.4

In the case of lead, and several other high Z materials, ignoring the photoelectric contribution results in low albedo estimates.

By assuming the attenuation coefficients are not greatly energy dependent and incorporating them into the constant terms, one arrives at the much simplified equation

$$a_d(\theta_o, \theta, \phi) = \frac{CK(\theta_s) \cdot 10^{26} + C'}{1 + \cos \theta_o \sec \theta} \qquad \text{Eq. 4.5}$$

Where C and C' are the C-H parameters which must be adjusted for each incident photon energy. Comparison with Monte Carlo results appear to justify this assumption (though since the

parameters C and C' are obtained from a least-squares fit to Monte Carlo data, this would follow). Their first paper (49) gave values of C and C' only for concrete at incident energies of 0.2, 0.5, 1, 2, 4, 6, and 10 MeV.

In 1965, Chilton and Davisson (51) published values for the C-H parameters in water, concrete, iron, and lead for incident photons of energies up to 6.13 MeV.

A later paper by Chilton (54) revised the formula, to that shown in Eq. 2.11, to more closely match updated Monte Carlo runs. However, only values for 0.662 and 1.25 MeV reflected from concrete have been published. Consequently the revised formula cannot be used in this development.

Appendix N considers these empirical developments with "effective" x-ray energies from the machines used in this dissertation.

Leimdorfer (46) has developed an analytical expression for the total albedo (not considering the angular distribution and making much the same assumptions as Chilton-Huddleston). His development covers the same area as that of Chilton and Huddleston and lacks some of their flexibility; further work with it is not considered.

## 4.2 MONTE CARLO METHODS

The Monte Carlo method is a computerized experiment in which individual photon "case histories" are compiled until a statistically valid distribution is obtained. An individual photon enters the program at a given energy. On the basis of this energy, a probability generating subroutine assigns an interaction with energy loss, change of direction, etc. This process is continued until the photon is emitted from the material (transmitted or backscattered) or drops in energy below some pre-set cut-off level. At this point a new photon is introduced into the program.

Raso (45), in 1963, published values of total dose rate albedo from concrete with incident photon energies of 0.2 to 10.0 MeV. However, the data of Wells (43) published in 1964, is of a format more nearly that of this research. His data gives differential dose albedos for photon reflection from concrete. Source energies of 0.6, 1, 2, 4, and 7 MeV are used with angles of incidence of $\theta_o = 0^o$, $30^o$, $45^o$, $60^o$, and $75^o$.

His representation of the differential dose albedo is given by the relation

$$a(\theta_o, \theta, \phi, E_o) = \frac{D(\theta_o, \theta, \phi, E_o)}{F(E_o) \sec \theta_o} \qquad \text{Eq. 4.6}$$

where:

$\alpha(\theta_o,\theta,\phi,E_o)$ = the ratio of the dose rate current reflected per steradian in the $\theta,\phi$ direction to the dose rate per photon of energy incident upon the slab surface at an angle $\theta_o$

$D(\theta_o,\theta,\phi,E_o)$ = the scattered photon rate current per steradian leaving the concrete surface in the direction $\theta,\phi$ per photon incident at an angle $\theta_o$ per unit area on the concrete surface

$F(E_o)\sec\theta_o$ = the dose rate incident to the surface per photon per $cm^2$ crossing the surface in the direction $\theta_o$

The cited literature deals only with monoenergetic incident sources. The author finds no published results of Monte Carlo runs having been made for bremsstrahlung, and since each bremsstrahlung spectrum would be a function of the particular generating machine, information of this type would be of limited value.

For comparison purposes in this dissertation, a number of Monte Carlo runs have been made and their results plotted. The program used (Appendix K) is based on a publication by K. G. Adams and C. R. Mehl (106) as updated generally in April, 1968, by Adams and with specific update features by Adams, August, 1970, for adaptation to the specific energies and materials encountered in the present

problem. A study of results from this particular Monte Carlo program with comparisons from DTF results (to be discussed in Section 4.3) and previously published experimental results is given in Appendix M.

## 4.3 METHOD OF DISCRETE ORDINATES

The method of discrete ordinates is a numerical procedure used to solve the Boltzmann transport equation. The solution of transport problems using the method of discrete ordinates is a well-established technique in neutron problems. These techniques have been adapted to photon transport problems at Sandia Laboratories (62) and other installations dealing with shielding or energy deposition problems.

The particular program (DTF-69) used in this research (Appendix L) was written by J. H. Renken and K. G. Adams (63) with updates specific to the problem of the dissertation by J. H. Flinchum of Sandia Corporation.

In any particular DTF run, the incident photon spectrum is divided into a finite number of energy groups (i.e. a multigroup approximation). The monoenergetic transport equation for each group is then solved numerically by finite difference equations. The photon energy loss due to scattering is accounted for by the transfer of photons from

one group to another of lower energy. Within the limitations of the numerical nature of the solution, the result of this procedure is believed to be a rigorous solution of the transport equation.

A number of other codes based on the same principle are presently in use. A comprehensive review of the "state-of-the-art" as regards the method of discrete ordinates may be obtained from the Radiation Shielding Information Center (107).

Runs have been made for each experimental configuration for comparison purposes. These results are presented in the discussion of experimental data in Section 6.2.

Various spectra were used as input. These spectra and results are discussed in Appendix D.

As with the Monte Carlo program, a number of runs were made for comparison with previously published experimental data with results presented in Appendix M.

# 5. EXPERIMENTAL DESIGN

## 5.1 BACKSCATTER MATERIALS

### 5.1.1 Introduction

For results of various experiments to be comparable, it is necessary that variance in the dimensions of the back-scatterer not affect the amount of radiation reflected. To this end experimenters generally use a "semi-infinite" slab of material, meaning that any increase in the irradiated slab area or the slab thickness must not result in a change in the albedo for the viewed area. Though all are agreed upon this principle, few are agreed upon what is necessary to constitute a semi-infinite piece of material. In the high energy bremsstrahlung experiments discussed previously (35, 36), variations from thicknesses of seven mean free path lengths and diameters of nine mean free path lengths to thickness of one half a mean free path length and less than one half a mean free path length in diameter are used.

Experiments with gamma ray sources have generally shown (12, 17, 18, 21) that increasing the thickness of

backscatter medium beyond two mean free path lengths does not significantly alter the albedo measured. Lateral dimensions are less well established however, perhaps because of variation in experimental design.

Hine (16) has demonstrated that for diameters of less than two mean free path lengths, variation in surface area significantly alters the measured albedo. Mizukami et al. (20) indicate that a surface area less than four mean free path lengths in diameter is inadequate, but that at a diameter of seven mean free path lengths no change in albedo will be observed by increasing the surface area. Steyn (12) feels that five mean free path lengths form an adequate surface. Other experimenters using gamma-ray sources (17, 24, 25) do not discuss the problem and use scatter surfaces of three to six mean free path lengths in diameter.

To insure that slabs used in this research were "semi-infinite", they were generally chosen to be two mean free path lengths thick at the point of minimum absorption for the energy spectrum being used and three and one half mean free path lengths from the edge of the viewed area (Appendix B) to any edge of the reflector. A number of measurements were made to insure the adequacy of the following calculations. These results are reported in Appendix G.

5.1.2 Lead

Lead exhibits a minimum mass attenuation coefficient of 0.0410 $cm^2/gm$ to 3.4 MeV photons. This corresponds to a mean free path length of 2.15 cm or 0.845 inches. A lead slab having adequate dimensions at this energy would be "semi-infinite" for any of the energies used in this work. Lead slabs 1.75 inches thick and 12.0 inches square were used for albedo measurements. The surface was uniformly irradiated (Appendix H).

5.1.2 Iron

Iron has a minimum mass attenuation coefficient of 0.0299 $cm^2/gm$ for photons at 8.5 MeV. This gives a mean free path length of 4.25 cm or 1.67 inches. Thus, a slab 3.34 inches thick and of diameter 11.69 inches plus viewed diameter (Appendix B) could be called "semi-infinite". For the majority of this research, a slab of this size would be larger than necessary. With a bremsstrahlung maximum energy of 2.0 MeV, a slab 2.32 inches thick and 8.14 inches plus viewed diameter would be semi-infinite. A slab 3.50 inches thick and 14.0 inches square was used for albedo measurements at 2.0 and 3.5 MeV, a slab 18.0 x 18.0 x 4.50 inches was used for 7.0 and 10.5 MeV.

5.1.3 Concrete

Normal density concrete (2.30 gm/cm$^3$) has a minimum absorption coefficient of 0.0204 or maximum mean free path length of 21.31 cm or 8.39 inches near 30 MeV. The energies considered in the present research are not that high and the absorption coefficient would therefore be somewhat higher. Also considerable differences exist in the atom densities of various concrete, depending upon how and where they are made. The concrete used was that typical of this area, poured with fine aggregate, stirred to prevent voids and formed without reinforcement steel to avoid high Z pertubation. The atom densities of this concrete are compared with other concretes in Table 1. The effect of differing concrete atom densities on albedo is studied through use of the discrete ordinates computer program at an incident bremsstrahlung energy of 2.0 MeV maximum in Figure 10. Aluminum is often used for computer comparisons to concrete due to the closeness in density, atomic number (Z), etc., and the relative ease of calculating one Z vs 10-13 Z. The effective atomic number of the concrete used here was 12.1, the density 2.16 gm/cm$^3$.

A slab 8 inches thick and 32 inches square was used as the concrete reflector at 2.0 and 3.5 MeV, a 10 inch thick,

36 inches square slab at 10.5 MeV. No concrete backscatter surface was used in the 7.0 MeV experiments due to the lack of handling equipment in that facility.

TABLE 1

CONCRETE COMPOSITIONS

ATOM DENSITIES (atoms/$cm^3$)

| ELEMENT | CONCRETE USED IN THIS DISSERTATION | O R N L STANDARD CONCRETE | RADIATION RESEARCH ASSOCIATES CONCRETE |
|---|---|---|---|
| H | $2.177 \times 10^{21}$ | $8.50 \times 10^{21}$ | $9.886 \times 10^{21}$ |
| C | $4.355 \times 10^{21}$ | $2.02 \times 10^{22}$ | $6.913 \times 10^{20}$ |
| O | $3.986 \times 10^{22}$ | $3.55 \times 10^{22}$ | $4.473 \times 10^{22}$ |
| Na | $3.473 \times 10^{20}$ | $1.63 \times 10^{19}$ | $9.1 \times 10^{20}$ |
| Mg | $2.6 \times 10^{19}$ | $1.86 \times 10^{21}$ | $9.922 \times 10^{20}$ |
| Al | $1.284 \times 10^{20}$ | $5.56 \times 10^{20}$ | $2.64 \times 10^{21}$ |
| Si | $1.775 \times 10^{22}$ | $1.70 \times 10^{21}$ | $1.355 \times 10^{22}$ |
| P | 0 | 0 | $3.326 \times 10^{19}$ |
| S | 0 | 0 | $3.326 \times 10^{19}$ |
| K | $1.257 \times 10^{19}$ | $4.03 \times 10^{19}$ | $5.862 \times 10^{20}$ |
| Ca | $2.274 \times 10^{21}$ | $1.11 \times 10^{22}$ | $4.334 \times 10^{21}$ |
| Ti | 0 | 0 | $9.577 \times 10^{19}$ |
| Fe | $2.515 \times 10^{19}$ | $1.93 \times 10^{20}$ | $7.794 \times 10^{20}$ |
| Cu | $5.156 \times 10^{18}$ | 0 | 0 |
| Zn | $4.872 \times 10^{19}$ | 0 | 0 |
| Sr | $2.406 \times 10^{18}$ | 0 | 0 |

Figure 10 Albedo dependence on concrete composition for 2.0 MeV Bremsstrahlung

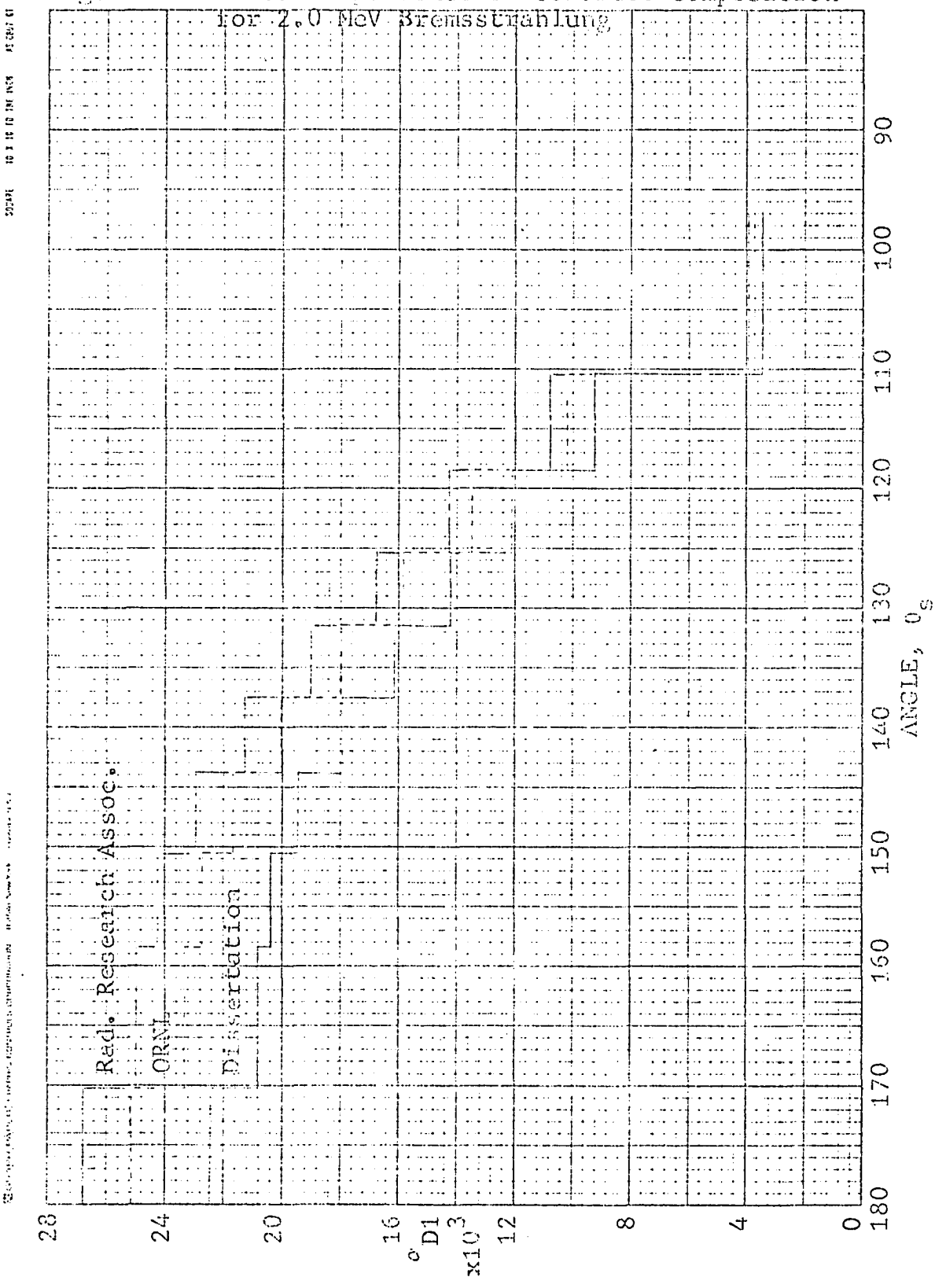

## 5.2 PHOTON SOURCES

### 5.2.1 Van de Graaff

The 2.0 MeV bremsstrahlung source used in this research was generated by an industrial radiographic Van de Graaff of High Voltage Engineering manufacture. The accelerating voltage is adjustable from 0.75 to 2.0 MeV, with sensitivity of ±40 KeV over 95% of a two hour period at 2.0 MeV. The electron beam current is adjustable from 0.01 to 0.25 milliamperes, with ±5 μamp at 0.250 milliamperes. The device generates 85 roentgens per minute at one meter. The accelerator is mounted with three degrees of freedom in a radiographic bay 19 feet wide, 26 feet high, and 26 feet from tube head to farthest wall.

Basic design and operating theory of Van de Graaffs are well discussed elsewhere (108, 109).

Beam divergence at the backscatter location is discussed in Appendix H for this and the following machines.

A previously published measured spectrum from this type of generator is given in Table 5. Rough absorption measurements were made with copper absorbers to determine an "effective energy for the beam used. These results are shown in Appendix D.

5.2.2 Flash x-ray devices (110, 111)

The 3.5, 7.0, and 10.5 MeV bremsstrahlung spectra were generated by high-energy flash x-ray generators. The major components of these machines are a low-inductance Marx generator, a Blumlein transmission line, and a field-emission vacuum tube. These components are housed within a steel cylinder filled with transformer oil for insulation.

During the charging cycle, storage capacitors are functionally placed in parallel with spark gaps acting as open circuits. When the desired charging voltage has been achieved, the power supply is electrically disconnected from the capacitor bank, and a high-voltage signal is initiated on the trigger line. Adjoining spark gaps are successively overvolted, causing the Marx generator to erect full output voltage. The negative voltage output of the Marx generator is placed on the intermediate cylinder of a folded Blumlein transmission line. During Blumlein charging, the outer and central cylinders, across which the tube is electrically located, are held near ground potential. When the Marx generator has erected to approximately 90 percent of its full output voltage, the Blumlein switch, between the central and intermediate cylinders, experiences self-breakdown, launching a traveling wave in the inner coaxial line. The voltage pulse formed by the Blumlein

structure is impressed across the x-ray tube which consists of an insulating and vacuum-holding structure, a field emission cathode, and an anode.

The x-ray mode anode is a thick, high-Z target (generally tungsten) for maximum efficiency in generation of bremsstrahlung radiation by deceleration of the electrons. A thick aluminum plate filters the remaining electrons and low energy x-rays from the beam as it is extracted into the experimental area. The output characteristics of the machine are dependent upon numerous parameters, including charge voltage, anode-cathode gap configuration, Blumlein oil gap, switch spacing, and the post-pulse switch position. Because of the complexity of calculations and measurements of these quantities and the large number of combinations of machine parameters, photon intensity and spectrum as a function of position and time are not totally available either in experimental or theoretical form. That which is known of the beam produced by the machine used in this research is discussed in the following sections.

5.2.2.1 3.5 MeV Generator

The Relativistic Electron Beam Accelerator (REBA) is a Sandia Corporation designed, Sandia built experimental device. The primary purpose of this device is to study the

deposition of energy in material by electron beams. By placing a high Z plate in the beam one can generate a bremsstrahlung photon spectrum. The time during which the experiments of this dissertation were carried out, is essentially the only time at which REBA has been operated in the x-ray mode. There exists, therefore, very little information about the x-ray beam. Various spectra for possible photon distributions are given in Appendix D. A few measurements were made with copper absorbers to give some idea of the beam quality. A plot of this determination is shown in Figure 41.

The beam intensity per burst of REBA at the point of backscatter was lower than required for good measurement. Therefore, a number of shots were made for each measurement to acquire sufficient dose. This had the effect of averaging out the machine's performance, as generators of this sort tend not to reproduce exactly from burst to burst. A sample set of shot parameters (tube voltage, $V_T$; and tube current, $I_T$) are given for REBA in Table 2. Tube voltage varied from averages of 3.38 to 3.52 MeV in the sets of experiments run for this paper. There is reason to believe (112) that these voltages may be high by as much as 10-15 percent. The tube output was monitored and normalized for each set as discussed in Section 6.

REBA consists of a single capacitor bank system which may dump into either of two Blumlein transmission lines (Figure 11). The irradiation cell in which the experiments discussed here were conducted was 14 feet wide, 15 feet from tube head to opposite wall and essentially open topped.

TABLE 2

REBA SHOT CHARACTERISTICS

| TUBE VOLTAGE $V_T$ (Mv) | TUBE CURRENT $I_T$ (kA) |
|---|---|
| 3.50 | 40.0 |
| 3.40 | 38.2 |
| 3.35 | 38.6 |
| 3.40 | 38.2 |
| 3.27 | 38.2 |
| 3.37 | 38.2 |
| 3.25 | 35.0 |
| 3.53 | 39.8 |
| 3.54 | 39.1 |
| 3.54 | 38.2 |
| 3.54 | 38.2 |
| 3.26 | 38.2 |
| 3.62 | 41.0 |
| 3.26 | 36.8 |
| 3.54 | 39.6 |

$(V_T)$ avg = $3.42 \pm 0.13$ (3.71%) Mv

$(I_T)$ avg = $38.49 \pm 1.40$ (3.64%) kA

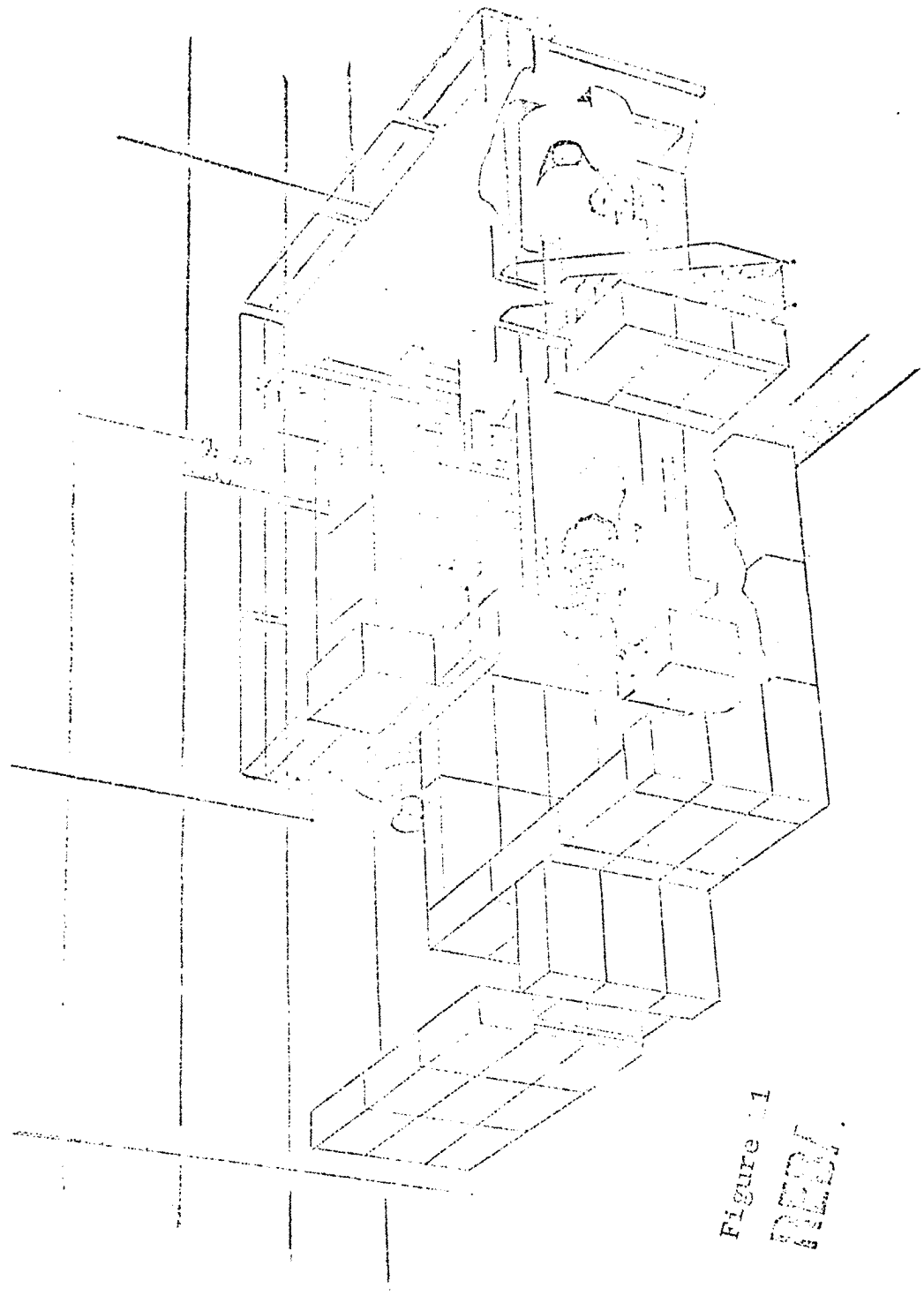

Figure 1

5.2.2.2 7.0 MeV Generator

The Transient Radiation Effects Facility (TREF) (113) is an Air Force Special Weapons Center laboratory designed for conducting transient radiation effects experiments to assess the survivability of systems in a prompt gamma radiation environment. The facility is perhaps less generator development oriented than Sandia, but due to the high priority of systems requiring tests in these environments, and the operating expense (~$1000/day) little more is known about the x-ray beam of the 7.0 MeV PulseRad 1590 (Figure 12) than that of the two other flash x-ray machines (REBA and HERMES II). Some absorption measurements have been made with absorbers of various atomic number which indicate an effective value of 4.1 - 4.2 MeV (114). Filtration of the output beam of TREF is somewhat (0.7934 cm Al and 0.076 cm Ta) heavier than that of REBA or HERMES (at the time of these measurements). To the primary purpose of these machines, this excess is of little consequence. The effect of reducing the low energy component of the incident bremsstrahlung through filtration of the beam (Figures 49 and 50), may be of greater importance (Figure 46) to albedo measurements. These figures indicate that, as pointed out by Zol'nikov and Sukhanova (115), specification of the

PULSERAD 1590

GAMMA SIMULATOR

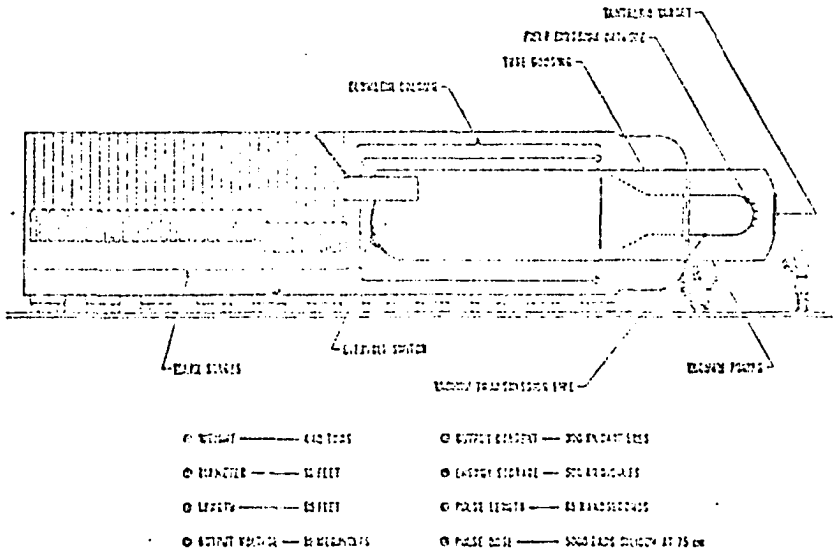

Figure 12

bremsstrahlung peak may give little information as regards albedo. This will be discussed more fully in Section 6.

The experimental area of TREF is separated from the flash x-ray device by a 10 foot high, 12 foot wide, 20 foot long RF shielded room. Facility design was such as to preclude the ready handling of the massive concrete slab used for previous backscatter experiments. Results are reported in Section 6 for iron and lead only.

Dose output for the PulseRad 1590 is rated at 4,000 rads in water at 75 centimeters per pulse. One pulse per experimental set-up was, therefore, adequate. Tube voltage varied from 6.48 to 7.10 MeV with an average of $6.98 \pm 0.18$ (2.57%) MeV for the shots made in this work.

5.2.2.3 10.5 MeV Generator

The second High Energy Radiation Megavolt Electron Source (HERMES II) is a Sandia designed and built flash x-ray device similar to those discussed previously. Somewhat more is known about the beam characteristics of this machine. Spectra and beam divergence are discussed in Appendix D and by Chodorow (110). Figures 13 and 14 detail the device and experimental area. Dose per pulse is about 2,500 Rad in water at one meter, and again only one burst per experimental set up was required to obtain adequate dose

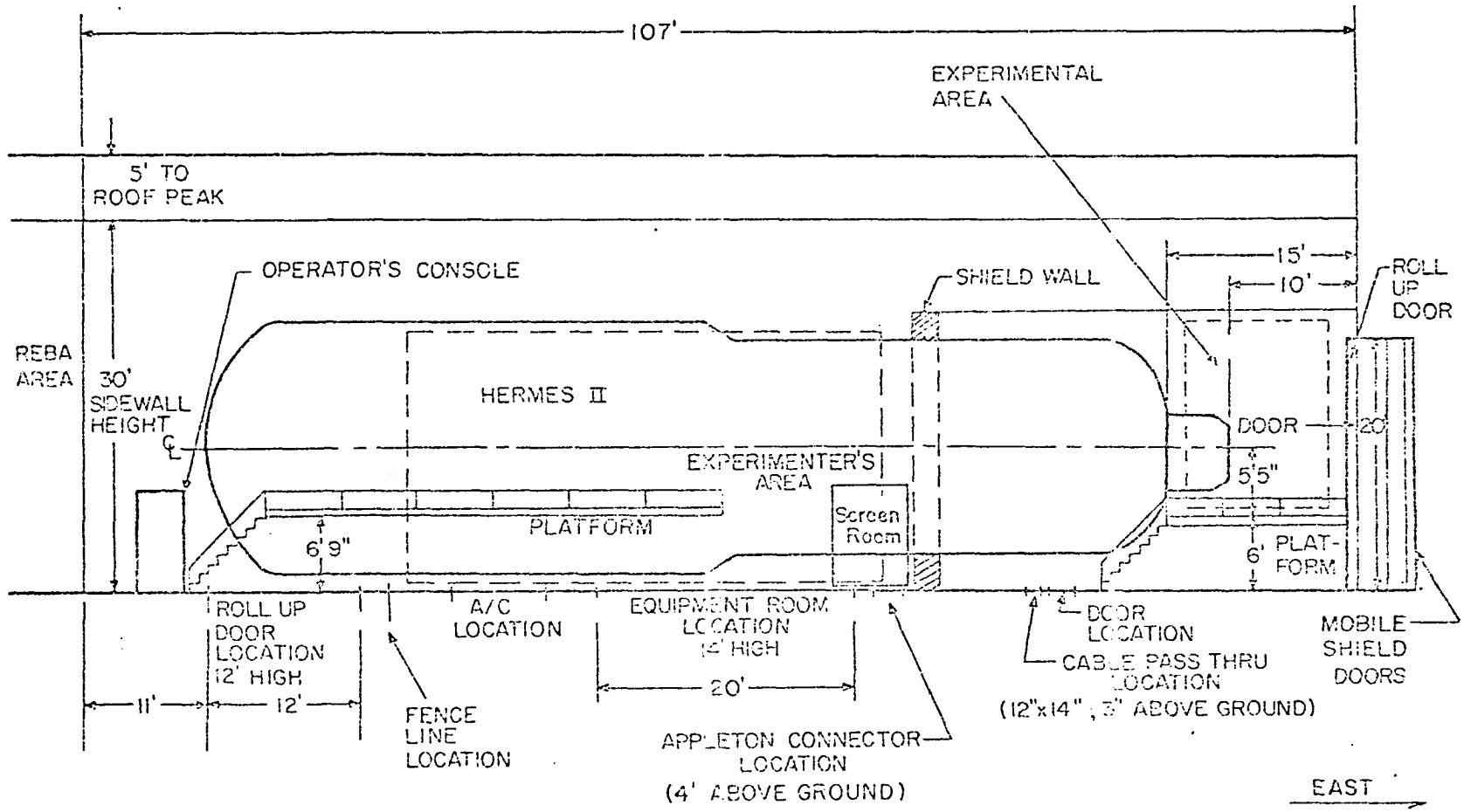


Figure 13 HERMES II

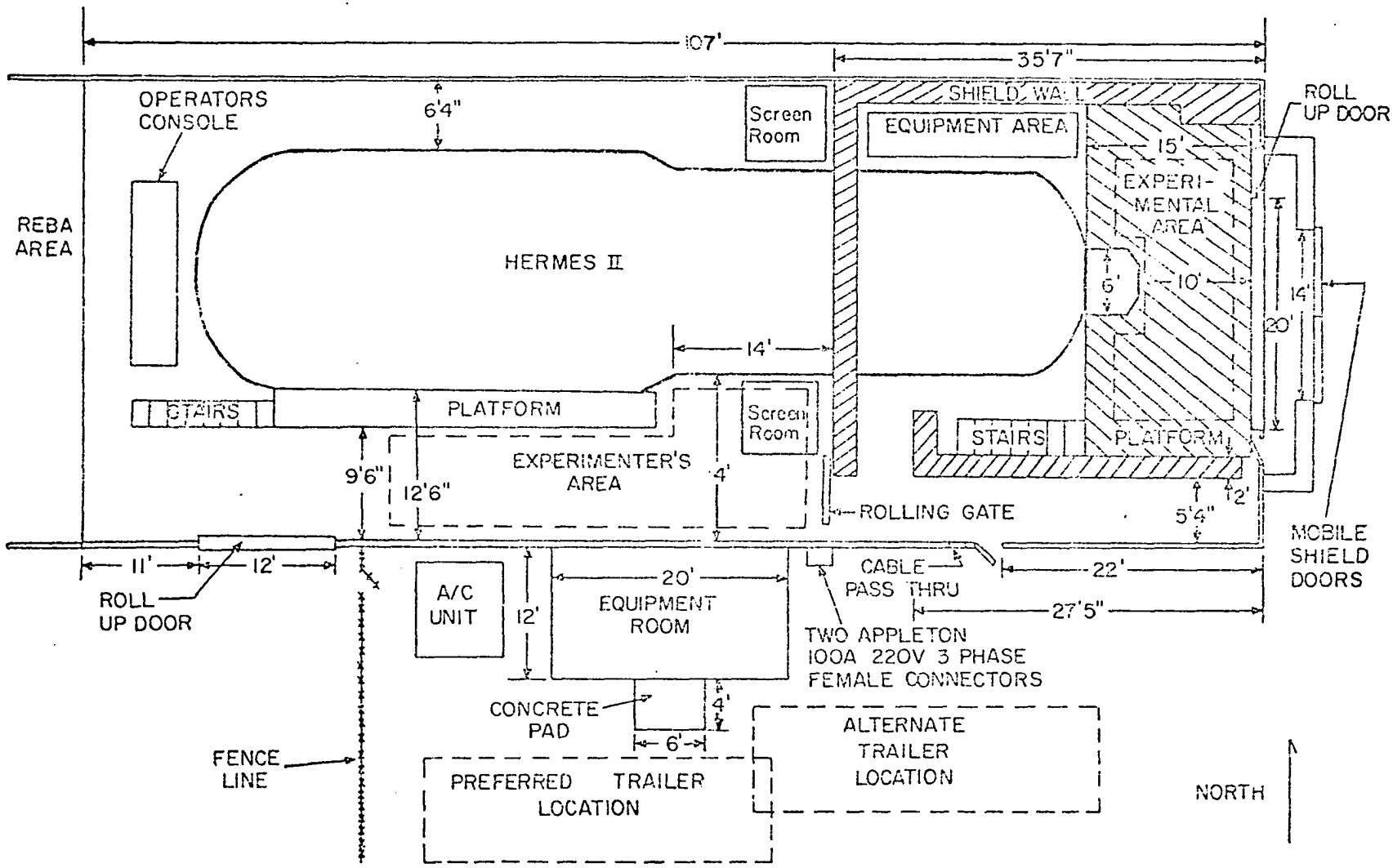


Figure 14 HERMES II

levels. Experimental configurations were repeated a number of times for statistical purposes. Peak tube voltage varied from 9.95 to 10.9 MeV with an average of 10.56 ± 0.28 (2.68%) MeV for runs made in this experiment.

## 5.3 BACKSCATTER SURFACE, COLLIMATOR, AND DETECTOR POSITION

The basic experimental design is diagramed in Figure 15.

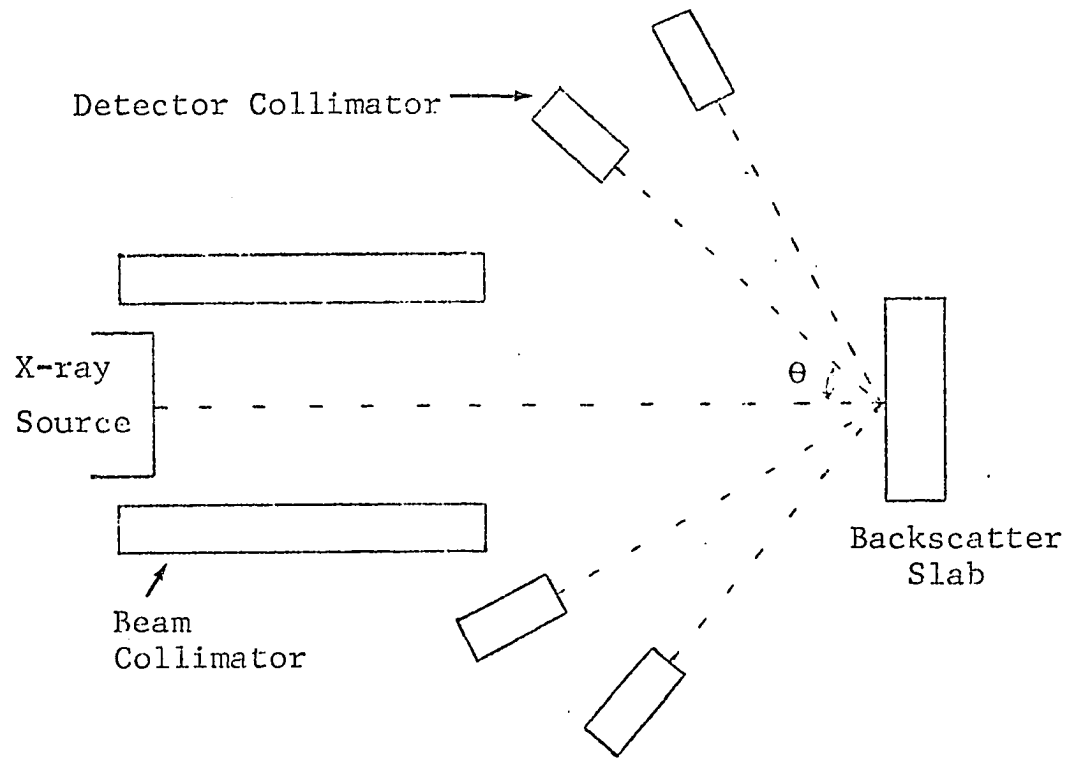


Figure 15. Experimental configuration

The x-ray source was shielded, not to restrict the beam, but to reduce air scatter at the detector locations. The beam was monitored at the center line and near the end of the beam collimator for normalization of each run.

The backscatter slab was placed normal to the x-ray beam axis at a distance adequate for uniform irradiation of the surface.

The detector collimators were placed as close to the backscatter slab as possible, without interrupting the incident beam. Distance from the slab and the angle between the slab and collimator axis determined the length of collimator required to restrict the viewed area sufficiently to maintain an "infinite" surface area slab. To provide flexibility in positioning the detector collimators and varying their length, the collimators were made up in segments. Standard lead bricks (2" x 4" x 8") were center drilled with 1.00" ID holes. One inch diameter copper rod was cut into 2.0, 3.0 and 4.0 inch lengths and center drilled with 0.50" ID holes. 0.25" slugs were cut from the copper rod to provide back-up shields. The copper was then pressure fitted to the lead and un-drilled lead bricks used around the assembly for additional shielding.

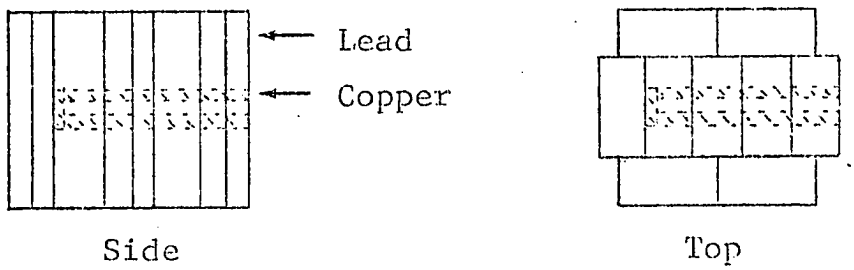


Figure 16. Detector collimator

The thermoluminescent dosimeters were packaged in polyethene bags and centered at the back of the detector collimator. The dosimeters were calibrated to Co-60 in the same configuration, so all results are measured in dose in LiF equivalent to Co-60.

The collimator lengths and detector distances used in individual measurements are given with the TLD data in Appendix I.

# 6. EXPERIMENTAL RESULTS

## 6.1 DATA ANALYSIS

The Radiation Shielding Information Center's report on Neutron and Gamma-Ray Albedos (1) defines three types of differential albedos for which the particle flux has been weighted by a dose response function: $\alpha_{D1}(E_o, \theta_o, \theta, \phi)$, differential current out (in dose units) per incident flux (in dose units); $\alpha_{D2}(E_o, \theta_o, \theta, \phi)$; differential current out (in dose units) per incident current (in dose units); and $\alpha_{D3}(E_o, \theta_o, \theta, \phi)$; differential flux out (in dose units) per incident flux (in dose units). As the incident beam is normal to the reflecting slab ($\theta_o = 90^o$), $\alpha_{D1}$ and $\alpha_{D2}$ are identical for the present research and may be defined as the ratio of the particle current (in dose units, $\mathcal{D}_R$, per steradian reflected in the direction $\theta, \phi$) to the dose, $D_o$, due to incident particles of energy, $E_o$.

$$\alpha_{D1} = \alpha_{D2} = \frac{\mathcal{D}_R}{D_o} \qquad \text{Eq. 6.1}$$

The experimental determination of $D_R$ and $D_o$, and transformation to a form comparable to computer estimates, is not straight forward. Measurement of the incident dose at the backscatter surface would result in a measurement of the incident dose plus a reflected dose, which is substantial due to the solid angle intercepted by the detectors being located at the scatter surface. (This is the quantity defined by Johns [109] as backscatter.) Therefore, two runs were made for each individual albedo measurement, one background and the other backscatter. During the background run, thermoluminescent dosimeters (TLD's) were located at the point where the center of the backscatter slab was to be placed for the albedo measurement, another set of TLD's was located midway between the x-ray target and the backscatter slab, and TLD's were located in each collimator to measure the background for that particular configuration due to air scatter, shield penetration, etc. The dosimeter positions were the same for albedo measurements less the set at the backscatter location (Figure 15). The TLD's monitoring the beam between the x-ray target and backscatter slab were never less than thirty inches to the slab. At this point the backscatter contribution was less than 0.5%. The dose actually deposited at the slab's surface was then calculated from measurements made during each of the runs.

$$DD = DI \left(\frac{BCS}{BCG}\right)\left[\frac{inc\left(\frac{\mu_{en}}{\rho}\right)_{slab}}{inc\left(\frac{\mu_{en}}{\rho}\right)_{LiF}}\right] \qquad \text{Eq. 6.2}$$

where:

DD = dose deposited at slab surface center during backscatter measurement

DI = dose deposited in TLD's during background run at same distance from x-ray target as DD

BCS = dose in TLD at some point between backscatter slab and x-ray target

BCG = dose in TLD at same point as BCS during background run

$inc\left(\frac{\mu_{en}}{\rho}\right)_{slab}$ = mass energy-absorption coefficient for the slab material and the incident beam

$inc\left(\frac{\mu_{en}}{\rho}\right)_{LiF}$ = mass energy-absorption coefficient for LiF and the incident beam

The dose to the slab surface was then averaged over the viewed area to account for beam divergence (Appendix H) to obtain $D_o$.

$\left(\frac{\mu_{en}}{\rho}\right)_{inc}$ is an effective value for the particular incident beam (Appendix D) considered and is estimated by:

$$\left(\frac{\mu_{en}}{\rho}\right)_{inc} = \frac{\sum_i \left(\frac{\mu_{en}}{\rho}\right)_i E_i}{\sum_i E_i} \qquad \text{Eq. 6.3}$$

where $\left(\frac{\mu_{en}}{\rho}\right)_i$ is the mass energy-absorption coefficient at the average energy of the "i"th energy interval and $E_i$ is the amount of energy in that interval.

The backscatter measurement was corrected for a background normalized to the backscatter input dose and expressed in terms of water dose.

$$BS = \left[DR - DBG\left(\frac{BCS}{BCG}\right)\right]\left[\frac{\left(\frac{\mu_{en}}{\rho}\right)_{ref,H_2O}}{\left(\frac{\mu_{en}}{\rho}\right)_{ref,LiF}}\right] \qquad \text{Eq. 6.4}$$

where:

BS = dose in water reflected by the backscatter slab at some angle and distance

DR = dose in TLD measured at same position as BS during backscatter run

DBG = dose in TLD measured at same position as BS during background run

$\left(\frac{\mu_{en}}{\rho}\right)_{ref}^{H_2O}$ = mass energy-absorption coefficient for water and reflected beam

$\left(\frac{\mu_{en}}{\rho}\right)_{ref}^{LiF}$ = mass energy-absorption coefficient for LiF and the reflected beam

$\left(\frac{BCS}{BCG}\right)$ as defined in Eq. 6.2

$\left(\frac{\mu_{en}}{\rho}\right)_{ref}$ is an effective value for the particular reflected beam spectrum (Appendix D) considered.

To determine the backscattered dose per steradian, BS was divided by the effective viewed solid angle of the particular collimator system used.

$$\Omega_{\epsilon} = \frac{A_{\epsilon}}{d^2} \qquad \text{Eq. 6.5}$$

where: $A_{\epsilon}$ = effective viewed area normal to the collimator axis (Appendix B)

d = detector to slab distance

The differential dose current per steradian is given by:

$$\mathcal{D}_R = \frac{BS}{\Omega_c} \cos \theta \qquad 6.6$$

where $\theta$ is the angle between the incident beam center line and the detector collimator axis. $\mathcal{D}_R$ has no meaning in the true physical sense, but is the form traditionally used in comparing albedo data. The differential current dose albedo per steradian, $\alpha_{D1}$, may then be calculated by Equation 6.1.

Beam intensity, for machines of the nature discussed in Section 5, is most frequently given as Rad in water per burst or per unit time at some point in the beam. Calculation of the dose in any particular shielding material involves detailed information as to incident beam energy spectra. Lacking such information, another expression of albedo might be more useful in shielding calculations.

$$\alpha_{D3(H_2O)} = \frac{\mathcal{D}_{R(H_2O)}}{D_{o(H_2O)}} \qquad \text{Eq. } 6.7$$

Derivation of Eq. 6.7 would follow as Eq. 6.1 above with $\left(\frac{\mu_{en}}{\rho}\right)_{inc}^{H_2O}$ replacing $\left(\frac{\mu_{en}}{\rho}\right)_{inc}^{slab}$ and the reflected dose being expressed as flux rather than current, a quantity with real physical meaning, useful in actual shielding calculations.

## 6.2 PRESENTATION OF RESULTS

Figures 17 through 27 compare the values of $\alpha_{D1}$ obtained experimentally with those obtained by the Monte Carlo program (Appendix K), the DTF program (Appendix L) and the Chilton-Huddleston formulation (Appendix N).

Error limits on the experimental points are discussed in Appendix J. Error bars for the Monte Carlo runs are not shown in an effort to avoid cluttering the graphs. In each plot, 200,000 case histories were run with a deviation of around ±8.5% for iron at 10.5 MeV to about ±16.2% for lead at 2.0 MeV. The precise error value was dependent upon the number of photons falling in a given angular spread. These errors are much increased when requesting an energy differentiation as plotted in Appendix D. DTF and the Chilton-Huddleston representations do not have readily representable error limits.

Figure 17 2.0 MeV lead scatterer $\alpha_{D1}$ vs Angle

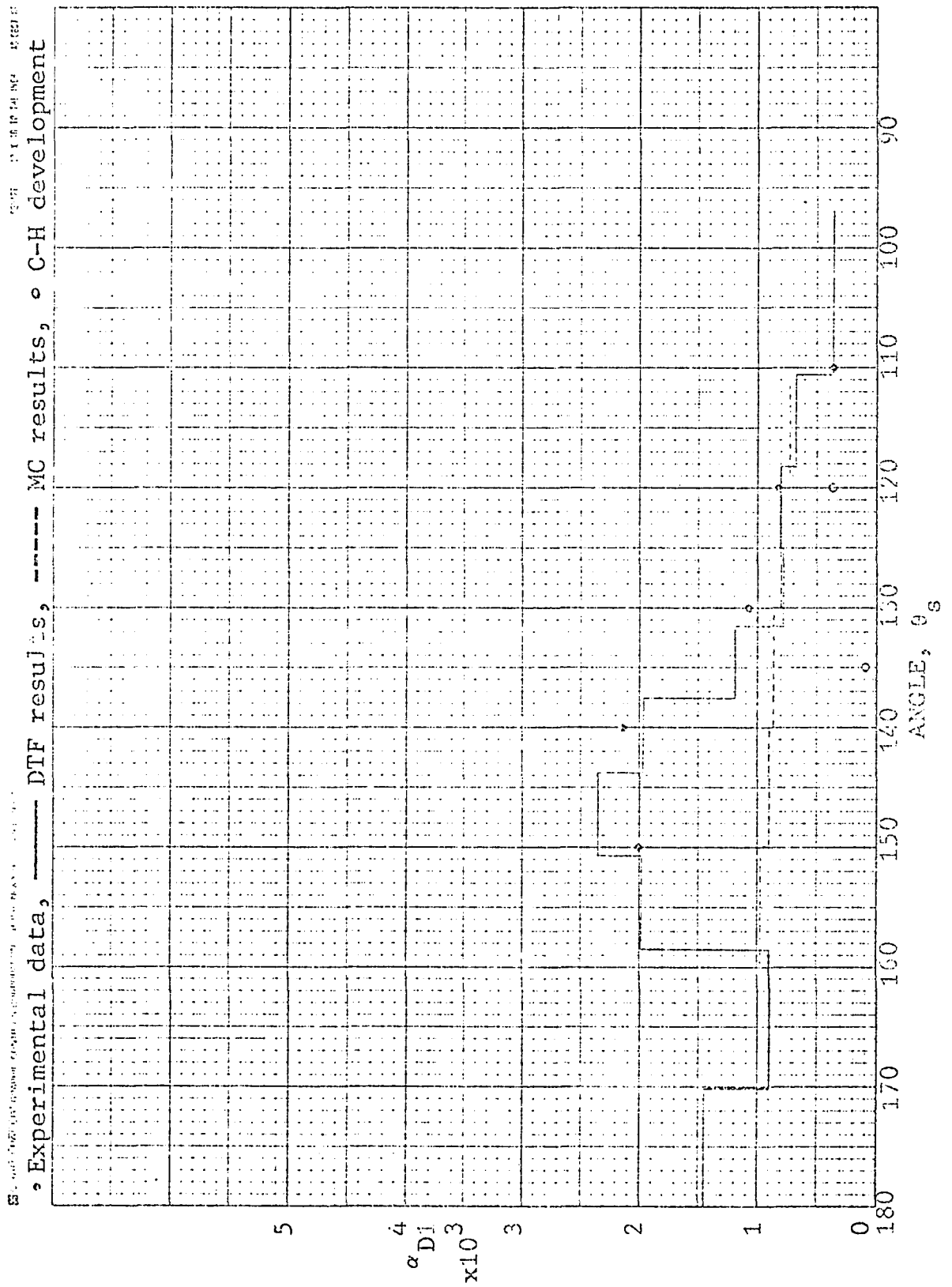

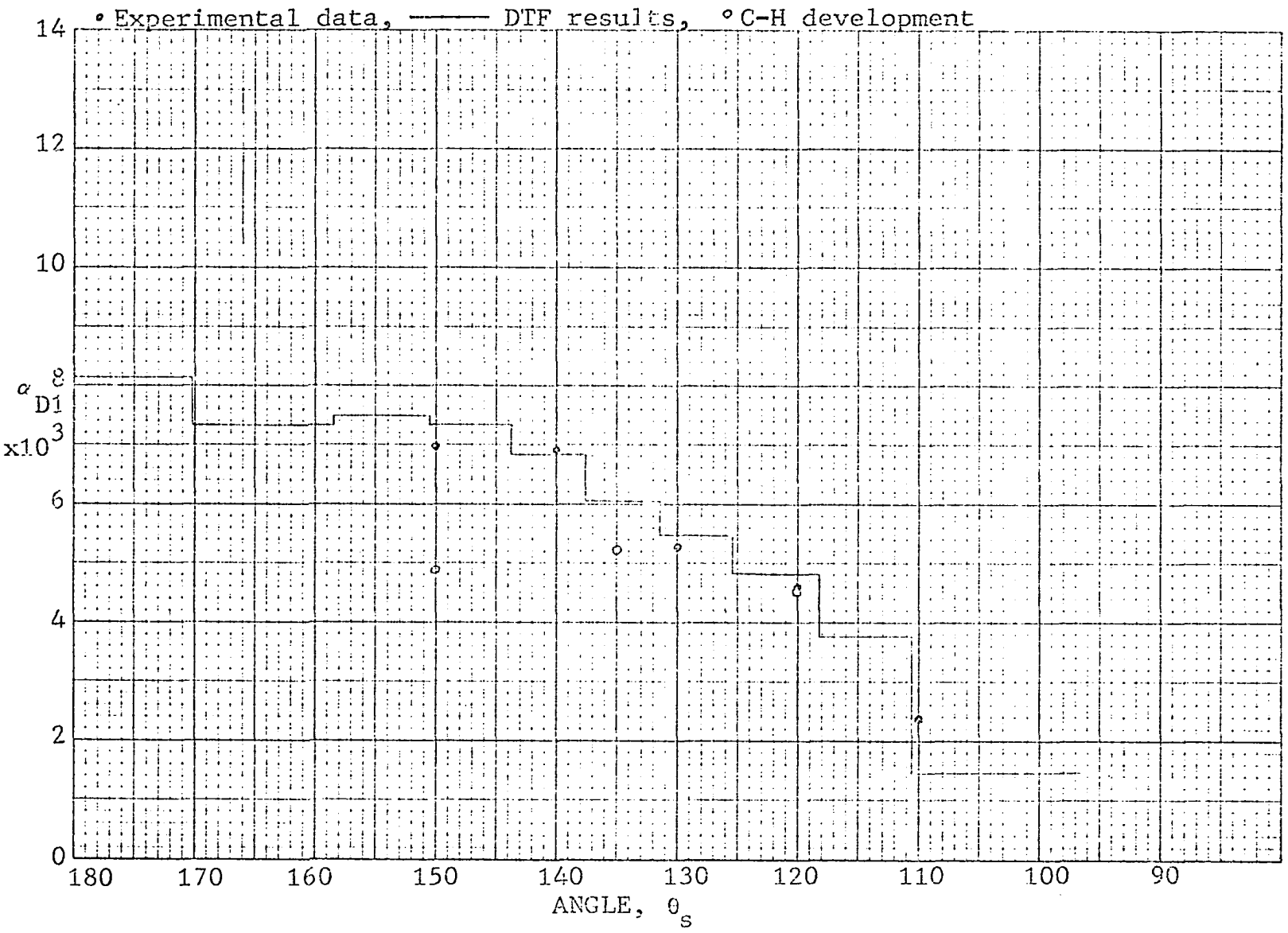


Figure 18 2.0 MeV iron scatterer $\alpha_{D1}$ vs Angle

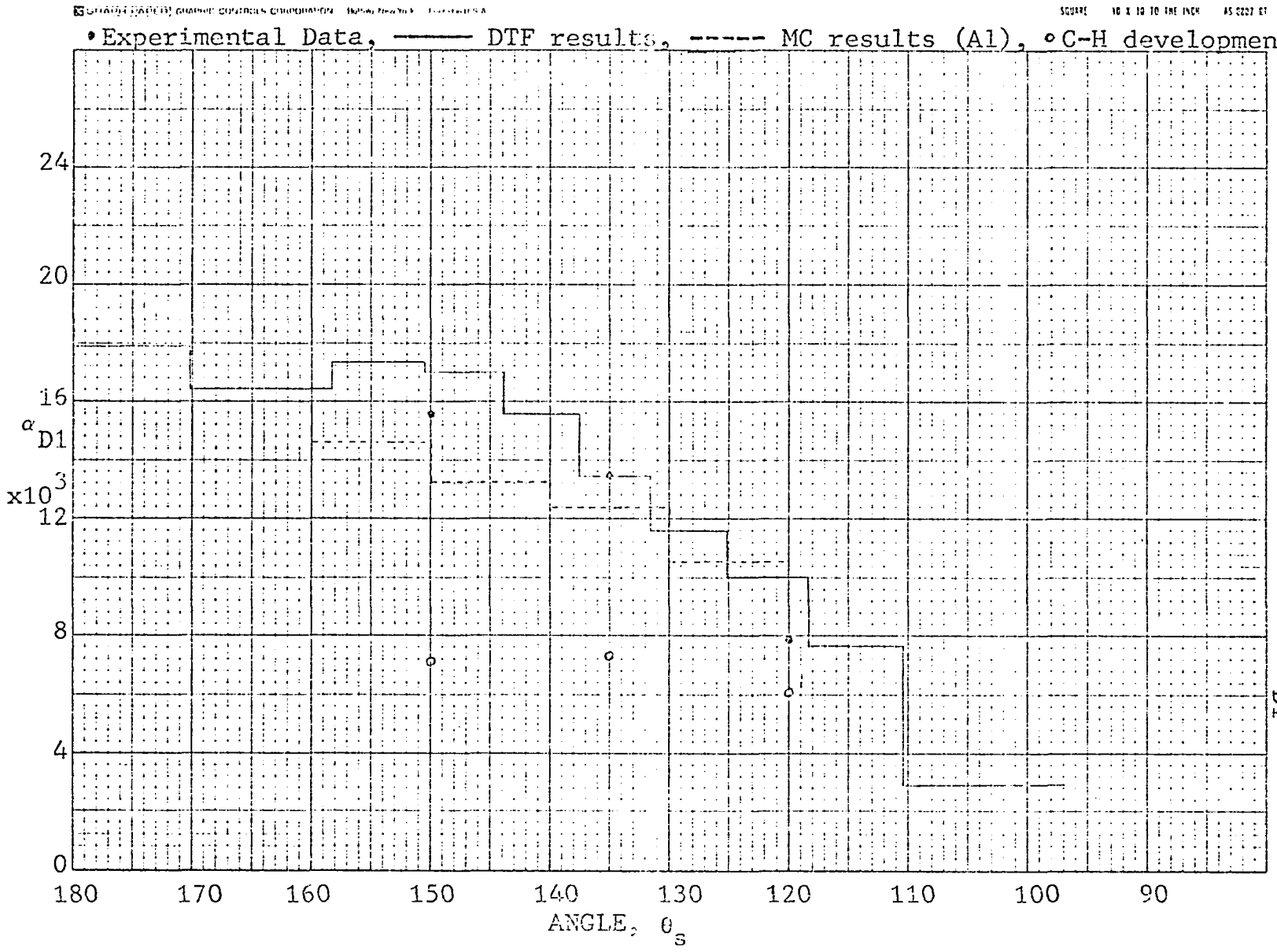


Figure 19 2.0 MeV concrete scatterer $\alpha_{D1}$ vs Angle

Figure 20 3.5 MeV lead scatterer $\alpha_{D1}$ vs Angle

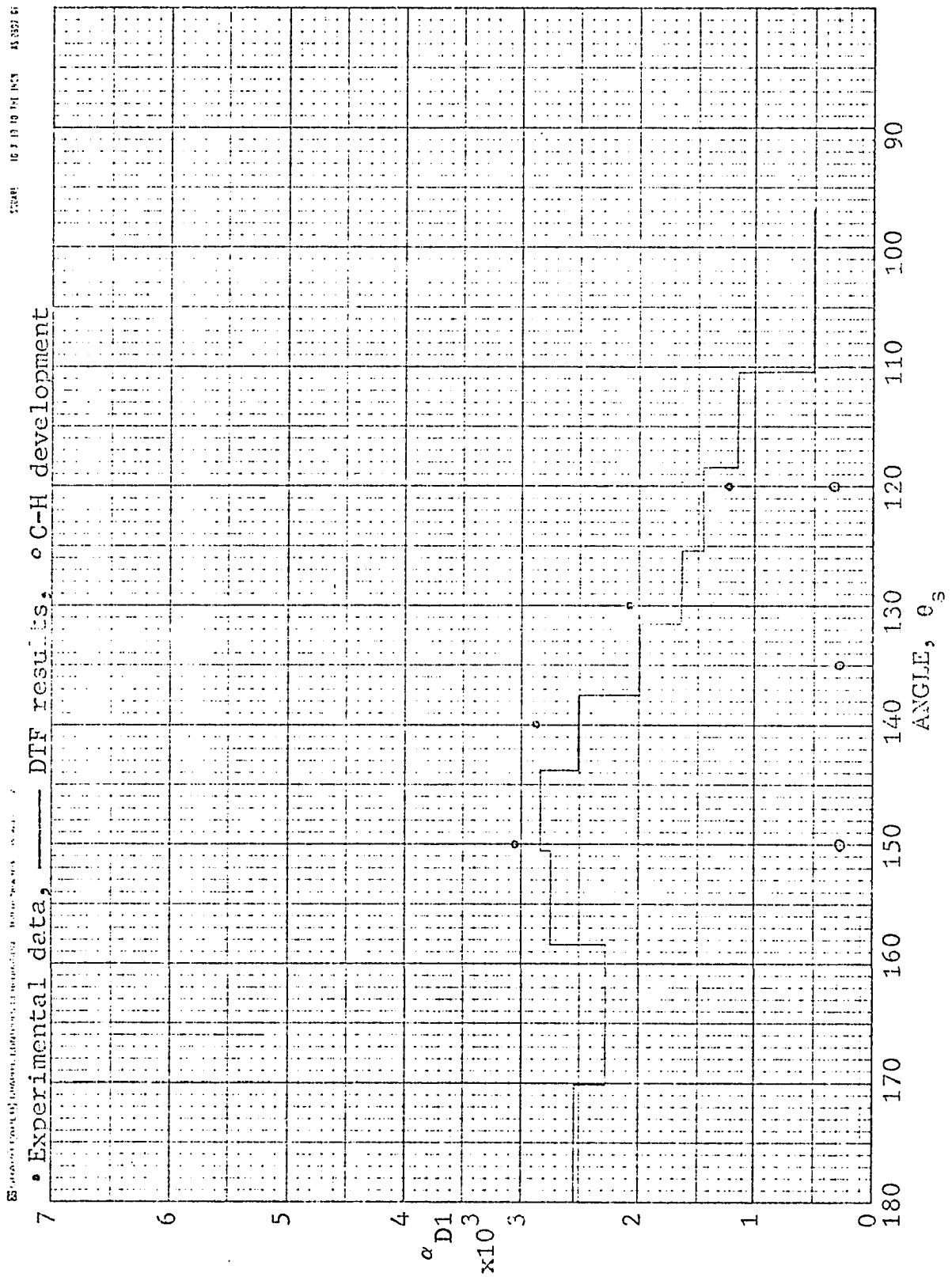

Figure 21 3.5 MeV iron scatterer $\alpha_{D1}$ vs Angle

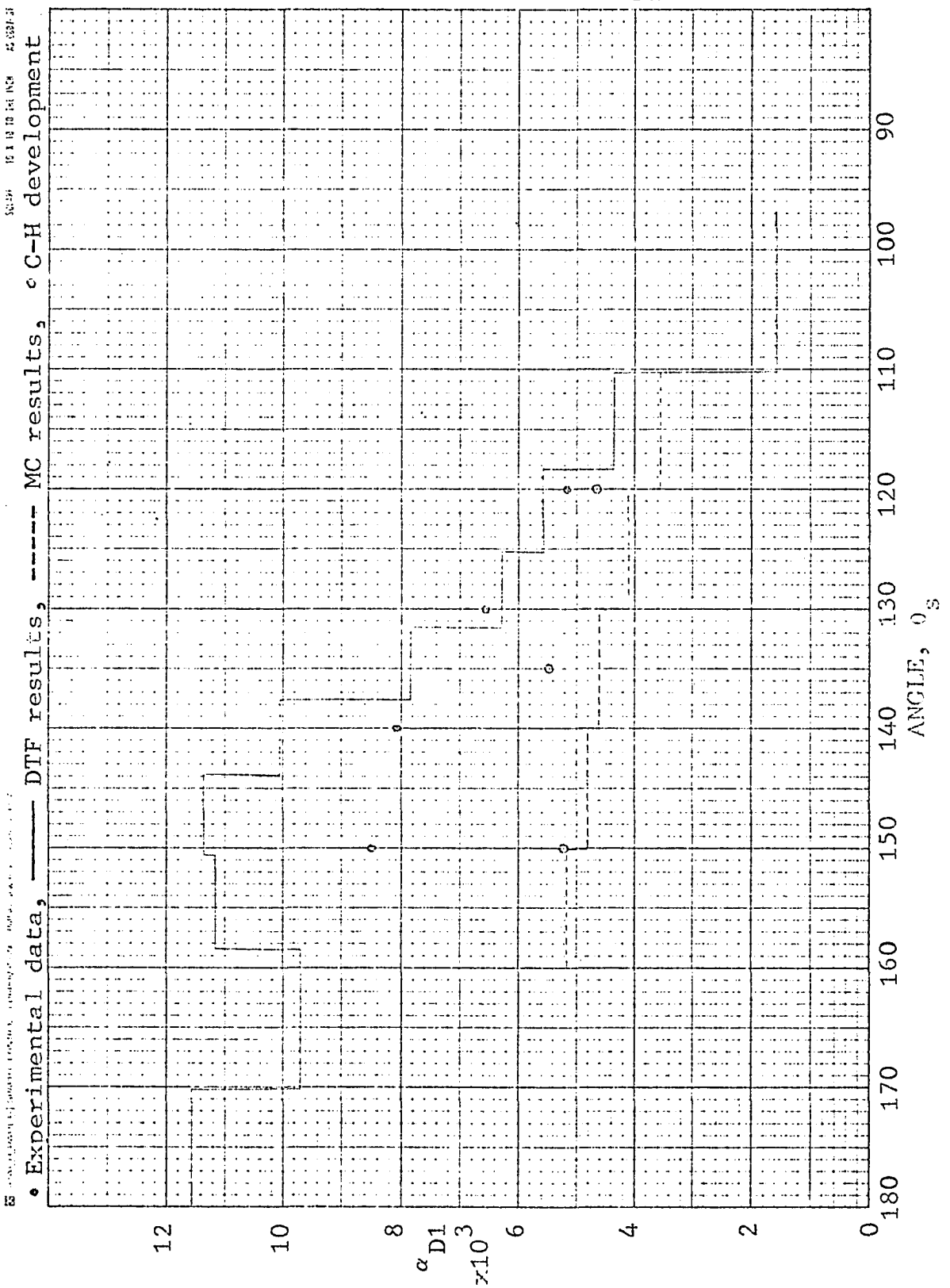

Figure 22 3.5 MeV concrete scatterer $\alpha_{D1}$ vs Angle

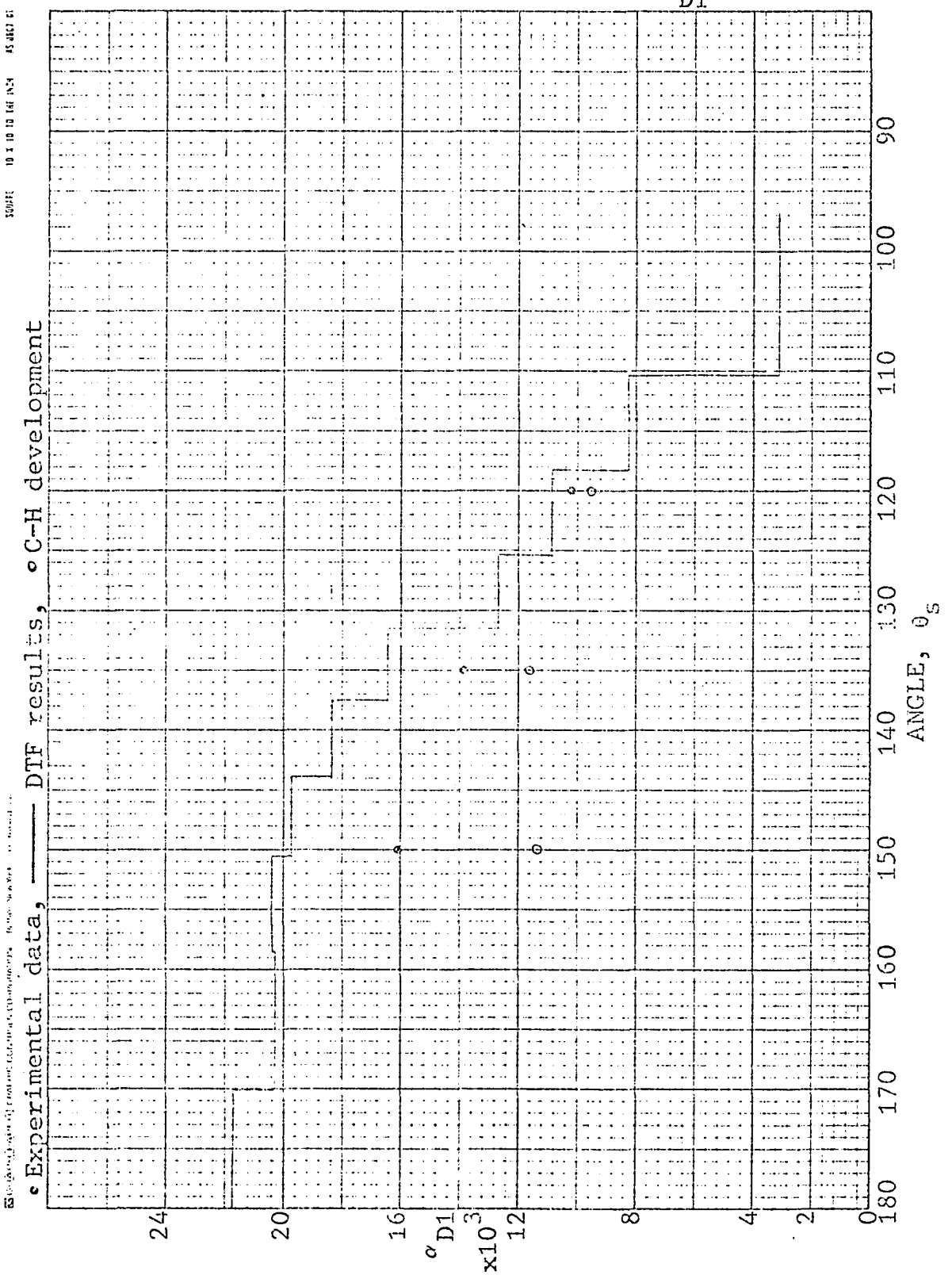

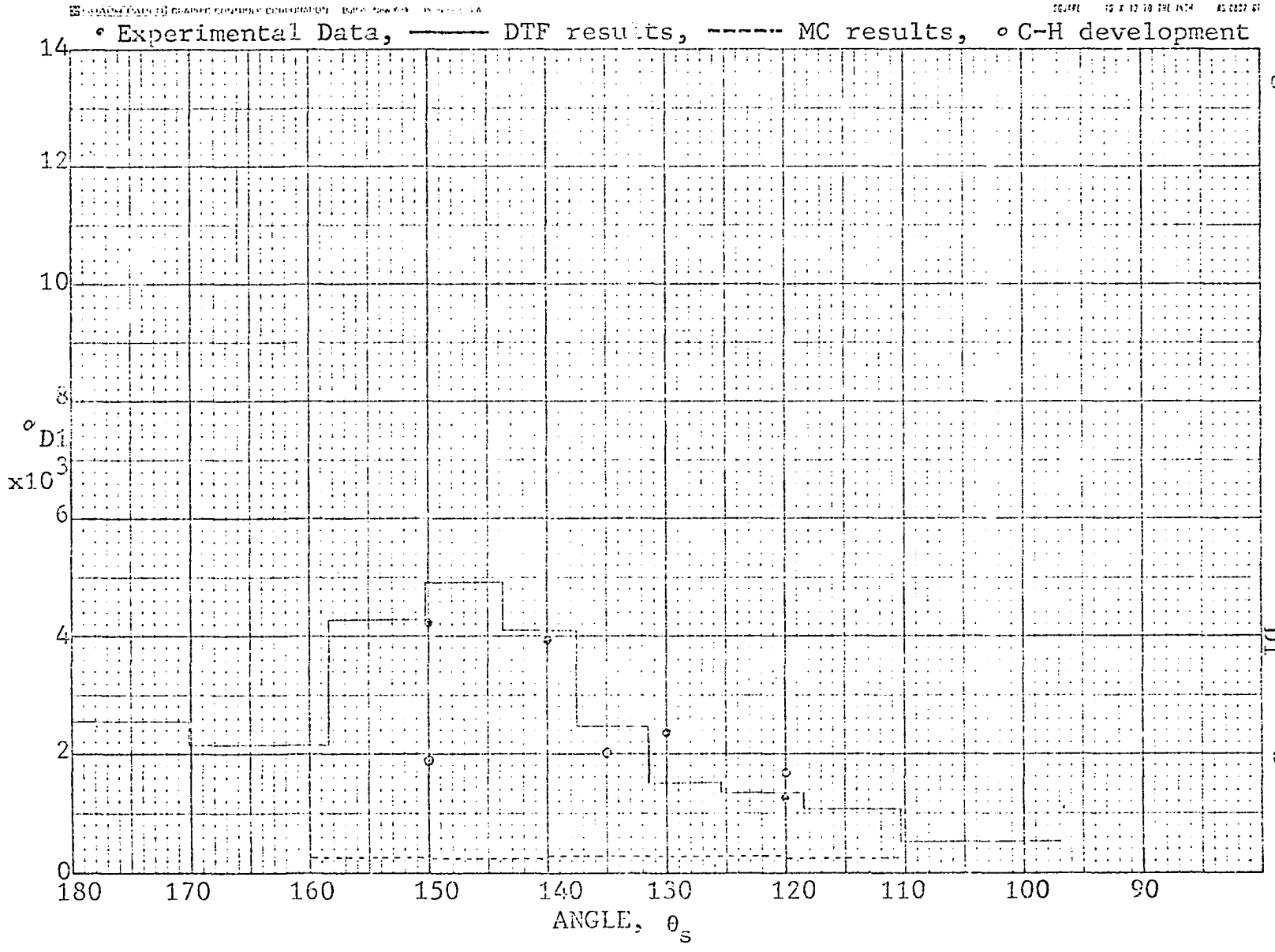


Figure 23 7.0 MeV lead reflector $^{\circ}_{D1}$ vs Angle

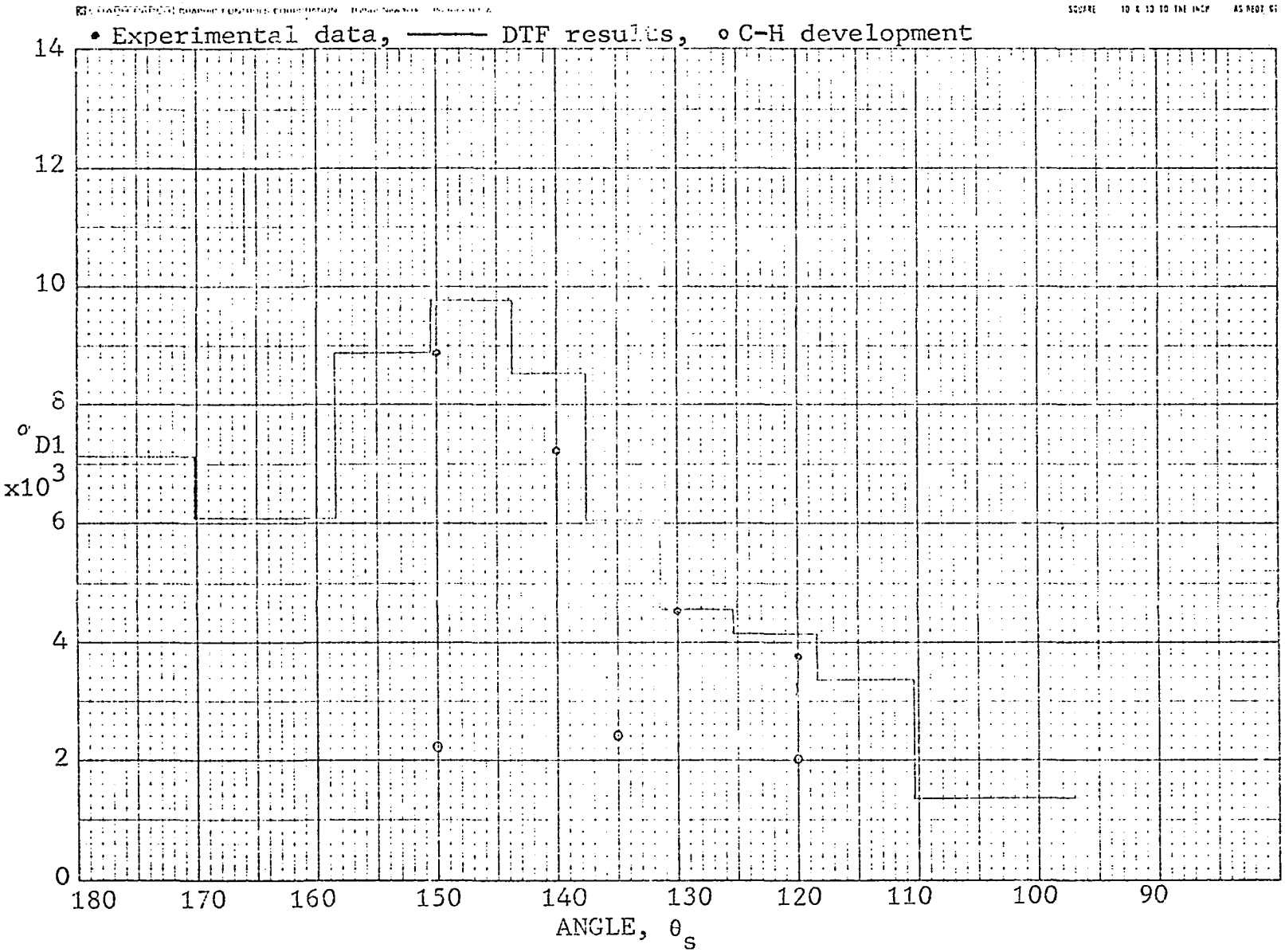


Figure 24 7.0 MeV iron reflector $\sigma_{D1}$ vs Angle

Figure 25 10.5 MeV lead scatterer $\alpha_{D1}$ vs Angle

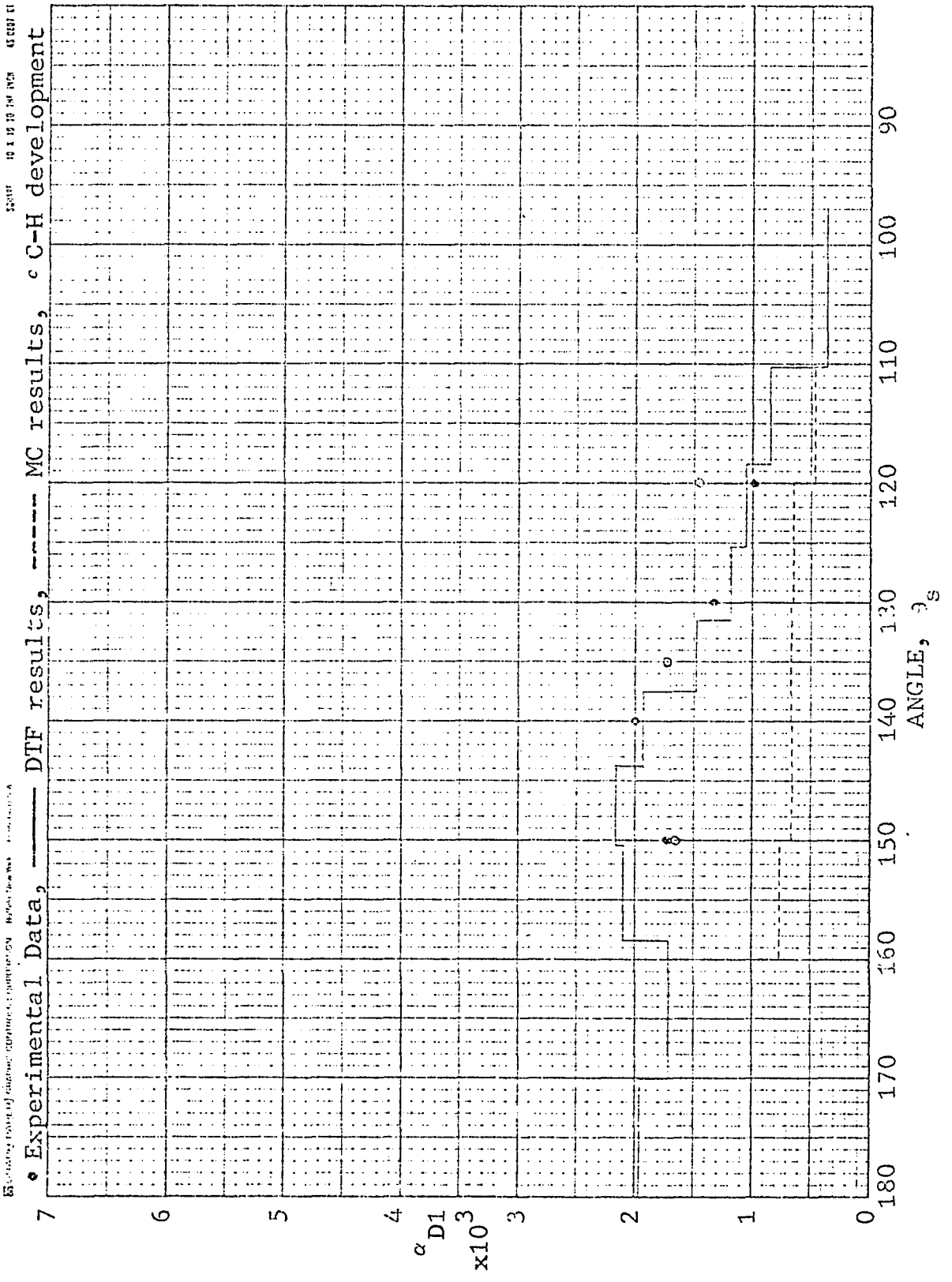

Figure 26 10.5 MeV iron scatterer $\alpha_{D1}$ vs Angle

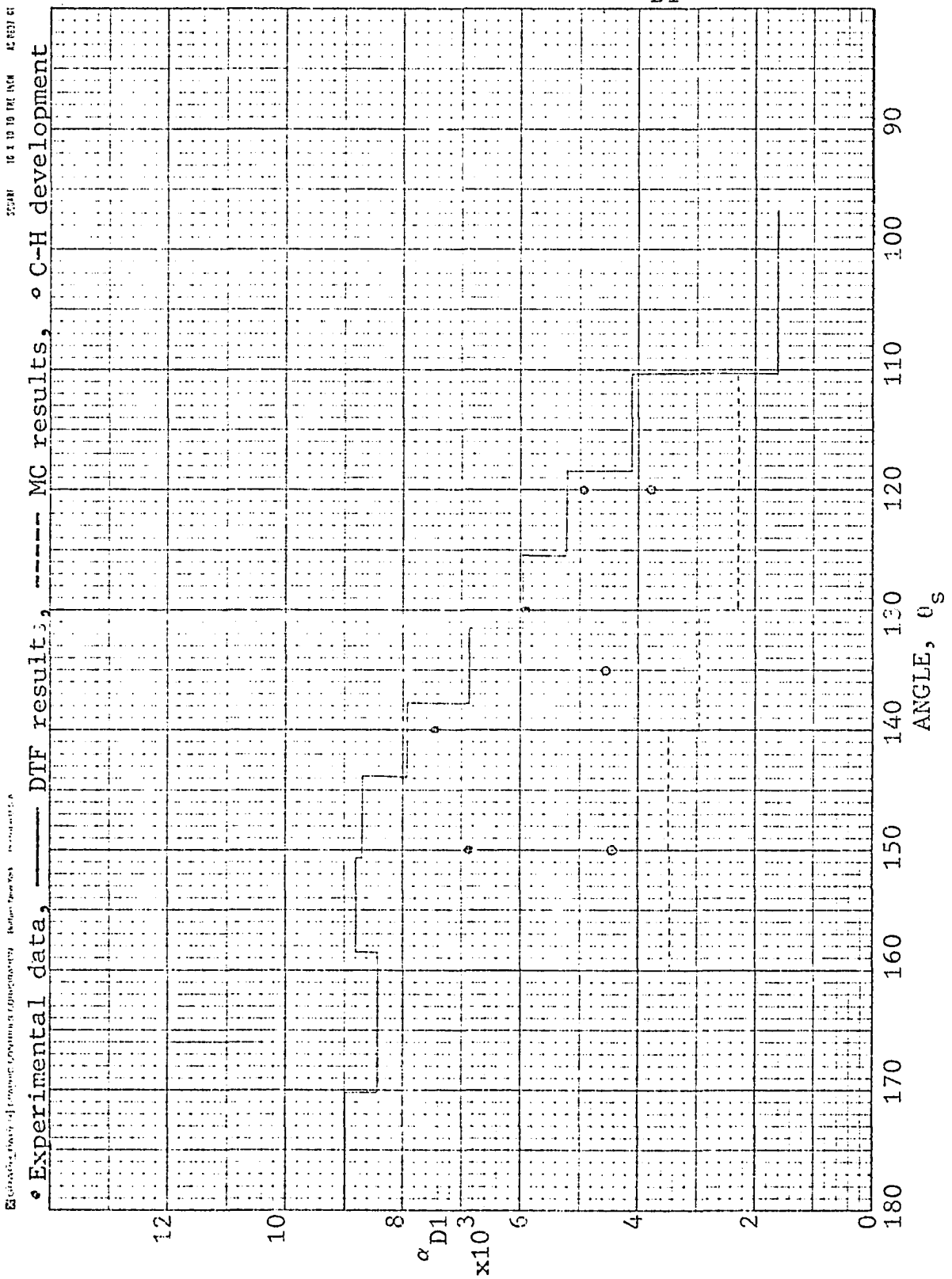

Figure 27 10.5 MeV concrete scatterer $\alpha_{D1}$ vs Angle

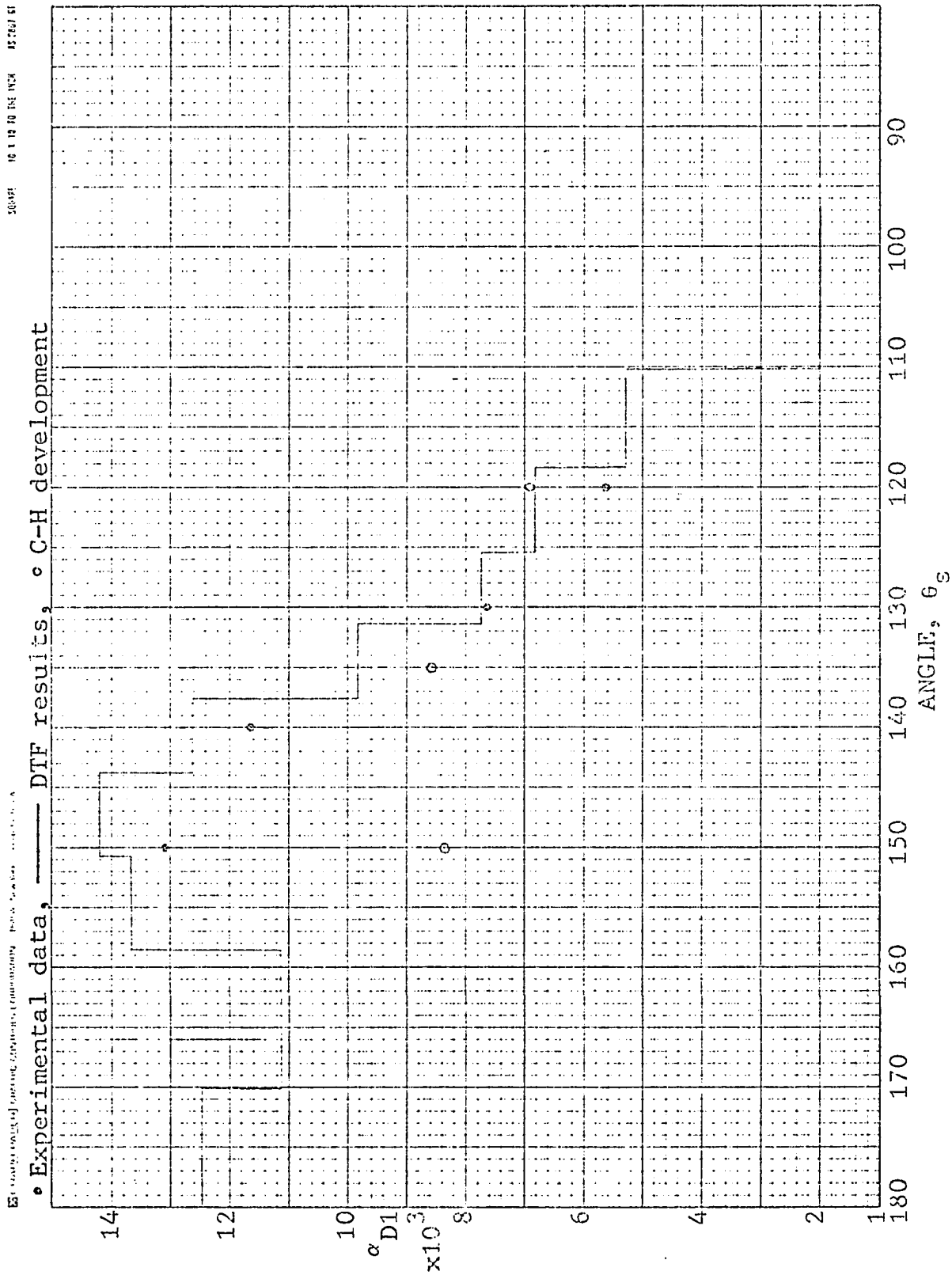

Table 3 lists the values of the differential dose in water flux albedo, $a_{D3(H_2O)}$, obtained experimentally.

TABLE 3

$a_{D3(H_2O)} \times 10^3$

| ANGLE OF SCATTER $\theta_s$ | SCATTER MATERIAL | | |
|---|---|---|---|
| **2.0 MeV** | | | |
| | Lead | Iron | Concrete |
| 150° | 19.10 ± 8.5% | 14.05 ± 8.9% | 17.96 ± 8.6% |
| 140° | 24.12 ± 9.6% | 14.72 ± 9.7% | |
| 135° | | | 19.06 ± 14.2% |
| 130° | 14.43 ± 10.9% | 14.44 ± 9.1% | |
| 120° | 19.98 ± 9.5% | 15.73 ± 6.6% | 15.55 ± 9.9% |
| 110° | 7.95 ± 13.0% | 17.30 ± 10.4% | |
| **3.5 MeV** | | | |
| | Lead | Iron | Concrete |
| 150° | 29.76 ± 9.5% | 14.17 ± 15.3% | 14.99 ± 12.9% |
| 140° | 31.96 ± 13.0% | 15.34 ± 11.2% | |
| 135° | | | 18.23 ± 9.5% |
| 130° | 27.72 ± 9.0% | 14.97 ± 9.5% | |
| 120° | 10.79 ± 9.6% | 15.19 ± 12.9% | 19.33 ± 11.5% |
| **7.0 MeV** | | | |
| | Lead | Iron | |
| 150° | 71.26 ± 21.3% | 45.19 ± 13.6% | |
| 140° | 75.98 ± 9.2% | 41.58 ± 12.9% | |
| 130° | 61.79 ± 11.2% | 31.08 ± 10.0% | |
| 120° | 38.11 ± 31.7% | 33.18 ± 15.2% | |
| **10.5 MeV** | | | |
| | Lead | Iron | Concrete |
| 150° | 21.91 ± 13.7% | 7.64 ± 11.0% | 10.11 ± 16.0% |
| 140° | 29.07 ± 10.1% | 9.36 ± 15.4% | 10.30 ± 18.7% |
| 130° | 23.03 ± 7.4% | 9.03 ± 9.4% | 8.08 ± 17.1% |
| 120° | 22.55 ± 8.5% | 9.83 ± 11.2% | 7.80 ± 16.1% |

For purposes of examining $\alpha_{D3(H_2O)}$ as a function of atomic number and maximum bremsstrahlung energy, the albedo currents are "integrated" over the angular range studied so as to have one value, $A_{D1(H_2O)}$, for each material-energy combination. This value should not be confused with $A_{DJ}$ values published elsewhere, as the dose references differ and $A_{D1(H_2O)}$ is the current dose summed across ten degree averages for measurements of dose reflected only from 115° to 155°. Figure 28 is a plot of $A_{D1(H_2O)}$ against the bremsstrahlung peak energy and Figure 29 against atomic number.

Figure 28 $A_{D1(H_2O)}$ vs $E_{max}$

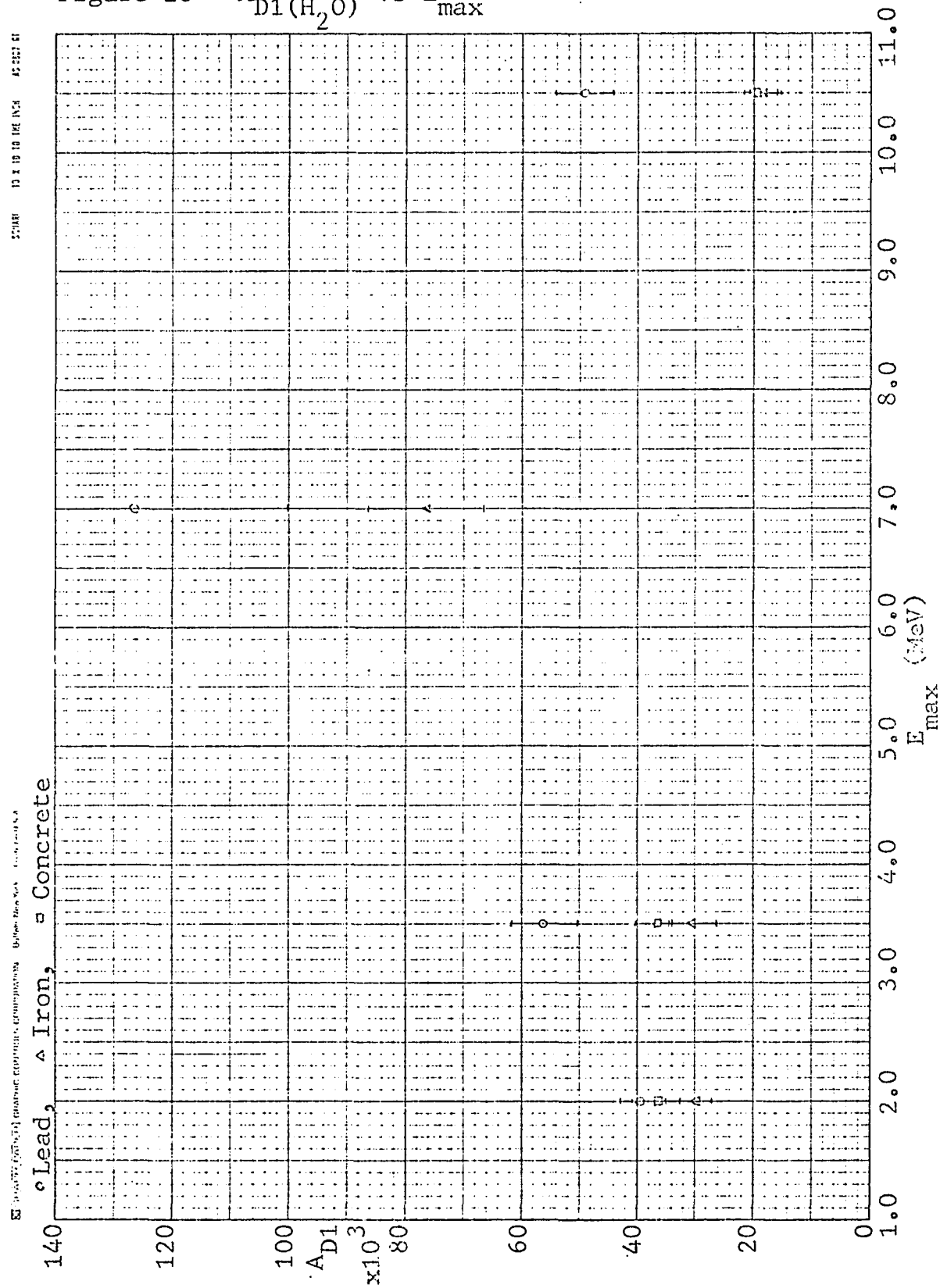

Figure 29 $A_{D1(H_2O)}$ vs Atomic Number

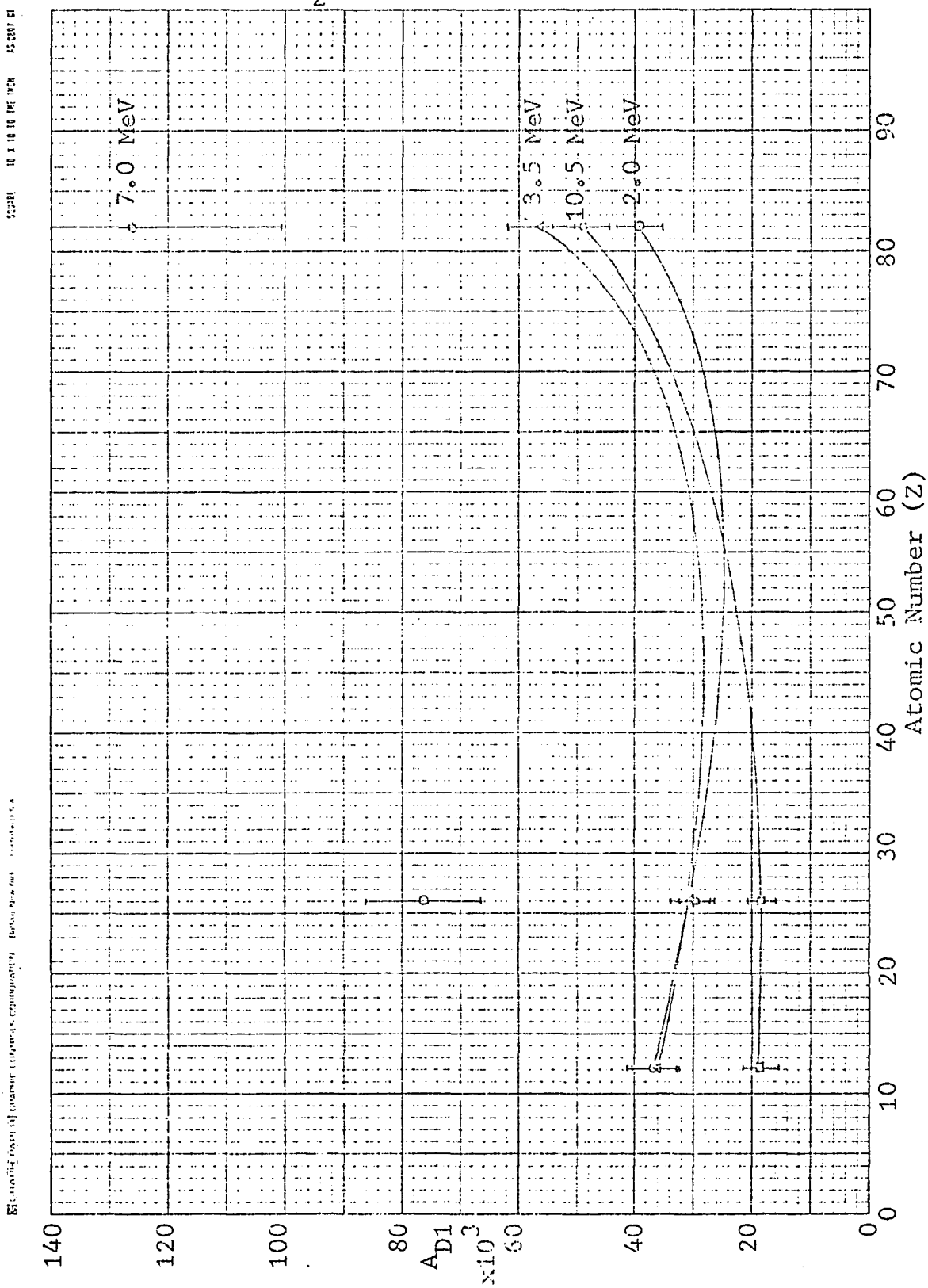

## 6.3 DISCUSSION OF RESULTS

In general the experimental values determined for $\alpha_{D1}$, the differential dose current albedo, quite closely follow the estimate obtained from DTF, the discrete ordinate computer solution. No error limits are specified on the experimental points plotted in Figures 17 through 27 due to their very strong dependence, through the function

$$\frac{\left(\frac{\mu_{en}}{\rho}\right)_{inc}^{slab}}{\left(\frac{\mu_{en}}{\rho}\right)_{inc}^{LiF}},$$ upon the incident energy spectra

considered. Errors due to measurement are discussed in Appendix J and are similar to those given in Table 3 of Section 6.2.

Results of the Chilton-Huddleston approximation are generally lower than the experimental data, in particular at the higher scattering angles. Still these numbers are within the order of error often accepted in radiation shielding estimates and though unfortunately low, they are not as low as results obtained with the Monte Carlo program used here. As fluorescence is not considered in the Chilton-Huddleston development, the generally poor fit with lead

might be expected.

Error limits for the $\alpha_{D3(H_2O)}$ values in Table 3 are given with each value. This limit includes those errors considered in Appendix J and the error introduced by

$$\left[\frac{\text{inc}\left(\frac{\mu_{en}}{\rho}\right)_{H_2O}}{\text{inc}\left(\frac{\mu_{en}}{\rho}\right)_{LiF}}\right]$$

due to various incident energy spectra. This factor is not nearly so variant as

$$\left[\frac{\text{inc}\left(\frac{\mu_{en}}{\rho}\right)_{\text{slab}}}{\text{inc}\left(\frac{\mu_{en}}{\rho}\right)_{LiF}}\right]$$

due to the absorption coefficient of LiF rather closely following that of $H_2O$ throughout the spectra (Appendix E).

$$\left[\frac{\text{ref}\left(\frac{\mu_{en}}{\rho}\right)_{H_2O}}{\text{ref}\left(\frac{\mu_{en}}{\rho}\right)_{LiF}}\right]$$

is the same in either data set and also

does not widely vary ( ~ 5% over the reflected spectra considered in Appendix D).

The values for $A_{D1(H_2O)}$ are for comparison within this data set only and the error limits given in those plots are an indication of the measurement errors only, not considering the practice of integrating over a small number of data points. The summation performed does, however, provide a single value for each (Z,E) combination, formed under the same conditions, by which Table 3 values may be considered for materials of different atomic number, exposed to different incident energies.

The plot of $A_{D1(H_2O)}$ against the maximum incident bremsstrahlung energy (Figure 28) tends to confirm the Zol'nikov, et al. report (115) that albedos have little dependence upon $E_{max}$ in the bremsstrahlung spectra. The plot against atomic number (Figure 29) is very similar to other plots made from data obtained with mono-energetic sources (1). The closeness of points obtained from different reflecting materials and different incident spectra is perhaps the most interesting feature of this graph. The points at 7.0 MeV maximum, that spectrum reported to have a small low energy component, are an exception, perhaps indicating the energy contributions below a few hundred KeV to be more important

in albedo considerations than the rest of the spectrum. This concept is explored, by computer, in Appendix D.

# 7. CONCLUSIONS AND RECOMMENDATIONS

Differential dose flux albedos were measured experimentally for broad-beam, normally incident bremsstrahlung spectra photons reflected from common shielding materials. These values were translated, through dose absorption ratios and angular relationships, to differential dose current albedos for comparison to various methods of estimating albedo. The comparison of experimental data to results of the discrete ordinates computer program (DTF) output was excellent, though the reliability of this fit is unknown due to the limited spectra information available on the generating devices studied. The results of the Chilton-Huddleston development, applied to the effective energies of the spectra studied, fall between the two computer estimates made and compare much better to the experimental results (generally within a factor of two) than might be expected considering the assumptions of this formulation. (Lead scatterers compare less well.)

The current albedo, though widely used in albedo studies, is an awkward form for shielding use as it lacks physical

meaning. Typical dose albedos, where the incident dose is based on energy deposition in the reflecting body, differ considerably from albedos calculated with the normally reported incident beam dose (based on water). These differences are dependent upon the reflecting material and can be interchanged only through an accurate knowledge of the energy spectra involved. To be of greatest value to those performing shielding calculations, results of this dissertation are reported as differential flux dose in water albedo.

The albedos reported in Table 3 are much less dependent upon reflector material and bremsstrahlung peak energy than might be expected. Figure 29 indicates the low energy make-up of the incident bremsstrahlung spectra to be of considerable importance.

In addition to the primary subject of the dissertation: a DTF modification is presented which yields results in a form more convenient to radiation protection use (Appendix L); and a thermoluminescent dosimeter annealing procedure is developed which greatly facilitates dosimeter handling, while losing none of the advantages of other procedures in terms of reliability and stability (Appendix F).

The following areas might be of interest for future experimental study:

a) Backscattering measurements to determine the influence of the low energy portion of an incident bremsstrahlung spectrum, as more information as to the beam character in that region becomes available.

b) A study of the effect of surface areas much smaller than "semi-infinite" on albedo to examine the trend indicated in Figures 74 and 76.

c) Backscattering measurements with materials of atomic numbers between 26 and 82, which though not generally of radiation protection interest, have value to others.

d) Angles of beam incidence, other than normal.

## 8. BIBLIOGRAPHY


1. Selph, Wade E. Neutron and Gamma-ray Albedos. Oak Ridge National Laboratory, Oak Ridge, Tennessee; February, 1958.

2. International Commission on Radiological Units. Report 11, September 1, 1968.

3. Jaeger, R. G.; Eisenlake, H. A., et al., editors. Shielding Fundamentals and Methods. Vol. I of Engineering Compendium on Radiation Shielding. Sponsored by International Atomic Energy Agency.

4. National Bureau of Standards. Safety Standard for Non-Medical X-ray and Sealed Gamma-ray Sources. Part I. General. Handbook 93. U. S. Government Printing Office, 1966.

5. National Bureau of Standards. Shielding for High-Energy Electron Accelerator Installations. Handbook 97. U. S. Government Printing Office, 1964.

6. Rockwell, T. III, editor. Introduction and Outline of Basic Shielding Theory. Reactor Shielding Design Manual.

7. Walker, R. L. and Grotenhuis, M. A Summary of Shielding Constants for Concrete. Argonne National Laboratory; November, 1961.

8. Kirn, Frederick S. and Kennedy, Robert J. "How Much Concrete for Shielding?" Nucleonics, Vol. 12, No. 6 (June, 1954), pp. 44-48.

9. Murray, Kenneth M. "Shielding Moderate-Energy Electron Accelerators," Nucleonics, Vol. 22, No. 2 February, 1964, pp. 61-67.

10. Raso, D. J. "Transmission of Scattered Gamma-Rays Through Concrete and Iron Slabs," Health Physics, Vol. 5 (1961), pp. 126-141.

11. Evans, R. D. The Atomic Nucleus. New York: McGraw-Hill, 1955.

12. Steyn, Julian Jack. "Backscatter of Normally Incident Gamma Photons from Semi-Infinite Media of Varying Atomic Number." Thesis, University of Toronto, Canada, 1966.

13. Compton, A. H. Phys. Rev. 21, 5 (1923), pg. 483.

14. Klein, D. and Nishina, Y. Zeit Fur Physik 52, (1929), pg. 853.

15. Hayward, E. and Hubbell, J. A. "The Backscattering of $Co^{60}$ Gamma Rays from Infinite Media," J. Applied Physics, 25, 4, (April, 1954).

16. Hine, J. and McCall, R. C. "Gamma-ray Backscattering," Nucleonics 12, No. 4 (April, 1954), pp. 27-30.

17. Bulatov, B. P. and Garusov, E. A. "$^{60}Co$ and $^{198}Au$ Gamma-ray Albedo of Various Material," Journal of Nuclear Energy, Part A: Reactor Science, Vol. 11, (1960), pp. 159-64.

18. Hyodo, T. "Backscattering of Gamma Rays," Nucl. Sci. & Eng., 12, (1962), pp. 178-84.

19. Fumita, H.; Kobayashi, K.; and Hyodo, T. "Backscattering of Gamma Rays from Iron Slabs," Science and Engineering, 19: 437-440, 1964.

20. Nakamura, T. and Hyodo, T. "Radial Distribution of Photons Backscattered from the Surface of Semi-infinite Scatterer," Nucl. Sci. & Technol. 6[3], pp. 143-152, March, 1969.

21. Mizukami, K.; Matsumoto, T.; and Hyodo, T. "Backscattering of Gamma Rays from Polyethylene, Aluminum and Lead Slabs,: Journal of Nuclear Science and Technology, 4 (12), pp. 607-613, (December, 1967).

22. Clarke, E. T. and Batten, J. F. "Gamma-ray Scattering by Concrete Surfaces," Nuclear Science and Engineering, 17:125-30, (1963).

23. Hendee, W. R. and Ellis, J. L. "Scattering of Gamma Radiation from Semi-Infinite Slabs," Health Physics, Vol. 12, (1966), pp. 673-681.

24. Jones, T. H.; Scofield, N. E.; Haggmark, L. G.; and Gurney, W. J. Experimental Determination of the Gamma-ray Angular Dose Albedos of Concrete, Aluminum, and Steel. U. S. Naval Radiological Defense Laboratory, San Francisco, California 94135, (#USNRDL-TR-790), 6 October 1964.

25. Haggmark, L. G.; Jones, T. H.; Scofield, N. E.; and Gurney, W. J. "Differential Dose-Rate Measurements of Backscattered Gamma Rays from Concrete, Aluminum, and Steel," Nucl. Sci. & Eng., 23:138-149, (1965).

26. Steyn, J. J. and Andrews, D. G. "Experimental Differential Number, Energy and Exposure Albedos for Semi-Infinite Media, for Normally Incident Gamma Photons," Nucl. Sci. & Eng., 27:318-327, (1967).

27. Cormack, D. V.; Burke, D. G.; and Davitt, W. E. "Spectral Distributions of 140 KVP X-rays," Radiology, 70 (1958), pg. 91.

28. Cormack, D. V. and Mak, S. "Spectra of Scattered Radiation at Points off the Beam Axis," Radiology, 72 (1959), pg. 107.

29. Jones, H. E. and Skarsgard, L. D. "The Spectral Distribution of Scattered Radiation Produced in a Water Phantom by X-rays in the Range 100 KV to 1.25 MeV," Rad. Research, 9, (1958), pg. 135.

30. Baran, J. A.; Faw, R. E.; and Kimel, W. R. "Reflection of $Co^{60}$ Gamma Rays from Concrete," Nucl. Inst. and Methods, 75, (1969), pp. 141-148.

31. Kitazume, Mitsuyaki. "Gamma-ray Scattering from Point Sources by Infinite Plane Surfaces," Journal of Nuclear Science and Technology, 5, (3), (March, 1968), pp. 98-103.

32. Pozdnew, D. B.; Churin, S. A.; and Gokhshtein, L. F. "Backward Scattering of Y-Radiation from Aluminum Barriers of Finite Thickness," Atomnaya Energiya, Vol. 22, No. 4, April, 1967.

33. Viktorov, A. A.; Efimenko, B. A.; Zolotukhin, V. G.; Klimanov, V. A., and Mashkovich, V. P. "Differential Albedo for Gamma Rays from a Point Unidirectional Source," Atomnaya Energiya Vol. 23, No. 3, pp. 187-191 (Sept., 1967.)

34. Kruglov, S. P., and Lopatin, S. P. "A Study of the Dispersion of the Energy of an Impact Radiation Beam from an Absorption Calorimeter," Zhurnal Tekhnicheskoi Fiziki, Vol. 30, No. 4, (April, 1960), pp. 424-432.

35. Pruitt, J. S. "High Energy X-ray Photon Albedo," Nucl. Inst. and Methods, 27, (1964), pp. 23-28.

36. Sugiyama, S. and Tomimasu, T. "High Energy X-ray Albedo for Pb, Cu and Duralumin," Nucl. Inst. and Methods, 53, (1967), pp. 346-348.

37. Karzmark, C. J. and Capone, T. "Measurements of 6 MV X-rays; II: Characteristics of Secondary Radiation," Br. J. Radiol., 41, (March, 1968), pp. 222-226.

38. Hayward, E. and Hubbell, J. "The Albedo of Various Materials for 1-MeV Photons," The Physical Review, Second Series, Vol. 93, No. 5, March 1, 1954.

39. Perkins, J. G. "Monte Carlo Calculation of Gamma-ray Albedos of Concrete and Aluminum," Journal of Applied Physics, Volume 26, No. 6, June, 1955.

40. Berger, J. J. "Calculation of Energy Dissipation by Gamma Radiation near the Interface between Two Media," J. Applied Physics, 28, Vol. 12, (1957) pp. 1502-1508.

41. Wells, M. B. "Air and Concrete Scattering of Gamma Rays," Convair; ANP Doc. No. NARF-59-11T MR-N-29 (20 March 1959).

42. Attix and Roesch, editors, Radiation Dosimetry, Volume 1, 1968.

43. Wells, M. B. "Differential Dose Albedos for Calculation of Gamma-ray Reflection from Concrete," Radiation Research Associate Document RRA-T46, December, 1964.

44. Davisson, Charlotte and Beach, L. A. "A Monte Carlo Study of Backscattered Gamma Radiation," Trans. Am. Nucl. Soc. Vol. 5, No. 2, (1962), pg. 391.

45. Raso, Dominic J. "Monte Carlo Calculations on the Reflection and Transmission of Scattered Gamma Rays," Nucl. Sci. & Eng. 17:411-418 (1963).

46. Leimdorfer, Martin. "The Backscattering of Gamma Radiation from Plane Concrete Walls," Nucl. Sci. & Eng., 17:345-351, (1963).

47. Bulatov, B. P. and Leipunski, O. I. "The Albedo of X-rays and the Reflection Build-up Factor," Soviet J. At. Energy, 7, (1961), pg. 1015.

48. Bulatov, B. P. "Method of Calculating the Intensity of Backscattered Gamma Radiation," Translated from Atomnaya Energiya, Vol. 21, No. 5, (November, 1966), pp. 345-356.

49. Chilton, A. B. and Huddleston, C. M. "A Semi-empirical Formula for Differential Dose Albedo for Gamma Rays on Concrete," Nucl. Sci. & Eng., 17:419-424 (1963).

50. Chilton, A. B. "Backscattering of Gamma Rays from Point Sources by an Infinite-Plane Concrete Surface," Nucl. Sci. & Eng., 21:194-200 (1965).

51. Chilton, A. B.; Davisson, C. M.; and Beach, L. A. "Parameters for C-H Albedo Formula for Gamma Rays Reflected from Water, Concrete, Iron and Lead," Trans. Am. Nucl. Soc. 8, (1965), pg. 656.

52. Huddleston, C. M. Comparison of Experimental and Theoretical Gamma Ray Albedo - An Interim Report. U. S. Naval Civil Engineering Laboratory, Point Hueneme, California, Doc. TN-567, 10 January 1964.

53. Huddleston, C. M. and Shoemaker, N. F. A Mathematical Derivation of Contour Lines for Constant Albedo of Gamma Rays on Concrete. U. S. Naval Civil Engineering Laboratory, Point Hueneme, Calif. Doc. TN-539.

54. Chilton, A. B. "A Modified Exposure Albedo Formula for Gamma Rays Reflected from Concrete," (1966 Winter Meeting American Nuclear Society), Trans. Am. Nucl. Soc., Vol. 9, No. 2, Pg. 368.

55. Chilton, A. B. "The Close-in Exposure Field from Point Isotropic Gamma-ray Sources Located at an Air-Ground Interface," Nucl. Sci. & Eng., 27: 403-410, (1967).

56. Eisenhauer, C. "An Image Source Technique for Calculating Reflection of Gamma Rays or Neutrons," Health Physics, Vol. II (1965) pp. 1145-1154.

57. Kaiser, R. E. and Mingle, J. O. "Reflections of High-Energy Photons from Semi-Infinite Homogeneous Slabs by Invariant Imbedding Techniques," Am. Nucl. Soc. Trans., Vol. 10, No. 2.

58. Doggett, W. O. and Bryan, F. A. "Theoretical Dose Transmission and Reflection Probabilities for 0.2 - 10.0 MeV Photons Obliquely Incident on Finite Concrete Barriers," Nucl. Sci. & Eng. Vol. 39, pp. 92-104 (1970).

59. Trubey, D. K. "The Single-scattering Approximation to the Solution to the Gamma-Ray Air-scattering Problem," Nucl. Sci. & Eng., 10, (1961), pp. 102-116.

60. Carlson, B. G.; Lee, C. E.; and Worlton, W. J. "The DSN and TDC Neutron Transport Codes," USAEC Document MAMS-2346 (1959).

61. Lathrop, K. D. "Use of Discrete-Ordinates Methods for Solution of Photon Transport Problems," Nucl. Sci. and Eng., 24:381-388, (1966).

62. Renken, James H. and Adams, K. G. Application of the Method of Discrete Ordinates to Photon Transport Calculations: A Research Report; Sandia Laboratories, SC-RR-67-419, June, 1967.

63. Renken, J. H. and Adams, K. G. An Improved Capability for Solution of Photon Transport Problems by the Method of Discrete Ordinates; Sandia Laboratories, SC-RR-739, December, 1969.

64. Segre, E., editor. Experimental Nuclear Physics. Vol. 1. New York: John Wiley and Sons, Inc. 1953.

65. Pratt, R. H. "Atomic Photoelectric Effect at High Energies," Physical Review, 117, (1960), pg. 1017-28.

66. Fink, R. W.; Jopson, R. C.; Mark, H.; and Swift, C. D. "Atomic Fluorescent Yields," Rev. Mod. Phys. Vol. 38, No. 3, June, 1966, pp. 513-540.

67. Morgan, K. Z. and Turner, J. E., editors. Principles of Radiation Protection. New York: John Wiley and Sons, 1967.

68. Bethe, H. A. and Heitler. Proc. Roy. Soc., (London). 146, (1934), pg. 83.

69. Berger, J. J.; Hubbel, J. H.; and Reingold, I. H. "Contribution of Annihilation Radiation to the Gamma Ray Flux in Lead," Physical Review, Vol. 113, No. 3 (Feb., 1959), pp. 857-862.

70. Motz, J. W.; Olsen, H. A.; and Koch, H. W. "Pair Production by Photons," Reviews of Modern Physics, Vol. 41, No. 4, pp. 581-591 (Oct., 1969).

71. Johns, H. E.; Katz, L.; Douglas, R. A.; and Haslam, R. N. H. "Gamma-Neutron Cross Section," Physical Review, 80, 6, (1950), pp. 1062-1068.

72. Baldwin, G. C. and Koch, H. W. "Threshold Measurements on the Nuclear Photo-effect," Physical Review, 67 (1945), pp. 1-11.

73. Weinstock, E. V. and Halpern, J. "Systematics of Photoproton Reaction," Physical Review, 94, 6, (1954), pp. 1651-54.

74. Levinger, J. S. Nuclear Photo-Disintegration. Oxford Univ. Press, 1960.

75. Price, W. J. Nuclear Radiation Detection. New York: McGraw-Hill, 1964.

76. Attix, F. H. and Roesch, W. C., editors. Radiation Dosimetry, Vol. II. Academic Press, 1966.

77. Attix, R. H. Present Status of Dosimetry by Radiophotoluminescence and Thermoluminescence Methods. U. S. Naval Research Laboratory Document NRL-6145, September, 1964.

78. Hendee, W. R.; Ibbott, G. S.; and Gilbert, D. B. "Effects of Total Dose on Energy Dependence of TLD-100 LiF Dosimeters," International Journal of Applied Radiation and Isotopes, Vol. 19, (1968), pp. 431-437.

79. Durke, R. K.; Lucas, A. C.; York, N. B.; Dahlstrom, T. S.; and Blair, G. E. Energy and Rate-Dependence Studies, Edgerton, Germeshauser, and Grier, Inc. Document EGG-S-237-R.

80. Schayes, R.; Brooke, C.; Kozlowitz, I.; and Lheureux, M. "New Developments in Thermoluminescent Dosimetry," Health Physics, Vol. 14 (1968), pp. 251-263.

81. Tochilin, E. and Goldstein, N. Dose Rate and Spectral Measurements from Pulsed X-ray Generators, U. S. Naval Radiological Defense Laboratory Document DASA-1703, December, 1965.

82. Bernstein, B. H. "Pulsed X-ray Prompt Gamma Simulation," U. S. Air Force Document BSD-TR 66-386, November, 1966.

83. Storm, E. and Shlaer, S. "Development of Energy-Independent Film Badges with Multi-Element Filters," Health Physics, Vol. 11, pp. 1127-1144.

84. Yokota, R.; Nakajima, S.; and Sakai, E. "High Sensitivity Silver-Activated Phosphate Glass for the Simultaneous Measurement of Thermal Neutrons, γ- and/or β-Rays," Health Physics, Vol. 5, pp. 219-224.

85. Endres, G. W. R. and Kocher, L. F. "The Response of Selected Thermoluminescent Materials to Fast-Neutron Exposures," Proceedings of Second International Conference on Luminescent Dosimetry; Conf-680920, September, 1968.

86. Reddy, A. R.; Ayyangar, K.; and Brownell, G. L. "Thermoluminescence Response of LiF to Reactor Neutrons," Rad. Research Vol. 40, pp. 552-562 (1969).

87. Zimmerman, D. W.; Rhyner, C. R.; and Cameron, J. R. "Thermal Annealing Effects on the Thermoluminescence of LiF," Health Physics, Vol. 12, (1966), pp. 525-531.

88. Carlsson, C. A. "Thermoluminescence of LiF: Dependence of Thermal History," Phys. Med. Biol. 1969, Vol. 14, No. 1, pp. 107-118.

89. Martensson, B. K. A. "Thermoluminescence of LiF: A Statistical Analysis of the Influence of Pre-Annealing on the Precision of Measurement," Phys. Med. Biol., 1969, Vol. 14, No. 1, pp. 119-130.

90. Harshaw Chemical Co. "High Sensitivity Ribbon Lithium Fluoride Thermoluminescent Dosimeters," Standard Data Sheets 074, 060, and 045.

91. Cameron, J. R.; Zimmerman, D.; Kenney, G.; Buck, R.; Bland, R.; and Grant, R. "Thermoluminescent Radiation Dosimetry Utilizing LiF," Health Physics, Vol. 10, pp. 25-29.

92. Randall, J. T. and Wilkins, M. H. F. "Phosphorescence and Electron Traps I and II; The Study of Trap Distribution," Proc. Roy. Soc. (London), Vol. 184, (1945), pp. 347-433.

93. Attix, F. H., editor. Proceedings of International Conference on Luminescence Dosimetry, June, 1965.

94. Greening, J. R. "The Derivation of Approximate X-ray Spectral Distribution and an Analysis of X-ray 'Quality' Specification," Brit. J. Radiol. Vol. 34, No. 425, (May, 1963), pp. 363-371.

95. Silberstein, L. "Determination of the Spectral Composition of X-ray Radiation from Filtration Data," J. Opt. Soc. Amer., 22, (1932), pg. 265.

96. Greening, J. R. "The Determination of X-ray Wavelength Distributions from Absorption Data," Proc. Phys. Soc., (London), 63A, (1950), pp. 1227-1234.

97. Twidell, J. W. "The Determination of X-ray Spectra Using Attenuation Measurements and a Computer Program," Phys. Med. Biol., 1970, Vol. 15, No. 3, pp. 529-539.

98. O'Dell, A. A., Jr.; Sandifer, C. W.; Knowles, R. B.; and George, W. D. Measurement of Absolute Thick-Target Bremsstrahlung Spectra, EG&G, Inc. 1183-2139, May 19, 1967.

99. Edelsack, E. A.; Kreger, W. E.; Mallet, W.; and Scofield, N. E. "Experimental Investigation of Thick-Target Bremsstrahlung Radiation Produced by Electrons of 1.00, 1.50, and 2.00 MeV," Health Physics, Vol. 4, pp. 1-15.

100. Pace, A. L. "Radiographic Characteristics of High Energy X-rays," Non-Destructive Testing, March-April, 1953.

101. Sandifer, C. W. and George, W. D. Radiation Calibration of a 20-MeV Linac, EG&G, Inc. # S-333-R May, 1965.

102. Goldie, C. H.; Wright, K. A.; Anson, J. H.; Cloud, R. W.; and Trump, J. G. "Radiographic Properties of X-rays in the Two-to-Six-Million-Volt Range," ASTM Bulletin, October, 1954.

103. Evans, W. W.; Granke, R. C.; Wright, K. A.; and Trump, J. G. "Absorption of 2-MeV Constant Potential Roentgen Rays by Lead and Concrete," Dept. of Elect. Eng., M.I.T, October, 1951.

104. Motz, J. W.; Miller, W.; and Wyckoff, H. O. "Eleven-MeV Thick Target Bremsstrahlung," Physical Review, Vol. 89, No. 5, March, 1953.

105. Hoffman-Pinther, P. X-ray Distribution from Sources Operating at Five to Fifteen Million Electron Volts, OTAC-RR-45.

106. Adams, K. G. and Mehl, C. R. Calculation of the Deposition of Energy by Photons, Sandia Laboratories, SC-RR-66-666, October, 1966.

107. Trubey, D. K. and Maskewitz, B. F. A Review of the Discrete Ordinates Sn Method for Radiation Transport Calculations, USAEC Document ORNL-RSIC-19-UC-80, March, 1968.

108. Kaplan, I., Nuclear Physics, Addison-Wesley Publ. Co., Inc. 1963.

109. Johns, H. E. and Cunningham, J. R. The Physics of Radiology; Charles C. Thomas, Publisher, 1969.

110. Chodorow, A. M. HERMES II Experimenters' Manual, Sandia Laboratories, SC-M-70-242, June, 1970.

111. Bernstein, B. H. Pulsed X-ray Prompt Gamma Simulator, BSD-TR-66-386, Nov., 1966, Air Force Systems Command.

112. Johnson, D. L., Sandia Corporation, private communication, April, 1970.

113. TREF, Technical Planning Document, Dept. of Air Force Headquarters; Air Force Special Weapons Center, Kirtland Air Force Base, Albuquerque, New Mexico.

114. Dye, D. Air Force Special Weapons Center, Private Communication, April, 1970.

115. Zol'nikov, P. P. and Sukhanova, K. A. "Energy and Space Distribution of Backscattered γ-Radiation," Atomnaya Energiya, Vol. 25, No. 6, pg. 518, December, 1968.

116. Dahlstrom, T. S. and Thompson, W. E. "The Angular Distribution of Dose Rate from Gamma Rays Scattered Through Various Thicknesses of Iron and Aluminum," USNRDL-TR-558, April 19, 1962.

117. Plimpton, J. D. Sandia Corporation, Private communication, September, 1970.

118. Mather, R. L. "Gamma-Ray Collimator Penetration and Scattering Effects," Journal of Applied Physics, Vol. 23, No. 10, October, 1957.

119. Martin, T. H. A Computerized Method of Predicting Electron Beam Bremsstrahlung Radiation with Specific Application to High Voltage Flash X-ray Machines. Sandia Corporation; SC-RR-69-241, May, 1969.

120. Bonzon, L. L. and Rivard, J. B. Method for Calculation of Bremsstrahlung and Neutron Production from Electron Driven Target. Sandia Corporation SC-TM-70-629, December, 1970.

121. Golden, J. C., Jr. Analytical Expressions for Bremsstrahlung Spectra Emitted by Highly Filtered Thick High-Z Targeted X-ray Devices from 2 to 20 MeV. Sandia Corporation; SC-TM-67-2900, December, 1967.

122. Bailey, F. A. Sandia Corporation, Private communication, October 26, 1970.

123. Buckalew, W. Sandia Corporation, Private communication, August, 1970.

124. Tochilin, E.; Goldstein, N.; and Lyman, J. T. "The Quality and LET Dependence of Three Thermoluminescent Dosimeters and Their Potential Use as Secondary Standards," Proceedings of the Second International Conference on Luminescence Dosimetry, Conf-680929, September, 1968.

125. Almond, P. R. et al. "The Energy Response of LiF, $CaF_2$, and $Li_2B_4O_7$:Mn from 26 KeV to 22 MeV," Luminescence Dosimetry, USAEC Doc., April, 1967.

126. Almond, P. R.; McCray, K.; Espejo, D.; and Watanabe, S. "The Energy Response of LiF, $CaF_2$, and $Li_2B_4O_7$:Mn from 26 KeV to 22 MeV," Proceedings of the Second International Conference on Luminescence Dosimetry, Conf-680920, September, 1968.

127. Frank, M. "Thermoluminescent Dosimetry with LiF and Energy Dependence of Thermoluminescent Dosimeters of $CaF_2$:Mn and LiF," Kernenergie, 6, 76, (1963).

128. Barford, N. C. Experimental Measurements: Precision, Error and Truth. Addison-Wesley Publishing Co. 1967.

## A. NOMENCLATURE

$A_\epsilon$ = effective viewed area normal to the collimator axis

$a$ = collimator radius

$\alpha_{D1}(E_o, \theta_o, \theta, \phi)$ = differential current out (in dose units) per incident flux (in dose units)

$\alpha_{D2}(E_o, \theta_o, \theta, \phi)$ = differential current out (in dose units) per incident current (in dose units)

$\alpha_{D3}(E_o, \theta_o, \theta, \phi)$ = differential flux out (in dose units) per incident flux (in dose units)

$A_{D1}(E_o, \theta_o)$ = total dose albedo, defined by integration of $\alpha_{D1}$ over all $\theta, \phi$

$A_{D2}(E_o, \theta_o)$ = total dose albedo, defined by integration of $\alpha_{D2}$ over all $\theta, \phi$

$D_{D3}(E_o, \theta_o)$ = total dose albedo, defined by integration of $\alpha_{D3}$ over all $\theta, \phi$

$\alpha_E$ and $A_E$ are defined as above for energy albedo

$\alpha$ and $A$ are defined as above for particle albedo

$\alpha(H_2O)$ = albedo determined when both dose terms are calculated for deposition in water

$\alpha = \frac{E_o}{m_o c^2}$

BCG = dose in TLD at some point between backscatter slab location in absence of slab and x-ray target

BCS = dose in TLD at some point between backscatter slab and x-ray target

BS = dose in water reflected by the backscatter slab at some angle and distance

c = the velocity of light -- $2.998 \times 10^{10}$ cm/sec, or collimator length, dependent upon use

d = collimator to slab distance

$D_o$ = incident dose

$\mathcal{D}_R$ = dose reflected per steradian

DBG = dose in TLD measured at same position as BS during background run

DD = dose deposited at backscatter surface center

DI = dose deposited at backscatter surface location in absence of reflector

DR = dose in TLD measured at same position as BS during backscatter run

e = the electronic charge -- $4.8 \times 10^{-10}$ statcoulomb

E = photon energy

exp = exponential

$h\nu$ = photon energy

K = Boltzmann's constant

$_{e}K(\theta_s)$ = Klein-Nishina energy scattering cross-section per electron

ln = natural logarithm

$m_o$ = the electronic mass -- $9.1083 \times 10^{-28}$ gms

$\left(\frac{\mu_{en}}{\rho}\right)$ = mass energy-absorption coefficient

$\mu_T$ = total attenuation coefficient

$\Omega$ = solid angle disignation

$\Pi$ = 3.14159.....

$\phi$ = the angle between the projection on the surface of the backscatter material of the incident radiation beam and the projection of the reflected radiation

$\Phi$ = fluence

$_{e}\sigma$ = total microscopic Compton interaction cross-section

$_{e}\sigma_s$ = the Compton scattering coefficient

$\sigma_{(\gamma,n)}$ = photonuclear absorption coefficient for the emission of a single neutron

$\Sigma_r$ = removal cross-section for neutrons

T = kinetic energy of a particle or temperature, dependent upon use

$\tau_K$ = the K-shell photoelectric cross-section in barns per atom

$\tau_{pe}$ = the total photoelectric cross-section in barns per atom

$\theta$ = the angle between the reflected radiation and the perpendicular to the surface of the backscatter material

$\theta_o$ = the angle between the incident radiation beam and the perpendicular to the surface of the backscatter material

$\theta_s$ = the angle between the transmitted beam axis and the reflected radiation

Additional specialized abbreviations are defined at the point of their use.

## B. VIEWED AREA CONSIDERATIONS

The area of a slab, normal to the collimator, viewed by a TLD crystal at the back of the collimator is the envelope of the family of circles generated by considering each point on the crystal.

If one considers a plane of origin through the leading edge of the collimator (Figure 30) such that a circle of radius "a" (the collimator radius) is defined in the plane, 1, another parallel plane, 2, at distance "c" (the collimator length) in the positive direction, and a third parallel plane, 3, at a negative distance "d" (the distance from the collimator to the scattering center), he may derive the equation of the envelope defining the viewed area. The collimator radius, a, will appear in Plane 3 as

$$r = \frac{(c + d)\, a}{c} \qquad \text{Eq. B.1}$$

with center displacement $\bar{x}$ and $\bar{y}$ given by

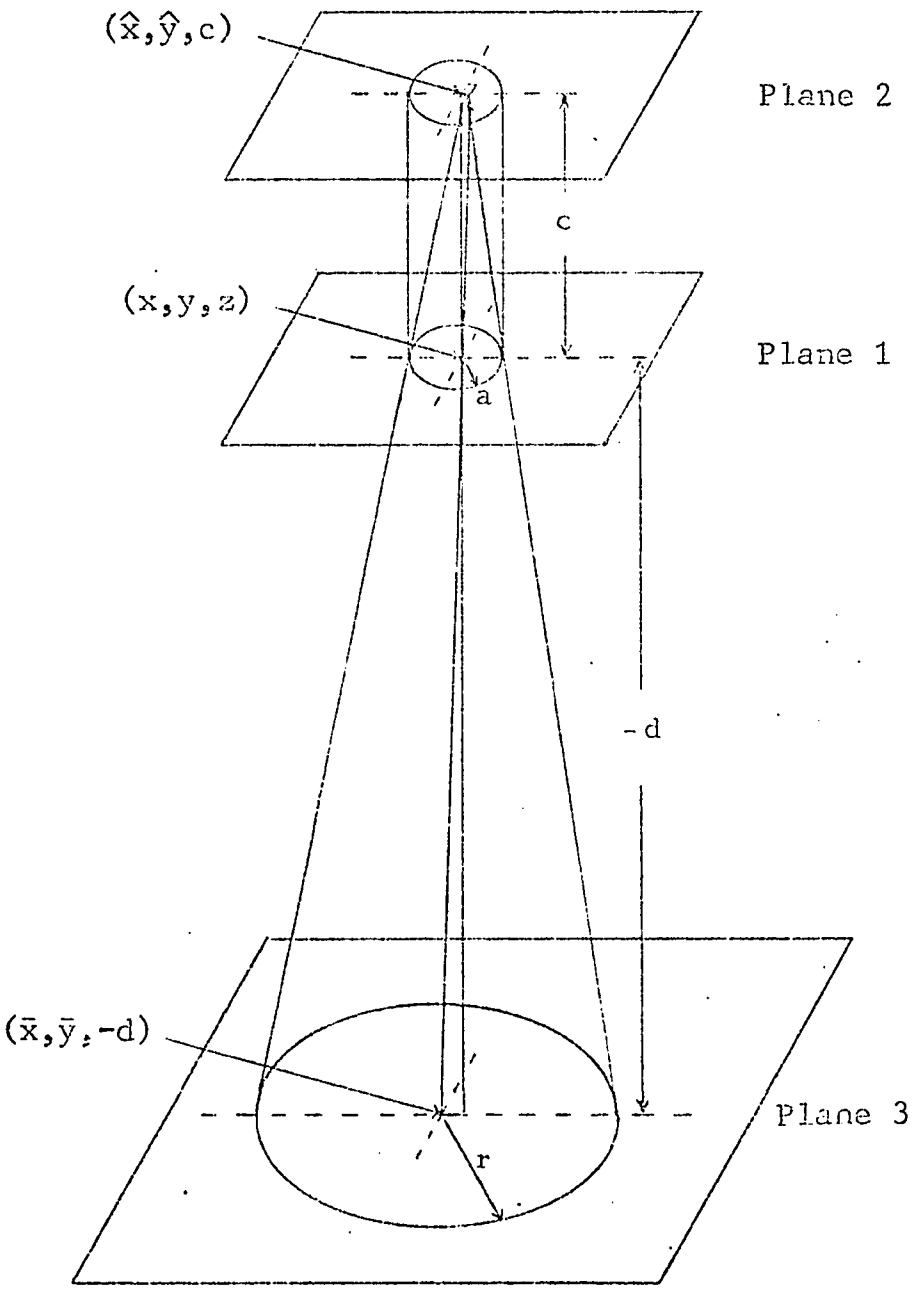


Figure 30. Viewed area geometry

$$\bar{x} = -\frac{\hat{x}\, d}{c} \qquad \text{Eq. B.2}$$

$$\bar{y} = -\frac{\hat{y}\, d}{c} \qquad \text{Eq. B.3}$$

from $(\hat{x},\hat{y})$ in Plane 2.

The equation of the circle in Plane 3 defined by point $(\hat{x},\hat{y})$ on the detecting crystal in Plane 2 and the collimator opening specified in Plane 1 is

$$(x - \bar{x})^2 + (y - \bar{y})^2 = r^2 \qquad \text{Eq. B.4}$$

or, substituting equations B.2 and B.3,

$$\left(x + \frac{\hat{x}d}{c}\right)^2 + \left(y + \frac{\hat{y}d}{c}\right)^2 = r^2 \qquad \text{Eq. B.5}$$

The envelope of the set of circles generated by tracing the outline of the detector is the outside boundary of the desired area.

Setting

$$\hat{x} = \hat{x}(t) \qquad \text{Eq. B.6}$$

and $$\hat{y} = \hat{y}(t) \qquad \text{Eq. B.7}$$

The equation for the general circle will then be:

$$\left(x + \frac{\hat{x}(t)d}{c}\right)^2 + \left(y + \frac{\hat{y}(t)d}{c}\right)^2 = r^2 \qquad \text{Eq. B.8}$$

To find the envelope of a set of lines, the general equation of the generating line is set equal to zero, differentiated with respect to the variable and the variable then eliminated between the two equations.

$$F(t) = \left(x + \frac{\hat{x}(t)d}{c}\right)^2 + \left(y + \frac{\hat{y}(t)d}{c}\right)^2 - r^2 = 0$$

Eq. B.9

$$\frac{dF(t)}{dt} = 2\left(x + \frac{\hat{x}(t)d}{c}\right)\frac{d}{c}\hat{x}'(t)$$

$$+ 2\left(y + \frac{\hat{y}(t)d}{c}\right)\frac{d}{c}\hat{y}'(t) = 0 \qquad \text{Eq. B.10}$$

In the particular case being considered, several special cases arise as follows:

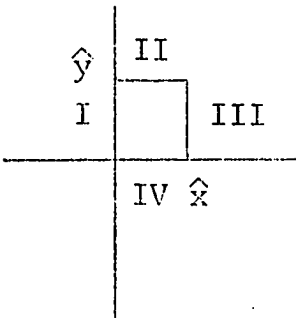


Figure 31. Crystal geometry considerations

Case I

$$\hat{x} = 0 \qquad \text{Eq. B.11}$$

and

$$\hat{x}' = 0 \qquad \text{Eq. B.12}$$

So

$$F(t) = x^2 + \left(y + \frac{\hat{y}(t)d}{c}\right)^2 - r^2 = 0 \qquad \text{Eq. B.13}$$

$$\frac{F(t)}{dt} = 2\left(y + \frac{\hat{y}(t)d}{c}\right)^2 \frac{d}{c}\,\hat{y}'(t) = 0 \qquad \text{Eq. B.14}$$

$$\hat{y} = -\frac{c}{d}\,y \qquad \text{Eq. B.15}$$

Substituting back into F(t):

$$x^2 + (y - y)^2 - r^2 = 0 \qquad \text{Eq. B.16}$$

$$x = \pm r \qquad \text{Eq. B.17}$$

Therefore, a set of circles has been generated parallel to the y-axis of radius "r" along the x-axis.

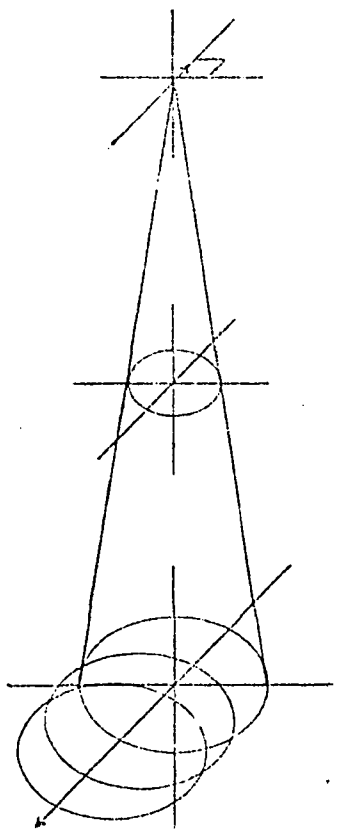

Figure 32. Edge generated envelope

The total envelope in Case I is then the set of parallel lines joining the circles formed by viewing points at the first two corners of the crystal.

Case II is similar in a perpendicular direction along a line parallel to the x-axis at distance $-\bar{y}$. The envelope has equation

$$y = \pm r \qquad \text{Eq. B.18}$$

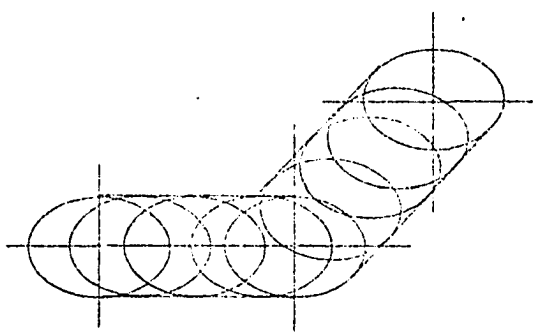

Figure 33. Envelope generated by two edges

Cases III and IV close the viewed area with a resultant figure:

curvature of radius, $r = \frac{(c + d)}{c} a$ Eq. B.19

center line separation of (crystal length)$\left(\frac{d}{c}\right)$ Eq. B.20

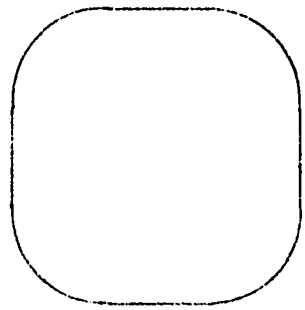

Figure 34. Total viewed area

This area includes the area seen by any point on the crystal. Only a fraction of this is seen by every point on the crystal (umbra), the rest being seen by a decreasing amount of the crystal (penumbra). The umbral region is defined by the area determined by the common area of the circles defined by points originating at the greatest extents of the detector (i.e. the four corners).

To find the umbral area consider the four defining circles:

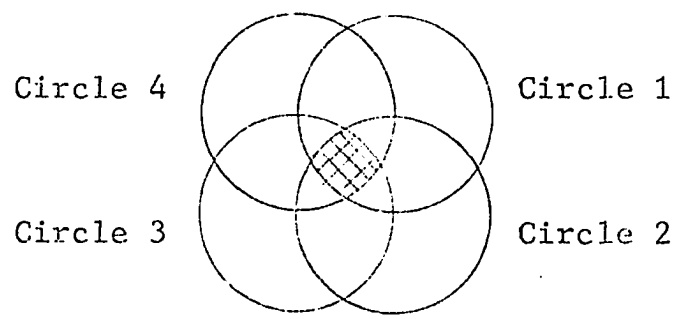


Figure 35. Umbral area

Circle 1; $x^2 + y^2 = r^2$ Eq. B.21

Circle 2; $x^2 + (y + \bar{y})^2 = r^2$ Eq. B.22

Circle 3; $(x + \bar{x})^2 + (y + \bar{y})^2 = r^2$ Eq. B.23

Circle 4; $(x + \bar{x})^2 + y^2 = r^2$ Eq. B.24

The intersection of Circles 1 and 2 provides the least value of x:

Circle 1 - Circle 2: $y^2 - (y + \bar{y})^2 = 0$ Eq. B.25

$$y^2 - y^2 - 2\bar{y}y - \bar{y}^2 = 0 \qquad \text{Eq. B.26}$$

$$2y = -\bar{y} \qquad \text{Eq. B.27}$$

$$y = -\left(\frac{\bar{y}}{2}\right) \qquad \text{Eq. B.28}$$

$$x^2 + \left(-\frac{\bar{y}}{2}\right)^2 = r^2 \qquad \text{Eq. B.29}$$

$$x^2 = r^2 - \left(\frac{\bar{y}}{2}\right)^2 \qquad \text{Eq. B.30}$$

$$x = \pm\sqrt{r^2 - \left(\frac{\bar{y}}{2}\right)^2} \qquad \text{Eq. B.31}$$

the negative solution for x being the one of interest. The intersection of either Circles 1 and 4 or Circles 2 and 3 provides a mid-point value of x.

Circle 1 - Circle 4: $x^2 - (x + \bar{x})^2 = 0$ Eq. B.32

$$x^2 - x^2 - 2x\bar{x} - \bar{x}^2 = 0 \qquad \text{Eq. B.33}$$

$$x = -\left(\frac{\bar{x}}{2}\right) \qquad \text{Eq. B.34}$$

Solution of the intersection of Circles 3 and 4 would yield the right-most boundary of x, but is not necessary as the two halves are symmetrical.

The total area of the umbra may then be found by:

$$A_u = 2\int_{-\sqrt{r^2 - \left(\frac{\bar{y}}{2}\right)^2}}^{-\left(\frac{\bar{x}}{2}\right)} [(\text{Circle 2 boundary}) - (\text{Circle 1 boundary})]\, dx \qquad \text{Eq. B.35}$$

Circle 1: $y = \pm\sqrt{r^2 - x^2}$ Eq. B.36

the negative radical being of interest.

Circle 2: $y^2 + 2y\bar{y} + (\bar{y}^2 + x^2 - r^2) = 0$ Eq. B.37

$$y = \frac{-2\bar{y} \pm \sqrt{4\bar{y}^2 - 4\bar{y}^2 - 4x^2 + 4r^2}}{2}$$ Eq. B.38

$$y = -\bar{y} \pm \sqrt{r^2 - x^2}$$ Eq. B.39

the positive radical being of interest.

Eq. B.35 then becomes:

$$A_u = 2\int_{-\sqrt{r^2 - \left(\frac{\bar{y}}{2}\right)^2}}^{-\left(\frac{\bar{x}}{2}\right)} \left(-\bar{y} + 2\sqrt{r^2 - x^2}\right) dx$$ Eq. B.40

$$A_u = -2\bar{y}x\Bigg|_{-\sqrt{r^2-\left(\frac{\bar{y}}{2}\right)^2}}^{-\left(\frac{\bar{x}}{2}\right)} + 4\int_{-\sqrt{r^2-\left(\frac{\bar{y}}{2}\right)^2}}^{-\left(\frac{\bar{x}}{2}\right)} \sqrt{r^2 - x^2}\, dx$$ Eq. B.41

$$A_u = -2\bar{y}\left[\frac{\bar{x}}{2} + \sqrt{r^2 - \left(\frac{\bar{y}}{2}\right)^2}\right] + 4\left[\frac{x}{2}\sqrt{r^2 - x^2} + \frac{r^2}{2}\arcsin\frac{x}{r}\right]\Bigg|_{-\sqrt{r^2 - \left(\frac{\bar{y}}{2}\right)^2}}^{-\left(\frac{\bar{x}}{2}\right)}$$

Eq. B.42

$$A_u = \bar{y}\bar{x} - 2\bar{y}\sqrt{r^2 - \left(\frac{\bar{y}}{2}\right)^2} + 2\left\{\left[\left(-\frac{\bar{x}}{2}\right)\sqrt{r^2 - \left(\frac{\bar{x}}{2}\right)^2} + r^2 \arcsin\left(-\frac{\bar{x}}{2r}\right)\right] - \left[-\sqrt{r^2 - \left(\frac{\bar{y}}{2}\right)^2}\sqrt{r^2 - r^2 + \left(\frac{\bar{y}}{2}\right)^2} + r^2 \arcsin\frac{-\sqrt{r^2 - \left(\frac{\bar{y}}{2}\right)^2}}{r}\right]\right\}$$

Eq. B.43

$$A_u = \bar{y}\bar{x} - 2\bar{y}\sqrt{r^2 - \left(\frac{\bar{y}}{2}\right)^2} - \bar{x}\sqrt{r^2 - \left(\frac{\bar{x}}{2}\right)^2} + 2r^2 \arcsin\left(-\frac{\bar{x}}{2r}\right)$$

$$+ \bar{y}\sqrt{r^2 - \left(\frac{\bar{y}}{2}\right)^2} - 2r^2 \arcsin\left(\frac{-\sqrt{r^2 - \left(\frac{\bar{y}}{2}\right)^2}}{r}\right) \qquad \text{Eq. B.44}$$

$$A_u = \bar{y}\bar{x} - \bar{y}\sqrt{r^2 - \left(\frac{\bar{y}}{2}\right)^2} - \bar{x}\sqrt{r^2 - \left(\frac{\bar{x}}{2}\right)^2}$$

$$+ 2r^2 \left[\arcsin\left(-\frac{\bar{x}}{2r}\right) - \arcsin\frac{-\sqrt{r^2 - \left(\frac{\bar{y}}{2}\right)^2}}{r}\right]$$

Eq. B.45

Substituting absolute values from Eqs. B.1, B.2, and B.3 to obtain the actual area of interest, Eq. B.45 becomes:

$$A_u = \hat{x}\hat{y}\left(\frac{d}{c}\right)^2 - \frac{\hat{y}d}{c}\sqrt{\frac{(c+d)^2}{c^2}a^2 - \frac{\hat{y}^2d^2}{4c^2}}$$

$$- \frac{\hat{x}d}{2}\sqrt{\frac{(c+d)^2a^2}{c^2} - \frac{\hat{x}^2d^2}{4c^2}}$$

$$+ 2\frac{(c+d)^2a^2}{c^2}\left[\arcsin\left(-\frac{\hat{x}d}{2a(c+d)}\right) - \arcsin\frac{-\sqrt{\frac{(c+d)^2a^2}{c^2} - \frac{\hat{y}^2d^2}{4c^2}}}{\frac{(c+d)a}{c}}\right]$$

Eq. B.46

The penumbral area is most easily found by determining the total enclosed area and subtracting the umbral area.

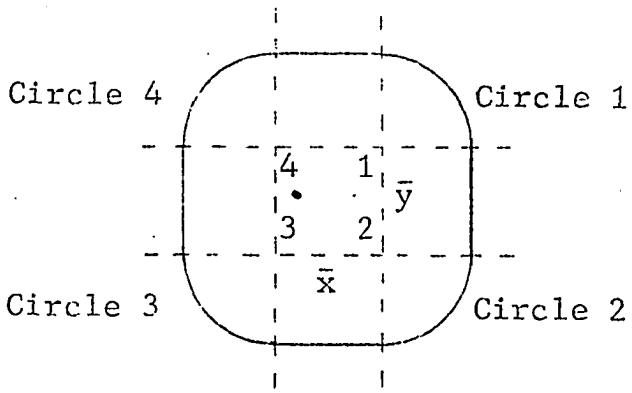


Figure 36. Total enclosed area

The total area can be seen by examination to be:

$$A_T = \Pi r^2 + \bar{y}\bar{x} + 2\bar{x}r + 2\bar{y}r \qquad \text{Eq. B.47}$$

$$A_T = \Pi r^2 + \bar{y}\bar{x} + 2r\,(\bar{x} + \bar{y}) \qquad \text{Eq. B.48}$$

Using absolute values for $\bar{x}$ and $\bar{y}$ from Equations B.1, B.2 and B.3, Eq. B.48 becomes

$$A_T = \frac{\Pi a^2 (c+d)^2}{c^2} + \hat{x}\hat{y}\left(\frac{d}{c}\right)^2 + \frac{2a(c+d)}{c}(\hat{x} + \hat{y})\left(\frac{d}{c}\right) \qquad \text{Eq. B.49}$$

and

$$A_p = A_T - A_u \qquad \text{Eq. B.50}$$

As pointed out by Dahlstrom and Thompson (116) and demonstrated by Steyn (12), radiation originating in the penumbra is not as effective as that from the umbra and either must be weighted as such or the area weighted in such a manner as to accomplish the same end. The method chosen by Dahlstrom and Thompson was to consider the radiation density as decreasing linearly to zero between the umbra and penumbra limits and choosing an "effective area" which, emitting a constant radiation density, would

emit the same amount as the true umbral and penumbral areas.

$$A_\epsilon \rho_o = A_u \rho_o + \int dA_p \, \rho(r) \qquad \text{Eq. B.51}$$

with $\rho_o$ = a constant radiation density

$\rho(r)$ = penumbral radiation density

$A_\epsilon$ = an effective viewed area

Steyn carried out a more detailed consideration of the intersected detector area and found that a numerical integration of Eq. B.51 (since it does not reduce to an exact solution) compared to within 0.005% of the area determined by a point detector viewing the same surface. As the detector used in his calculations occupied the full back of the collimator the error involved would be greater than that for which a smaller detector is used (other dimensions remaining comparable).

Field and experimental use of a variety of detector shapes in collimators of differing aperture configurations (117) indicate the error between a precise solution of Equation B.51 and the point detector approximation to be in the order of the square of the ratio of the greatest detector dimension to the collimator length. In the worst

case of the data used here, that would be:

$$\left(\frac{0.236}{6.00}\right)^2 \text{ or } 0.155\%$$

In view of these considerations and the untractable form the preceding development takes when considering other than normally viewed surfaces, the point source estimate is used in the actual data reduction. The maximum error involved is far below the statistical variation of the thermoluminescent dosimeter readings.

## B.2 POINT DETECTOR VIEWED AREA

The area of a slab viewed by a point detector located in a collimator is determined by the detector to slab distance (c + d), the collimator length (c) and radius (a), and the angle (θ) between the collimator axis and a normal to the slab.

$$x = h(\sec \theta) \qquad \text{Eq. B.52}$$

$$y = (c+d) - g \qquad \text{Eq. B.53}$$

$$\frac{a}{c} = \frac{h}{g} \qquad \text{Eq. B.54}$$

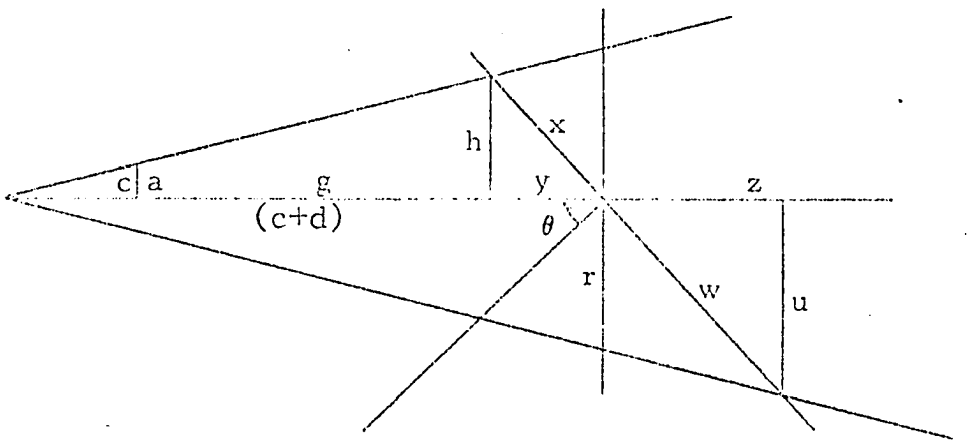


Figure 37. Point detector viewed area

$$g = \frac{c}{a} h \qquad \text{Eq. B.55}$$

$$y = h \tan \theta \qquad \text{Eq. B.56}$$

$$h \tan \theta = (c+d) - \frac{c}{a} h \qquad \text{Eq. B.57}$$

$$h = \frac{(c+d)}{\tan \theta + \frac{c}{a}} \qquad \text{Eq. B.58}$$

$$\cos \theta = \frac{h}{x} \qquad \text{Eq. B.59}$$

$$x = \frac{(c+d)\ \sec\theta}{\tan\theta + \left(\frac{c}{a}\right)} \qquad \text{Eq. B.60}$$

$$x = \frac{\left(\frac{a}{c}\right)(c+d)\ \sec\theta}{1 + \left(\frac{a}{c}\right)\tan\theta} \qquad \text{Eq. B.61}$$

$$x = \frac{r\ \sec\theta}{1 + \left(\frac{a}{c}\right)\tan\theta} \qquad \text{Eq. B.62}$$

$$\frac{a}{c} = \frac{u}{(c+d) + z} \qquad \text{Eq. B.63}$$

$$\tan\theta = \frac{z}{u} \qquad \text{Eq. B.64}$$

$$z = u\tan\theta \qquad \text{Eq. B.65}$$

$$\frac{a}{c} = \frac{u}{(c+d) + u\tan\theta} \qquad \text{Eq. B.66}$$

$$\left(\frac{a}{c}\right)(c+d) + u\left(\frac{a}{c}\tan\theta\right) = u \qquad \text{Eq. B.67}$$

$$\left(\frac{a}{c}\right)(c+d) = u\left[1 - \left(\frac{a}{c}\right)\tan\theta\right] \qquad \text{Eq. B.68}$$

$$u = \frac{\left(\frac{a}{c}\right)(c+d)}{1 - \left(\frac{a}{c}\right)\tan\theta} \qquad \text{Eq. B.69}$$

$$\cos\theta = \frac{u}{w} \qquad \text{Eq. B.70}$$

$$w = u \sec\theta \qquad \text{Eq. B.71}$$

$$w = \frac{\left(\frac{a}{c}\right)(c+d)\sec\theta}{1 - \left(\frac{a}{c}\right)\tan\theta} \qquad \text{Eq. B.72}$$

$$w = \frac{r \sec\theta}{1 - \left(\frac{a}{c}\right)\tan\theta} \qquad \text{Eq. B.73}$$

$$G = \text{semi-major ellipse} = \tfrac{1}{2}(w + x) \qquad \text{Eq. B.74}$$

$$G = \tfrac{1}{2}\left[\frac{r \sec\theta}{1 - \left(\frac{a}{c}\right)\tan\theta} + \frac{r \sec\theta}{1 + \left(\frac{a}{c}\right)\tan\theta}\right] \qquad \text{Eq. B.75}$$

$$G = \frac{r \sec\theta}{1 - \left(\frac{a}{c}\right)^2 \tan^2\theta} \qquad \text{Eq. B.76}$$

$H$ = semi-minor ellipse = $r$ Eq. B.77

$A$ = area of ellipse = $\Pi HG$ Eq. B.78

$$A = \frac{\Pi r^2 \sec^2 \theta}{1 - \left(\frac{a}{c}\right)^2 \tan^2 \theta} \qquad \text{Eq. B.79}$$

The area viewed on the reflecting slab by a point detector where:

$a$ = collimator radius

$c$ = collimator length

$r$ = detector to scattering center distance

$\theta$ = angle between collimator axis and a normal to the slab

## C. COLLIMATOR EFFECTS

One of the most complete and most frequently referenced works on collimator penetration and scattering is by Mather (118). He develops expressions which give the amount of radiation passing through a cylindrical hole in a slab of material, including the amount of radiation which penetrates the edges of the hole and that due to scattering from the walls of the collimator.

In Mather's report, it is shown, that to a first approximation, the results are the same as the geometric aperture for a like diameter hole in a similar slab with one mean free path of material removed from each side.

Figure 38 details the collimator construction where c is the collimator length, specified in Appendix I for each measurement made.

A copper liner was pressure-fitted to the lead in an effort to eliminate any lead fluorescence response in the TLD's due to the shield.

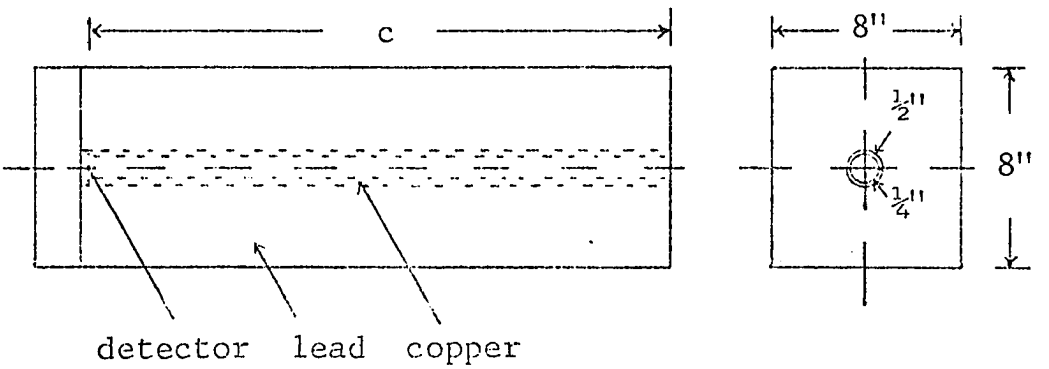


Figure 38. Collimator detail

The mean free path was calculated by the standard equation (11):

$$(mfp) = \frac{1}{\mu_o} \qquad \text{Eq. C.1}$$

where: $\mu_o$ is the total linear attenuation coefficient (as found in Reference 38).

Since the reflected radiation is certainly not monoenergetic (see Appendix D, Figures 49 - 66 for example spectra) a $\mu_{eff}$ must be used.

$$\mu_{eff} = \frac{\sum_i \mu_{o_i} E_i}{\sum_i E_i} \qquad \text{Eq. C.2}$$

where $E_i$ is the amount of energy emitted in the "i"th energy interval. $\mu_{o_i}$ is the total attenuation coefficient at the average energy of the "i"th energy interval.

The computer-generated spectra in Appendix D were used to obtain the following table.

TABLE 4

DETECTOR COLLIMATOR CORRECTION

| Incident Bremsstrahlung Spectra Max. (MeV) | Scatterer Material | Collimator Correction (Inches) |
|---|---|---|
| 2.0 | Lead | 0.11 |
| | Iron | 0.32 |
| | Concrete | 0.15 |
| 3.5 | Lead | 0.15 |
| | Iron | 0.31 |
| | Concrete | 0.18 |
| 7.0 | Lead | 0.20 |
| | Iron | 0.31 |
| 10.5 | Lead | 0.26 |
| | Iron | 0.32 |
| | Concrete | 0.26 |

## D. SPECTRA CONSIDERATIONS

### D.1 INPUT SPECTRA

In order to obtain a computer solution to the back-scatter problem, one must have some knowledge of the incident beam energy spectra. Spectra for the machines studied in this dissertation are quite difficult to obtain. For the purposes of gaining some computer comparison to the experimental data, the author has relied heavily on previously published spectra. At 2.0, 3.5, and 10.5 MeV, very rough absorption measurements were made to have an "effective" energy measurement for comparison to the published spectra in DTF runs. Copper was used in the absorption study and calibrated against Co-60 and Cs-137. Absorption measurements at 7.0 MeV had been made previously by facility operators.

Figure 39 was obtained from copper absorption of the 2.0 MeV Van de Graaff beam. An effective energy (determined by the method of Greening [96]) of 0.85 MeV was used as input to the DTF program. These results are compared in

Figure 39 Cu absorption 2.0 MeV

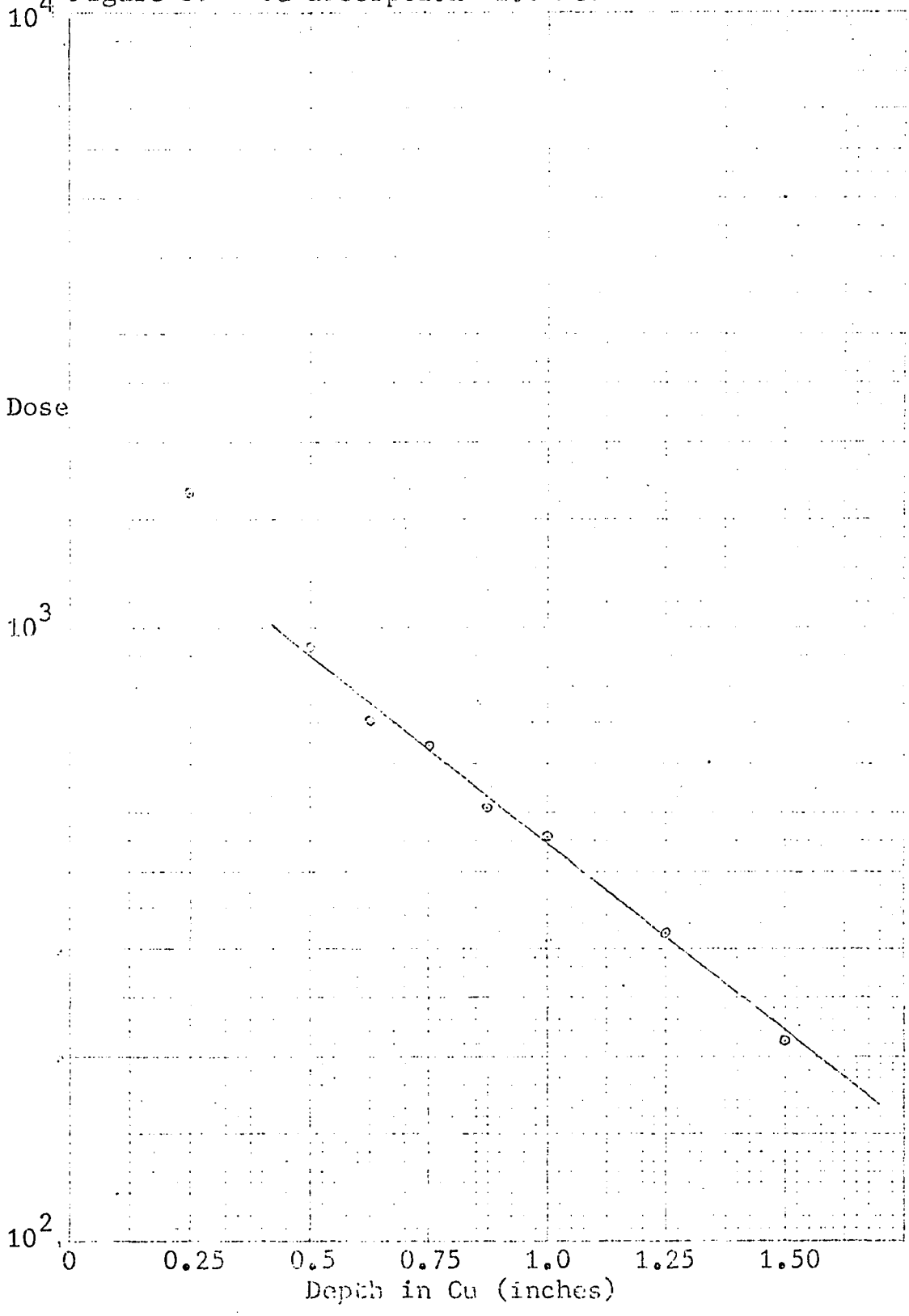

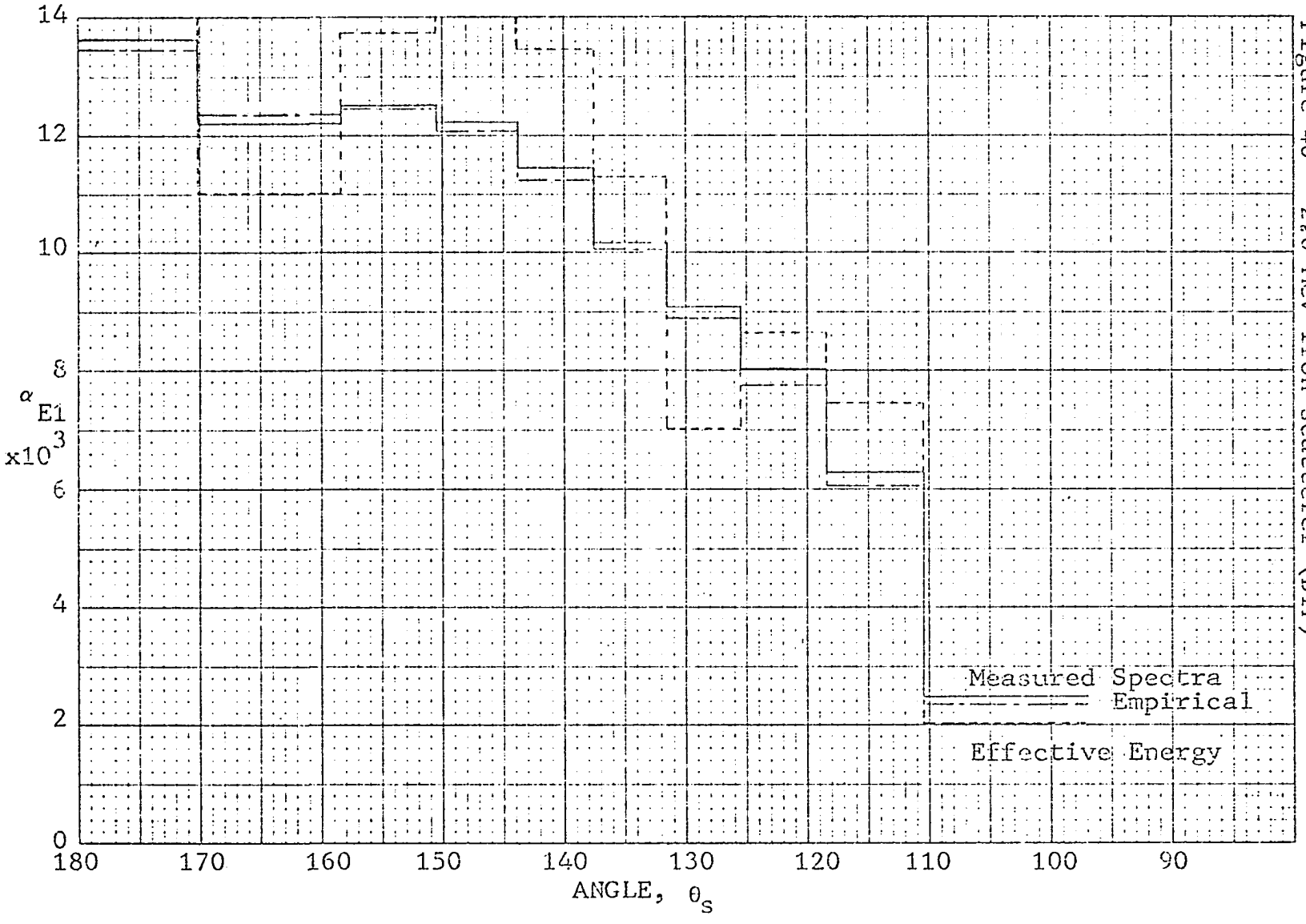


Figure 40 2.0 MeV iron scatterer (DTF)

Figure 40 with DTF results obtained when inputting a measured 2.0 MeV spectrum (Table 5). Iron was used as an example reflecting material.

TABLE 5

2.0 MeV MEASURED SPECTRA (99, 100)

| GROUP BOUNDS (MeV) | INPUT FLUX (Photons/MeV) |
|---|---|
| 2.0 | 5.6 |
| 1.5 | 13.6 |
| 1.02 | 22.0 |
| 0.80 | 35.0 |
| 0.60 | 60.0 |
| 0.52 | 65.0 |
| 0.50 | 68.0 |
| 0.44 | 75.0 |
| 0.38 | 85.0 |
| 0.32 | 87.0 |
| 0.28 | 90.0 |
| 0.25 | 90.0 |
| 0.225 | 90.0 |
| 0.20 | 80.0 |
| 0.175 | 70.0 |
| 0.15 | 60.0 |
| 0.13 | 50.0 |
| 0.12 | 40.0 |
| 0.10 | 40.0 |
| 0.088 | 40.0 |
| 0.07684 | 40.0 |
| 0.07664 | 35.0 |
| 0.68 | 35.0 |
| 0.060 | 30.0 |
| 0.055 | 25.0 |
| 0.050 | 20.0 |
| 0.045 | 15.0 |
| 0.040 | 10.0 |
| 0.035 | 5.0 |
| 0.030 | |

A similar process was carried out on the 3.5 MeV flash x-ray machine. Figure 41 shows the absorption curve, Figure 42 the DTF results, and Table 6 the measured spectra (102) used for comparison. By Greening's technique the 3.5 MeV beam was estimated to be 43.2% 0.24 MeV and 56.8% 1.34 MeV. The measured spectra in this case are somewhat rougher than before as they were used for input to both the Monte Carlo program and DTF. The Monte Carlo spectra input is limited to twenty-five energy groups. The scattering material is again iron.

TABLE 6

3.5 MeV MEASURED SPECTRA (102)

| GROUP BOUNDS (MeV) | INPUT FLUX (Photons/MeV) |
|---|---|
| 3.5 | 0.0143 |
| 3.3 | 0.0845 |
| 3.1 | 0.1194 |
| 2.75 | 0.1746 |
| 2.35 | 0.2553 |
| 1.95 | 0.3692 |
| 1.55 | 0.5355 |
| 1.36 | 0.6471 |
| 1.15 | 0.8261 |
| 0.78 | 1.2821 |
| 0.68 | 1.4412 |
| 0.58 | 1.6724 |
| 0.48 | 1.875 |
| 0.38 | 1.5789 |
| 0.32 | 0.312 |
| 0.30 | 0.0 |
| 0.10 | 0.0 |
| 0.06 | 0.0 |
| 0.03 | |

Figure 41 3.5 MeV Cu absorption

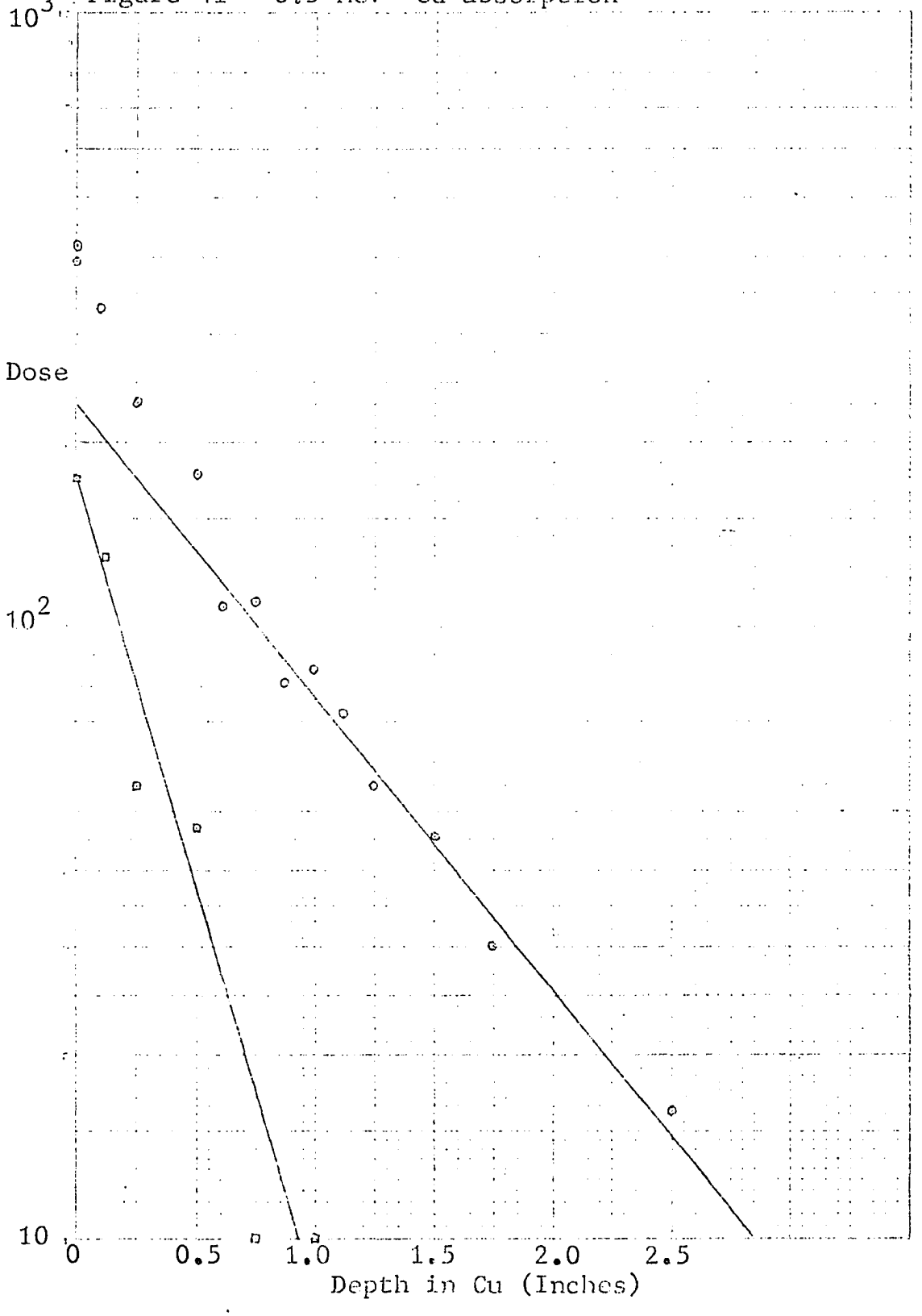

Figure 42 DTF 3.5 MeV iron scatterer

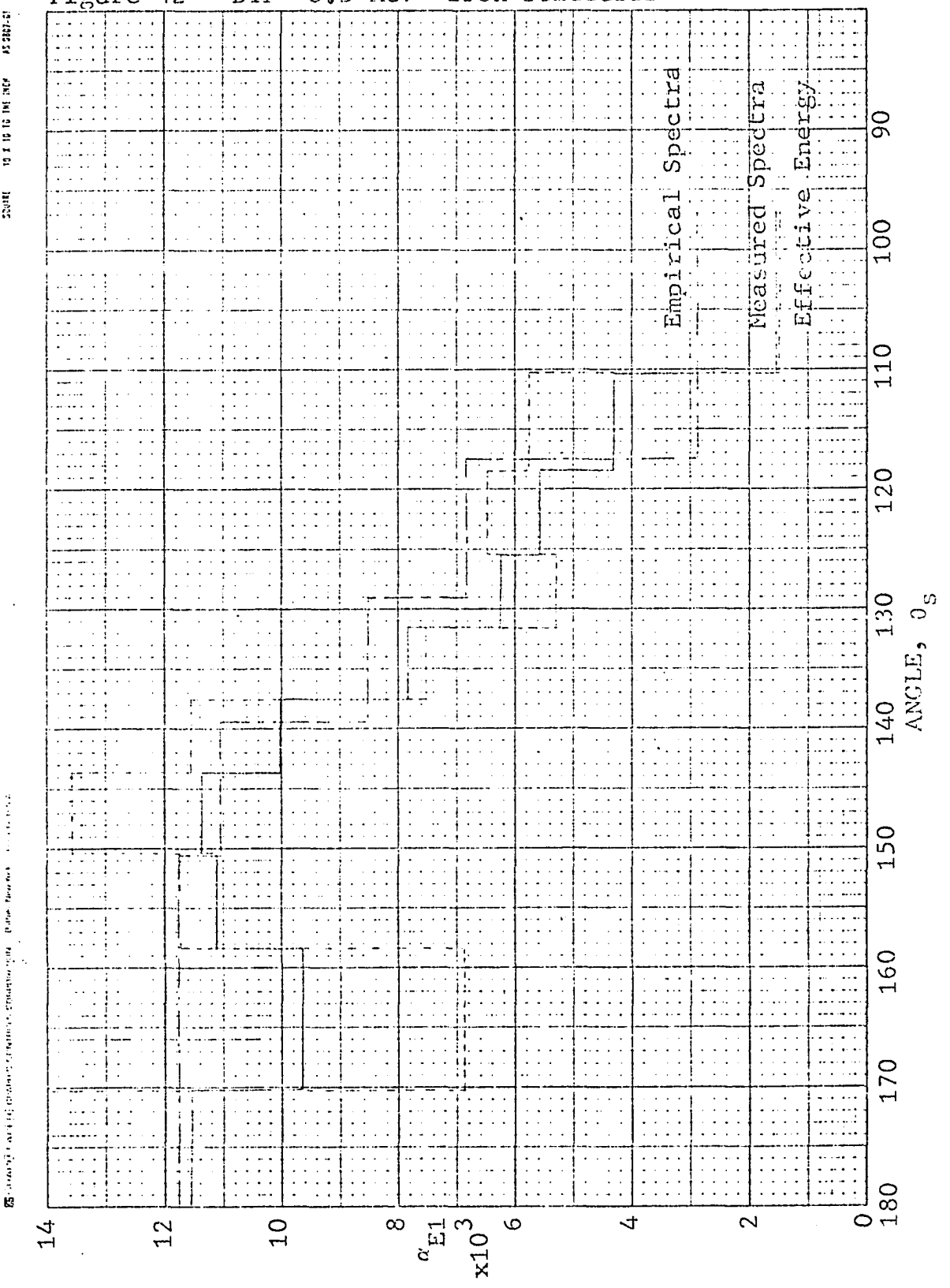

Due to the relative scarcity of measured spectra from flash x-ray devices, several methods of calculating spectra have been derived. Most of these are computerized methods of studying electron transport in a target material. (119, 120). One (121), however, is based on an analytical approximation requiring only a maximum and minimum energy input to obtain a spectra guess. The measured spectrum reported for a 3.5 MeV machine (not that used in this work) is compared with the spectrum obtained from an electron transport code (122) and the empirical approximation spectra in Figure 43. Normalization of the three curves differs to more clearly show each. Results of the empirical method are compared with results previously discussed in Figures 40 and 42. The spectra are given in Tables 7 and 8. The results obtained using the empirical spectra with 7.0 MeV and 10.5 MeV are compared with measured spectra inputs for the same energies in Figures 44 and 45. Lead is used as a reflector in these examples. The input spectra used are found in Tables 9, 10, 11, and 12.

Figure 43 Various 3.5 MeV input spectra

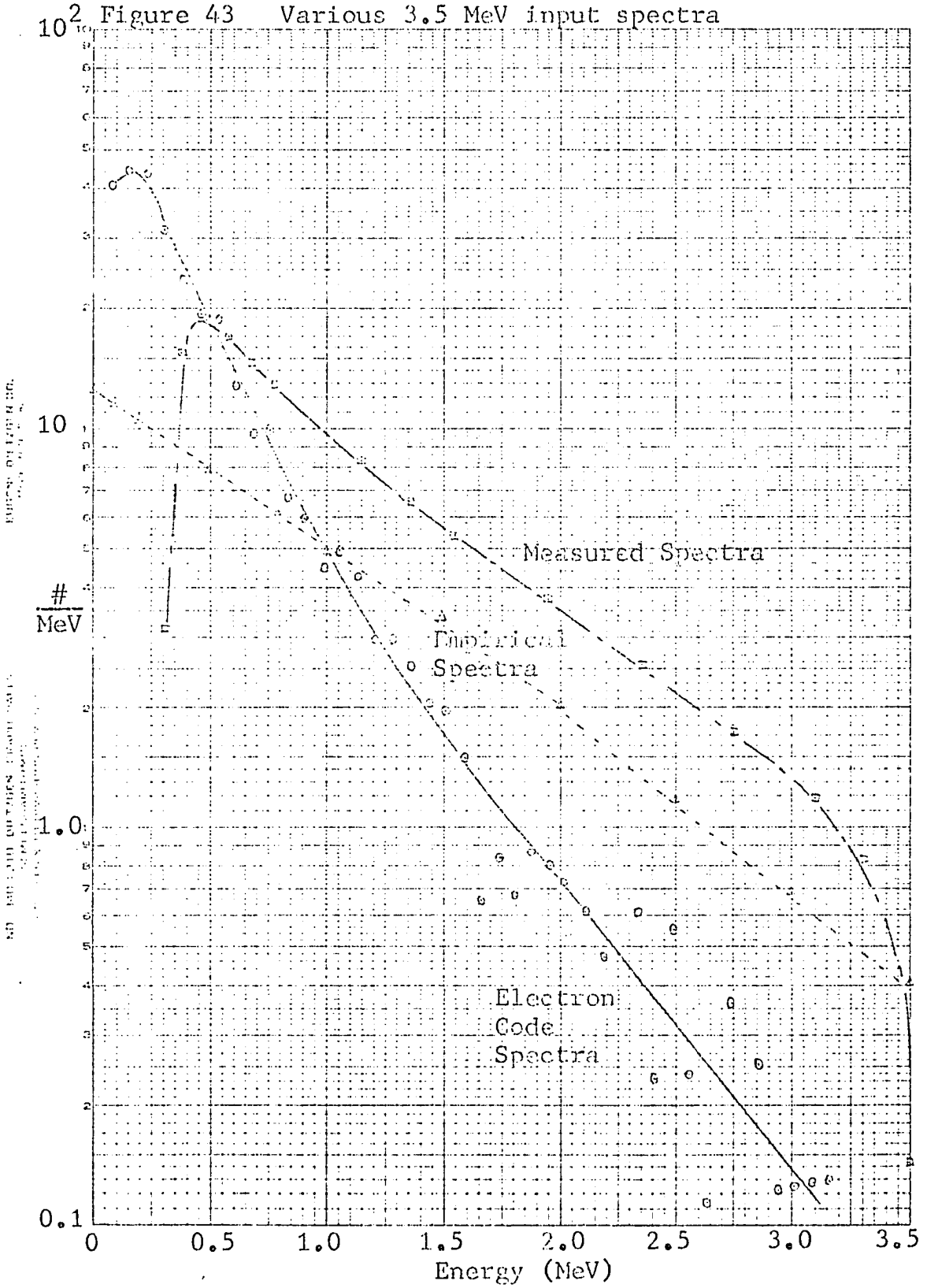

TABLE 7

2.0 MeV EMPIRICAL SPECTRA

| GROUP BOUNDS (MeV) | INPUT FLUX (Photons/MeV) |
|---|---|
| 2.00 | 0.15186 |
| 1.50 | 0.38412 |
| 1.02 | 0.72064 |
| 0.80 | 1.06659 |
| 0.60 | 1.37958 |
| 0.52 | 1.51365 |
| 0.50 | 1.63223 |
| 0.44 | 1.82633 |
| 0.38 | 2.04373 |
| 0.32 | 2.24355 |
| 0.28 | 2.39530 |
| 0.25 | 2.52180 |
| 0.225 | 2.64268 |
| 0.20 | 2.76940 |
| 0.175 | 2.90216 |
| 0.15 | 3.02695 |
| 0.13 | 3.11310 |
| 0.12 | 3.20190 |
| 0.10 | 3.29921 |
| 0.08805 | 3.37152 |
| 0.07684 | 3.40500 |
| 0.07664 | 3.43588 |
| 0.068 | 3.48987 |
| 0.060 | 3.53260 |
| 0.055 | 3.56580 |
| 0.050 | 3.59940 |
| 0.045 | 3.63320 |
| 0.040 | 3.66740 |
| 0.035 | 3.70200 |
| 0.030 | |

TABLE 8

3.5 MeV EMPIRICAL SPECTRA

| GROUP BOUNDS (MeV) | INPUT FLUX (Photons/MeV) |
|---|---|
| 3.5 | 0.040306 |
| 3.0 | 0.068831 |
| 2.5 | 0.117541 |
| 2.0 | 0.200724 |
| 1.5 | 0.338811 |
| 1.02 | 0.48852 |
| 0.8 | 0.61139 |
| 0.6 | 0.70908 |
| 0.52 | 0.74785 |
| 0.50 | 0.78068 |
| 0.44 | 0.83246 |
| 0.38 | 0.88767 |
| 0.32 | 0.93638 |
| 0.28 | 0.97209 |
| 0.25 | 1.0111 |
| 0.225 | 1.02083 |
| 0.2 | 1.05614 |
| 0.175 | 1.0848 |
| 0.15 | 1.1112 |
| 0.13 | 1.1292 |
| 0.12 | 1.14747 |
| 0.1 | 1.16727 |
| 0.088 | 1.18183 |
| 0.077 | 1.19135 |
| 0.068 | 1.20536 |
| 0.060 | 1.21377 |
| 0.055 | 1.22029 |
| 0.050 | 1.22683 |
| 0.045 | 1.23342 |
| 0.040 | 1.24003 |
| 0.035 | 1.24669 |
| 0.030 | |

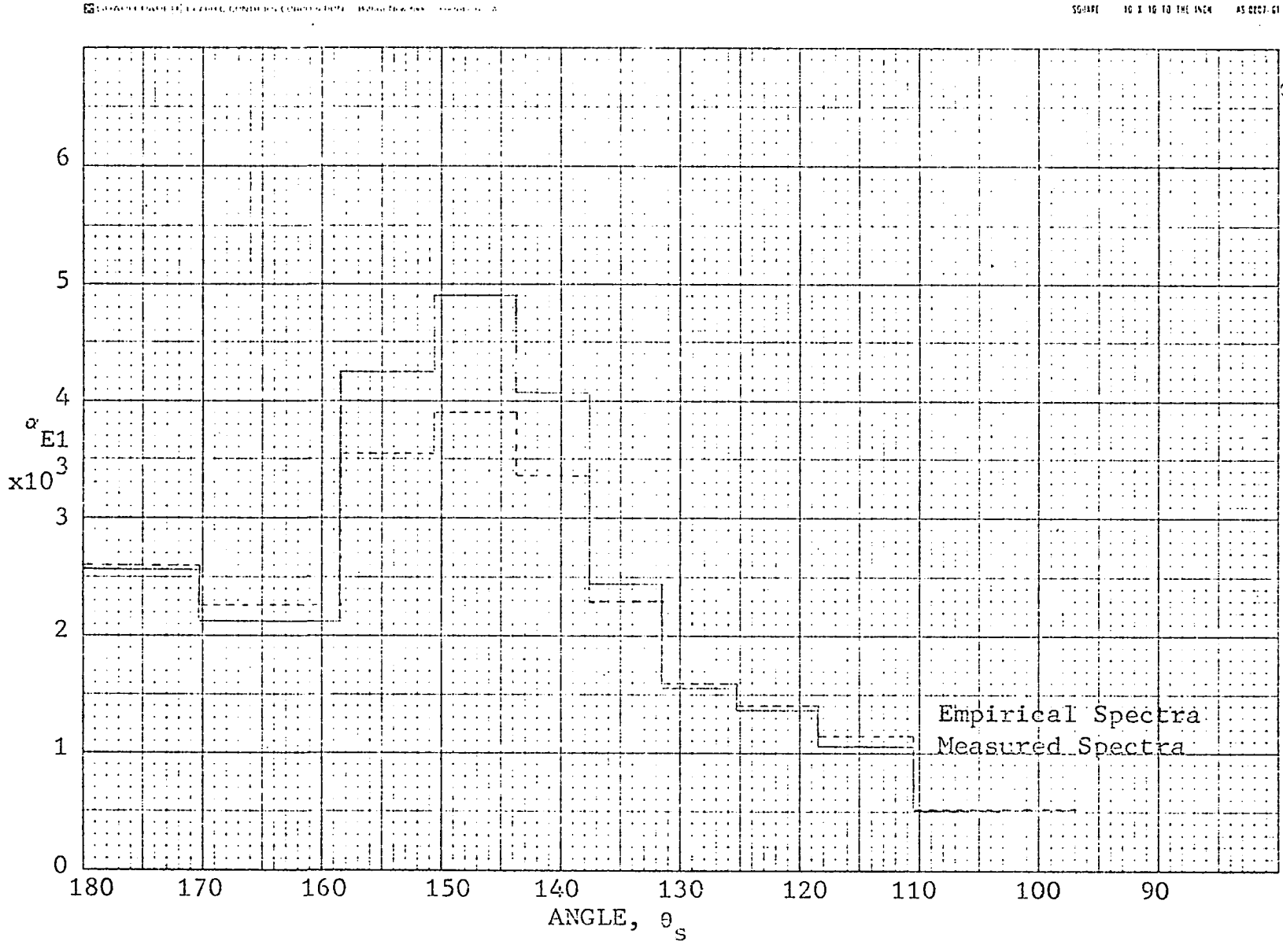


Figure 44 DTF 7.0 MeV lead scatterer

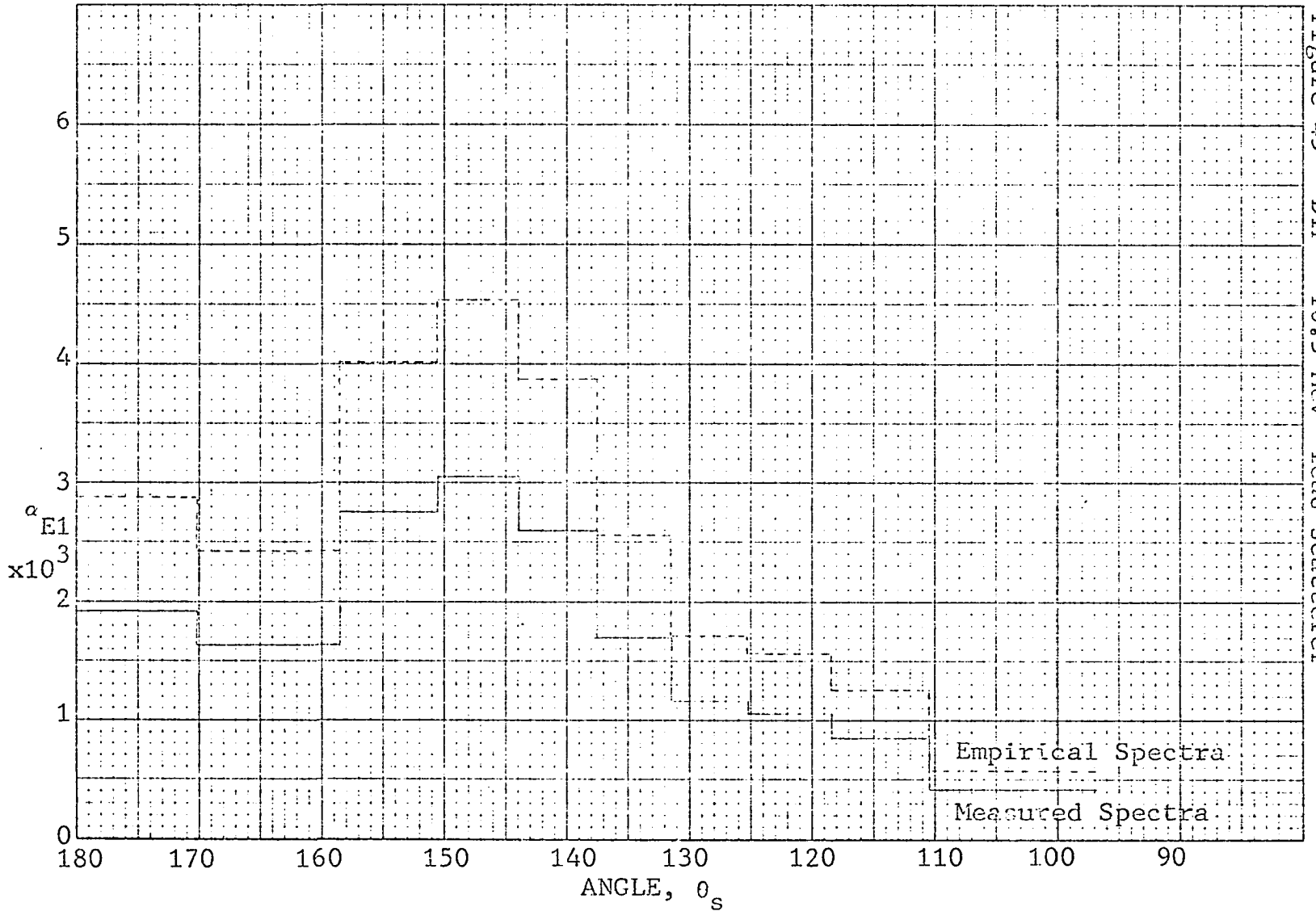


Figure 45 DTF 10.5 MeV lead scatterer

TABLE 9

7.0 MeV MEASURED SPECTRA (105)

| GROUP BOUNDS (MeV) | INPUT FLUX (Photons/MeV) |
|---|---|
| 7.0 | 1.4286 |
| 6.63 | 4.5249 |
| 6.12 | 6.5359 |
| 5.61 | 8.7344 |
| 5.1 | 10.784 |
| 4.59 | 13.508 |
| 4.08 | 16.667 |
| 3.57 | 21.008 |
| 3.06 | 26.471 |
| 2.55 | 34.118 |
| 2.04 | 46.078 |
| 1.53 | 63.399 |
| 1.275 | 76.471 |
| 1.02 | 93.137 |
| 0.765 | 95.425 |
| 0.51 | 107.840 |
| 0.40 | 0.0 |
| 0.30 | 0.0 |
| 0.10 | 0.0 |
| 0.06 | 0.0 |
| 0.03 | |

TABLE 10

7.0 MeV EMPIRICAL SPECTRA

| GROUP BOUNDS (MeV) | INPUT FLUX (Photons/MeV) |
|---|---|
| 7.0 | 0.0100723 |
| 6.0 | 0.0172003 |
| 5.0 | 0.0293728 |
| 4.0 | 0.0501598 |
| 3.0 | 0.0742656 |
| 2.5 | 0.0970494 |
| 2.0 | 0.126823 |
| 1.5 | 0.164807 |
| 1.02 | 0.198325 |
| 0.8 | 0.221891 |
| 0.6 | 0.239058 |
| 0.52 | 0.245523 |
| 0.5 | 0.250845 |
| 0.44 | 0.25903 |
| 0.38 | 0.267482 |
| 0.32 | 0.274729 |
| 0.28 | 0.279921 |
| 0.25 | 0.28407 |
| 0.225 | 0.287896 |
| 0.2 | 0.291773 |
| 0.175 | 0.295703 |
| 0.15 | 0.299285 |
| 0.13 | 0.301695 |
| 0.12 | 0.304128 |
| 0.10 | 0.306742 |
| 0.088005 | 0.308649 |
| 0.07684 | 0.309588 |
| 0.07664 | 0.310322 |
| 0.068 | 0.311706 |
| 0.06 | 0.312792 |
| 0.055 | 0.31363 |
| 0.05 | 0.314471 |
| 0.045 | 0.315313 |
| 0.04 | 0.316158 |
| 0.035 | 0.317005 |
| 0.03 | |

TABLE 11

10.5 MeV MEASURED SPECTRA (110)

| GROUP BOUNDS (MeV) | INPUT FLUX (Photons/MeV) |
|---|---|
| 10.5 | 1.18 |
| 10.0 | 2.3 |
| 9.5 | 5.3 |
| 9.0 | 12.5 |
| 8.0 | 18.5 |
| 7.0 | 24.0 |
| 6.0 | 31.0 |
| 5.0 | 38.0 |
| 4.5 | 46.0 |
| 4.0 | 53.0 |
| 3.5 | 70.0 |
| 3.0 | 87.0 |
| 2.5 | 125.0 |
| 2.0 | 190.0 |
| 1.5 | 300.0 |
| 1.2 | 450.0 |
| 1.02 | 640.0 |
| 0.8 | 760.0 |
| 0.6 | 830.0 |
| 0.52 | 870.0 |
| 0.5 | 900.0 |
| 0.44 | 980.0 |
| 0.38 | 1112.0 |
| 0.32 | 1500.0 |
| 0.28 | 1500.0 |
| 0.25 | 1500.0 |
| 0.225 | 1112.0 |
| 0.2 | 980.0 |
| 0.175 | 900.0 |
| 0.15 | 450.0 |
| 0.13 | 0.0 |
| 0.12 | 0.0 |
| 0.10 | 0.0 |
| 0.0880 | 0.0 |
| 0.07684 | 0.0 |
| 0.07664 | 0.0 |

TABLE 11 (cont'd)

| GROUP BOUNDS (MeV) | INPUT FLUX (Photons/MeV) |
|---|---|
| 0.070 | 0.0 |
| 0.06 | 0.0 |
| 0.05 | 0.0 |
| 0.04 | 0.0 |
| 0.03 | |

TABLE 12

10.5 MeV EMPIRICAL SPECTRA

| GROUP BOUNDS (MeV) | INPUT FLUX (Photons/MeV) |
|---|---|
| 10.5 | 0.035003 |
| 10.0 | 0.045268 |
| 9.0 | 0.065839 |
| 8.0 | 0.0957568 |
| 7.0 | 0.13927 |
| 6.0 | 0.202555 |
| 5.0 | 0.294598 |
| 4.0 | 0.428466 |
| 3.0 | 0.564976 |
| 2.5 | 0.681355 |
| 2.0 | 0.821707 |
| 1.5 | 0.987151 |
| 1.02 | 1.12425 |
| 0.8 | 1.2162 |
| 0.6 | 1.28143 |
| 0.52 | 1.30561 |
| 0.5 | 1.32535 |
| 0.44 | 1.35547 |
| 0.38 | 1.38629 |
| 0.32 | 1.41248 |
| 0.28 | 1.43111 |
| 0.25 | 1.44593 |
| 0.225 | 1.45954 |
| 0.2 | 1.47327 |
| 0.175 | 1.48713 |
| 0.15 | 1.49972 |
| 0.13 | 1.50816 |
| 0.12 | 1.51666 |
| 0.10 | 1.52578 |
| 0.088005 | 1.53241 |
| 0.07684 | 1.53567 |
| 0.07664 | 1.53764 |
| 0.07 | 1.54244 |
| 0.06 | 1.54823 |
| 0.05 | 1.55404 |
| 0.04 | 1.55988 |
| 0.03 | |

Absorption measurements by Kirtland Air Force personnel indicate an effective energy of 4.1 - 4.2 MeV for the 7.0 MeV flash x-ray machine, as discussed in Section 5.

Absorption measurements of the HERMES II beam are shown in Figures 46 and 47. The curve in Figure 46 was made with a 70 mil tantalum x-ray target and 0.3125 inch aluminum filter while Figure 47 was made with a 60 mil tantalum target and 0.4 inch aluminum filter. The effect of the additional filter in "hardening" the beam can be seen. In the first case one gets a 58% component at 3.8 to 4.2 MeV and a 42% component of 0.27 - 0.28 MeV. The second set-up indicates about 75% at 4.9 - 5.5 MeV and 25% at 0.11 - 0.15 MeV. The tube configuration at the time data was taken for this research was a 60 mil tantalum target backed by a 0.3125 inch aluminum plate.

None of the measured spectra referenced give photon flux for less than 200 - 300 KeV. There is considerable debate as to the amount of energy carried in the low energy range of the spectra. Some (123) feel that the low energy count goes significantly higher than any other portion of the spectra, while others (104, 105) indicate a drop to zero below 100 KeV. Something in between these two views

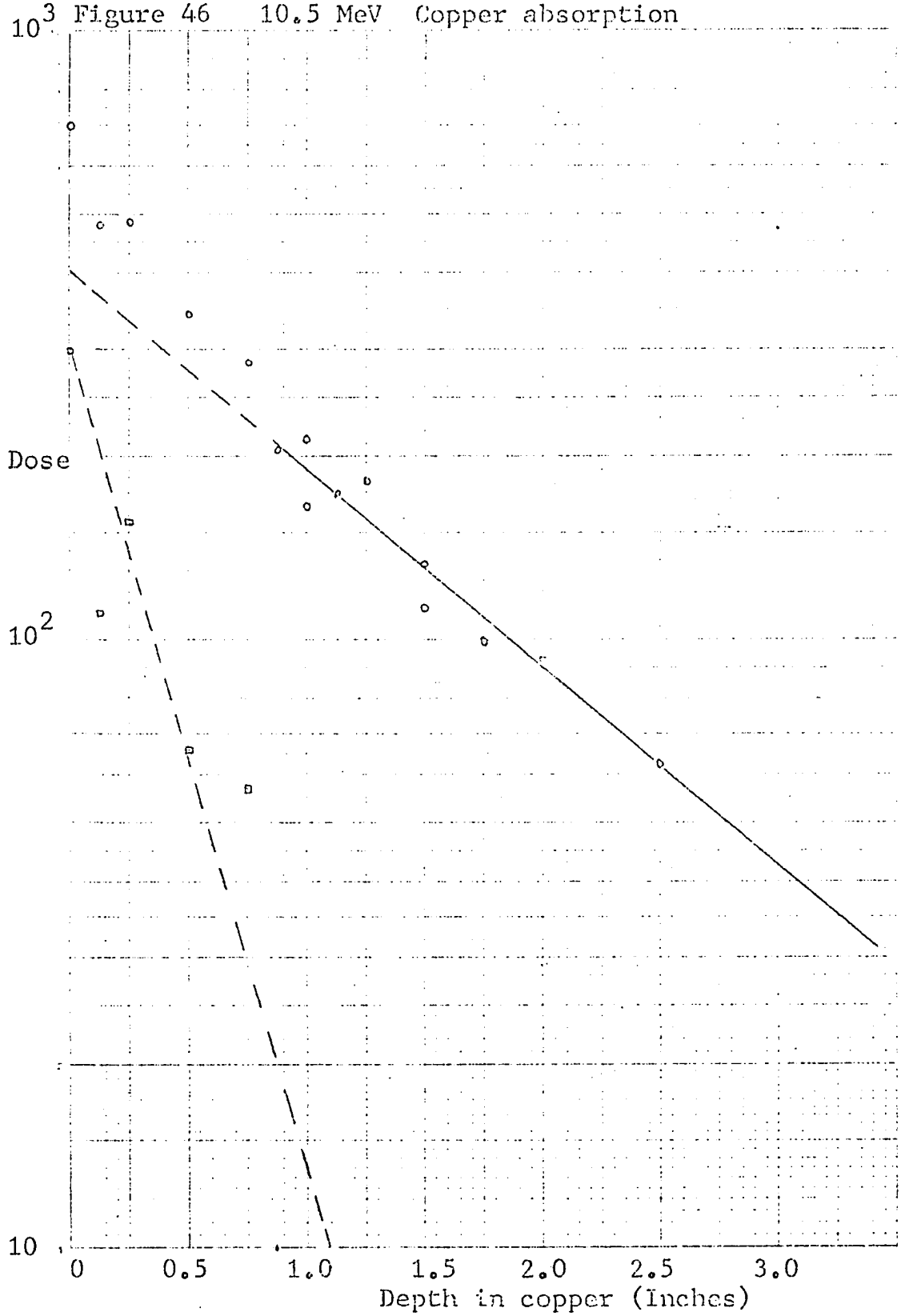
$10^3$ Figure 46 10.5 MeV Copper absorption
Dose
$10^2$
10
0
0.5
1.0
1.5
2.0
2.5
3.0
Depth in copper (Inches)

Figure 47 10.5 MeV copper absorption

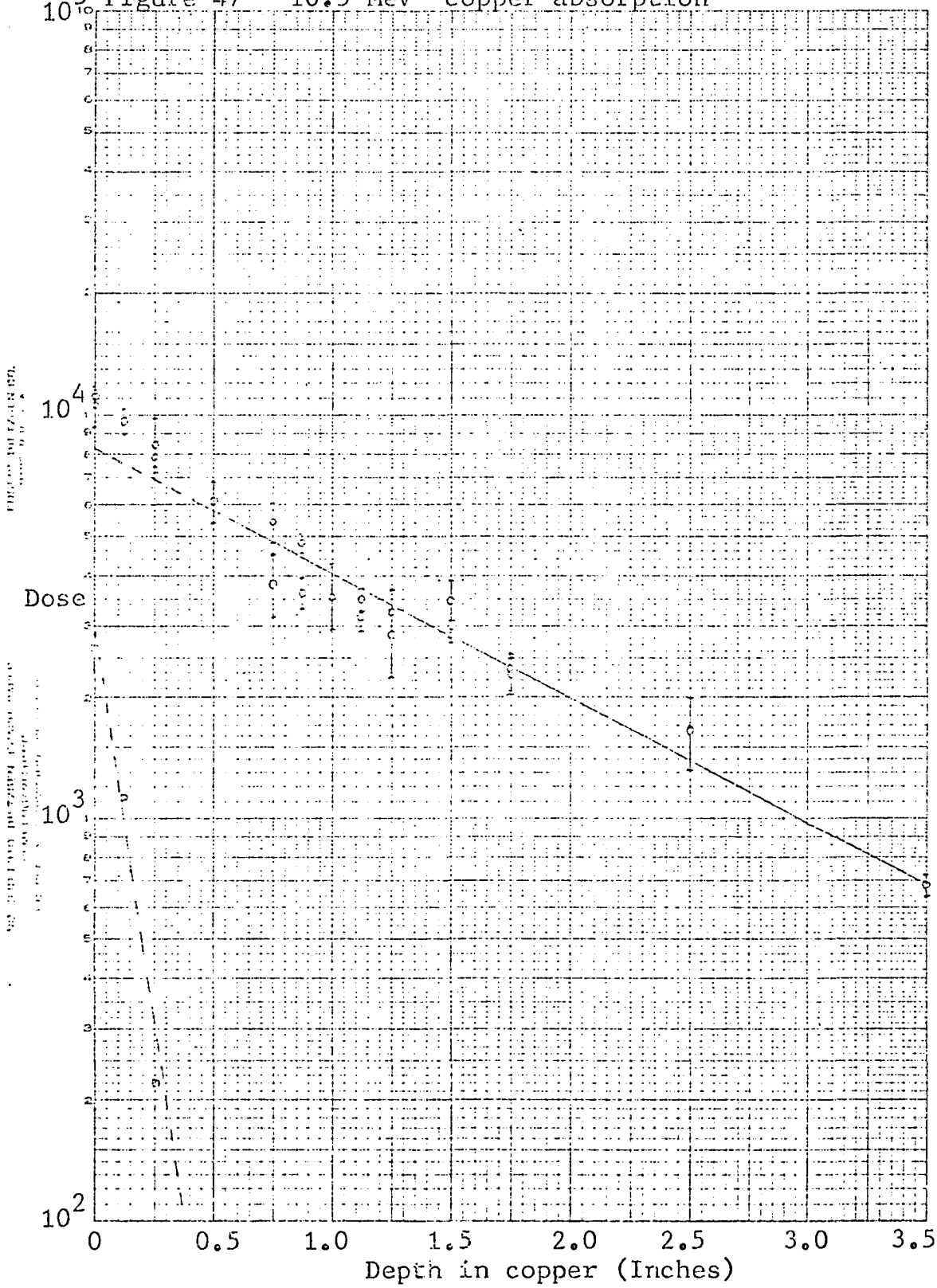

is probably more nearly the correct representation. To the primary mission of the x-ray devices studied (i.e. dose deposition inside a steel-encased body) the question of low energy population is largely academic. The effect on the present experiments is shown in Figure 48. The input spectra for these curves are given in Table 13. The total energy albedo from iron is reduced 31.8% by increasing the low energy component of the beam by the amounts shown. The difference the additional filter used at 7.0 MeV would make on the 10.5 MeV spectrum is shown in Figures 49 and 50.

Figure 48 DTF 10.5 MeV iron scatterer

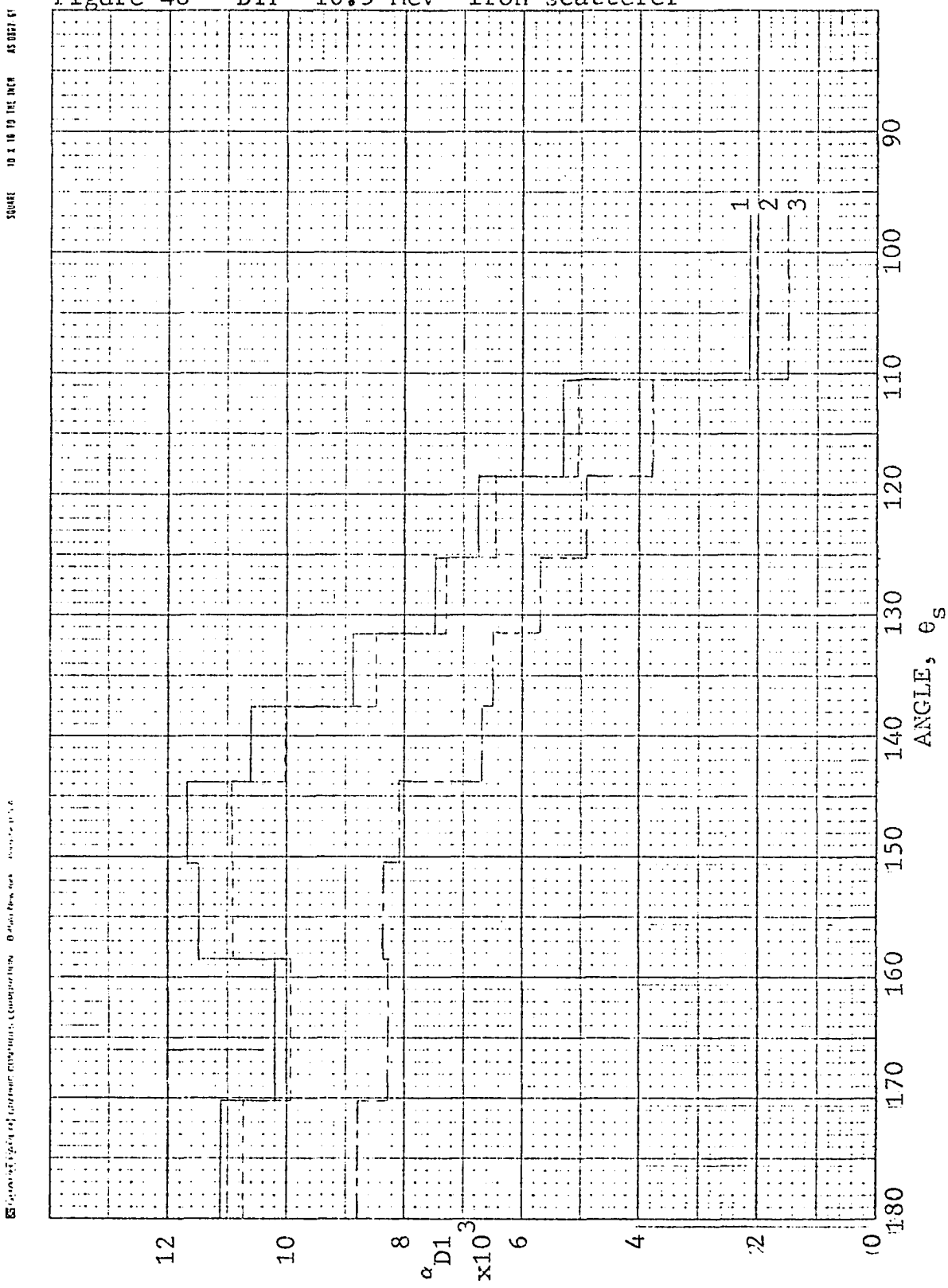

TABLE 13

10.5 MeV SPECTRA

| GROUP BOUNDS (MeV) | INPUT FLUX 1 (Photons/MeV) | INPUT FLUX 2 (Photons/MeV) | INPUT FLUX 3 (Photons/MeV) |
|---|---|---|---|
| 10.5 | 1.18 | 1.18 | 1.18 |
| 10.0 | 2.3 | 2.3 | 2.3 |
| 9.5 | 5.3 | 5.3 | 5.3 |
| 9.0 | 12.5 | 12.5 | 12.5 |
| 8.0 | 18.5 | 18.5 | 18.5 |
| 7.0 | 24.0 | 24.0 | 24.0 |
| 6.0 | 31.0 | 31.0 | 31.0 |
| 5.0 | 38.0 | 38.0 | 38.0 |
| 4.5 | 46.0 | 46.0 | 46.0 |
| 4.0 | 53.0 | 53.0 | 53.0 |
| 3.5 | 70.0 | 70.0 | 70.0 |
| 3.0 | 87.0 | 87.0 | 87.0 |
| 2.5 | 125.0 | 125.0 | 125.0 |
| 2.0 | 190.0 | 190.0 | 190.0 |
| 1.5 | 300.0 | 300.0 | 300.0 |
| 1.2 | 450.0 | 450.0 | 450.0 |
| 1.02 | 640.0 | 640.0 | 640.0 |
| 0.8 | 760.0 | 760.0 | 760.0 |
| 0.6 | 830.0 | 830.0 | 830.0 |
| 0.52 | 870.0 | 870.0 | 870.0 |
| 0.5 | 900.0 | 900.0 | 900.0 |
| 0.44 | 980.0 | 980.0 | 980.0 |
| 0.38 | 1112.0 | 1112.0 | 1112.0 |
| 0.32 | 1500.0 | 1500.0 | 1500.0 |
| 0.28 | 1500.0 | 1500.0 | 1800.0 |
| 0.25 | 1500.0 | 1500.0 | 2600.0 |
| 0.225 | 1112.0 | 1500.0 | 3000.0 |
| 0.20 | 980.0 | 1500.0 | 4000.0 |
| 0.175 | 900.0 | 1500.0 | 5600.0 |
| 0.15 | 450.0 | 1500.0 | 8000.0 |
| 0.13 | 0.0 | 1500.0 | 10000.0 |
| 0.12 | 0.0 | 1500.0 | 13000.0 |
| 0.10 | 0.0 | 1500.0 | 17000.0 |
| 0.088 | 0.0 | 1500.0 | 18500.0 |
| 0.07684 | 0.0 | 1500.0 | 19000.0 |
| 0.07664 | 0.0 | 1500.0 | 19000.0 |
| 0.07 | 0.0 | 1500.0 | 19500.0 |
| 0.06 | 0.0 | 1500.0 | 20000.0 |
| 0.05 | 0.0 | 1500.0 | 21500.0 |
| 0.04 | 0.0 | 1500.0 | 22500.0 |

Figure 49 10.5 MeV Spectra 1

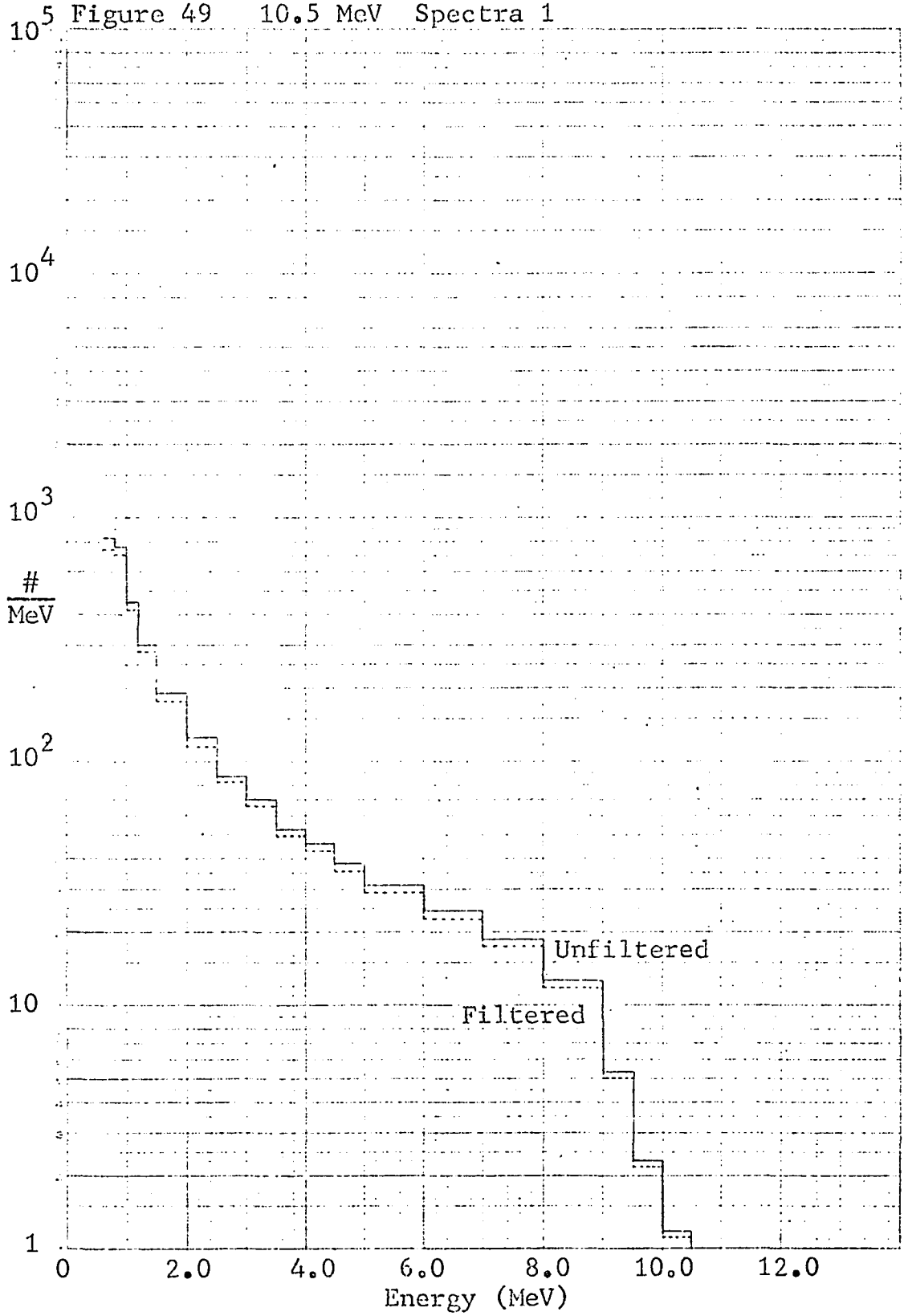

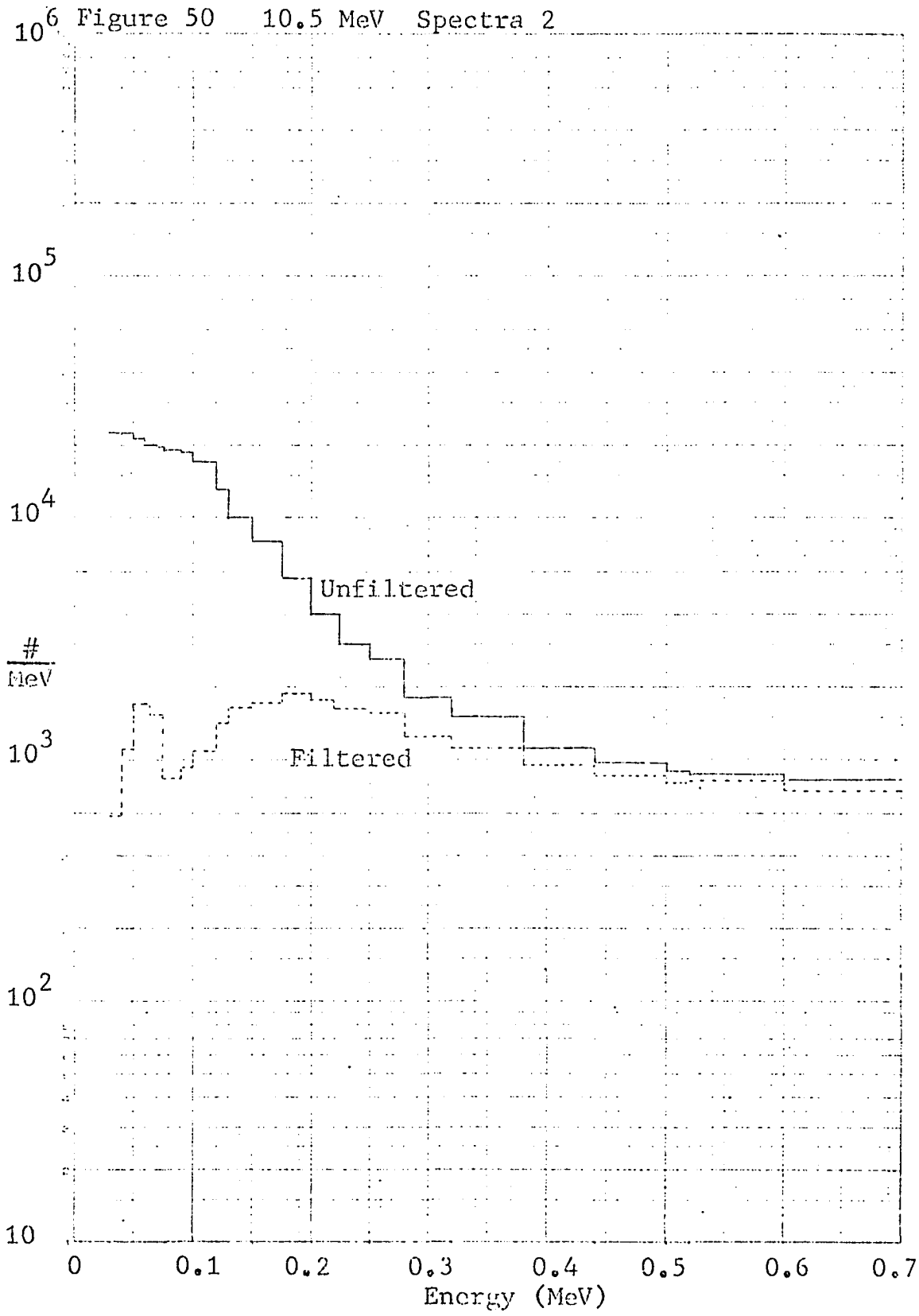
Figure 50 10.5 MeV Spectra 2
$10^6$
$10^5$
$10^4$
$10^3$
$10^2$
10
# / MeV
Unfiltered
Filtered
0
0.1
0.2
0.3
0.4
0.5
0.6
0.7
Energy (MeV)

Differential albedo plots for input bremsstrahlung spectra of different peak energies are given in Figure 51 with concrete as the scattering medium. As the input energy increases, DTF can be seen to predict a somewhat cyclic variation with angle. This tendency is more pronounced with higher Z materials and is shown to be quite distinct in Figure 45. This variation is also evident with single energy spectra inputs and is at odds with experimental data previously published for gamma sources. A comparison of DTF and Monte Carlo results with experimental data published elsewhere is shown in Figures 88 and 89.

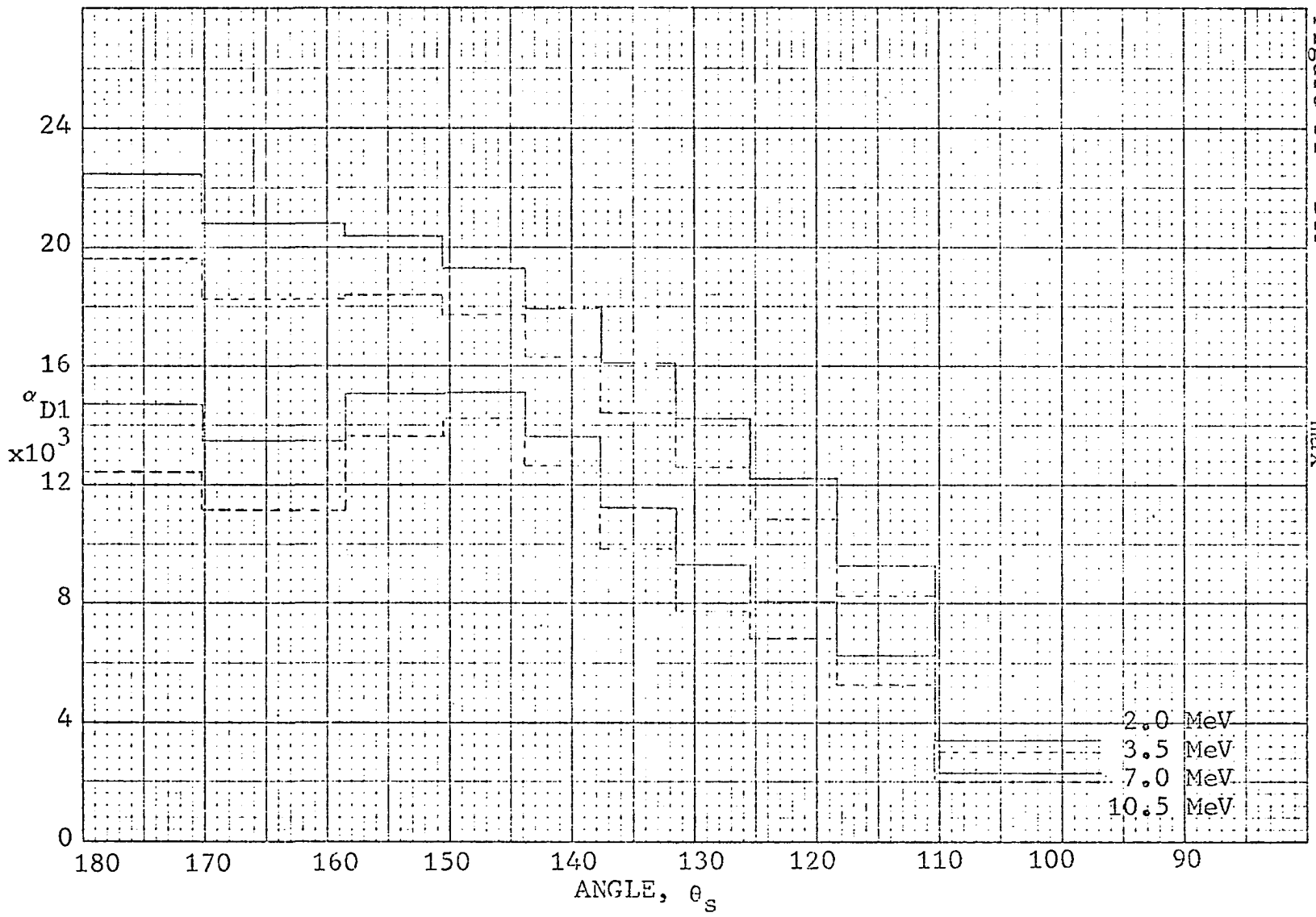


Figure 51 DTF Various $E_{max}$ concrete scatterer

D.29 REFLECTED SPECTRA

Physical measurement of the reflected spectra for backscatter flux with the flash x-ray machines was not possible, as is discussed in Section 3. Due to the steady-state operation mode of the Van de Graaff, some scintillation measurements of reflected spectra were possible at 2.0 MeV. The crystal used (described in Section 3) was canned in 0.032" aluminum which gives a transmission of about 65% at 70 KeV decreasing to 12% at 30 KeV. Due to the rapidly shifting gain evidenced by the detector system functioning in the high radiation background existing in the radiographic bay, no effort was made to correct the spectra obtained. Figures 52 and 53 are examples of the spectra obtained.

Greater spectra information is necessary to make collimator length and TLD response corrections. Spectral results from DTF and Monte Carlo runs are plotted in Figures 54 to 71 for the materials and energies used in this work. These spectra were used for the corrections discussed in Appendices C and E.

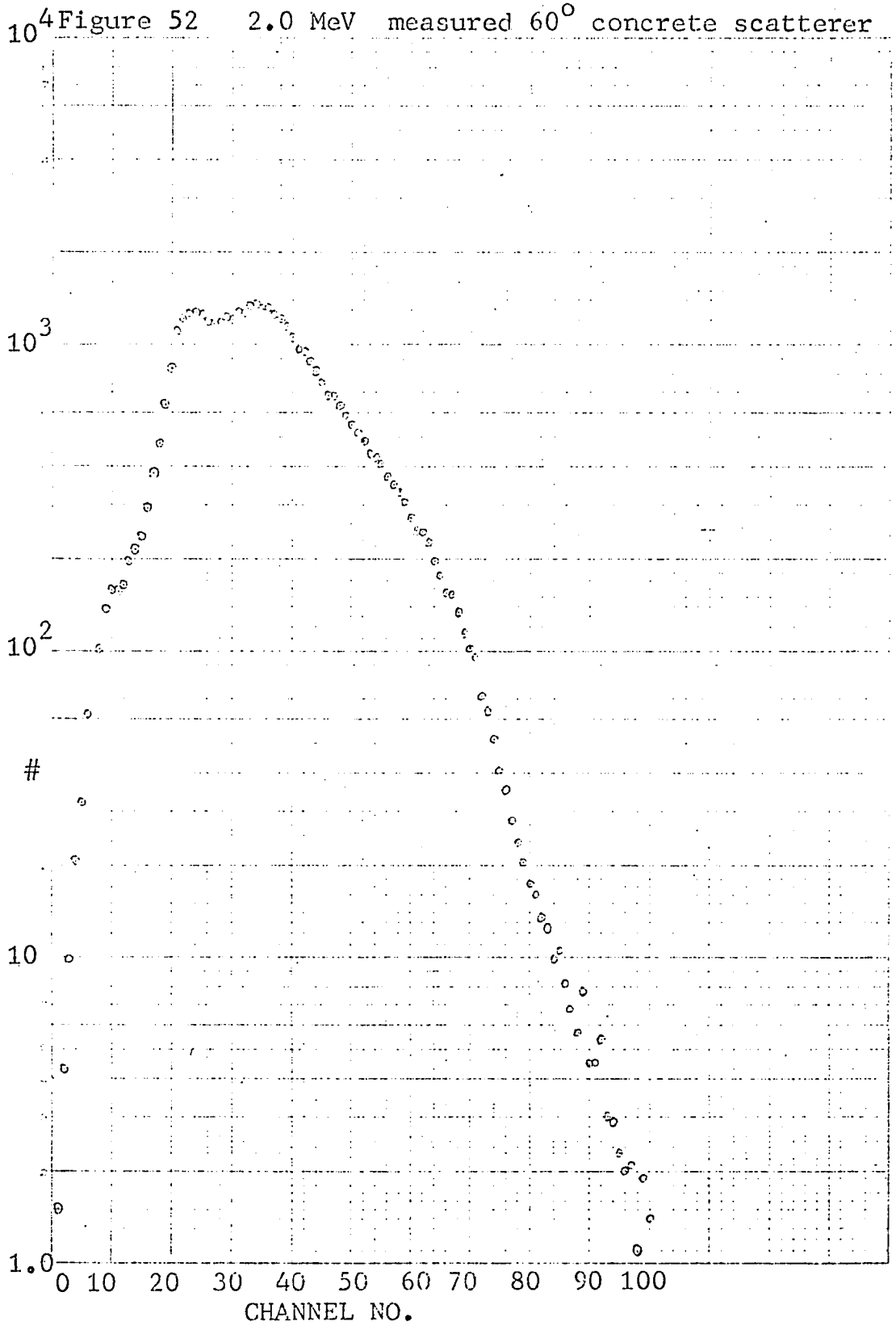


Figure 52 2.0 MeV measured $60^o$ concrete scatterer

4Figure 53 2.0 MeV measured 30° lead scatterer

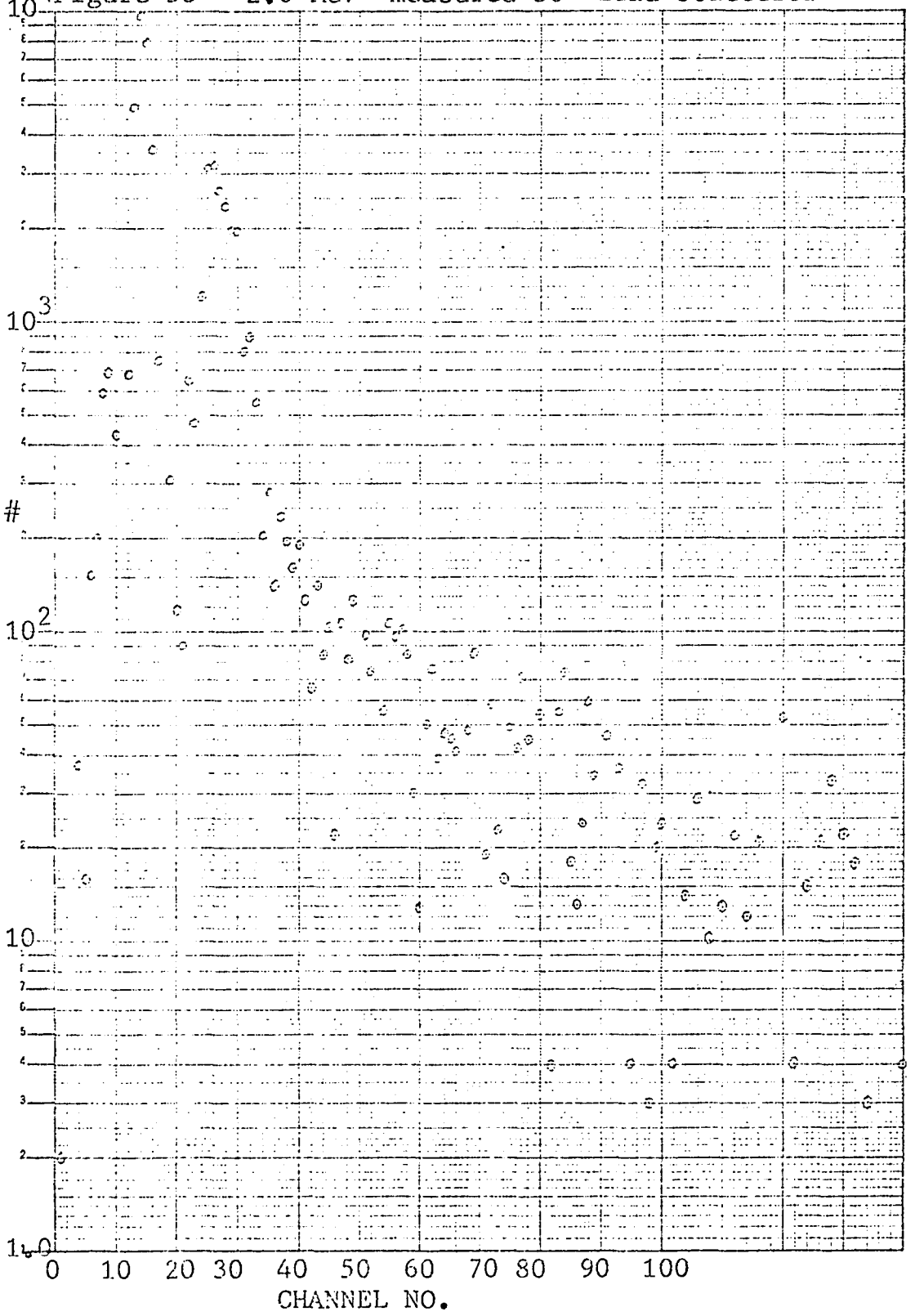

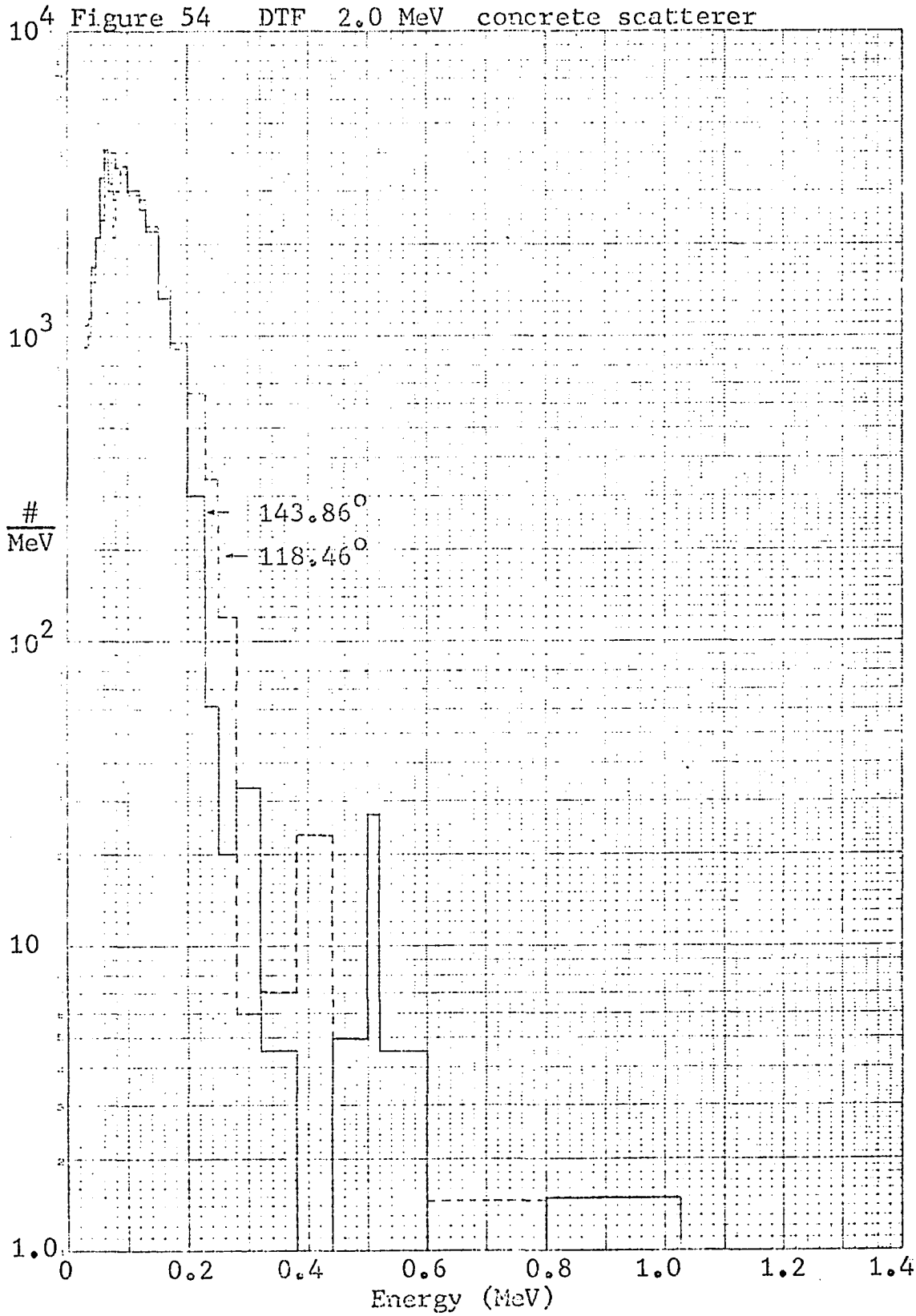
Figure 54 DTF 2.0 MeV concrete scatterer
10^4
10^3
#/MeV
10^2
10
1.0
143.86°
118.46°
0
0.2
0.4
0.6
0.8
1.0
1.2
1.4
Energy (MeV)

Figure 55 DTF 2.0 MeV iron scatterer

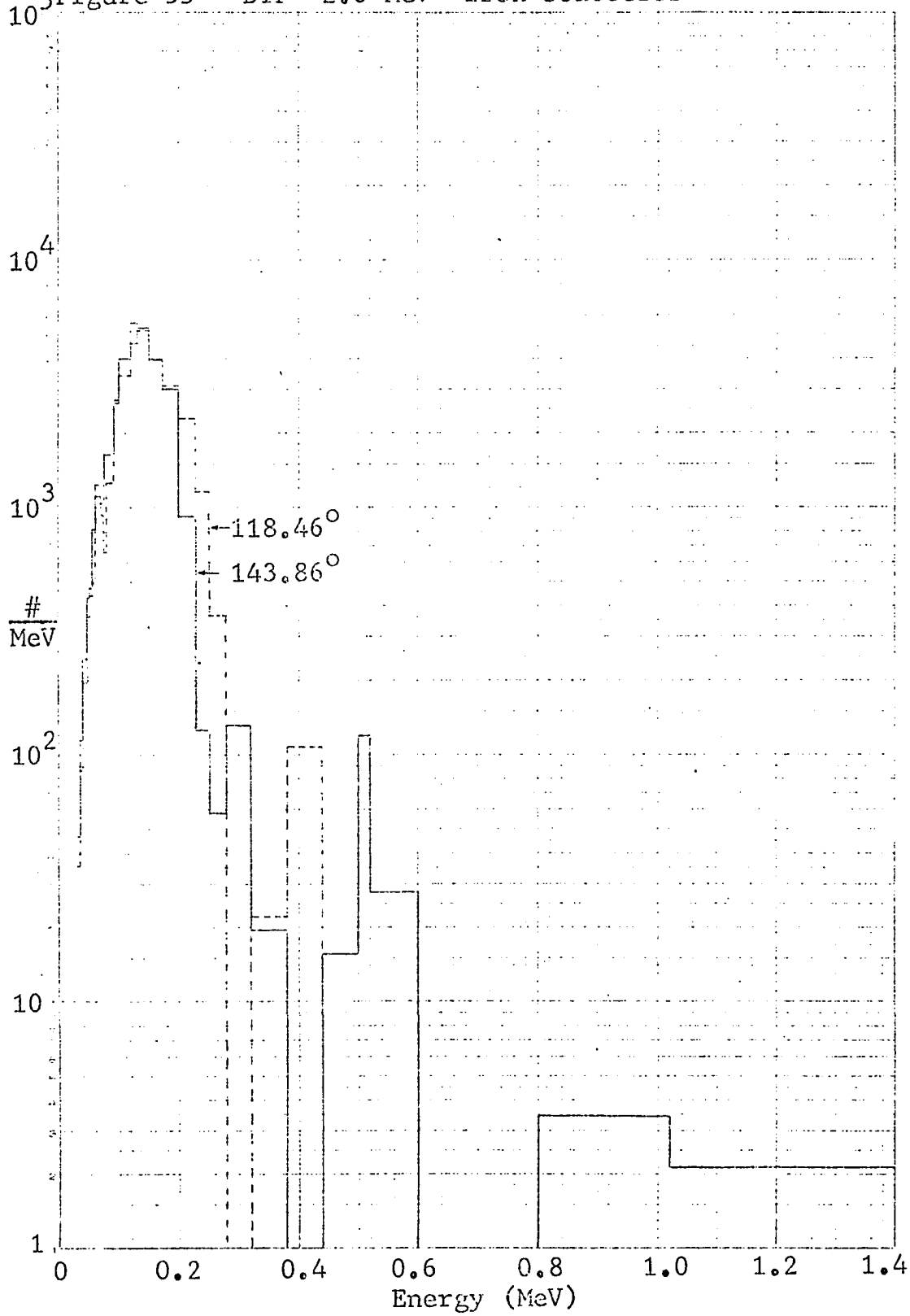

Figure 56 DTF 2.0 MeV lead scatterer

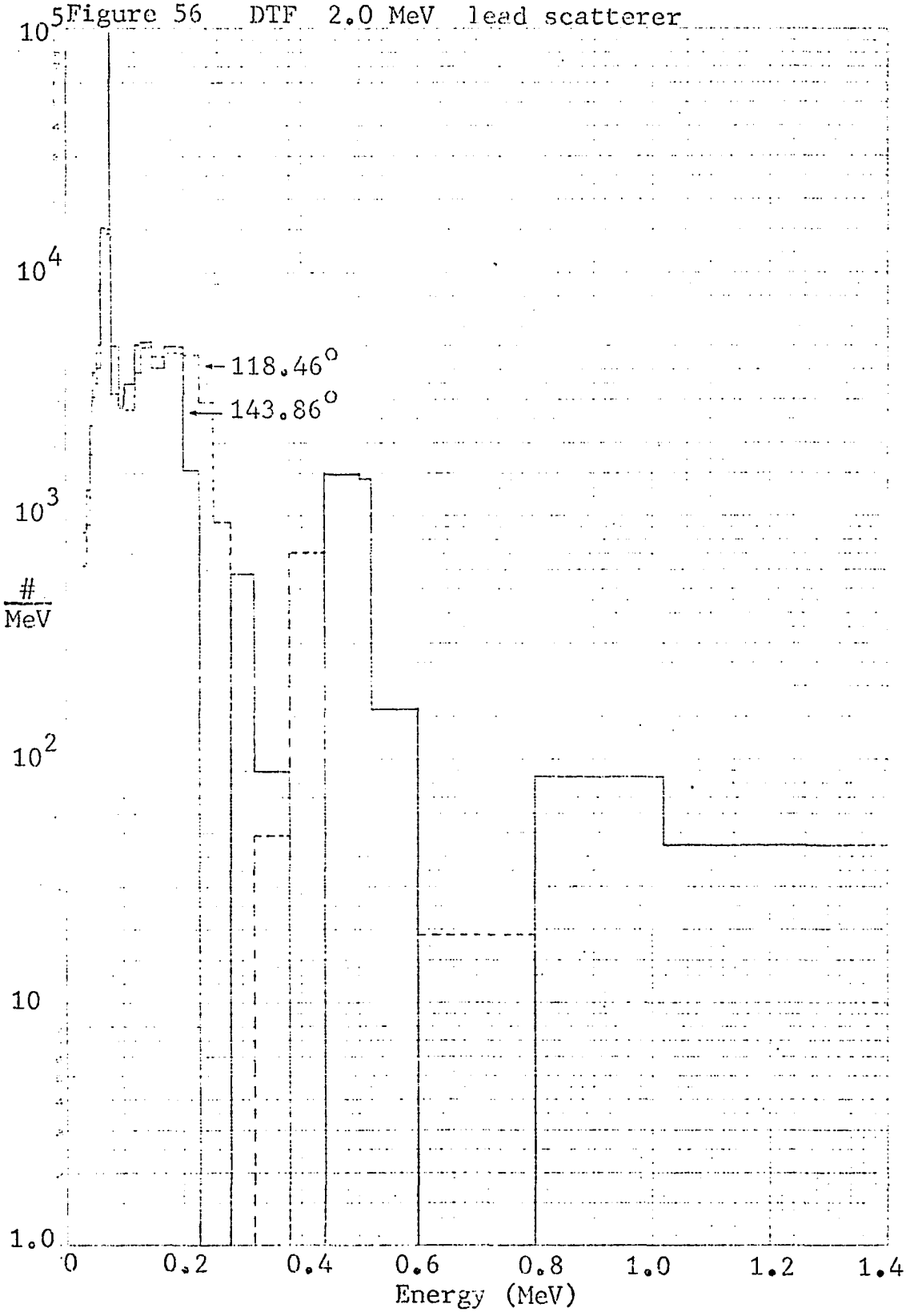

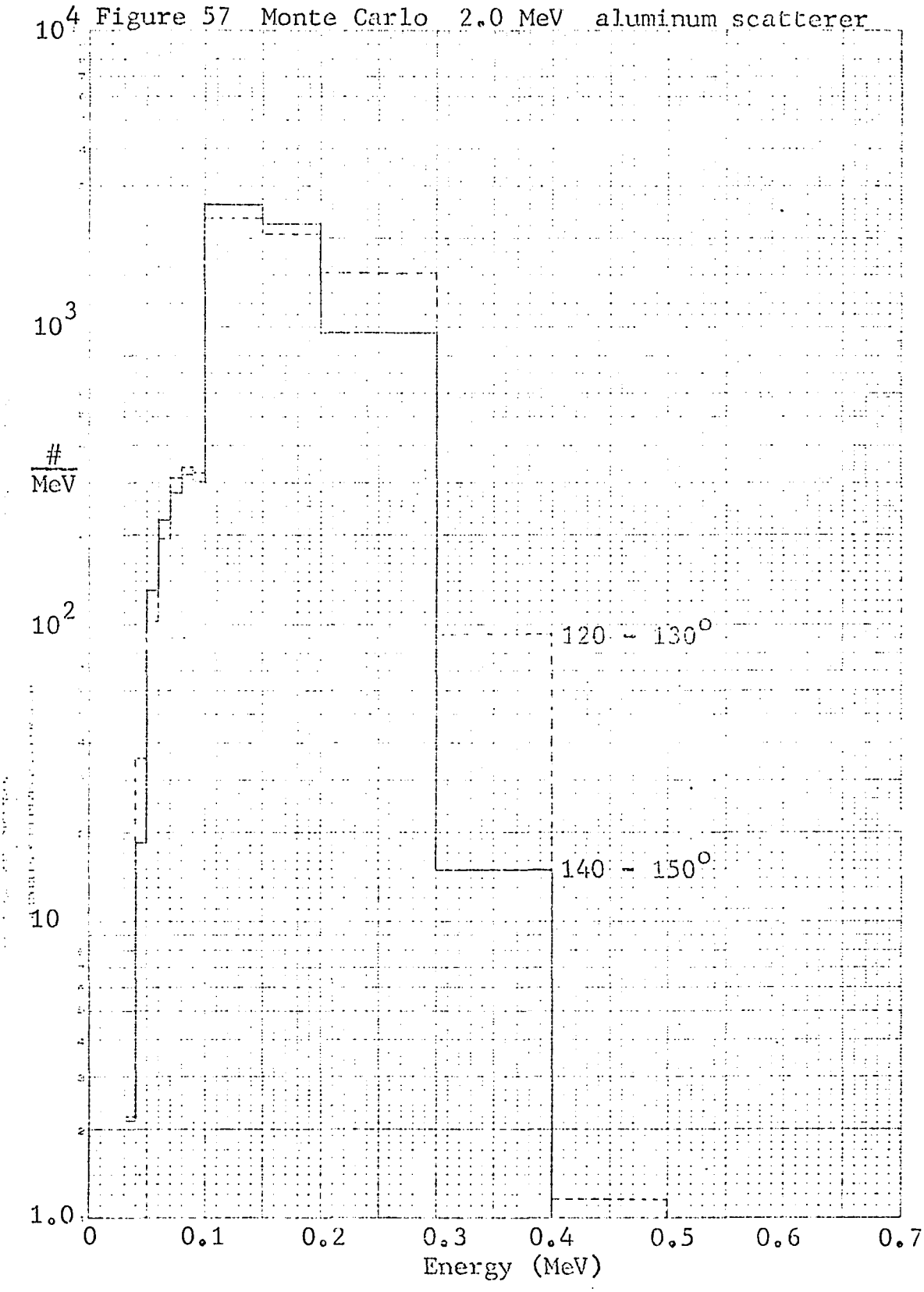
Figure 57 Monte Carlo 2.0 MeV aluminum scatterer
$10^4$
$10^3$
$10^2$
10
1.0
# / MeV
120 - 130°
140 - 150°
0
0.1
0.2
0.3
0.4
0.5
0.6
0.7
Energy (MeV)

Figure 58 Monte Carlo 2.0 MeV lead scatterer

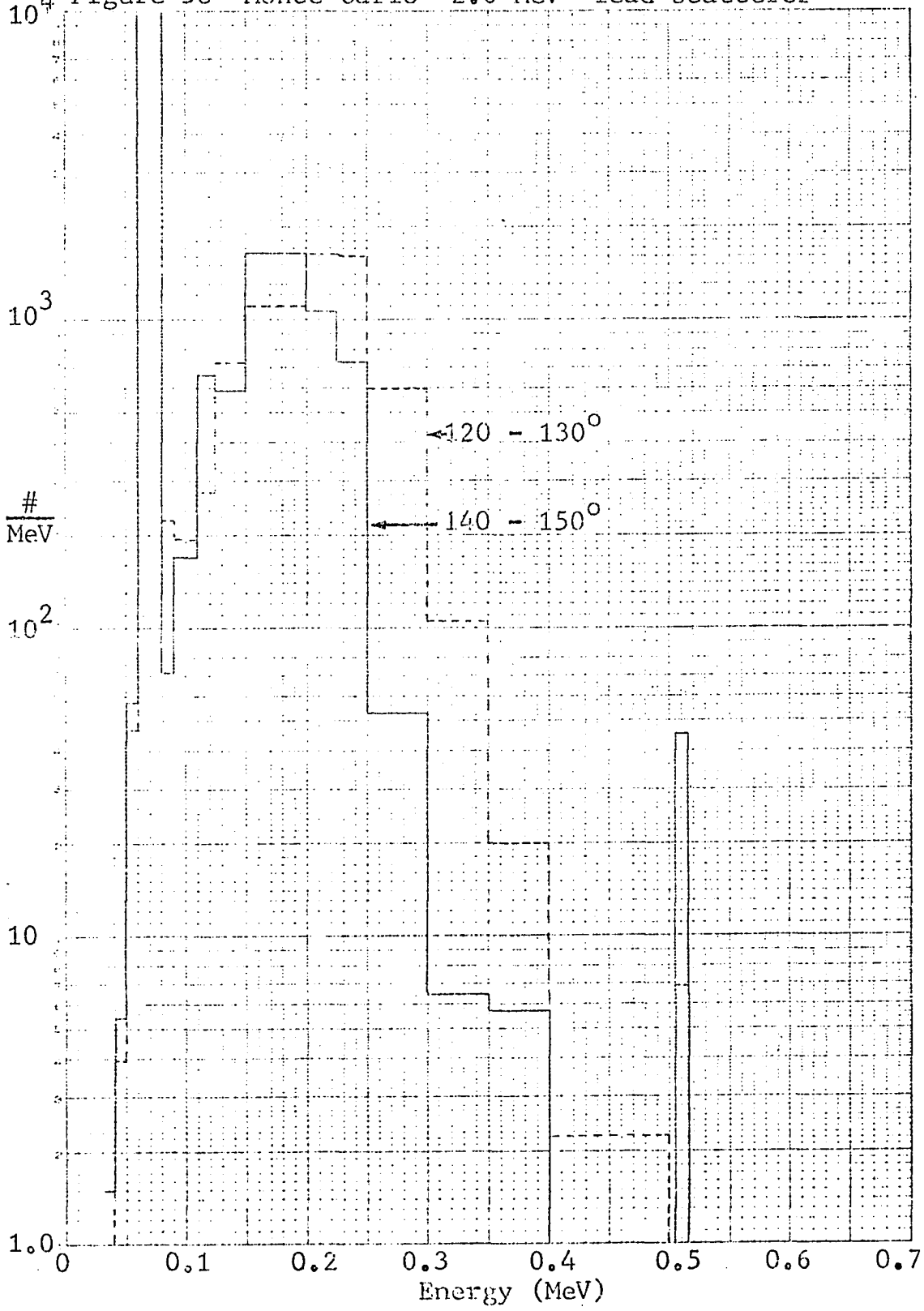

Figure 59 DTF 3.5 MeV concrete scatterer

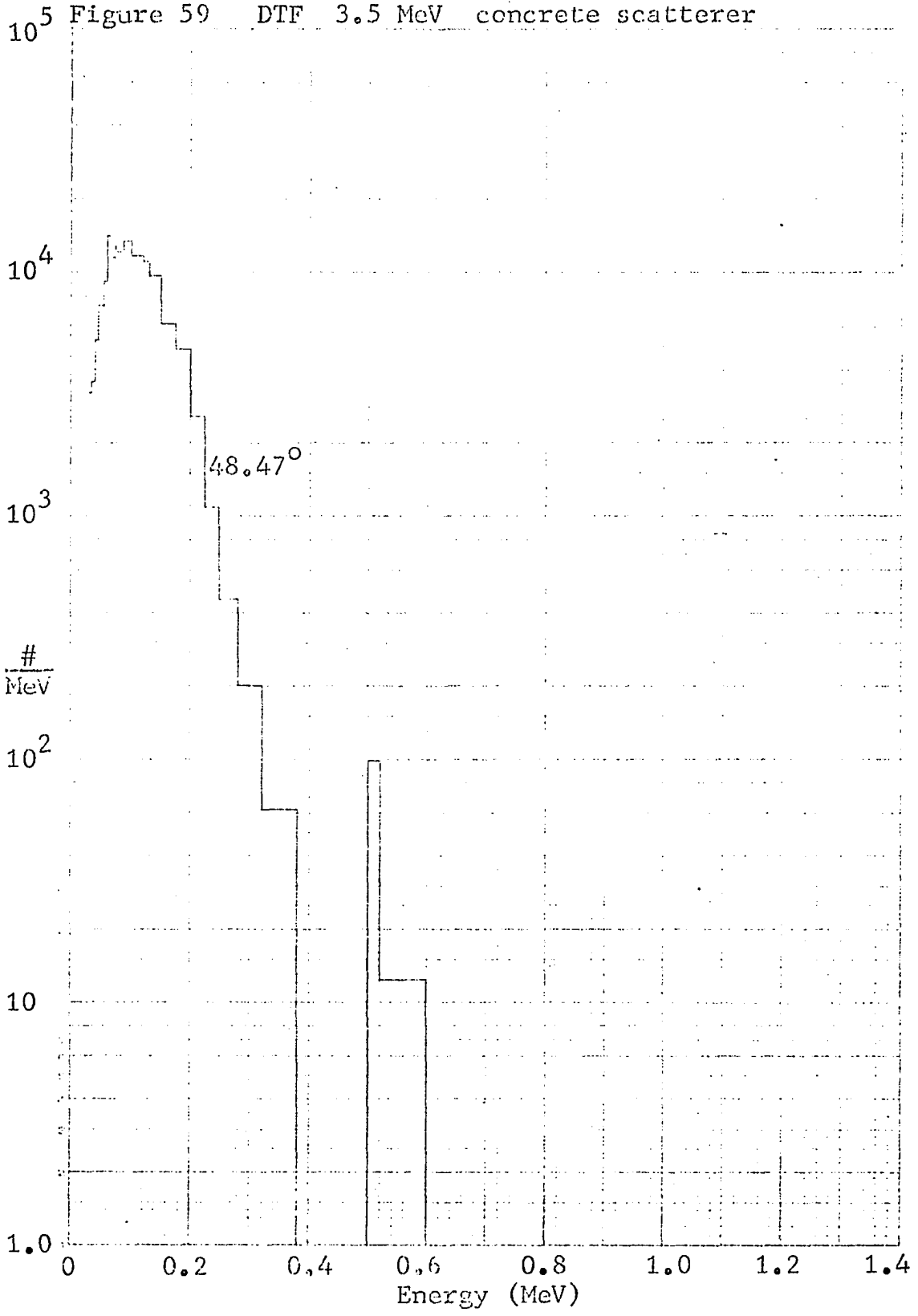

$10^5$ Figure 60 DTF 3.5 MeV iron scatterer

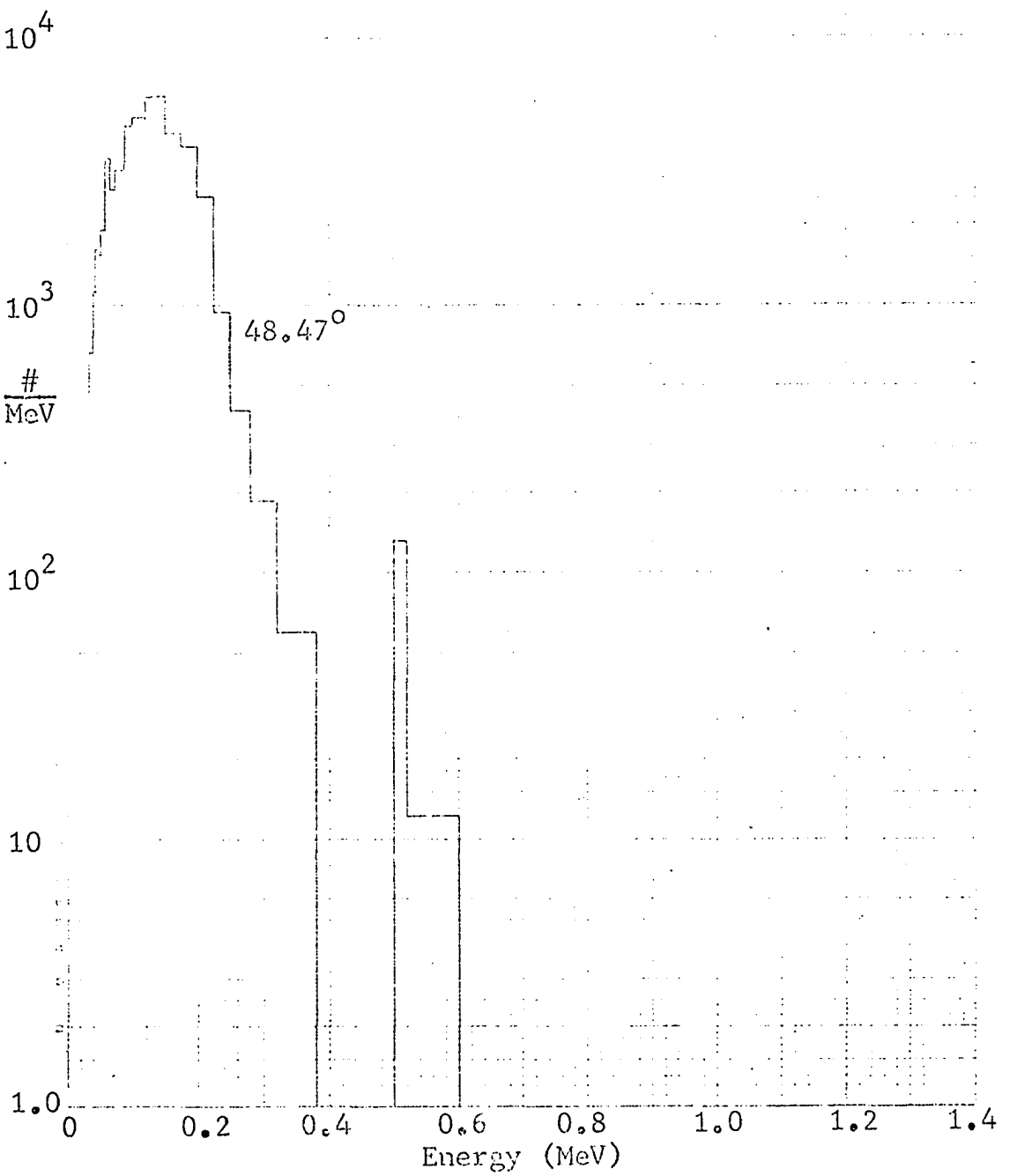

Figure 61 DTF 3.5 MeV lead scatterer

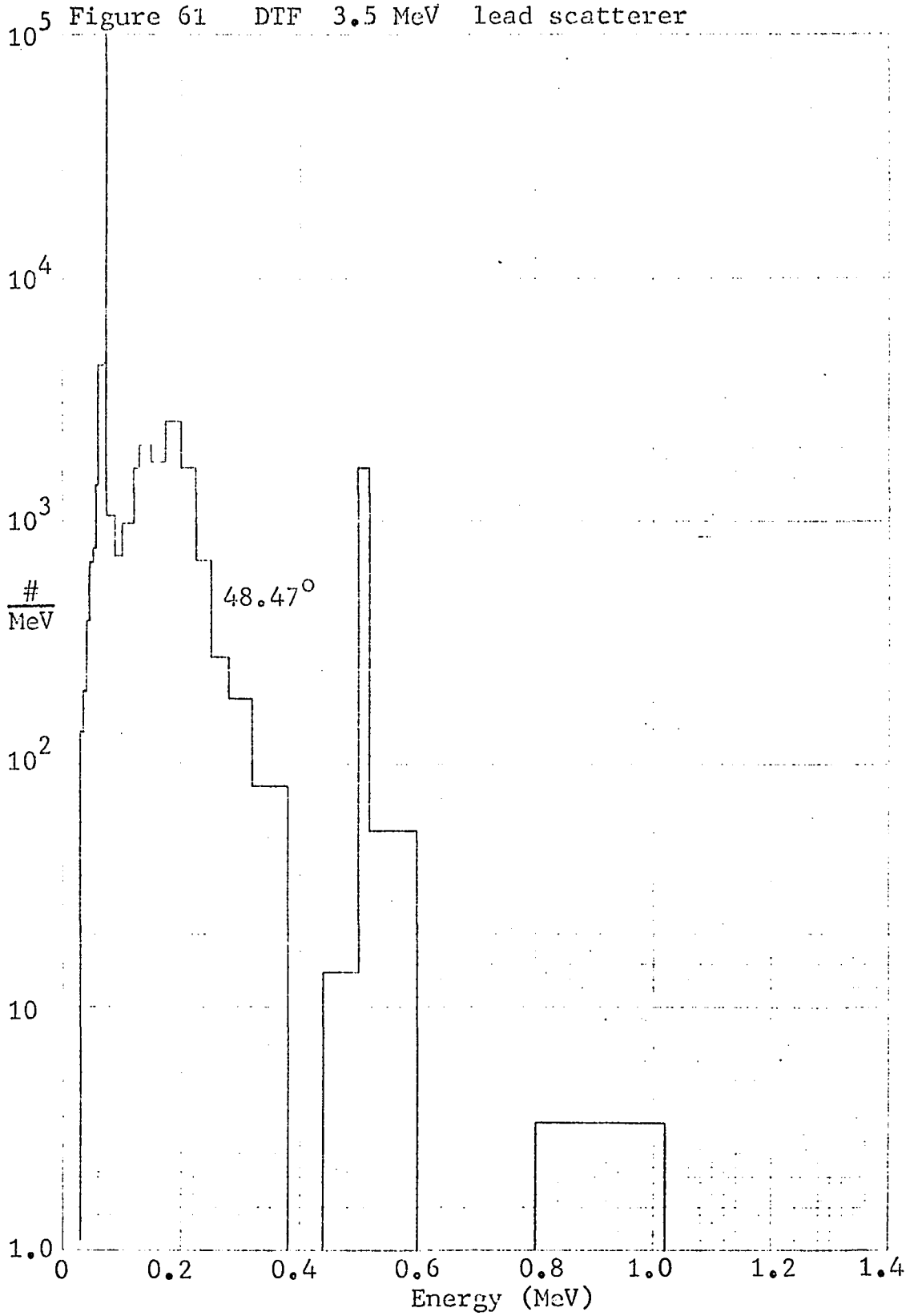

Figure 62 Monte Carlo 3.5 MeV iron scatterer

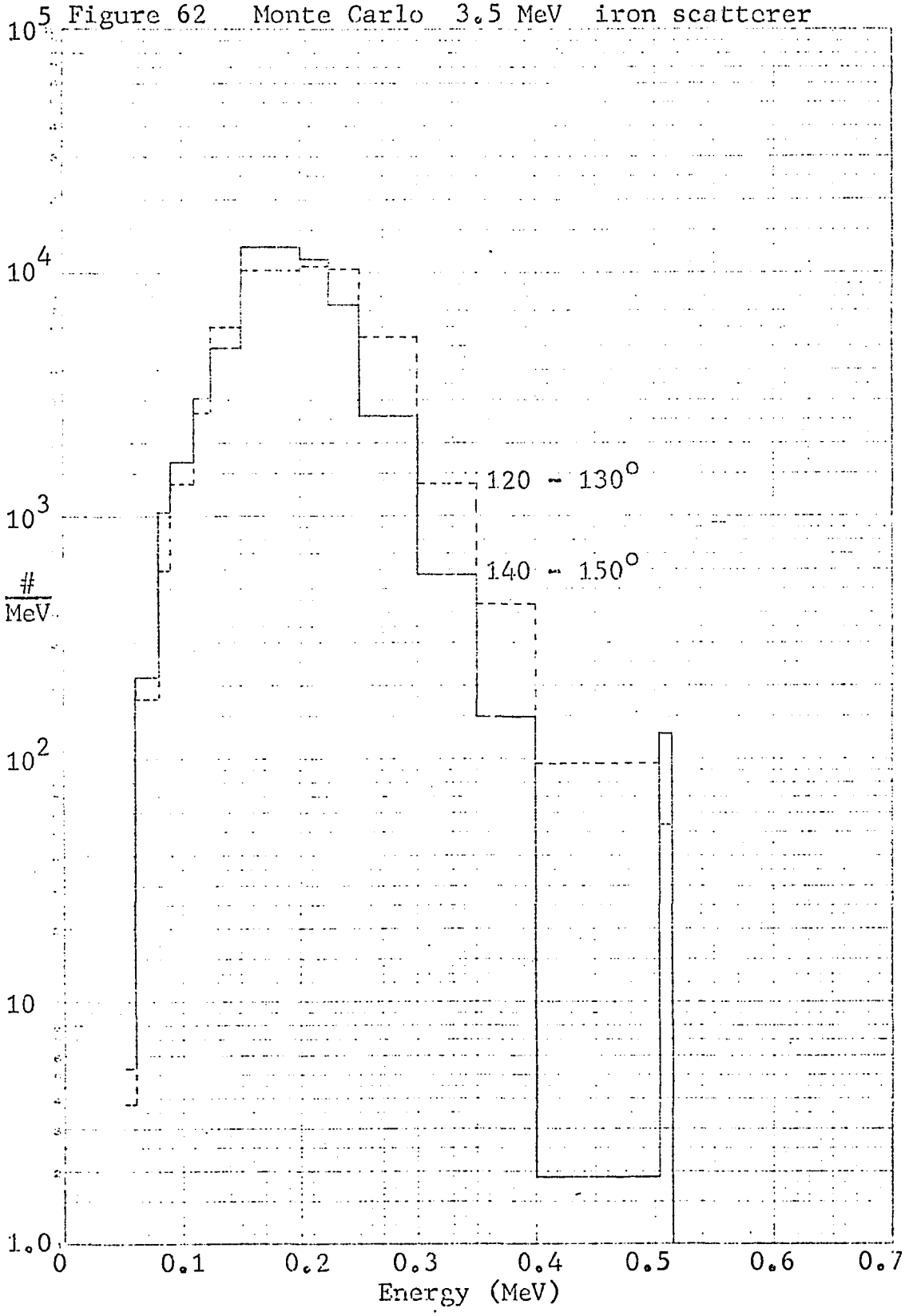

Figure 63 DTF 7.0 MeV concrete scatterer

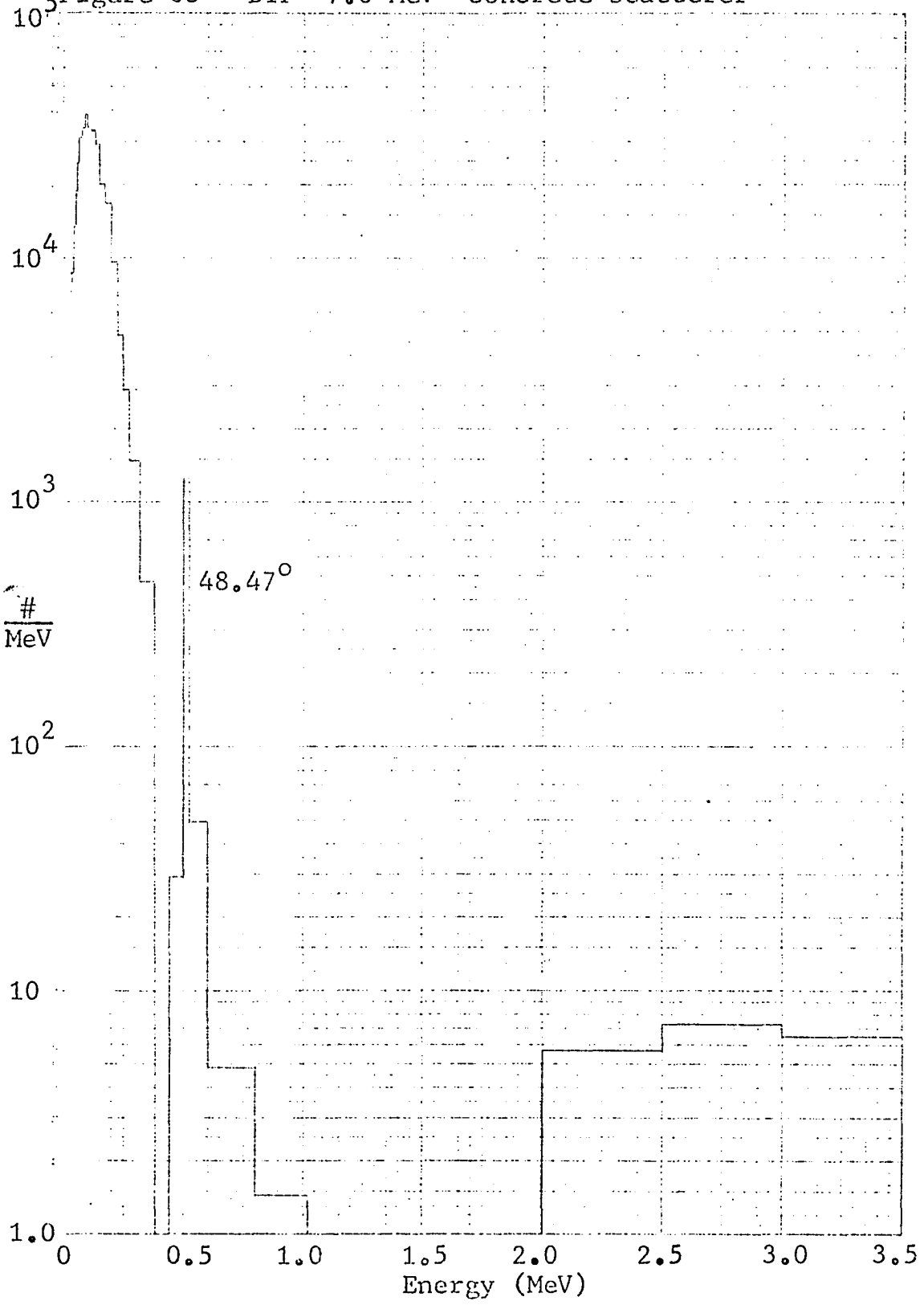

Figure 64 DTF 7.0 MeV iron scatterer

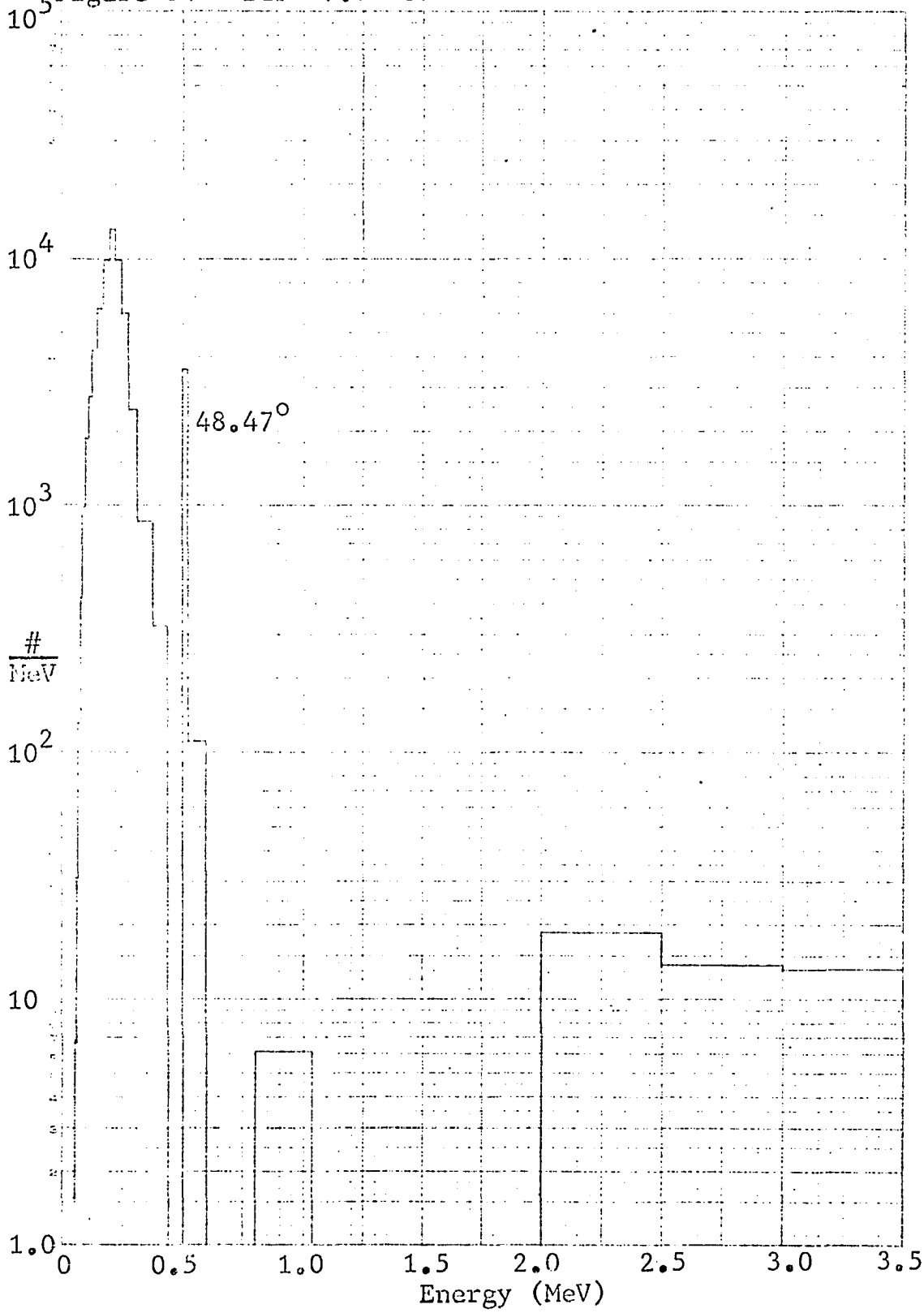

Figure 65 DTF 7.0 MeV lead scatterer

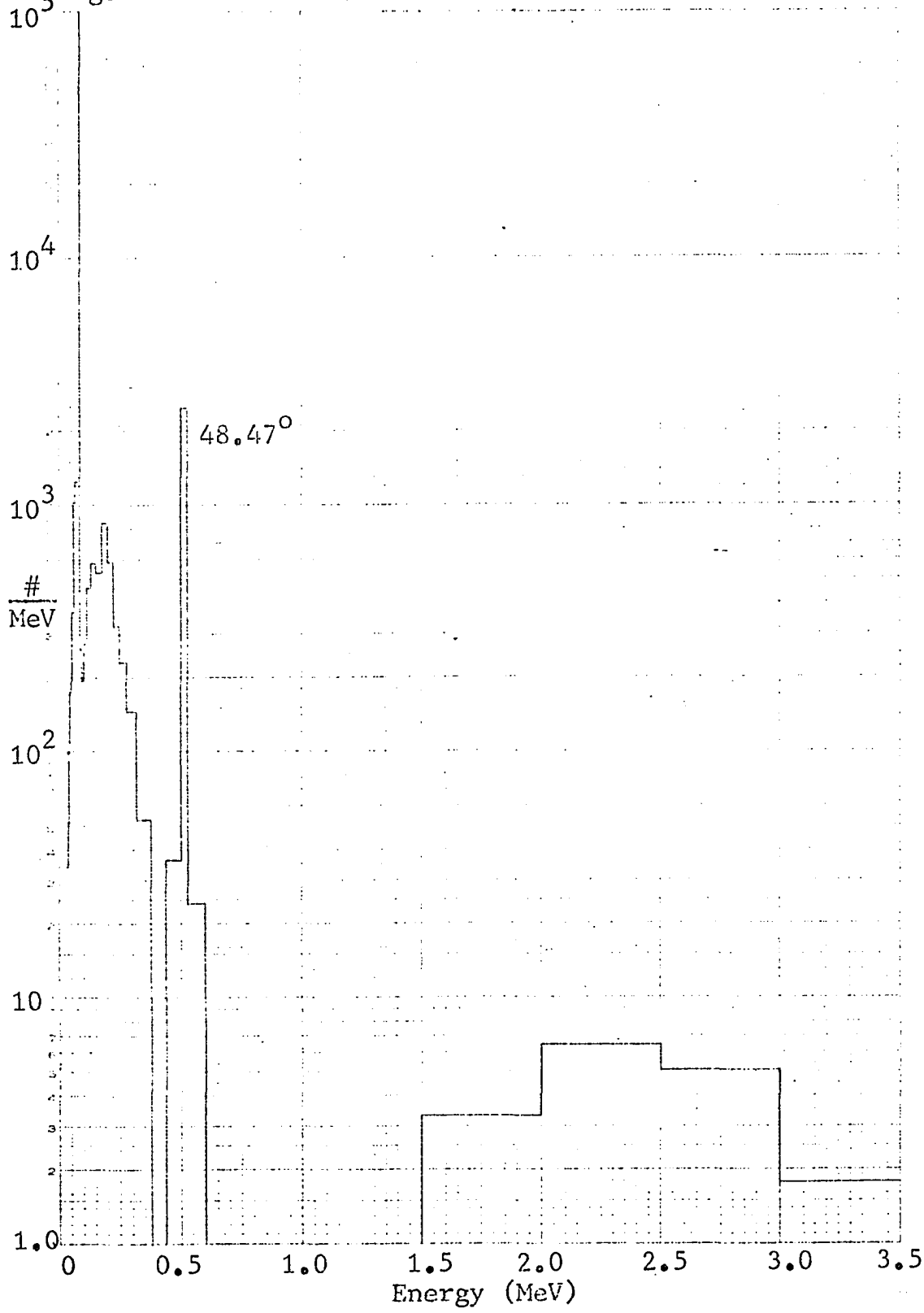

Figure 66 Monte Carlo 7.0 MeV lead scatterer

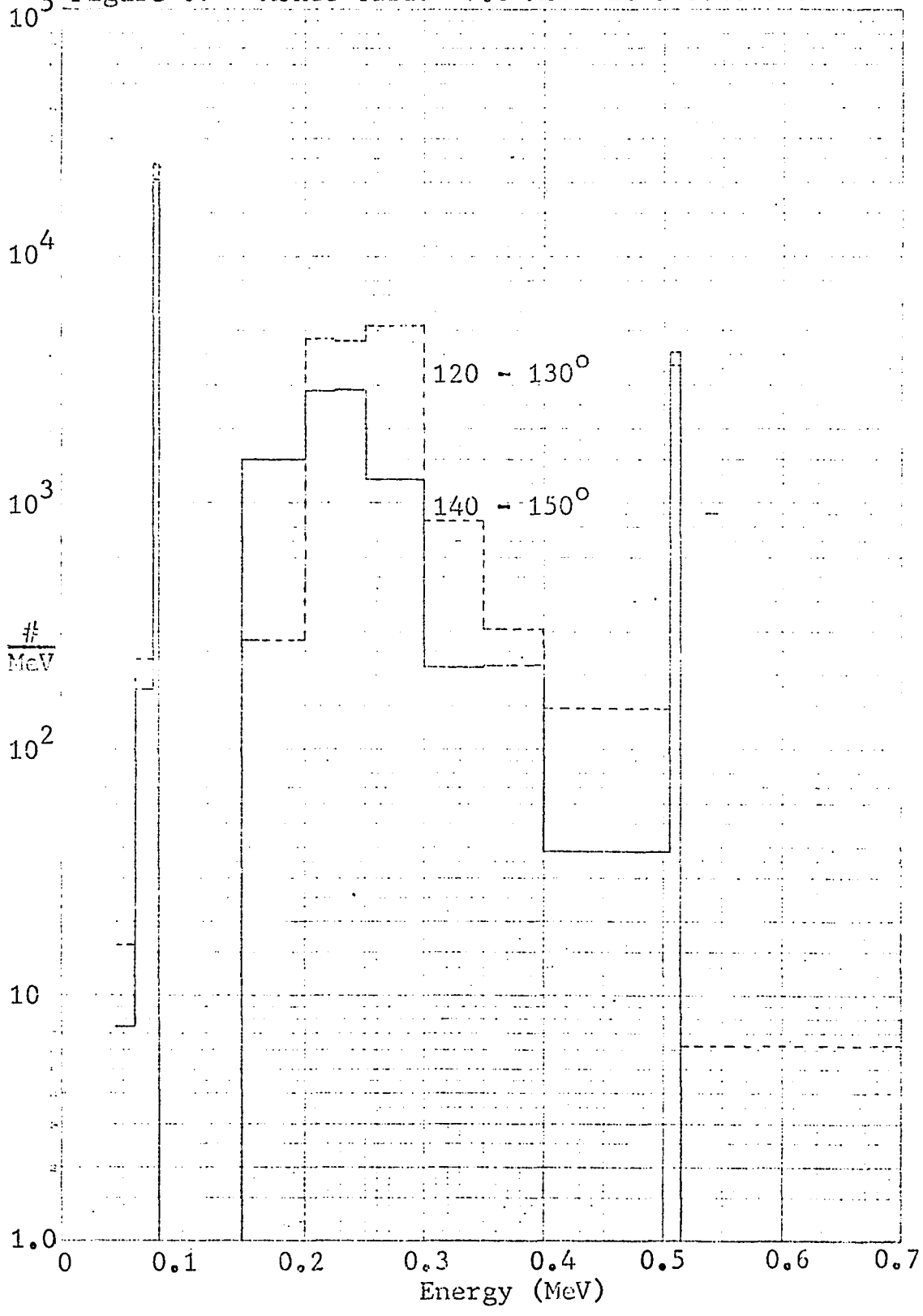

Figure 67 DTF 10.0 MeV concrete scatterer

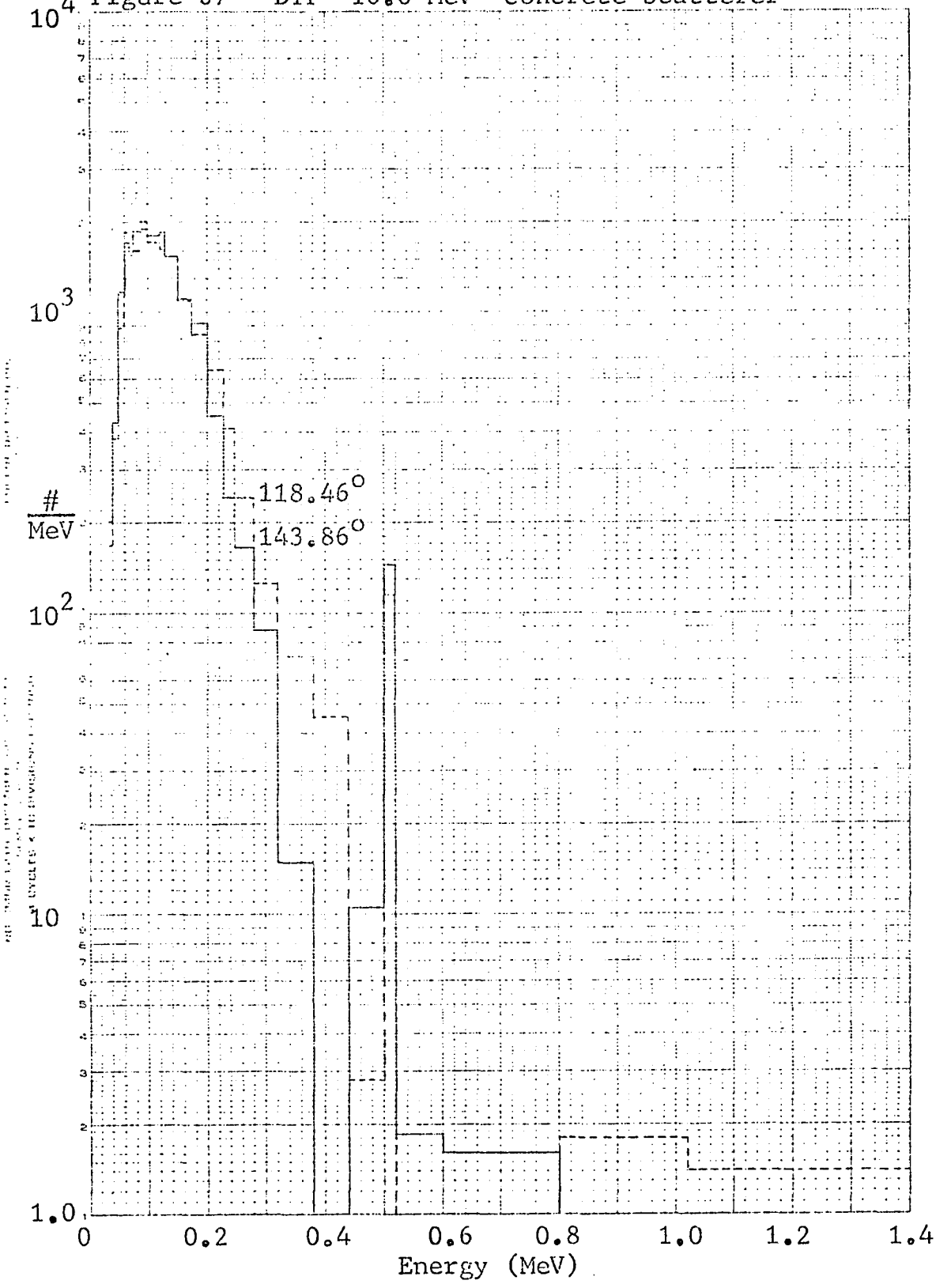

Figure 68 DTF 10.5 MeV iron scatterer

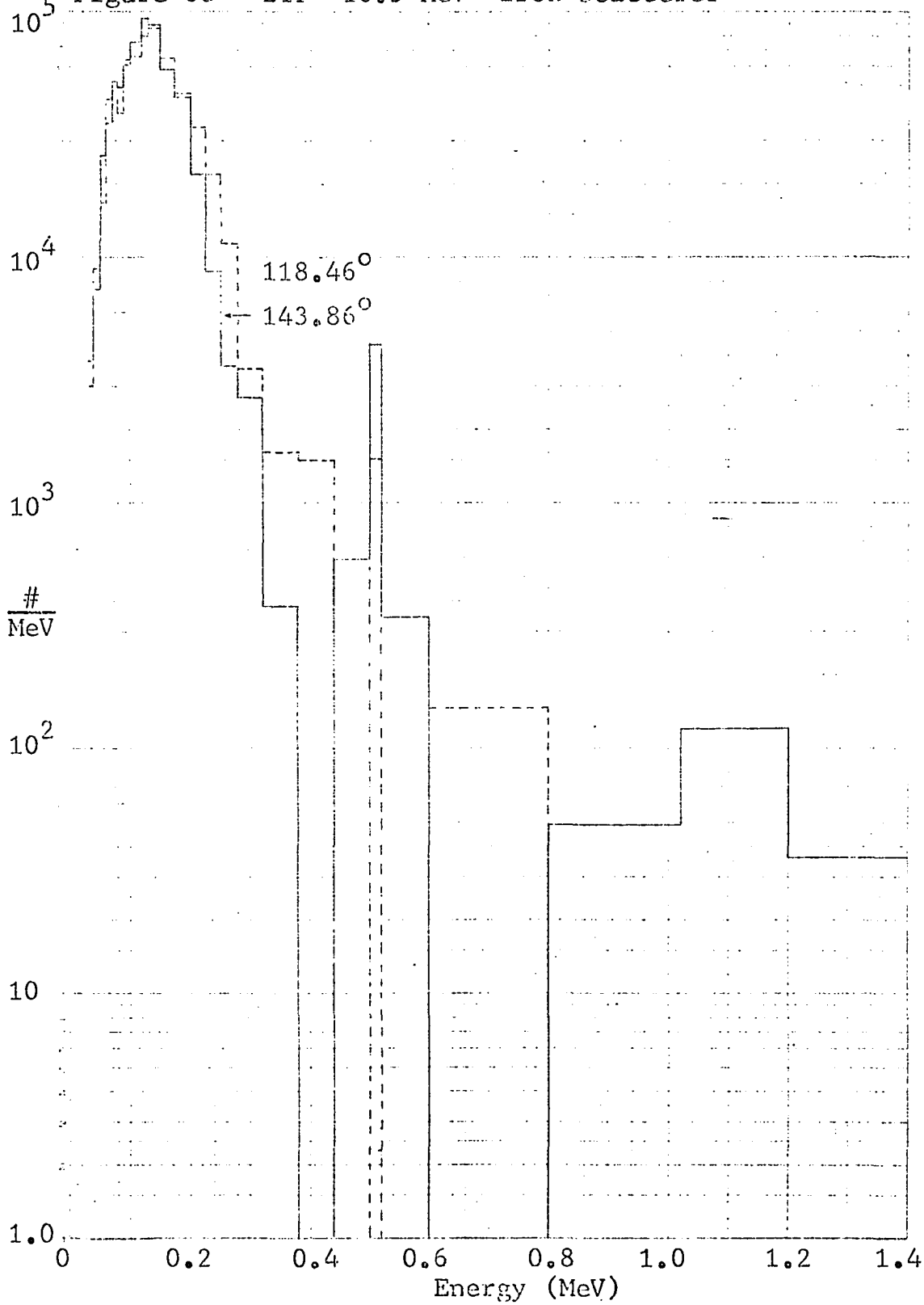

Figure 69 DTF 10.5 MeV lead scatterer

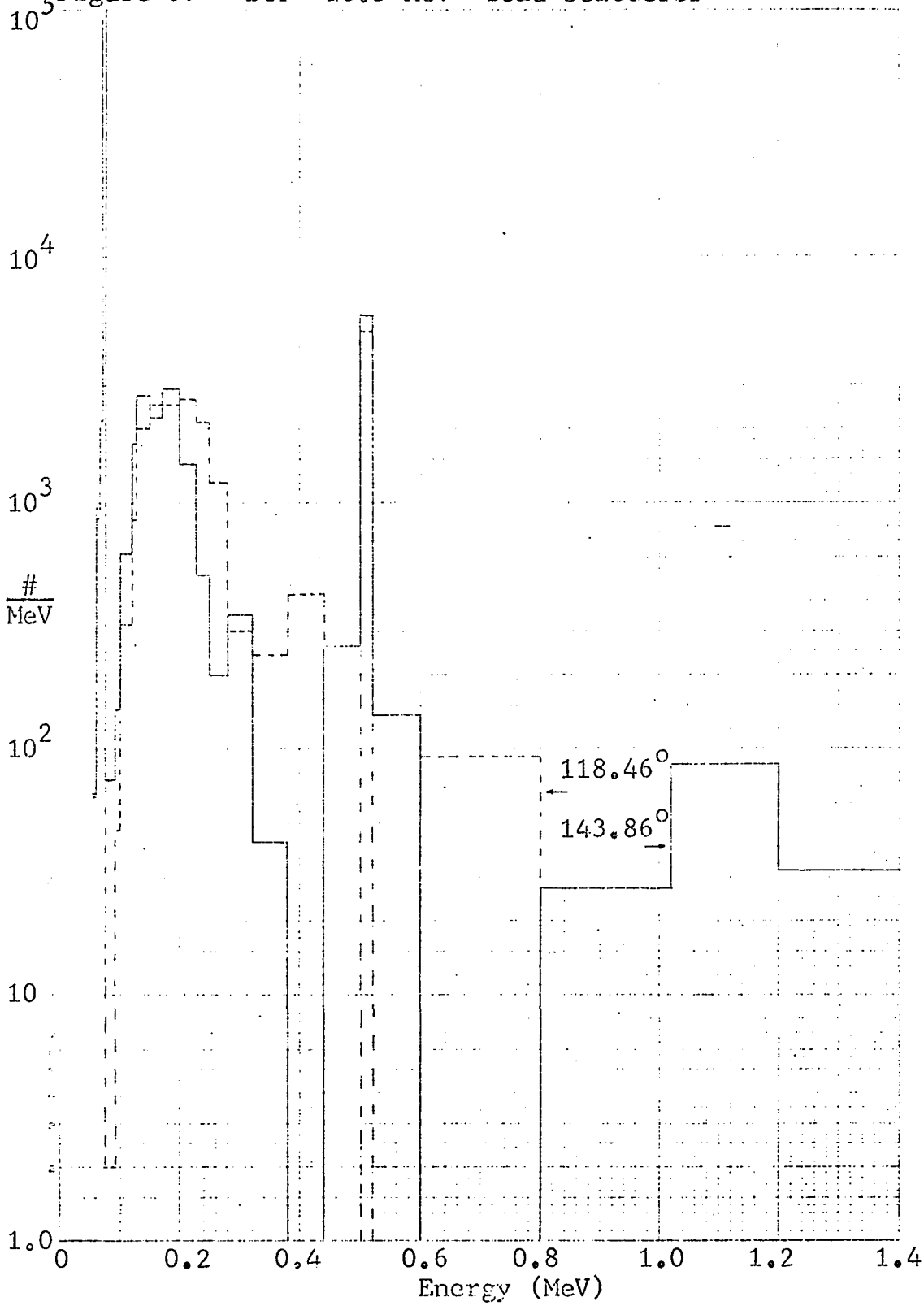

Figure 70 Monte Carlo 10.5 MeV iron scatterer

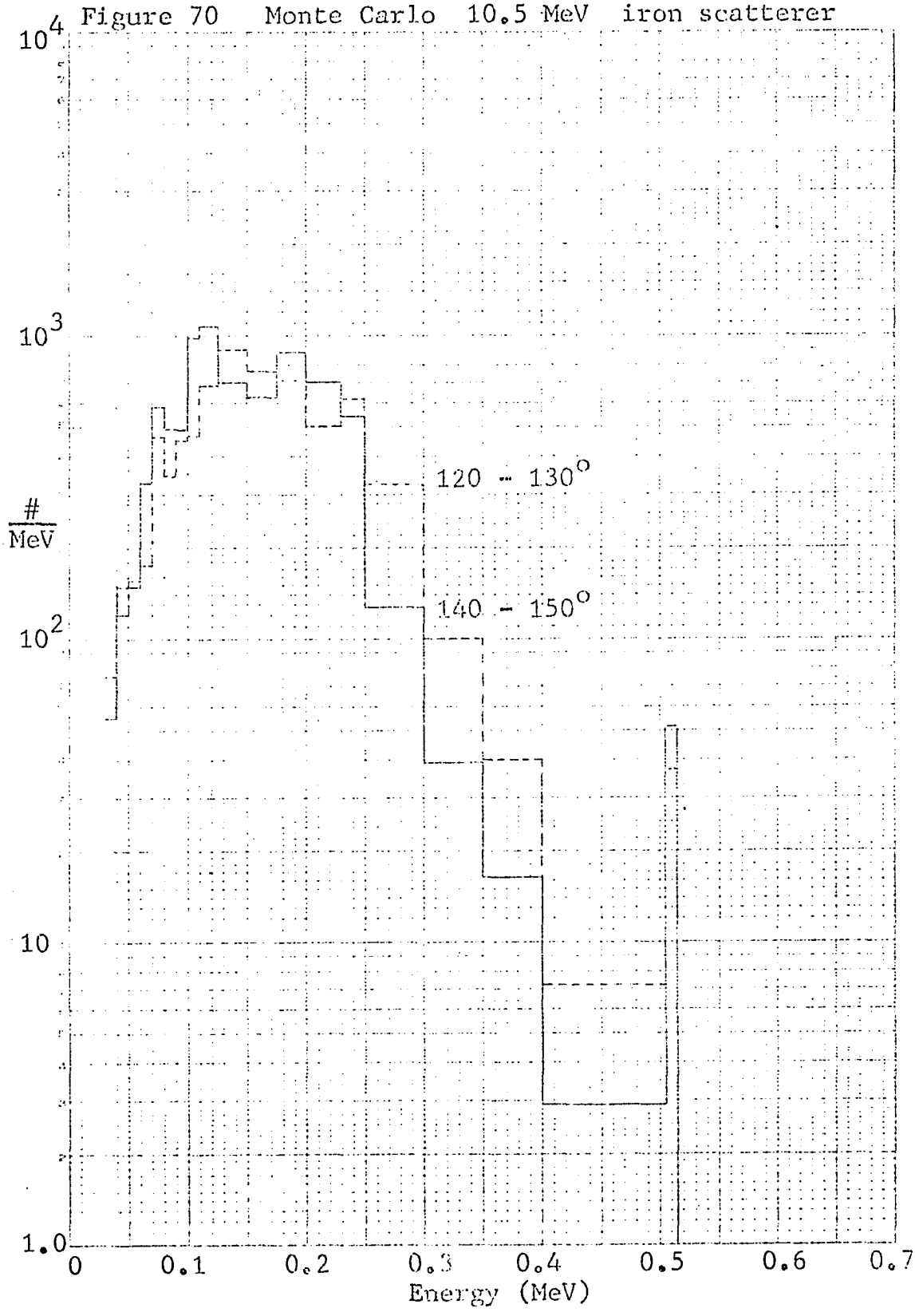

Figure 71 Monte Carlo 10.5 MeV lead scatterer

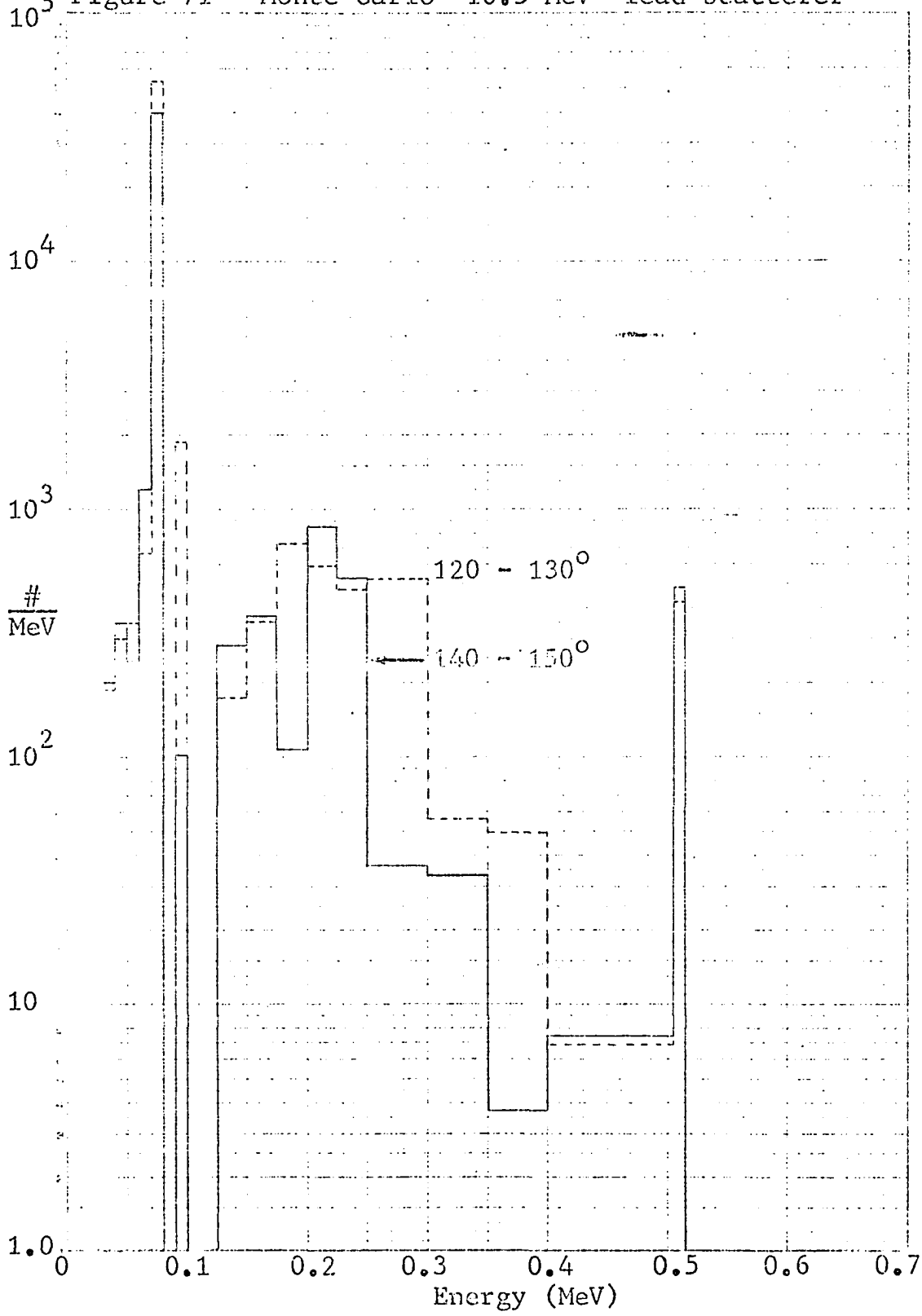

## E. LiF ENERGY DEPENDENCY

A large number of experiments have been carried out in an effort to determine the relative response of LiF as a function of energy (79, 81, 91, 93, 124, 125, 126, 127, 128). Though there is some disagreement in the literature, the response is well enough understood for a large number of private and government agencies to adopt thermoluminescent dosimetry for personnel exposure documentation and to consider it for use as a secondary standard in radiation measurement.

Energy dependency of TLD's is most frequently plotted as "Thermoluminescent response per R relative to that for Co-60" vs "Energy", and in this form shows a marked over-response at energies below 100 KeV (Figure 72).

This dissertation, however, is concerned with the measurement of dose albedos. A plot of energy dependency as "Response of LiF per rad in water" vs "Energy" is therefore a more visible representation of the energy dependency of the present measurements.

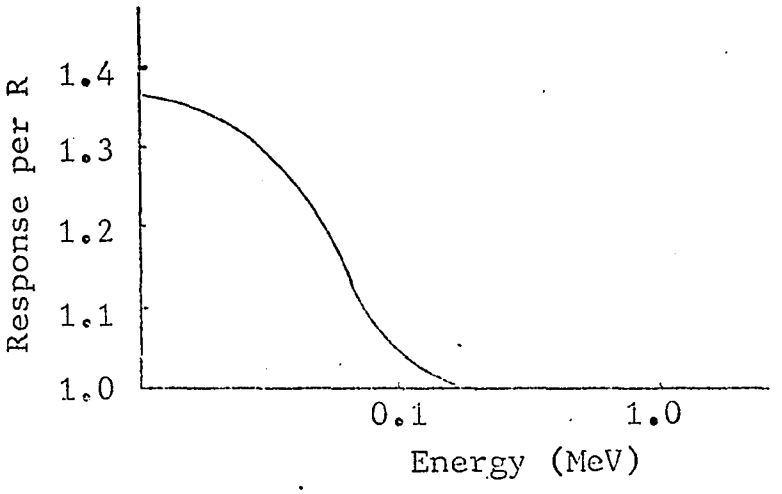


Figure 72. TLD energy response per R (81)

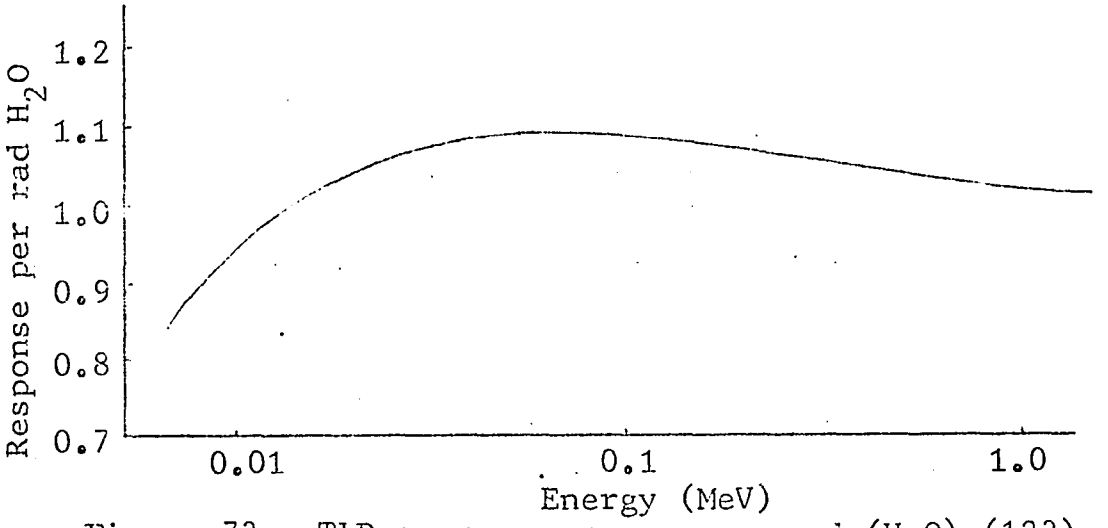


Figure 73. TLD energy response per rad ($H_2O$) (123)

The TLD response per rad ($H_2O$), essentially the $\left[\frac{\left(\frac{\mu_{en}}{\rho}\right)_{H_2O}}{\left(\frac{\mu_{en}}{\rho}\right)_{LiF}}\right]$ function discussed in Section 6 inverted, is energy independent above 40 KeV. Reportedly (78) the dosimeters are even less energy sensitive at high dose levels.

Correction to the TLD data for calculation of "water dose" albedos is therefore relatively small and not rapidly varying as a function of x-ray spectra.

## F. THERMOLUMINESCENT DOSIMETER READ-OUT AND ANNEALING PROCEDURES

A series of experiments were carried out to determine the most convenient annealing - read-out procedure, with results comparable to "standard" procedures, using the available equipment. The experimental procedure consisted of adjusting the time and temperature of the "Pre-heat" and "Integrate" cycles by means of glow curves, to insure that essentially all the thermoluminescence was given off in as short a time and with as low a temperature as possible.

Groups consisting of fifteen to twenty TLD's were treated according to several "standard" pre-irradiation annealing procedures (80, 87, 89, 90), exposed to 1 R ±5% of $^{60}Co$ radiation, treated according to their corresponding post-irradiation annealing procedure and read out in the "Integrate" cycle. The time and temperature of the "Pre-heat" cycle were then adjusted, by means of glow curves, to eliminate the lower temperature traps, and thus serve effectively as a post-irradiation annealing procedure. Upon

establishment of a suitable "Pre-heating" cycle, groups of 15 TLD crystals were pre-irradiation annealed according to a particular "standard" procedure, exposed to 1 R $^{60}Co$, read out in the determined cycle and compared statistically to the groups which received a post-irradiation annealing before read-out. To verify the results more substantially, the experiment was repeated using fifty dosimeters in each procedure.

The read-out cycle, as determined by the use of glow curves, consisted of a "Pre-heat" period of 7 seconds at 165°C and an "Integrate" period of 15 seconds at 250°C. The time interval allows the dosimeter to be read out and the heating element to cool back to an acceptable level in approximately 30 seconds with a minimum amount of dark current.

The data for that "standard" annealing cycle recommended for use with those TLD crystals used and the abbreviated annealing cycle developed here were compared statistically and found to be equivalent at the 99.5% confidence level under chi square testing. Compared with other "standard" annealing procedures, the abbreviated procedure yielded as great a mean sensitivity (light units/R) and was quite comparable in accuracy.

Table 14 lists the annealing procedures studied and the results obtained with each, using twenty-five dosimeters per set. Table 15 summarizes the mean sensitivity and standard deviation obtained with each set. Individual TLD readings are found in Appendix I.

TABLE 14

TLD ANNEALING PROCEDURES

1) 1 hr. 400°C Pre-anneal
2 hr. 100°C
10 min. 100°C Post-anneal
No Pre-heat cycle
15 sec. 250°C Integrate
Mean = 718.5
% = 3.53

2) 1 hr. 400°C Pre-anneal
2 hr. 100°C
10 min. 100°C Post-anneal
7 sec. 165°C Pre-heat
15 sec. 250°C Integrate
Mean = 696.8
% = 6.50

3) 1 hr. 400°C Pre-anneal
2 hr. 100°C
No Post-anneal
7 sec. 165°C Pre-heat
15 sec. 250°C Integrate
Mean = 711
% = 3.40

4) 1 hr. 400°C Pre-anneal
24 hr. 80°C
No Post-anneal
No Pre-heat
15 sec. 250° Integrate
Mean = 704
% = 2.98

5) 1 hr. 400°C Pre-anneal
24 hr. 80°C
No Post-anneal
7 sec. 165°C Pre-heat
15 sec. 250°C Integrate
Mean = 706
% = 2.94

6) 1 hr. 400°C Pre-anneal
24 hr. 80°C
10 min. 100°C Post-anneal
No Pre-heat
15 sec. 250°C Integrate
Mean = 695
% = 2.94

7) 1 hr. 400°C Pre-anneal
24 hr. 80°C
10 min. 100°C Post-anneal
7 sec. 165°C Pre-heat
15 sec. 250°C Integrate
Mean = 672
% = 5.12

8) 1 hr. 400°C Pre-anneal
24 hr. 80°C
No Post-anneal
7 sec. 165° Pre-heat
15 sec. 250°C Integrate
Mean = 706
% = 2.94

TABLE 14 (cont'd)

9) 1 hr. 400°C Pre-anneal
10 min. 100°C Post-anneal
No Pre-heat
15 sec. 250°C Integrate
Mean = 964
% = 2.89

10) 1 hr. 400°C Pre-anneal
10 min. 100°C Post-anneal
7 sec. 165°C Pre-heat
15 sec. 250° Integrate
Mean = 932
% = 4.27

11) 1 hr. 400°C Pre-anneal
No Post-anneal
7 sec. 165°C Pre-heat
15 sec. 250°C Integrate
Mean = 936
% = 3.20

12) 1 hr. 400°C Pre-anneal
No Post-anneal
7 sec. 165°C Pre-heat
15 sec. 250°C Integrate
Mean = 960
% = 3.82

TABLE 15

TLD ANNEALING PROCEDURE SUMMARY

| TEST NO. | MEAN | STANDARD DEVIATION (Percent) |
|---|---|---|
| 1 | 718 | 3.53 |
| 2 | 697 | 6.50 |
| 3 | 711 | 3.40 |
| 4 | 704 | 2.98 |
| 5 | 706 | 2.94 |
| 6 | 695 | 2.94 |
| 7 | 672 | 5.12 |
| 8 | 706 | 2.94 |
| 9 | 964 | 2.89 |
| 10 | 932 | 4.27 |
| 11 | 936 | 3.20 |
| 12 | 960 | 3.82 |

To verify that the accuracy and the stability of the dosimeters were not affected by the abbreviated annealing procedure, a calibration curve was obtained yielding a slope of 1.016 and a maximum standard deviation at the 68% confidence interval for a 10 MR exposure of ±6.0%; fading characteristics were demonstrated to be negligible in a three-month period.

The author was aided in work on this Appendix by B. L. O'Neal, Sandia Corporation, and D. Rudy, New Mexico State University.

## G. INFINITE SLAB SIZE MEASUREMENTS

In order to simplify the geometry associated with beam perimeter fall-off and increasing slab size, all "infinite-size" studies were conducted with the incident beam restricted to 2.0" square at the backscatter surface. The distance from beam edge to backscatter slab edge was then increased, holding thickness constant, and the resulting albedos considered. Slab thickness effects were studied with a constant slab area. Lead slab areas of 4.0, 6.0, 7.0, 8.0, 9.0, and 10.0 inches square and thicknesses of 0.25, 0.50, 0.625, 0.75, 1.00, 1.25, 1.375, 1.50, and 2.00 inches were studied at 2.0 MeV. Slabs of 4.0, 6.0, 8.0, 12.0, and 14.0 inches square and thicknesses of 0.15, 0.35, 0.58, 0.78, 1.15, 1.40, 1.72, and 2.10 inches were studied at 60.0 MeV. Infinite size calculations were checked at 2.0 MeV for iron and steel but the full plot not made due to machine time considerations.

A hypothesis test that the iron slabs are equally effective reflectors falls well within the 95% acceptance level. The concrete results are similar (Tables 16 and 17).

TABLE 16

IRON REFLECTOR RATIOS ($\times 10^5$)

| ANGLE | SLAB SIZE 12" x 12" x 2.5" | 12" x 12" x 4.125" | 14" x 14" x 2.5" |
|---|---|---|---|
| 150° | 4.04 ± 8.35% | 4.00 ± 8.30% | 4.04 ± 10.05% |
| 135° | 3.96 ± 9.34% | 4.04 ± 8.61% | 4.16 ± 8.70% |
| 120° | 2.97 ± 9.02% | 2.97 ± 7.97% | 2.92 ± 9.5 % |

TABLE 17

CONCRETE REFLECTOR RATIOS ($\times 10^5$)

| ANGLE | SLAB SIZE 32" x 32" x 8" | 32" x 32" x 10" | 36" x 36" x 8" |
|---|---|---|---|
| 150° | 4.59 | 4.60 | 4.55 |
| 135° | 4.40 | 4.22 | 4.43 |
| 120° | 3.25 | 2.89 | 3.21 |

The following graphs, 74, 75, 76, and 77 show results of the above experiments.

At small backscatter surface areas, an increase in albedo was noted. These measurements were made with very little collimation, which might have recorded scatter from the sides of the backscatter slab as well as the face. This effect might better be studied with a gamma source-scintillation detector arrangement.

Figure 74 2.0 MeV lead surface area effects

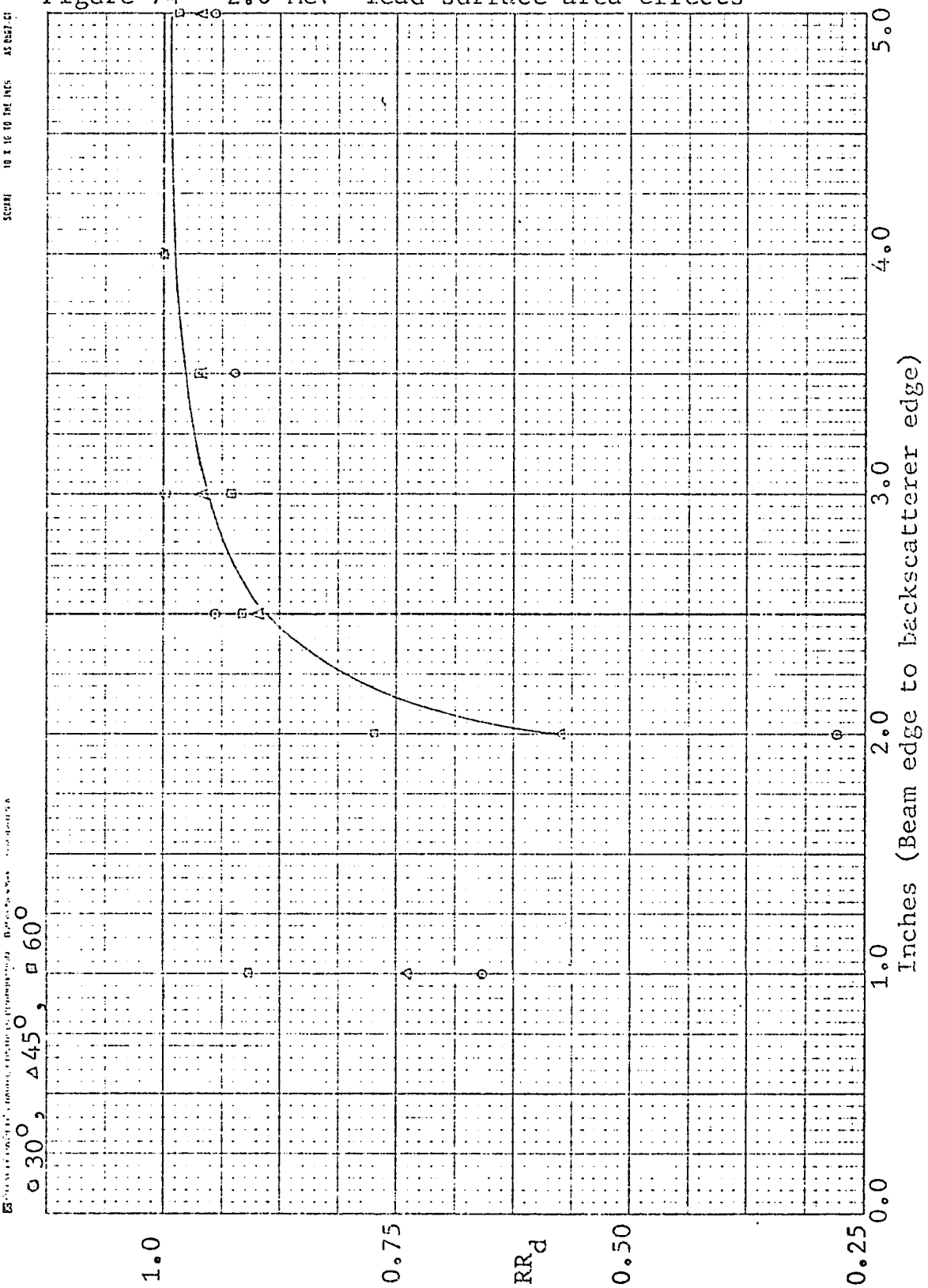

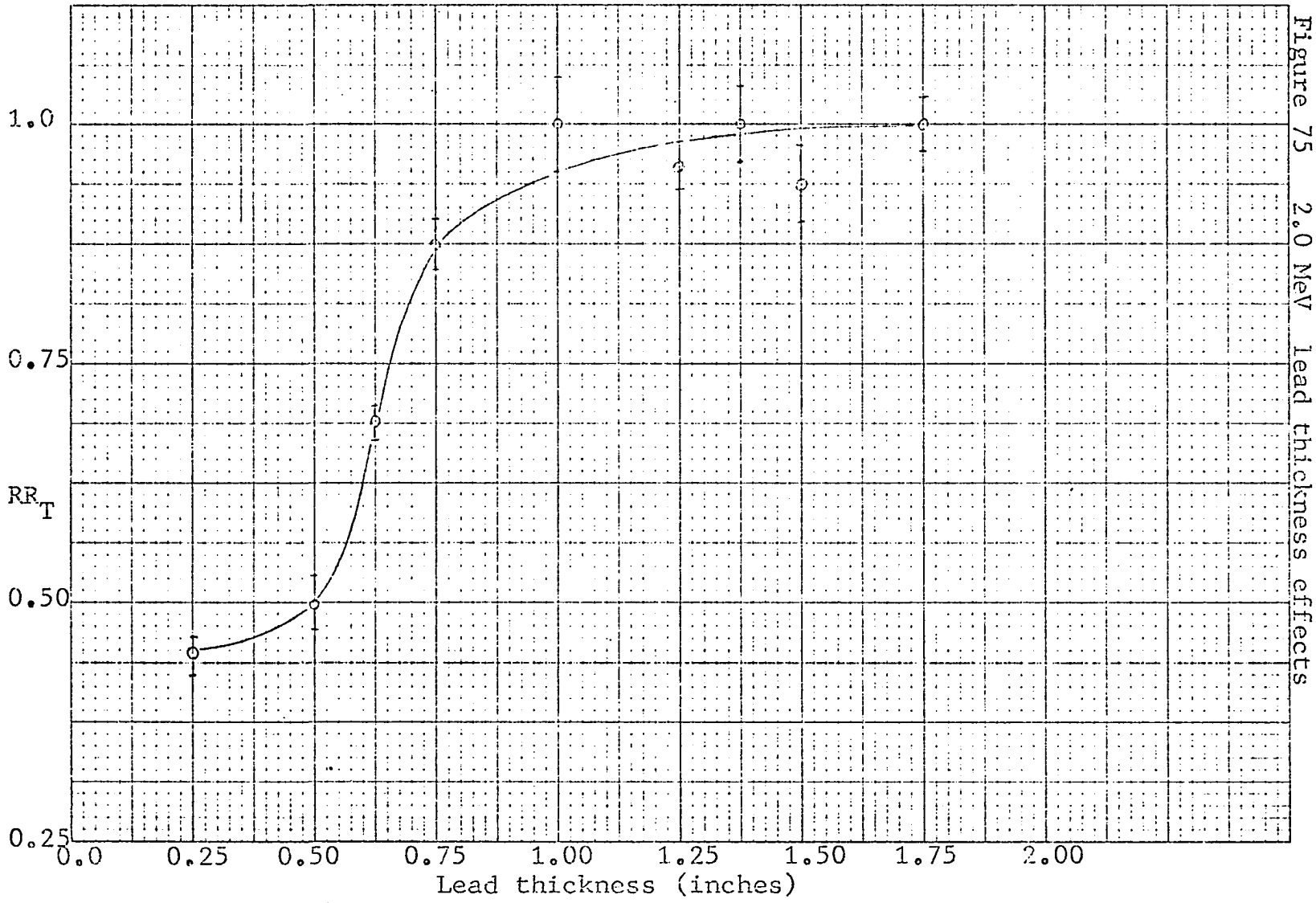


Figure 75 2.0 MeV lead thickness effects

Figure 76 60 MeV lead surface area effects

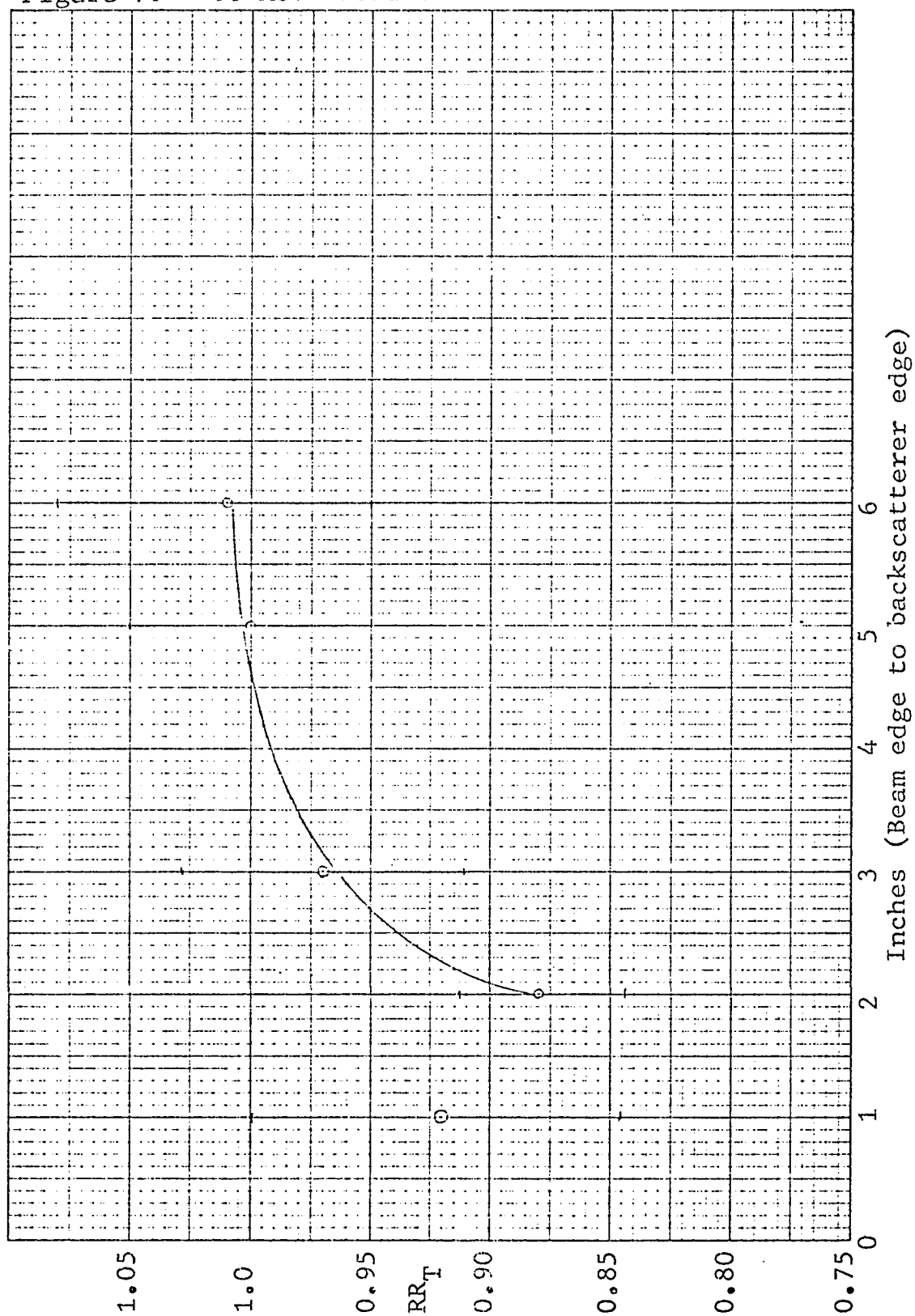

Figure 77 60 MeV lead thickness effects

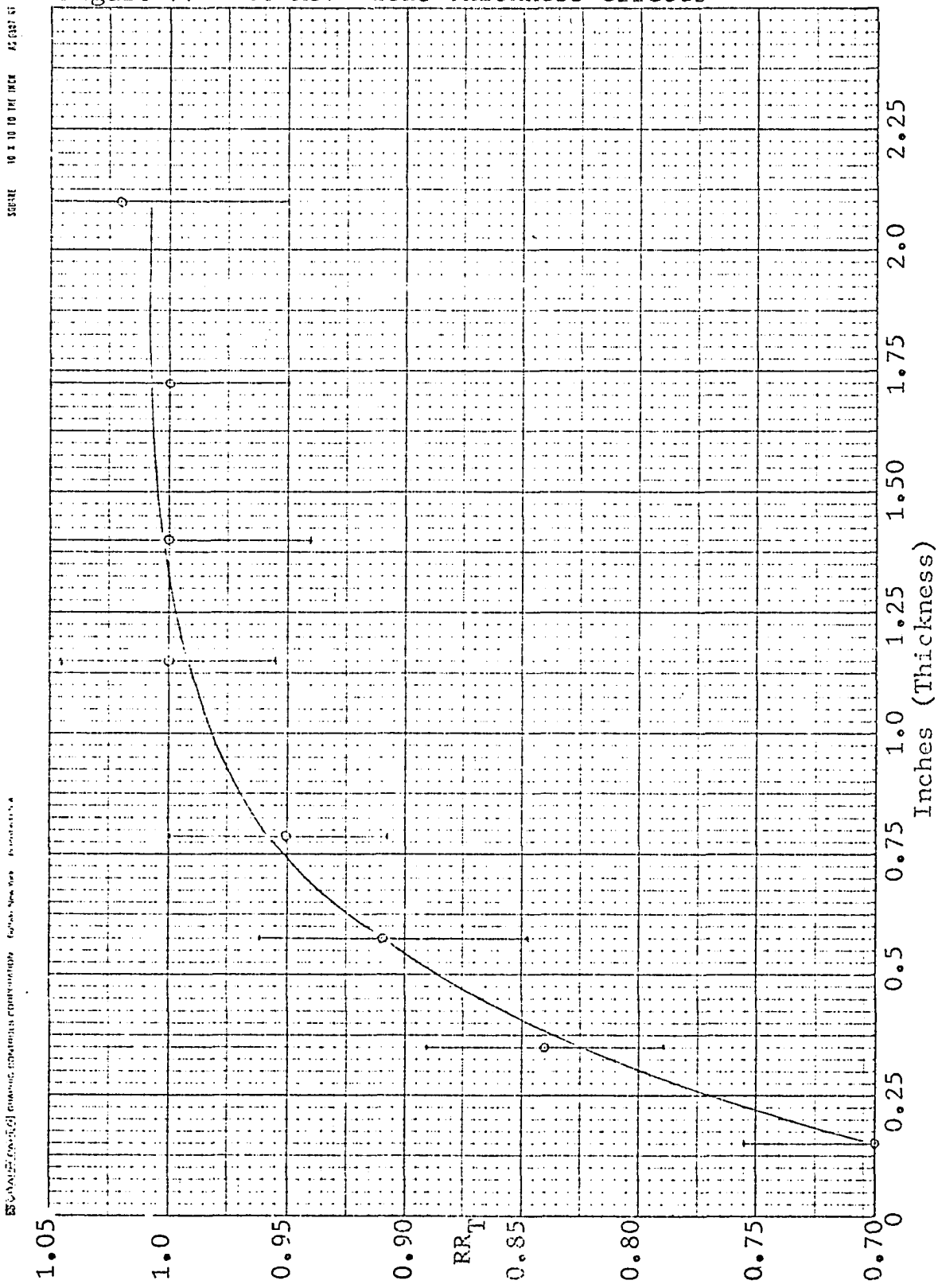

## H. BEAM DIVERGENCE

X-ray beams are inherently more directional than are isotopic sources. Beam divergence is a function of the particular generating machine used. Horizontal and vertical beam cross-sections are given for the machines used (except at 10.5 MeV for which published cross-sectional measurements exist) in Figures 78 to 83. Cylindrical symmetry is then assumed and a least squares fit made to determine beam fall-off as a function of radius (Figures 84 to 86). The incident slab dose is then averaged at the center of the "effective viewed area".

Albedo would be expected to vary with the amount of semi-infinite surface irradiated, up to some point, similar to the change experienced with increased surface area. The concept of "semi-infinite irradiated surface area" is even less well established than that of semi-infinite surface. Indeed, large numbers of albedo experiments have been conducted (Section 2) in which a uniformly irradiated surface could not have been achieved. In the experiments conducted in this research, only those with concrete at

Figure 78 2.0 MeV horizontal beam divergence

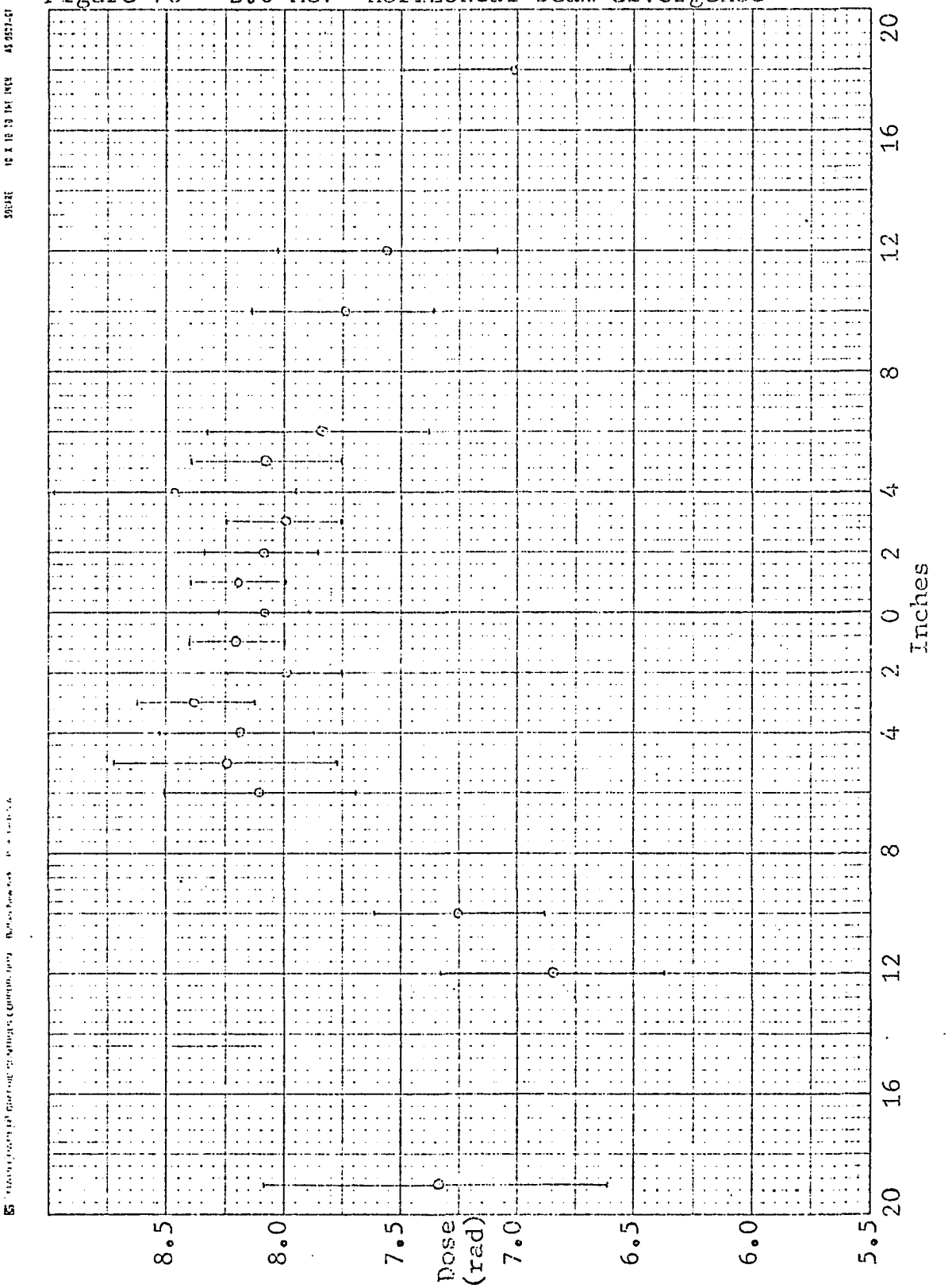

Figure 79 2.0 MeV vertical beam divergence

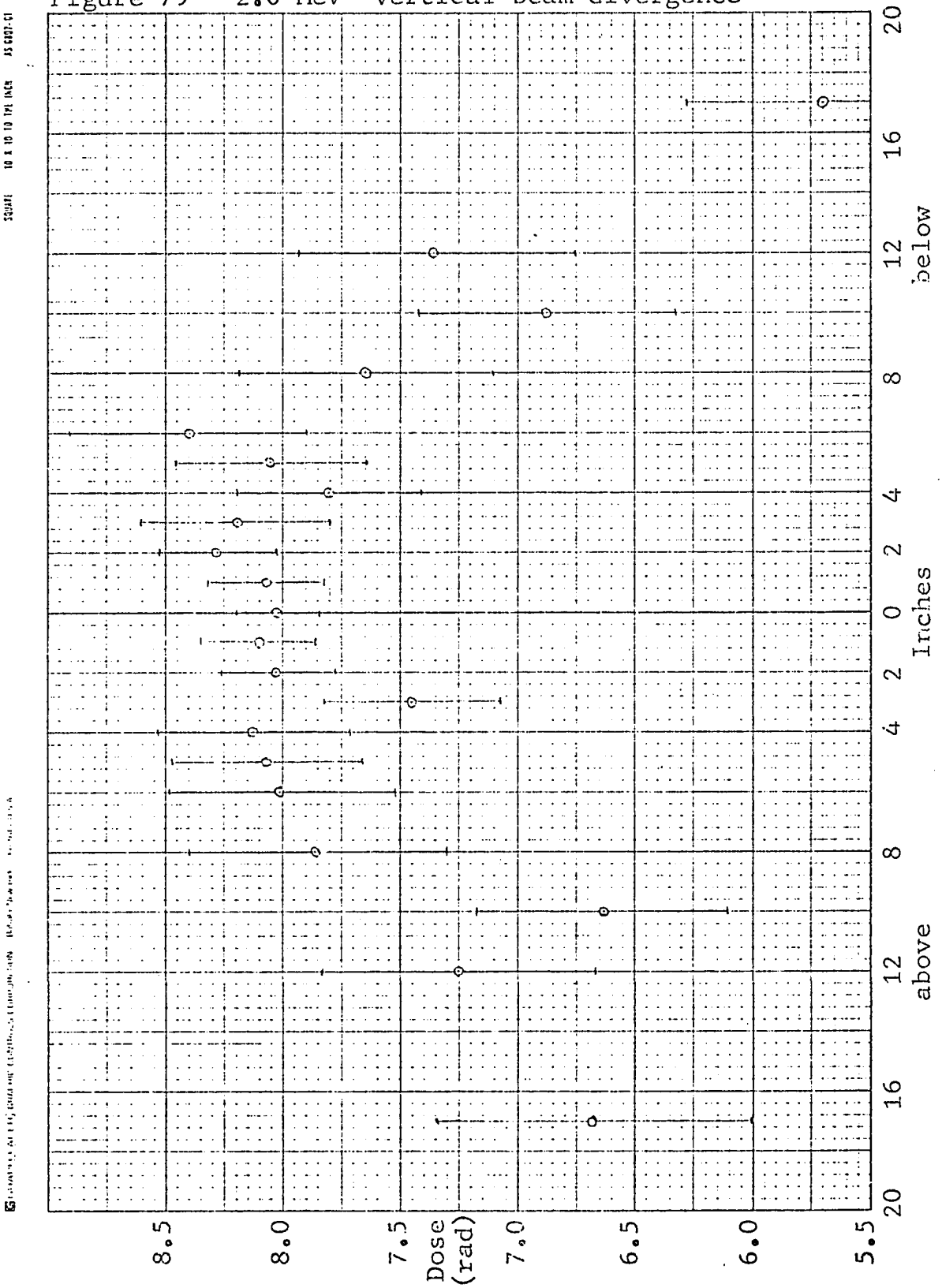

Figure 80 3.5 MeV vertical beam divergence

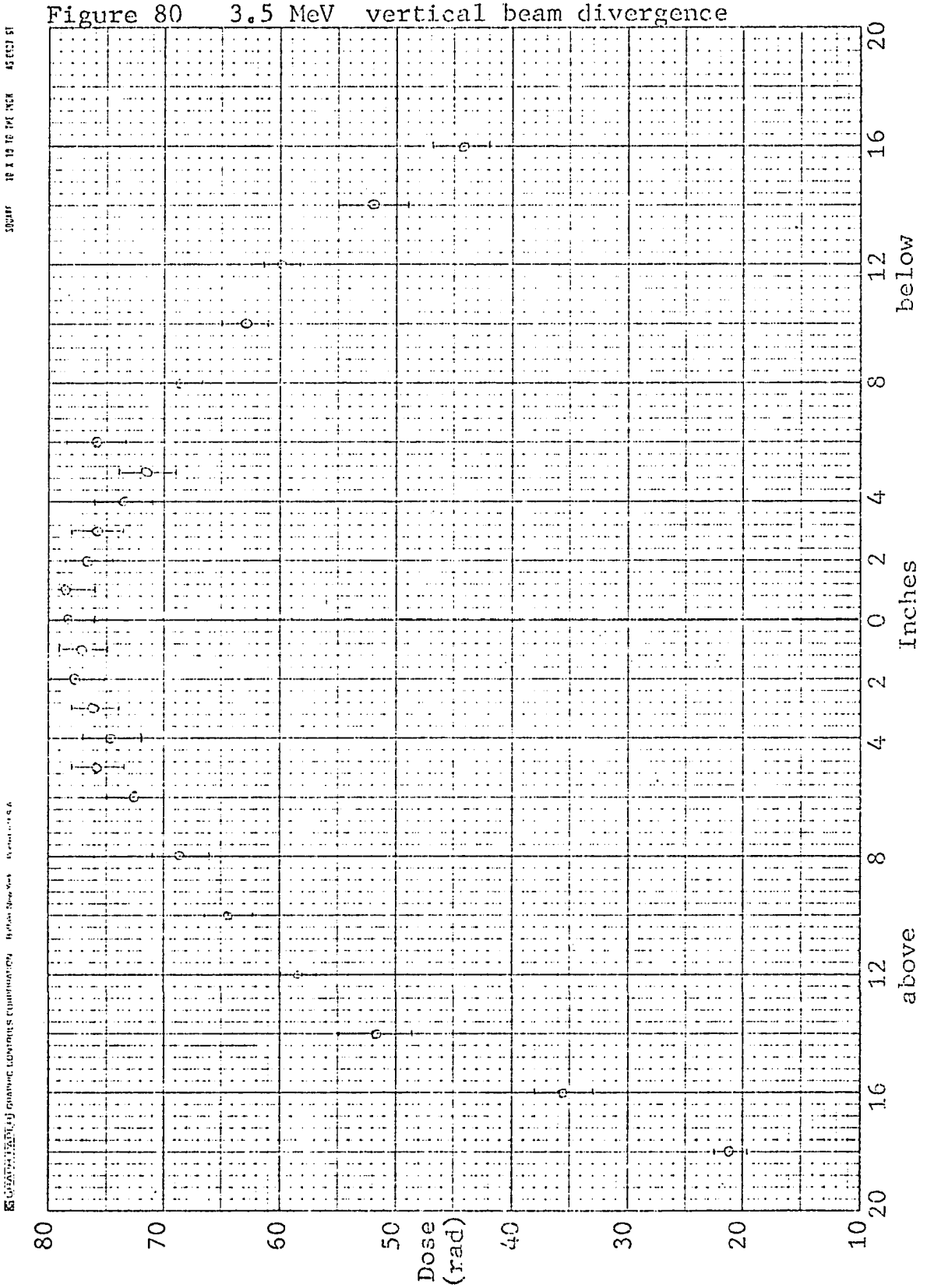

Figure 81 3.5 MeV horizontal beam divergence

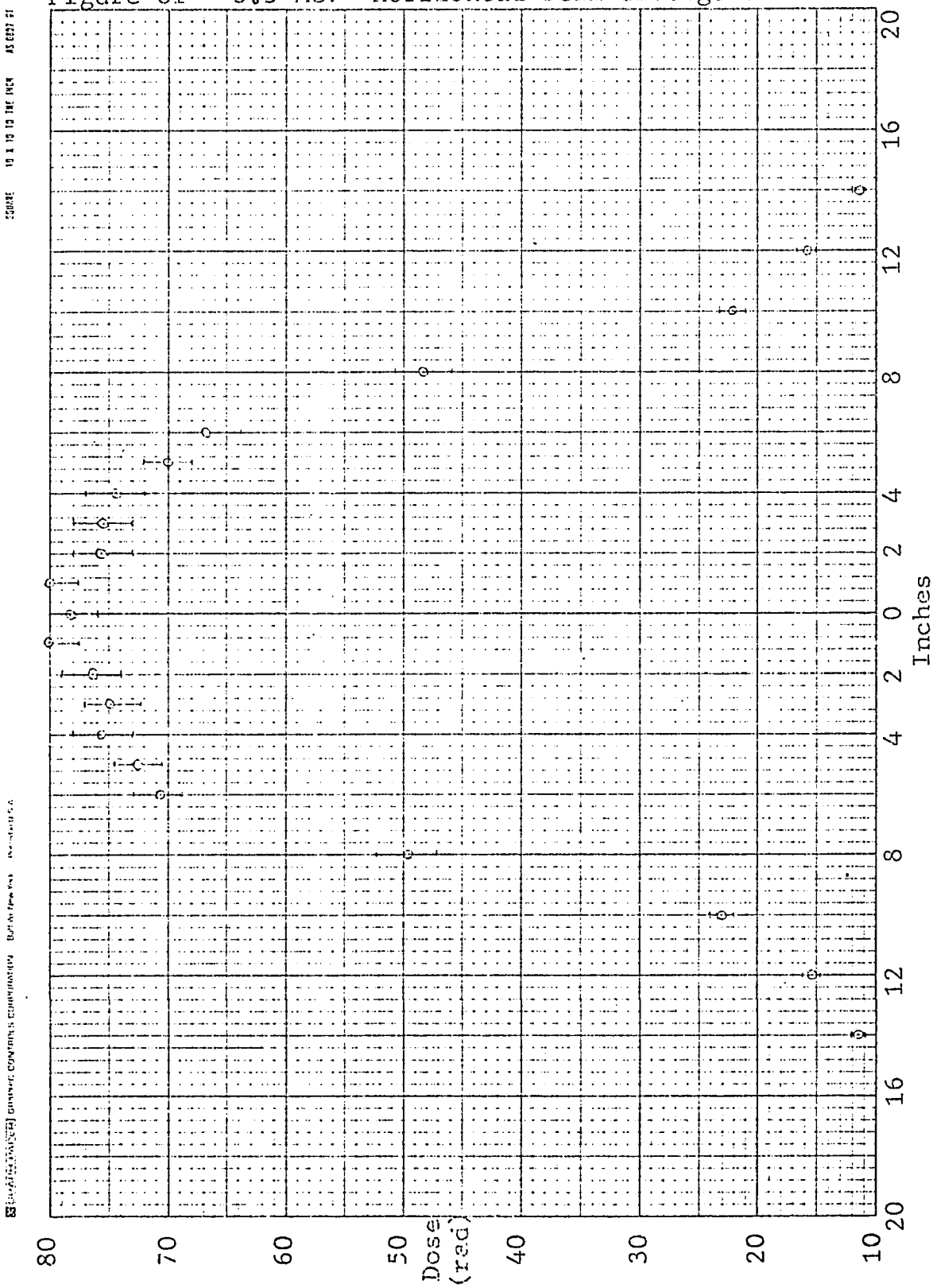

Figure 82 7.0 MeV horizontal beam divergence

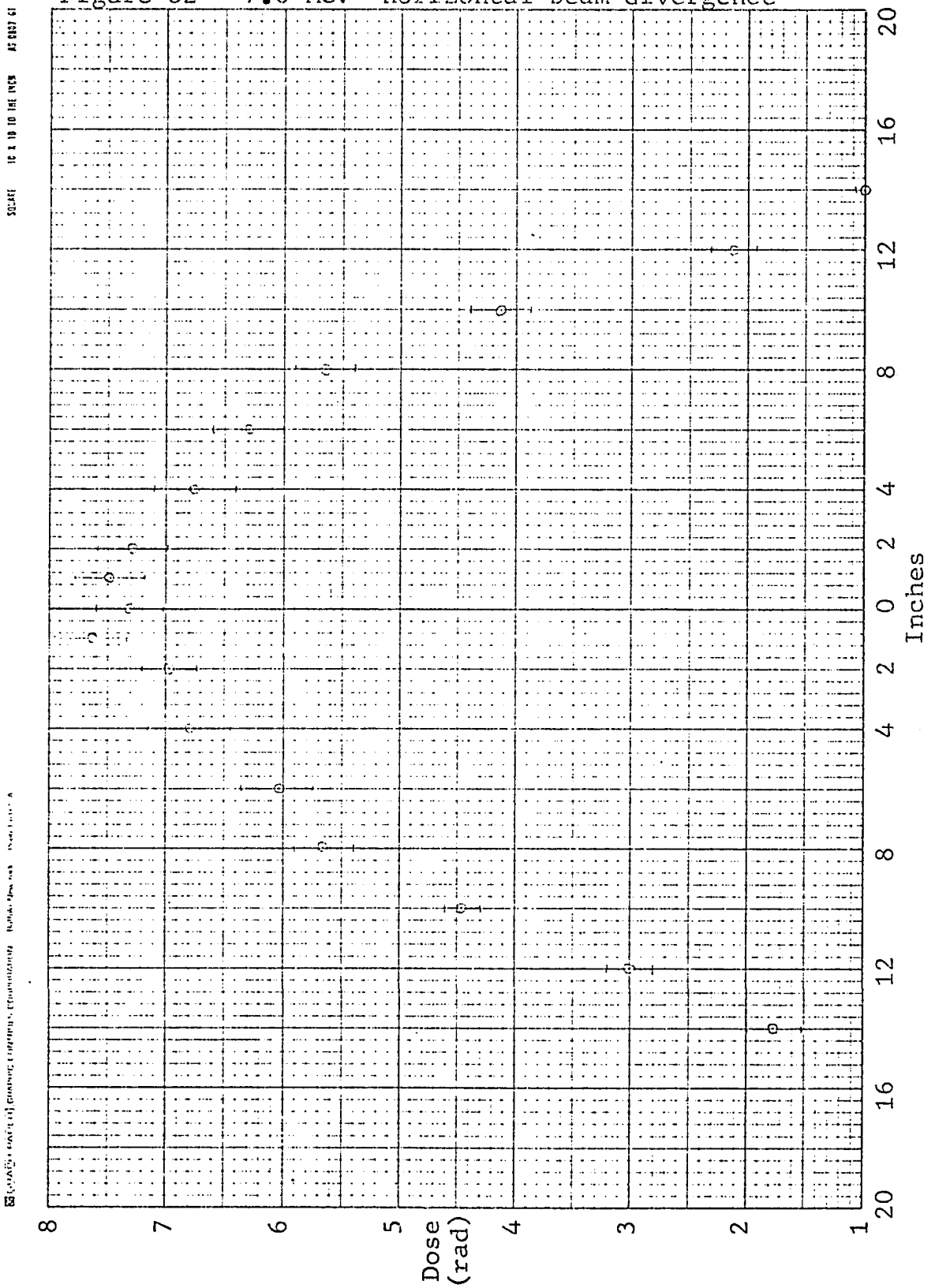

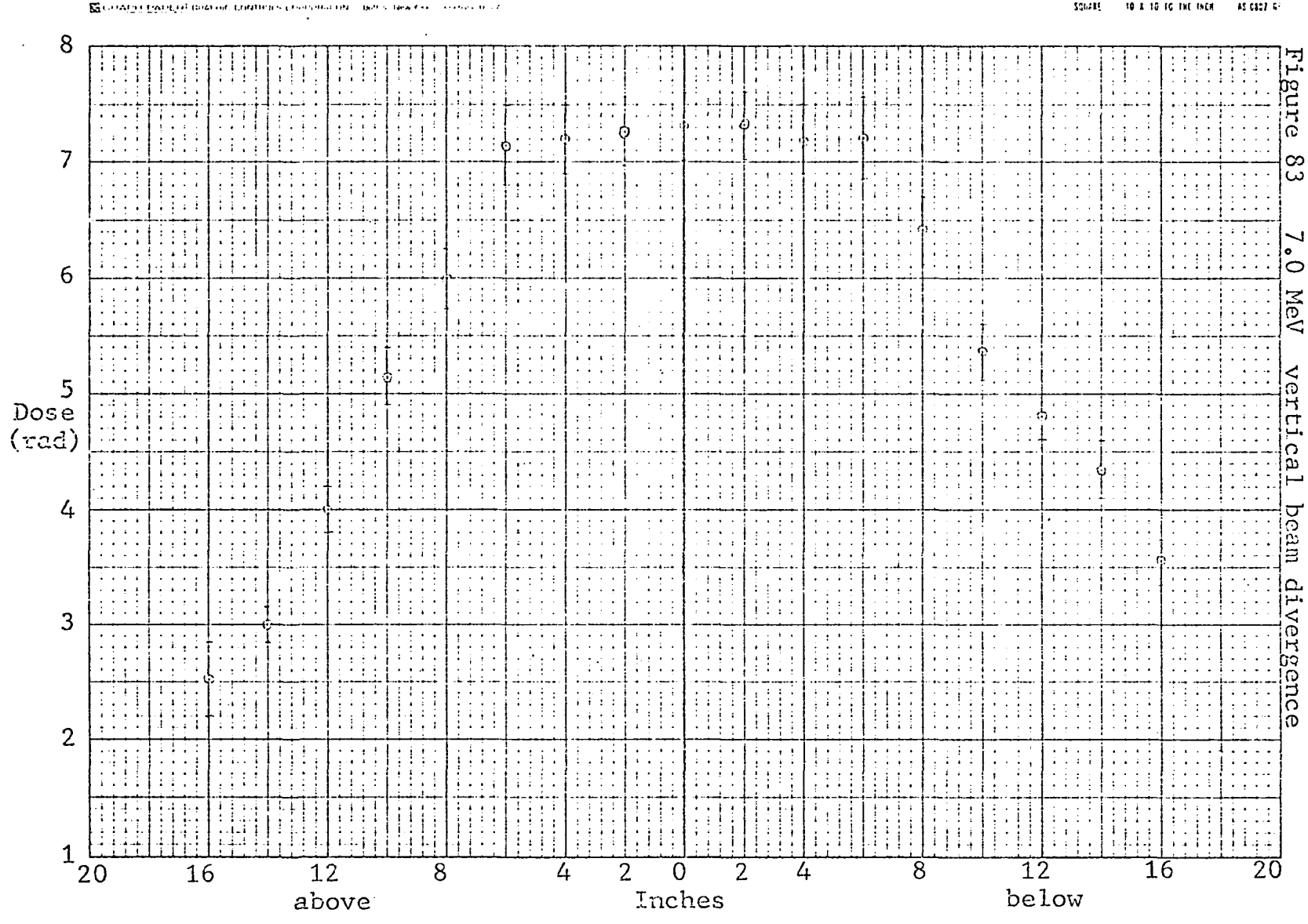


Figure 83 7.0 MeV vertical beam divergence

Figure 84 2.0 MeV beam divergence

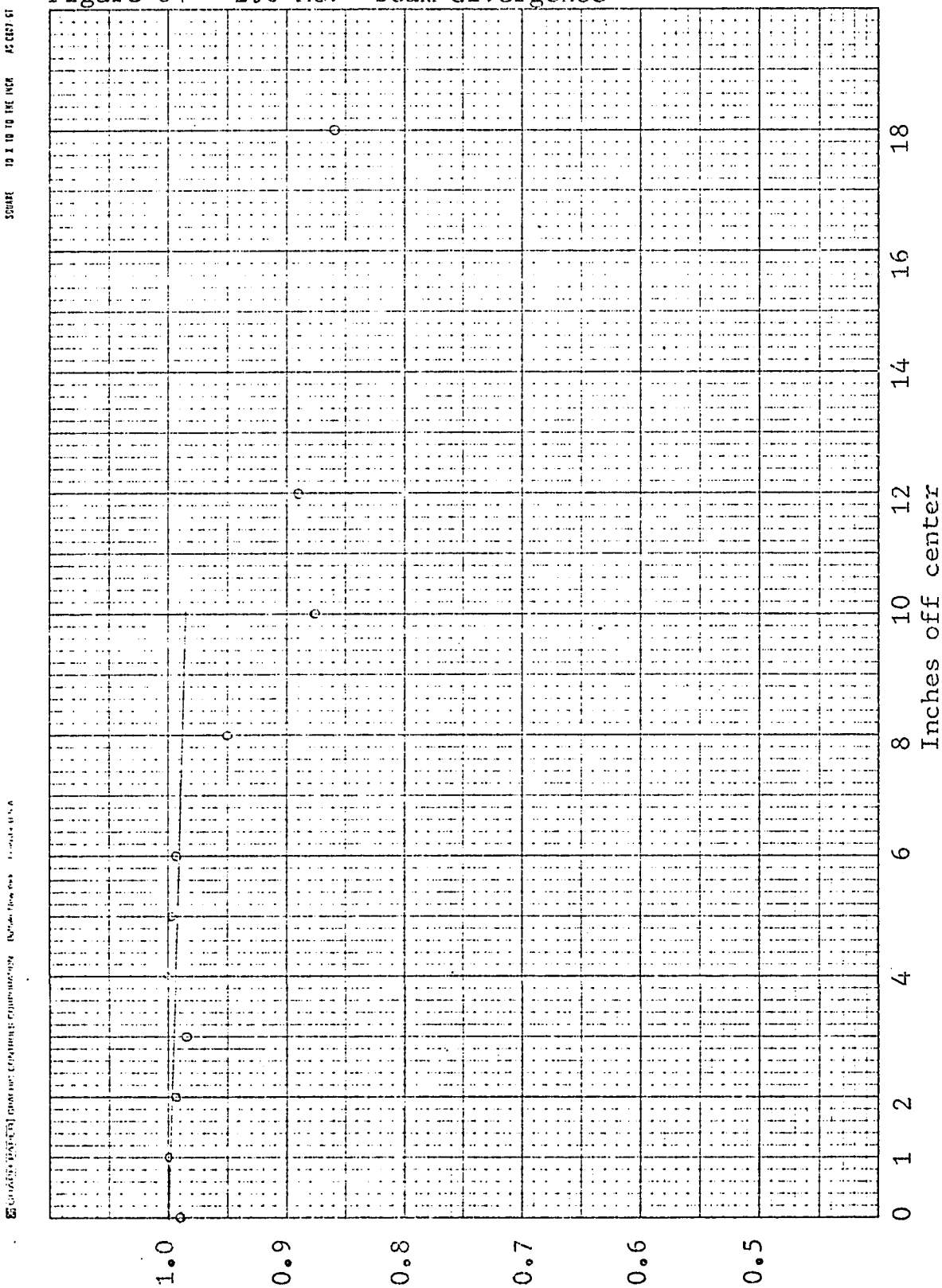

Figure 85 3.5 MeV beam divergence

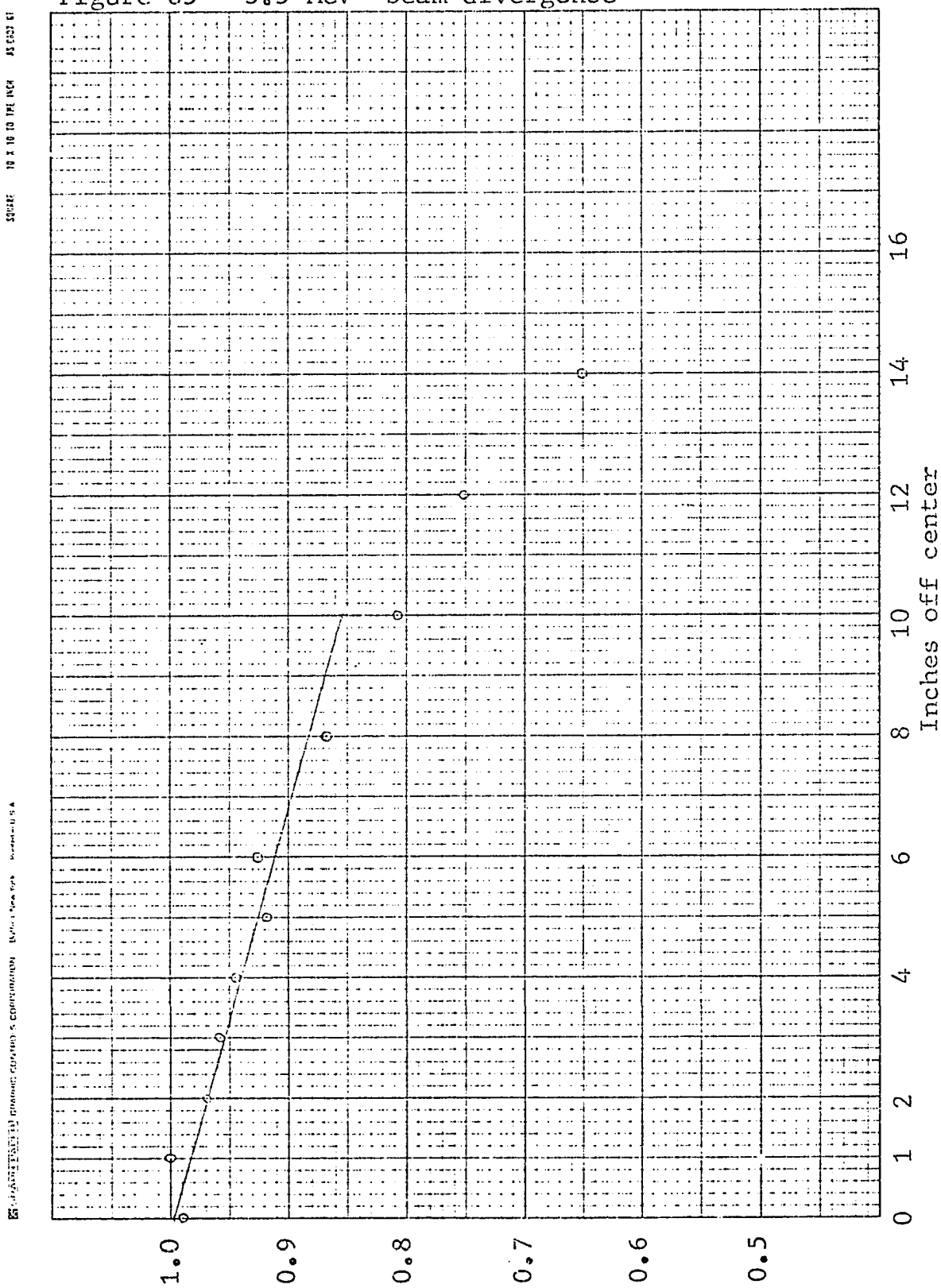

Figure 86 7.0 MeV beam divergence

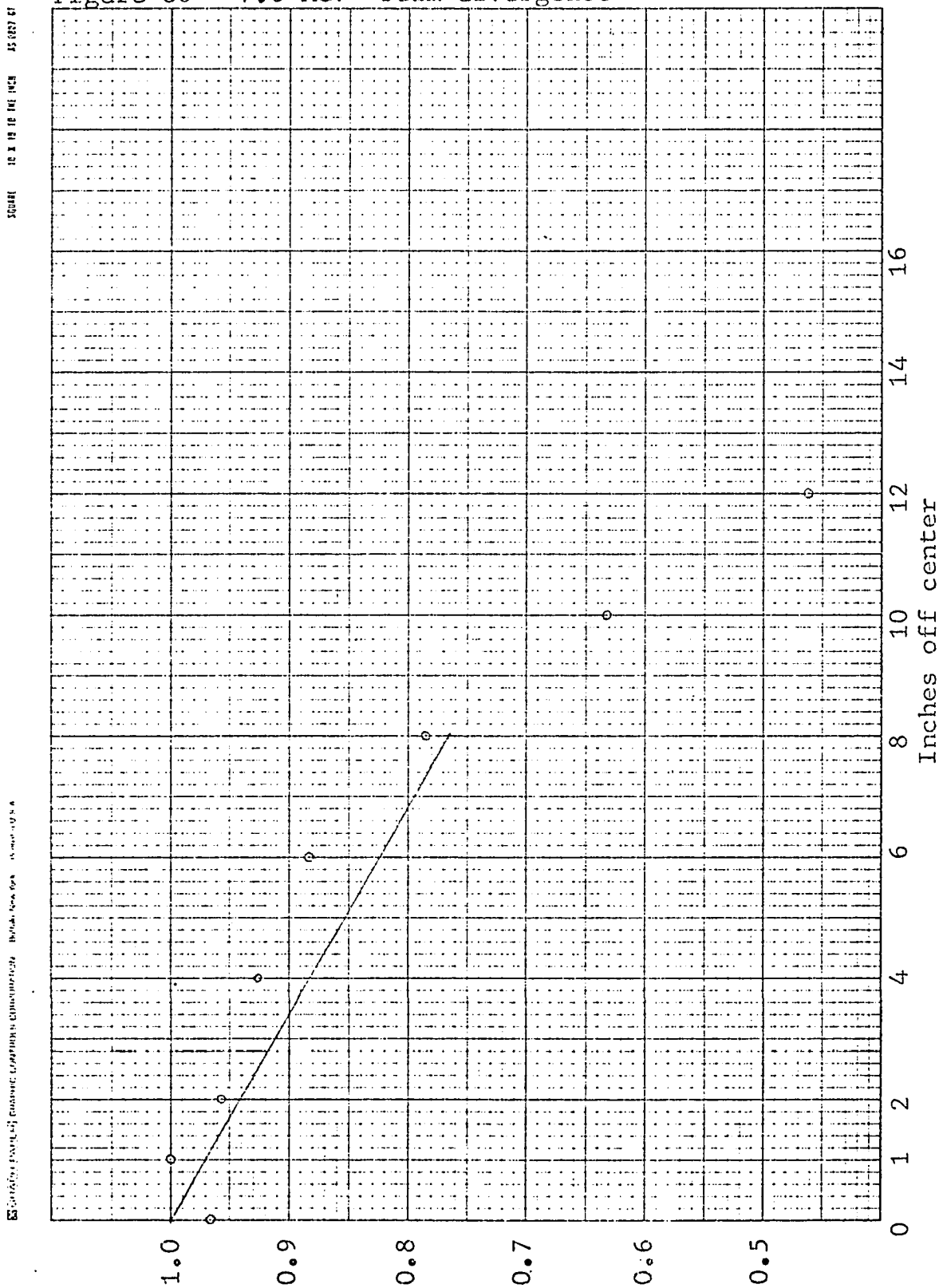

10.5 MeV are not clearly semi-infinite irradiated surface areas. And even in this case, results are not much below DTF results and the beam is as large as might generally be encountered.

# I. TLD EXPERIMENTAL DATA

The following tables list the data collected in this project.

As mentioned previously, two sizes of crystals were used; these are referred to as "square" (1/8" x 1/8") and "rod" (1mm x 6mm). The locations monitored are "Beam Collimator Exit", "Backscatterer Position", and the various angular positions which have the additional notation of "Background" or "Backscatter" depending upon the measurement made. "Beam Collimator Exit" was normally 30 to 35 inches from the x-ray target. The sides of the beam were shielded somewhat to lower background levels due to scatter out of the beam. "Backscatterer Position" denotes the location at which the backscatter slab was to be placed, 60 to 75 inches from the x-ray target. The experimental configuration is discussed in Section 5.

Calibration on the crystals was repeatedly checked throughout the period of this work so as to keep the reported readings comparable.

## 17.1 2 MeV

### 17.1.1 Backscatter

#### 17.1.1.1 Lead

| LOCATION | TLD READING | |
|---|---|---|
| | SQUARE | ROD |
| Beam collimator exit | 13939800 | 11369800 |
| | 15503200 | 11776600 |
| | 12931600 | 9662700 |
| | 13893600 | 11142500 |
| | 14839500 | 10335200 |
| | 13585800 | 10541700 |
| Backscatterer position | 1044600 | 894800 |
| | 973500 | 922600 |
| | 1150600 | 909200 |
| | 1047700 | 865100 |
| | 1152100 | 745900 |
| | 1236200 | 756300 |
| Background @ 14", 30° 3.75" collimator | 2992 | |
| | 2991 | |
| | 3653 | |
| | 3277 | |
| Background @ 12", 40° 3.75" collimator | | 3020 |
| | | 3018 |
| | | 2495 |
| | | 2892 |
| Background @ 11", 50° 3.75" collimator | 224 | |
| | 208 | |
| | 231 | |
| | 211 | |
| Background @ 10", 60° 3.75" collimator | | 407 |
| | | 371 |
| | | 339 |
| | | 372 |

| LOCATION | TLD READING | |
|---|---|---|
| | SQUARE | ROD |
| Beam collimator exit | 14928900 | 9575200 |
| | 13463800 | 10470300 |
| | 14424000 | 10695400 |
| | 13789500 | 10354900 |
| | 14846400 | 10812000 |
| | 13392100 | 9945700 |
| Backscatter @ 14", 30° | 4216 | |
| 3.75" collimator | 4051 | |
| | 4493 | |
| | 4533 | |
| Backscatter @ 12", 40° | | 3022 |
| 3.75" collimator | | 3360 |
| | | 2886 |
| | | 2907 |
| Backscatter @ 11", 50° | 1223 | |
| 3.75" collimator | 1353 | |
| | 1413 | |
| | 1338 | |
| Backscatter @ 10", 60° | | 1150 |
| 3.75" collimator | | 1119 |
| | | 1242 |
| | | 1092 |
| Beam collimator exit | 14889800 | 10441500 |
| | 13182100 | 10613400 |
| | 14603600 | 10730600 |
| | 14217200 | 11083800 |
| | 14906500 | 11726900 |
| | 14327600 | 11215300 |
| Backscatterer position | 1124000 | 776600 |
| | 1164700 | 764000 |
| | 1179400 | 856100 |
| | 1158500 | 857100 |
| | 1202500 | 890000 |
| | 1082300 | 824500 |

| LOCATION | TLD READING | |
|---|---|---|
| | SQUARE | ROD |
| Background @ 14", 30° 3.75" collimator | | 7314 |
| | | 7026 |
| | | 7377 |
| | | 6877 |
| Background @ 12", 40° 3.75" collimator | 448 | |
| | 448 | |
| | 477 | |
| | 461 | |
| Background @ 11", 50° 3.75" collimator | | 125 |
| | | 150 |
| | | 163 |
| | | 165 |
| Background @ 10", 60° 3.75" collimator | 208 | |
| | 233 | |
| | 215 | |
| | 211 | |
| Beam collimator exit | 14607400 | 10041300 |
| | 13355400 | 10525400 |
| | 14491300 | 11334800 |
| | 14496800 | 11050400 |
| | 15454400 | 11006400 |
| | 13785600 | 11440300 |
| Backscatter @ 14", 30° 3.75" collimator | | 4194 |
| | | 5798 |
| | | 4885 |
| | | 5470 |
| Backscatter @ 12", 40° 3.75" collimator | 1432 | |
| | 1410 | |
| | 1532 | |
| | 1485 | |
| Backscatter @ 11", 50° 3.75" collimator | | 775 |
| | | 799 |
| | | 815 |
| | | 885 |

| LOCATION | TLD READING | |
|---|---|---|
| | SQUARE | ROD |
| Backscatter @ 10", 60° | 1423 | |
| 3.75" collimator | 1397 | |
| | 1504 | |
| | 1343 | |
| Beam collimator exit | 5745500 | 4196400 |
| | 5401900 | 4079800 |
| | 5287200 | 4167900 |
| | 5795900 | 4079300 |
| | 5517800 | 4468300 |
| | 5364400 | 3949500 |
| Backscatterer position | 885100 | 708800 |
| | 905800 | 675000 |
| | 913300 | 748600 |
| | 991800 | 608700 |
| | 905300 | 712700 |
| | 826700 | 645400 |
| Background @ 27.12", 30° | | 4 |
| 11.50" collimator | | 3 |
| | | 3 |
| | | 3 |
| Background @ 23.0", 30° | 5 | |
| 7.75" collimator | 5 | |
| | 5 | |
| | 5 | |
| Background @ 16.5", 50° | | 5 |
| 6.375" collimator | | 4 |
| | | 6 |
| | | 5 |
| Background @ 10.0", 50° | 4 | |
| 7.5" collimator | 4 | |
| | 5 | |
| | 5 | |
| Background @ 24.88", 50° | | 3 |
| 13.25" collimator | | 3 |
| | | 3 |
| | | 3 |

| LOCATION | TLD READING | |
|---|---|---|
| | SQUARE | ROD |
| Beam collimator exit | 5984300 | 4293400 |
| | 5552100 | 4139400 |
| | 5429800 | 4178600 |
| | 5755500 | 4267400 |
| | 5096300 | 3465100 |
| | 5686200 | 4227700 |
| Backscatter @ 27.0", 30° | 12 | |
| 11.5" collimator | 13 | |
| | 11 | |
| | 12 | |
| Backscatter @ 23.0", 30° | | 9 |
| 7.75" collimator | | 8 |
| | | 9 |
| | | 8 |
| Backscatter @ 24.81", 50° | 10 | |
| 13.25" collimator | 9 | |
| | 8 | |
| | 9 | |
| Backscatter @ 18", 50° | | 7 |
| 7.5" collimator | | 6 |
| | | 6 |
| | | 7 |
| Backscatter @ 16.62", 50° | 120 | |
| 6.375" collimator | 121 | |
| | 121 | |
| | 143 | |
| Beam collimator exit | 5922300 | 4193900 |
| | 5515800 | 4429800 |
| | 5906900 | 4088500 |
| | 5886000 | 4355200 |
| | 5316000 | 4286300 |
| | 5651400 | 4161200 |

| LOCATION | TLD READING | |
|---|---|---|
| | SQUARE | ROD |
| Backscatterer position | 1073000 | 630400 |
| | 1006700 | 753600 |
| | 1042400 | 716800 |
| | 999800 | 716100 |
| | 947500 | 701000 |
| | 920800 | 723400 |
| Background @ 25.25", 40° | | 3 |
| 7.375" collimator | | 4 |
| | | 3 |
| | | 4 |
| Background @ 25.19", 40° | 4 | |
| 11.625" collimator | 6 | |
| | 5 | |
| | 5 | |
| Background @ 17.69", 40° | | 5 |
| 6.375" collimator | | 5 |
| | | 6 |
| | | 5 |
| Background @ 23.5", 60° | 5 | |
| 13.25" collimator | 4 | |
| | 5 | |
| | 4 | |
| Background @ 23.44", 60° | | 4 |
| 7.50" collimator | | 3 |
| | | 4 |
| | | 3 |
| Beam collimator exit | 5673000 | 3904800 |
| | 5329500 | 4340100 |
| | 5124900 | 4198700 |
| | 5340300 | 4336700 |
| | 5521100 | 3872100 |
| | 5892000 | 4243800 |
| Backscatter @ 25.19", 40° | 12 | |
| 11.625" collimator | 12 | |
| | 12 | |
| | 11 | |

| LOCATION | TLD READING | |
|---|---|---|
| | SQUARE | ROD |
| Backscatter @ 25.25", 40° | | 8 |
| 7.375" collimator | | 8 |
| | | 9 |
| | | 9 |
| Backscatter @ 17.69", 40° | 128 | |
| 6.375" collimator | 111 | |
| | 139 | |
| | 126 | |
| Backscatter @ 23.44", 60° | | 7 |
| 7.50" collimator | | 6 |
| | | 7 |
| | | 8 |
| Backscatter @ 23.50", 60° | 12 | |
| 13.25" collimator | 10 | |
| | 11 | |
| | 11 | |
| Beam collimator exit | 5608100 | 3562900 |
| | 5798300 | 4096800 |
| | 5159900 | 3605000 |
| | 5720600 | 3828100 |
| | 5391800 | 3256400 |
| | 5446200 | |
| Backscatterer position | 1022000 | 649800 |
| | 1029400 | 753500 |
| | 970300 | 706200 |
| | 1048700 | 719700 |
| | 1027500 | 804700 |
| | 902700 | 598400 |
| Background @ 21.88", 30° | | 8 |
| 5.562" collimator | | 8 |
| | | 8 |
| | | 9 |
| Background @ 18.69", 40° | 13 | |
| 5.312" collimator | 11 | |
| | 11 | |
| | 10 | |

| LOCATION | TLD READING | |
|---|---|---|
| | SQUARE | ROD |
| Background @ 18.75", 50°<br>7.625" collimator | | 5<br>6<br>5<br>5 |
| Background @ 15.94", 60°<br>5.875" collimator | 11<br>11<br>10<br>11 | |
| Background @ 21.19", 70°<br>7.875" collimator | | 5<br>5<br>4<br>5 |
| Beam collimator exit | 5081800<br>4928900<br>5148300<br>5189200<br>5236000<br>4891800 | 4371500<br>4421700<br>3569400<br>3854800<br>3919700<br>4033000 |
| Backscatter @ 21.88", 30°<br>5.562" collimator | | 102<br>91<br>98<br>99 |
| Backscatter @ 18.69", 40°<br>5.312" collimator | 211<br>218<br>216<br>227 | |
| Backscatter @ 18.75", 50°<br>7.625" collimator | | 41<br>43<br>41<br>37 |
| Backscatter @ 15.94", 60°<br>5.875" collimator | 170<br>172<br>154<br>173 | |

| LOCATION | TLD READING | |
|---|---|---|
| | SQUARE | ROD |
| Backscatter @ 21.19", 70° | | 27 |
| 7.875" collimator | | 25 |
| | | 29 |
| | | 28 |
| Beam collimator exit | 6143900 | 4696400 |
| | 6267800 | 4592300 |
| | 5677200 | 4331700 |
| | 6139700 | 4205500 |
| | 5501700 | 3977500 |
| | 5861100 | 4475500 |
| Backscatterer position | 1074900 | 785200 |
| | 1122600 | 795900 |
| | 1185400 | 757400 |
| | 1090500 | 737100 |
| | 1154700 | 859000 |
| | 1122700 | 776000 |
| Background @ 22.62", 30° | 12 | |
| 5.875" collimator | 12 | |
| | 12 | |
| | 12 | |
| Background @ 20.50", 40° | | 10 |
| 5.312" collimator | | 9 |
| | | 9 |
| | | 9 |
| Background @ 20.12", 50° | 6 | |
| 7.688" collimator | 6 | |
| | 6 | |
| | 7 | |
| Background @ 22.19", 60° | | 4 |
| 9.688" collimator | | 4 |
| | | 4 |
| | | 4 |

| LOCATION | TLD READING | |
|---|---|---|
| | SQUARE | ROD |
| Beam collimator exit | 5777300 | 3747600 |
| | 5933100 | 4476500 |
| | 5342900 | 4724600 |
| | 5437600 | 4324600 |
| | 6151100 | 3890700 |
| | 4913400 | 4466200 |
| Backscatter @ 22.62", 30° | 166 | |
| 5.875" collimator | 169 | |
| | 151 | |
| | 157 | |
| Backscatter @ 20.50", 40° | | 150 |
| 5.312" collimator | | 159 |
| | | 181 |
| | | 148 |
| Backscatter @ 20.12", 50° | 65 | |
| 7.688" collimator | 76 | |
| | 75 | |
| | 70 | |
| Backscatter @ 22.19", 60° | | 18 |
| 9.688" collimator | | 18 |
| | | 20 |
| | | 19 |

17.1.1.2 Iron

| LOCATION | TLD READING | |
|---|---|---|
| | SQUARE | ROD |
| Beam collimator exit | 5314100 | 4010400 |
| | 6179900 | 4253400 |
| | 5303000 | 4039300 |
| | 5642300 | 4131600 |
| | 5100300 | 3673700 |
| | 5494500 | 4298900 |
| Backscatterer position | 1110800 | 691300 |
| | 969400 | 698400 |
| | 1006300 | 734000 |
| | 1005300 | 667900 |
| | 1036800 | 559000 |
| | 986300 | 723900 |
| Background @ 22.69", 30° 5.75" collimator | | 7 |
| | | 7 |
| | | 6 |
| | | 6 |
| Background @ 20.15", 40° 3.25" collimator | 10 | |
| | 10 | |
| | 11 | |
| | 11 | |
| Background @ 20.19", 50° 7.625" collimator | | 4 |
| | | 5 |
| | | 4 |
| | | 6 |
| Background @ 21.88", 60° 9.688" collimator | 9 | |
| | 5 | |
| | 5 | |
| | 5 | |
| Beam collimator exit | 5691700 | 3898200 |
| | 5633900 | 4258900 |
| | 5797000 | 4211900 |
| | 5656600 | 4436800 |
| | 4865300 | 4504600 |
| | 5610400 | 4326800 |

| LOCATION | TLD READING | |
|---|---|---|
| | SQUARE | ROD |
| Backscatter @ 22.69", 30° 5.75" collimator | | 75 |
| | | 80 |
| | | 80 |
| | | 83 |
| Backscatter @ 20.25", 40° 5.25" collimator | 144 | |
| | 135 | |
| | 125 | |
| | 148 | |
| Backscatter @ 20.19", 50° 7.625" collimator | | 44 |
| | | 43 |
| | | 43 |
| | | 44 |
| Backscatter @ 21.88", 60° 9.688" collimator | 39 | |
| | 40 | |
| | 37 | |
| | 39 | |
| Beam collimator exit | 5318700 | 3936200 |
| | 5172700 | 4355700 |
| | 4736100 | 3830100 |
| | 5324300 | 4395200 |
| | 5576500 | 4915300 |
| | 5452300 | 4363500 |
| Backscatterer position | 1020500 | 803500 |
| | 889900 | 669900 |
| | 948600 | 669500 |
| | 881700 | 799900 |
| | 964500 | 786900 |
| | 1003000 | 721700 |
| Background @ 22.0", 30° 5.562" collimator | 9 | |
| | 8 | |
| | 8 | |
| | 9 | |
| Background @ 18.75", 40° 5.312" collimator | | 7 |
| | | 7 |
| | | 7 |
| | | 8 |

| LOCATION | TLD READING | |
|---|---|---|
| | SQUARE | ROD |
| Background @ 18.75", 50° | 7 | |
| 7.562" collimator | 5 | |
| | 6 | |
| | 6 | |
| Background @ 15.94", 60° | | 7 |
| 5.875" collimator | | 7 |
| | | 6 |
| | | 6 |
| Background @ 21.31", 70° | 7 | |
| 7.875" collimator | 6 | |
| | 7 | |
| | 7 | |
| Beam collimator exit | 5023700 | 4387500 |
| | 5254200 | 4207200 |
| | 5766400 | 4127400 |
| | 6038500 | 4670100 |
| | 5772900 | 3886900 |
| | 5635800 | 3691400 |
| Backscatter @ 22.0", 30° | 109 | |
| 5.562" collimator | 128 | |
| | 124 | |
| | 121 | |
| Backscatter @ 18.75", 40° | | 110 |
| 5.312" collimator | | 113 |
| | | 103 |
| | | 106 |
| Backscatter @ 18.75", 50° | 57 | |
| 7.562" collimator | 66 | |
| | 61 | |
| | 67 | |
| Backscatter @ 15.94", 60° | | 95 |
| 5.875" collimator | | 93 |
| | | 93 |
| | | 96 |

| LOCATION | TLD READING | |
|---|---|---|
| | SQUARE | ROD |
| Backscatter @ 21.31", 70° | 69 | |
| 7.875" collimator | 66 | |
| | 77 | |
| | 72 | |

17.1.1.3 Concrete

| LOCATION | TLD READING | |
|---|---|---|
| | SQUARE | ROD |
| Beam collimator exit | 6652900 | 5511400 |
| | 7201600 | 5400800 |
| | 7273400 | 5491600 |
| | 6833100 | 4900200 |
| | 5935200 | 5399400 |
| | 6879300 | 5290200 |
| Backscatterer position | 494800 | 339100 |
| | 443500 | 357800 |
| | 419800 | 236600 |
| | 487700 | 308600 |
| | 457300 | 347800 |
| | 442000 | 319100 |
| Background @ 43.25", 30° | 7 | 6 |
| 12.0" collimator | 8 | 5 |
| | 7 | 4 |
| | 7 | 5 |
| Background @ 35.62", 45° | 5 | 3 |
| 9.875" collimator | 4 | 4 |
| | 4 | 3 |
| | 4 | 3 |
| Background @ 37.88", 60° | 5 | |
| 14.625" collimator | 4 | |
| | 5 | |
| | 4 | |
| Beam collimator exit | 6198700 | 5268500 |
| | 6530300 | 5026100 |
| | 6062200 | 4752500 |
| | 6098000 | 5049600 |
| | 6217100 | 4602700 |
| | 6793000 | 5323200 |
| Backscatter @ 43.25", 30° | 17 | 13 |
| 12.0" collimator | 18 | 13 |
| | 18 | 14 |
| | 22 | 13 |

| LOCATION | TLD READING | |
|---|---|---|
| | SQUARE | ROD |
| Backscatter @ 35.62", 45° | 23 | 17 |
| 9.875" collimator | 24 | 18 |
| | 21 | 22 |
| | 22 | 19 |
| Backscatter @ 37.88", 60° | 13 | 11 |
| 14.625" collimator | 13 | 9 |
| | 12 | 10 |
| | 13 | 9 |

## 17.1.2 Copper absorption in beam

| DEPTH IN COPPER | TLD READING |
|---|---|
| 2.00 inches | 127 |
| | 146 |
| | 137 |
| | 124 |
| 1.50 | 210 |
| | 215 |
| | 195 |
| | 226 |
| 1.25 | 315 |
| | 340 |
| | 330 |
| | 295 |
| 1.00 | 474 |
| | 431 |
| | 457 |
| | 471 |
| 0.875 | 531 |
| | 475 |
| | 487 |
| | 546 |
| 0.75 | 625 |
| | 669 |
| | 670 |
| | 622 |
| 0.625 | 724 |
| | 684 |
| | 735 |
| | 662 |
| 0.50 | 936 |
| | 930 |
| | 949 |
| | 904 |
| 0.25 | 1700 |
| | 1605 |
| | 1619 |

## 17.1.3 Infinite size determinations (All measurements in this section were made with a 3.75" collimator)

### 17.1.3.1 Lead

#### 17.1.3.1.1 4" square, 1.75" thick

| LOCATION | TLD READING | |
|---|---|---|
| | SQUARE | ROD |
| Beam collimator exit | 6480700 | |
| | 5735200 | |
| | 5710500 | |
| | 6423100 | |
| | 5356600 | |
| | 5896500 | |
| | 5548300 | |
| | 5576500 | |
| | 5777500 | |
| Backscatterer position | 910000 | |
| | 822600 | |
| | 963500 | |
| | 970600 | |
| | 971400 | |
| | 864200 | |
| | 909700 | |
| | 886600 | |
| | 930300 | |
| Background @ 33.88", 30° | 8 | |
| | 7 | |
| | 7 | |
| | 7 | |
| Background @ 28.62", 45° | 9 | |
| | 7 | |
| | 8 | |
| | 7 | |

| LOCATION | TLD READING | |
|---|---|---|
| | SQUARE | ROD |
| Background @ 23.38", 45° | 7 | |
| | 8 | |
| | 9 | |
| | 8 | |
| Background @ 22.56", 60° | 10 | |
| | 7 | |
| | 7 | |
| | 9 | |
| Beam collimator exit | 6029600 | |
| | 6202700 | |
| | 6405100 | |
| | 6472100 | |
| | 6093800 | |
| | 5930100 | |
| | 6368300 | |
| | 6094400 | |
| | 6025500 | |
| Backscatter @ 33.88", 30° | 17 | |
| | 17 | |
| | 18 | |
| | 17 | |
| Backscatter @ 28.62", 45° | 20 | |
| | 21 | |
| | 18 | |
| | 20 | |
| Backscatter @ 23.38", 45° | 28 | |
| | 25 | |
| | 27 | |
| | 27 | |
| Backscatter @ 22.56", 60° | 28 | |
| | 29 | |
| | 27 | |
| | 28 | |

| LOCATION | TLD READING | |
|---|---|---|
| | SQUARE | ROD |
| Beam collimator exit | | 4338300 |
| | | 3227500 |
| | | 4221800 |
| | | 4391000 |
| | | 4206300 |
| | | 4361400 |
| | | 4246000 |
| | | 4084100 |
| | | 4298800 |
| Backscatterer position | | 604700 |
| | | 568600 |
| | | 629200 |
| | | 590600 |
| | | 662900 |
| | | 603800 |
| | | 616200 |
| | | 646700 |
| | | 578400 |
| Background @ 31.52", 30° | | 9 |
| | | 9 |
| | | 11 |
| | | 13 |
| Background @ 23.81", 45° | | 7 |
| | | 8 |
| | | 7 |
| | | 8 |
| Background @ 24.81", 45° | | 10 |
| | | 10 |
| | | 10 |
| | | 9 |
| Background @ 20.75", 60° | | 6 |
| | | 10 |
| | | 7 |

| LOCATION | TLD READING | |
|---|---|---|
| | SQUARE | ROD |
| Backscatterer position | | 4336800 |
| | | 4206400 |
| | | 3532300 |
| | | 4356900 |
| | | 3971800 |
| | | 3756700 |
| | | 4051000 |
| | | 4089200 |
| | | 4158800 |
| Backscatter @ 31.52", 30° | | 14 |
| | | 13 |
| | | 14 |
| | | 15 |
| Backscatter @ 23.81", 45° | | 21 |
| | | 19 |
| | | 19 |
| | | 20 |
| Backscatter @ 24.81", 45° | | 19 |
| | | 18 |
| | | 17 |
| | | 19 |
| Backscatter @ 20.75", 60° | | 20 |
| | | 20 |
| | | 21 |
| | | 20 |

17.1.3.1.2 6" square, 1.75" thick

| LOCATION | TLD READING | |
|---|---|---|
| | SQUARE | ROD |
| Beam collimator exit | | 4459000 |
| | | 4262300 |
| | | 4196600 |
| | | 4296100 |
| | | 4167300 |
| | | 4559700 |
| | | 3959300 |
| | | 4540100 |
| | | 4407900 |
| Background @ 34.19", 30° | | 8 |
| | | 7 |
| | | 6 |
| | | 8 |
| Background @ 28.50", 45° | | 6 |
| | | 7 |
| | | 6 |
| | | 6 |
| Background @ 22.69", 60° | | 7 |
| | | 8 |
| | | 8 |
| | | 7 |
| Beam collimator exit | | 4219700 |
| | | 3277000 |
| | | 4128100 |
| | | 4480800 |
| | | 5006400 |
| | | 4590700 |
| | | 4138400 |
| | | 4405200 |
| | | 4592100 |
| Backscatter @ 34.19", 30° | | 11 |
| | | 11 |
| | | 12 |
| | | 12 |

| LOCATION | TLD READING | |
|---|---|---|
| | SQUARE | ROD |
| Backscatter @ 28.50", 45° | | 13 |
| | | 15 |
| | | 15 |
| | | 13 |
| Backscatter @ 22.69", 60° | | 17 |
| | | 17 |
| | | 17 |
| | | 19 |
| Beam collimator exit | 5359200 | |
| | 5500800 | |
| | 5462800 | |
| | 5240900 | |
| | 5527500 | |
| | 5448500 | |
| | 4800700 | |
| | 5607800 | |
| | 5153100 | |
| Backscatterer position | 878800 | |
| | 868000 | |
| | 835500 | |
| | 790600 | |
| | 660800 | |
| | 933600 | |
| | 845400 | |
| | 836900 | |
| | 869100 | |
| Background @ 31.75", 30° | 38 | |
| | 33 | |
| | 35 | |
| | 38 | |
| Background @ 24.19", 45° | 33 | |
| | 31 | |
| | 36 | |
| | 34 | |

| LOCATION | TLD READING | |
|---|---|---|
| | SQUARE | ROD |
| Background @ 24.25", 45° | 38 | |
| | 33 | |
| | 42 | |
| | 33 | |
| Background @ 21.06", 60° | 30 | |
| | 25 | |
| | 34 | |
| | 29 | |
| Beam collimator exit | 6368200 | |
| | 5437800 | |
| | 6056400 | |
| | 5269500 | |
| | 5870700 | |
| | 5435900 | |
| | 5563100 | |
| | 6483500 | |
| | 5944600 | |
| Backscatter @ 31.75", 30° | 42 | |
| | 35 | |
| | 39 | |
| | 44 | |
| Backscatter @ 24.19", 45° | 53 | |
| | 48 | |
| | 57 | |
| | 46 | |
| Backscatter @ 24.25", 45° | 45 | |
| | 56 | |
| | 46 | |
| | 56 | |
| Backscatter @ 21.06", 60° | 51 | |
| | 50 | |
| | 47 | |
| | 55 | |

17.1.3.1.3 7" square, 1.75" thick

| LOCATION | TLD READING | |
|---|---|---|
| | SQUARE | ROD |
| Beam collimator exit | 5975100 | |
| | 6275500 | |
| | 5638400 | |
| | 6404600 | |
| | 6070900 | |
| | 6045900 | |
| Backscatterer position | 932500 | |
| | 887500 | |
| | 877800 | |
| | 936400 | |
| | 857800 | |
| | 919500 | |
| Background @ 30.25", 30° | 4 | |
| | 4 | |
| | 5 | |
| | 5 | |
| Background @ 14.50", 45° | 6 | |
| | 5 | |
| | 5 | |
| | 5 | |
| Background @ 19.62", 60° | 5 | |
| | 5 | |
| | 5 | |
| Beam collimator exit | 6319100 | |
| | 6396400 | |
| | 6025800 | |
| | 5905400 | |
| | 6037000 | |
| | 5949100 | |
| Backscatter @ 30.25", 30° | 16 | |
| | 15 | |
| | 16 | |
| | 15 | |

| LOCATION | TLD READING | |
|---|---|---|
| | SQUARE | ROD |
| Backscatter @ 14.50", 45° | 76 | |
| | 72 | |
| | 82 | |
| | 67 | |
| Backscatter @ 19.62", 60° | 30 | |
| | 31 | |
| | 30 | |
| | 31 | |
| Beam collimator exit | | 4340400 |
| | | 4721300 |
| | | 4371600 |
| | | 4298700 |
| | | 4203400 |
| | | 4734200 |
| Backscatterer position | | 765200 |
| | | 727900 |
| | | 649500 |
| | | 611600 |
| | | 642000 |
| | | 643000 |
| Background @ 30.06", 30° | | 3 |
| | | 2 |
| | | 3 |
| | | 3 |
| Background @ 14.56", 45° | | 4 |
| | | 3 |
| | | 4 |
| | | 4 |
| Background @ 19.19", 60° | | 4 |
| | | 4 |
| | | 4 |
| | | 3 |

| LOCATION | TLD READING | |
|---|---|---|
| | SQUARE | ROD |
| Beam collimator exit | | 4331500 |
| | | 4635500 |
| | | 4360300 |
| | | 4901400 |
| | | 4468100 |
| | | 4365400 |
| Backscatter @ 30.06", 30° | | 11 |
| | | 12 |
| | | 12 |
| | | 12 |
| Backscatter @ 14.56", 45° | | 55 |
| | | 54 |
| | | 53 |
| | | 56 |
| Backscatter @ 19.19", 60° | | 20 |
| | | 21 |
| | | 20 |
| | | 21 |
| Beam collimator exit | 4843000 | |
| | 4631300 | |
| | 5108500 | |
| | 5079200 | |
| | 5375700 | |
| | 5163500 | |
| Background @ 29.50", 30° | 13 | |
| | 14 | |
| | 13 | |
| | 15 | |
| Background @ 23.69", 45° | 20 | |
| | 21 | |
| | 23 | |
| | 22 | |
| Background @ 21.38", 60° | 20 | |
| | 20 | |
| | 20 | |
| | 19 | |

| LOCATION | TLD READING | |
|---|---|---|
| | SQUARE | ROD |
| Beam collimator exit | 5191800 | |
| | 5565100 | |
| | 5472400 | |
| | 5284500 | |
| | 5187600 | |
| | 5522000 | |
| Backscatter @ 29.50", 30° | 16 | |
| | 15 | |
| | 17 | |
| | 16 | |
| Backscatter @ 23.69", 45° | 22 | |
| | 19 | |
| | 21 | |
| | 22 | |
| Backscatter @ 21.38", 60° | 21 | |
| | 22 | |
| | 20 | |
| | 21 | |

17.1.3.1.4 8" square, 1.75" thick

| LOCATION | TLD READING | |
|---|---|---|
| | SQUARE | ROD |
| Beam collimator exit | 5788300 | |
| | 5680300 | |
| | 4898800 | |
| | 5905100 | |
| | 5762300 | |
| | 5975700 | |
| | 6004600 | |
| | 6101300 | |
| | 5492500 | |
| Backscatterer position | 890800 | |
| | 834800 | |
| | 859700 | |
| | 881500 | |
| | 821100 | |
| | 855800 | |
| | 928200 | |
| | 876500 | |
| | 902300 | |
| Background @ 28.81", 30° | 7 | |
| | 6 | |
| | 7 | |
| | 5 | |
| Background @ 22.38", 45° | 6 | |
| | 7 | |
| | 7 | |
| | 7 | |
| Background @ 25.00", 45° | 5 | |
| | 6 | |
| | 5 | |
| | 5 | |
| Background @ 20.19", 60° | 8 | |
| | 8 | |
| | 7 | |
| | 6 | |

| LOCATION | TLD READING | |
|---|---|---|
| | SQUARE | ROD |
| Beam collimator exit | 5997300 | |
| | 5886400 | |
| | 5027700 | |
| | 5736700 | |
| | 5675700 | |
| | 6063900 | |
| | 6047700 | |
| | 5976200 | |
| | 5587300 | |
| Backscatter @ 28.81", 30° | 19 | |
| | 18 | |
| | 18 | |
| | 17 | |
| Backscatter @ 22.38", 45° | 29 | |
| | 31 | |
| | 26 | |
| | 30 | |
| Backscatter @ 25.00", 45° | 24 | |
| | 20 | |
| | 23 | |
| | 21 | |
| Backscatter @ 20.19", 60° | 30 | |
| | 30 | |
| | 30 | |
| | 26 | |
| Beam collimator exit | | 3903800 |
| | | 4244200 |
| | | 4322700 |
| | | 3935000 |
| | | 4122800 |
| | | 4436200 |
| | | 4122900 |

| LOCATION | TLD READING | |
|---|---|---|
| | SQUARE | ROD |
| Backscatterer position | | 645500 |
| | | 627300 |
| | | 625700 |
| | | 635400 |
| | | 623700 |
| | | 619500 |
| | | 612600 |
| | | 657200 |
| Background @ 31.62", 30° | | 5 |
| | | 6 |
| | | 6 |
| | | 6 |
| Background @ 24.12", 45° | | 5 |
| | | 6 |
| | | 5 |
| | | 6 |
| Background @ 24.06", 45° | | 9 |
| | | 7 |
| | | 7 |
| | | 8 |
| Background @ 21.25", 60° | | 6 |
| | | 6 |
| | | 6 |
| | | 5 |
| Beam collimator exit | | 4193300 |
| | | 4131300 |
| | | 4019800 |
| | | 4555600 |
| | | 3970500 |
| | | 3159000 |
| | | 4081600 |
| | | 4070700 |
| Backscatter @ 31.62", 30° | | 12 |
| | | 10 |
| | | 11 |
| | | 11 |

| LOCATION | TLD READING | |
|---|---|---|
| | SQUARE | ROD |
| Backscatter @ 24.12", 45° | | 18 |
| | | 18 |
| | | 19 |
| | | 20 |
| Backscatter @ 24.06", 45° | | 20 |
| | | 16 |
| | | 18 |
| | | 20 |
| Backscatter @ 21.25", 60° | | 19 |
| | | 19 |
| | | 19 |
| | | 18 |

17.1.3.1.5 10" square, 1.75" thick

| LOCATION | TLD READING | |
|---|---|---|
| | SQUARE | ROD |
| Beam collimator exit | | 4201500 |
| | | 4177300 |
| | | 3034800 |
| | | 4124500 |
| | | 4347900 |
| | | 4341200 |
| | | 4400100 |
| | | 4033000 |
| | | 4202100 |
| Backscatterer position | | 604400 |
| | | 695200 |
| | | 699000 |
| | | 622300 |
| | | 689900 |
| | | 646900 |
| | | 444900 |
| Background @ 29.00", 30° | | 4 |
| | | 5 |
| | | 4 |
| | | 5 |
| Background @ 22.50", 45° | | 4 |
| | | 4 |
| | | 4 |
| | | 3 |
| Background @ 25.25", 45° | | 5 |
| | | 4 |
| | | 4 |
| | | 5 |
| Background @ 20.12", 60° | | 4 |
| | | 5 |
| | | 4 |
| | | 4 |

| LOCATION | TLD READING | |
|---|---|---|
| | SQUARE | ROD |
| Backscatter @ 29.00", 30° | | 14 |
| | | 13 |
| | | 12 |
| | | 13 |
| Backscatter @ 22.50", 45° | | 22 |
| | | 22 |
| | | 21 |
| | | 24 |
| Backscatter @ 25.25", 45° | | 14 |
| | | 15 |
| | | 15 |
| | | 14 |
| Backscatter @ 20.12", 60° | | 20 |
| | | 22 |
| | | 18 |
| | | 20 |
| Beam collimator exit | 5374900 | |
| | 4996800 | |
| | 5753600 | |
| | 5252100 | |
| | 5641100 | |
| | 5262100 | |
| | 5681400 | |
| Backscatterer position | 840100 | |
| | 838100 | |
| | 841500 | |
| | 824400 | |
| | 787500 | |
| | 882900 | |
| | 806000 | |
| Background @ 31.00", 30° | 9 | |
| | 8 | |
| | 6 | |
| | 7 | |

| LOCATION | TLD READING | |
|---|---|---|
| | SQUARE | ROD |
| Background @ 23.75", 45° | 7 | |
| | 6 | |
| | 7 | |
| | 6 | |
| Background @ 23.62", 45° | 9 | |
| | 9 | |
| | 9 | |
| | 10 | |
| Background @ 21.00", 60° | 8 | |
| | 7 | |
| | 8 | |
| | 8 | |
| Beam collimator exit | 4943200 | |
| | 4709400 | |
| | 5036200 | |
| | 5343500 | |
| | 5500300 | |
| | 5866100 | |
| | 4646300 | |
| | 5543300 | |
| Backscatter @ 31.00", 30° | 12 | |
| | 14 | |
| | 15 | |
| | 17 | |
| Backscatter @ 23.75", 45° | 25 | |
| | 25 | |
| | 25 | |
| | 25 | |
| Backscatter @ 23.62", 45° | 25 | |
| | 26 | |
| | 27 | |
| | 28 | |
| Backscatter @ 21.00", 60° | 26 | |
| | 28 | |
| | 25 | |
| | 25 | |

17.1.3.1.6 12" square, 1.75" thick

| LOCATION | TLD READING | |
|---|---|---|
| | SQUARE | ROD |
| Beam collimator exit | | 4179500 |
| | | 4103400 |
| | | 2933900 |
| | | 3748700 |
| | | 4084000 |
| | | 3795400 |
| Backscatterer position | | 569500 |
| | | 584200 |
| | | 664100 |
| | | 665200 |
| | | 582000 |
| | | 507100 |
| Background @ 29.44", 30° | | 2 |
| | | 3 |
| | | 3 |
| | | 3 |
| Background @ 23.69", 45° | | 3 |
| | | 2 |
| | | 2 |
| | | 3 |
| Background @ 21.62", 60° | | 3 |
| | | 3 |
| | | 3 |
| | | 2 |
| Beam collimator exit | | 4044700 |
| | | 4204900 |
| | | 4234200 |
| | | 4302300 |
| | | 4395000 |
| | | 3998900 |
| Backscatter @ 29.44", 30° | | 10 |
| | | 11 |
| | | 11 |
| | | 10 |

| LOCATION | TLD READING | |
|---|---|---|
| | SQUARE | ROD |
| Backscatter @ 23.69", 45° | | 18 |
| | | 15 |
| | | 16 |
| | | 15 |
| Backscatter @ 21.62", 60° | | 15 |
| | | 15 |
| | | 14 |
| | | 15 |
| Beam collimator exit | 5846700 | |
| | 4800800 | |
| | 6307000 | |
| | 5969500 | |
| | 5717500 | |
| | 5906000 | |
| Backscatterer position | 982300 | |
| | 913400 | |
| | 890300 | |
| | 969600 | |
| | 851400 | |
| | 807200 | |
| Background @ 29.25", 30° | 4 | |
| | 3 | |
| | 3 | |
| | 2 | |
| Background @ 23.50", 45° | 3 | |
| | 3 | |
| | 3 | |
| Background @ 21.25", 60° | 4 | |
| | 4 | |
| | 4 | |
| | 4 | |

| LOCATION | TLD READING | |
|---|---|---|
| | SQUARE | ROD |
| Beam collimator exit | 5514400 | |
| | 5327400 | |
| | 5356800 | |
| | 5056400 | |
| | 5416600 | |
| | 6150900 | |
| Backscatter @ 29.25", 30° | 15 | |
| | 17 | |
| | 16 | |
| | 15 | |
| Backscatter @ 23.50", 45° | 23 | |
| | 22 | |
| | 21 | |
| | 20 | |
| Backscatter @ 21.25", 60° | 22 | |
| | 21 | |
| | 26 | |
| | 24 | |

17.1.3.1.7 9" square, 0.25" thick

| LOCATION | TLD READING | |
|---|---|---|
| | SQUARE | ROD |
| Beam collimator exit | 5916900 | |
| | 6956400 | |
| | 6050700 | |
| | 6588100 | |
| | 6426800 | |
| | 6919600 | |
| | 6147600 | |
| | 6719600 | |
| | 6291300 | |
| Backscatterer position | 910900 | |
| | 923000 | |
| | 1058600 | |
| | 1051600 | |
| | 1049700 | |
| | 1037200 | |
| | 993000 | |
| | 961500 | |
| | 819400 | |
| Background @ 27.62", 30° | 9 | |
| | 7 | |
| | 8 | |
| | 9 | |
| Background @ 11.81", 45° | 11 | |
| | 10 | |
| | 11 | |
| | 11 | |
| Background @ 12.69", 60° | 13 | |
| | 12 | |
| | 10 | |
| Beam collimator exit | 5619800 | |
| | 5128300 | |
| | 5539300 | |
| | 5371900 | |
| | 5026800 | |
| | 5852100 | |

| LOCATION | TLD READING | |
|---|---|---|
| | SQUARE | ROD |
| Backscatter @ 27.62", 30° | 21 | |
| | 22 | |
| | 23 | |
| | 21 | |
| Backscatter @ 11.81", 45° | 141 | |
| | 132 | |
| | 132 | |
| | 126 | |
| Backscatter @ 12.69", 60° | 100 | |
| | 85 | |
| | 88 | |
| | 77 | |

17.1.3.1.8 9" square, 0.50" thick

| LOCATION | TLD READING | |
|---|---|---|
| | SQUARE | ROD |
| Beam collimator exit | 6165400 | |
| | 6250900 | |
| | 6426700 | |
| | 4938000 | |
| | 5716300 | |
| | 6004100 | |
| | 5386200 | |
| | 6356600 | |
| | 5807800 | |
| Backscatter @ 27.69", 30° | 20 | |
| | 16 | |
| | 18 | |
| | 19 | |
| Backscatter @ 11.88", 45° | 125 | |
| | 119 | |
| | 120 | |
| | 121 | |
| Backscatter @ 12.75", 60° | 82 | |
| | 86 | |
| | 97 | |
| | 96 | |

17.1.3.1.9 9" square, 0.625" thick

| LOCATION | TLD READING | |
|---|---|---|
| | SQUARE | ROD |
| Beam collimator exit | | 3752400 |
| | | 4125300 |
| | | 3733100 |
| | | 4058100 |
| | | 4217800 |
| | | 4681900 |
| Backscatterer position | | 654100 |
| | | 649600 |
| | | 677700 |
| | | 628500 |
| | | 663000 |
| | | 719200 |
| Background @ 30.00", 30° | | 3 |
| | | 5 |
| | | 3 |
| | | 5 |
| Background @ 14.50", 45° | | 5 |
| | | 4 |
| | | 5 |
| | | 6 |
| Background @ 19.25", 60° | | 5 |
| | | 6 |
| | | 6 |
| | | 6 |
| Beam collimator exit | | 5282000 |
| | | 4378000 |
| | | 4194200 |
| | | 4571100 |
| | | 4700800 |
| | | 3526000 |
| | | 4965600 |
| | | 4971200 |
| | | 4746300 |

| LOCATION | TLD READING | |
|---|---|---|
| | SQUARE | ROD |
| Backscatter @ 30.00", 30° | | 15 |
| | | 14 |
| | | 13 |
| | | 16 |
| Backscatter @ 14.50", 45° | | 63 |
| | | 68 |
| | | 60 |
| | | 80 |
| Backscatter @ 19.25", 60° | | 97 |
| | | 88 |
| | | 96 |
| | | 89 |

17.1.3.1.10 9" square, 0.75" thick

| LOCATION | TLD READING | |
|---|---|---|
| | SQUARE | ROD |
| Beam collimator exit | 5647500 | |
| | 5997300 | |
| | 5950300 | |
| | 5605700 | |
| | 5674900 | |
| | 6240300 | |
| Backscatter @ 27.75", 30° | 18 | |
| | 16 | |
| | 18 | |
| | 16 | |
| Backscatter @ 11.88", 45° | 122 | |
| | 112 | |
| | 107 | |
| | 103 | |
| Backscatter @ 12.75", 60° | 84 | |
| | 93 | |
| | 88 | |
| | 83 | |

17.1.3.1.11 9" square, 1.00" thick

| LOCATION | TLD READING | |
|---|---|---|
| | SQUARE | ROD |
| Beam collimator exit | | 4485400 |
| | | 4179200 |
| | | 4005100 |
| | | 3742500 |
| | | 3981100 |
| | | 4060800 |
| | | 4076500 |
| | | 4165300 |
| | | 2964900 |
| Backscatterer position | | 565400 |
| | | 698200 |
| | | 718800 |
| | | 656700 |
| | | 803100 |
| | | 600100 |
| | | 589100 |
| | | 829100 |
| | | 628200 |
| Background @ 27.69", 30° | | 3 |
| | | 3 |
| | | 3 |
| | | 4 |
| Background @ 9.56", 45° | | 5 |
| | | 5 |
| | | 5 |
| | | 5 |
| Background @ 11.31", 60° | | 5 |
| | | 5 |
| | | 5 |
| | | 5 |

| LOCATION | TLD READING | |
|---|---|---|
| | SQUARE | ROD |
| Beam collimator exit | | 4668400 |
| | | 4274200 |
| | | 3947400 |
| | | 4291300 |
| | | 4290500 |
| | | 4700800 |
| | | 4788000 |
| | | 4392200 |
| | | 3911400 |
| Backscatter @ 27.69", 30° | | 14 |
| | | 13 |
| | | 14 |
| | | 15 |
| Backscatter @ 9.56", 45° | | 109 |
| | | 109 |
| | | 116 |
| | | 114 |
| Backscatter @ 11.31", 60° | | 150 |
| | | 174 |
| | | 152 |
| | | 149 |

17.1.3.1.12 9" square, 1.25" thick

| LOCATION | TLD READING | |
|---|---|---|
| | SQUARE | ROD |
| Beam collimator exit | | 3772700 |
| | | 3903400 |
| | | 4611300 |
| | | 4182300 |
| | | 3993800 |
| | | 4173300 |
| | | 4005000 |
| | | 4161500 |
| | | 4031800 |
| Backscatter @ 27.5", 30° | | 22 |
| | | 17 |
| | | 17 |
| | | 14 |
| Backscatter @ 9.44", 45° | | 145 |
| | | 169 |
| | | 164 |
| | | 169 |
| Backscatter @ 11.25", 60° | | 87 |
| | | 91 |
| | | 90 |
| | | 64 |

17.1.3.1.13 9" square, 1.375" thick

| LOCATION | TLD READING | |
|---|---|---|
| | SQUARE | ROD |
| Beam collimator exit | | 4126300 |
| | | 4430100 |
| | | 4140800 |
| | | 4292500 |
| | | 4035800 |
| | | 4127300 |
| | | 4435600 |
| | | 3980400 |
| | | 4572000 |
| Backscatter @ 27.62", 30° | | 14 |
| | | 13 |
| | | 14 |
| | | 14 |
| Backscatter @ 11.81", 45° | | 89 |
| | | 97 |
| | | 81 |
| | | 83 |
| Backscatter @ 12.75", 60° | | 54 |
| | | 59 |
| | | 54 |
| | | 59 |

17.1.3.1.14 9" square, 1.50" thick

| LOCATION | TLD READING | |
|---|---|---|
| | SQUARE | ROD |
| Beam collimator exit | 6701400 | |
| | 6936700 | |
| | 5921000 | |
| | 6825300 | |
| | 6357500 | |
| | 6108500 | |
| | 6636100 | |
| | 6145900 | |
| | 6254900 | |
| Backscatter @ 31.12", 30° | 15 | |
| | 15 | |
| | 15 | |
| | 15 | |
| Backscatter @ 23.62", 45° | 27 | |
| | 27 | |
| | 27 | |
| | 26 | |
| Backscatter @ 9.19", 45° | 280 | |
| | 284 | |
| | 265 | |
| | 278 | |
| Backscatter @ 20.62", 60° | 27 | |
| | 26 | |
| | 28 | |
| | 24 | |
| Beam collimator exit | | 4754300 |
| | | 4658300 |
| | | 4515900 |
| | | 3268600 |
| | | 4135600 |
| | | 4261100 |
| | | 4784200 |
| | | 4752400 |
| | | 4770900 |

| LOCATION | TLD READING | |
|---|---|---|
| | SQUARE | ROD |
| Backscatter @ 31.38", 30° | | 17 |
| | | 20 |
| | | 19 |
| | | 20 |
| Backscatter @ 23.88", 45° | | 18 |
| | | 19 |
| | | 19 |
| | | 18 |
| Backscatter @ 9.62", 45° | | 167 |
| | | 163 |
| | | 166 |
| | | 169 |
| Backscatter @ 20.75", 60° | | 10 |
| | | 12 |
| | | 11 |
| | | 10 |

17.1.3.1.15 9" square, 1.75" thick

| LOCATION | SQUARE | ROD |
|---|---|---|
| Beam collimator exit | | 4041000 |
| | | 3913700 |
| | | 4212500 |
| | | 3631600 |
| | | 2898900 |
| | | 4214500 |
| | | 4229200 |
| | | 3899300 |
| | | 3831600 |
| Backscatterer position | | 627100 |
| | | 649200 |
| | | 637800 |
| | | 644400 |
| | | 622700 |
| | | 671600 |
| | | 599300 |
| | | 656900 |
| | | 695900 |
| Background @ 31.62", 30° | | 9 |
| | | 10 |
| | | 8 |
| | | 11 |
| Background @ 23.75", 45° | | 10 |
| | | 9 |
| | | 8 |
| | | 10 |
| Background @ 24.75", 45° | | 10 |
| | | 14 |
| | | 11 |
| | | 10 |
| Background @ 20.75", 60° | | 9 |
| | | 9 |
| | | 8 |
| | | 9 |

| LOCATION | TLD READING | |
|---|---|---|
| | SQUARE | ROD |
| Beam collimator exit | 6049200 | 2743000 |
| | 6133600 | 3734900 |
| | 5863600 | 3852000 |
| | 5548900 | 4067500 |
| | 5993500 | 3596600 |
| | 6285000 | 3694200 |
| | 4933000 | 4059500 |
| | 5916500 | 3680000 |
| | 5330600 | 4217300 |
| Backscatter @ 31.62", 30° | 19 | 15 |
| | 19 | 14 |
| | 19 | 15 |
| | 17 | 15 |
| Backscatter @ 23.75", 45° | 28 | 23 |
| | 27 | 24 |
| | 26 | 21 |
| | 30 | 20 |
| Backscatter @ 24.75", 45° | 28 | 21 |
| | 26 | 20 |
| | 28 | 21 |
| | 29 | 21 |
| Backscatter @ 20.75", 60° | 27 | 23 |
| | 27 | 20 |
| | 28 | 24 |
| | 30 | 23 |

17.1.3.1.16 9" square, 2.00" thick

| LOCATION | TLD READING | |
|---|---|---|
| | SQUARE | ROD |
| Beam collimator exit | 6347700 | |
| | 6077600 | |
| | 6247200 | |
| | 5567900 | |
| | 5849600 | |
| | 6068000 | |
| | 6296200 | |
| | 6619700 | |
| | 6183200 | |
| Backscatterer position | 950500 | |
| | 940300 | |
| | 1019600 | |
| | 902100 | |
| | 982000 | |
| | 960200 | |
| | 1013400 | |
| | 986100 | |
| | 1070800 | |
| Background @ 31.25", 30° | 4 | |
| | 3 | |
| | 4 | |
| | 4 | |
| Background @ 23.75", 45° | 3 | |
| | 3 | |
| | 3 | |
| | 4 | |
| Background @ 9.38", 45° | 6 | |
| | 6 | |
| | 6 | |
| | 6 | |
| Background @ 20.69", 60° | 4 | |
| | 3 | |
| | 4 | |
| | 4 | |

| LOCATION | TLD READING | |
|---|---|---|
| | SQUARE | ROD |
| Backscatterer position | 6632000 | |
| | 6615100 | |
| | 6515000 | |
| | 6960200 | |
| | 5833500 | |
| | 6599500 | |
| | 6472200 | |
| | 6512900 | |
| | 6562600 | |
| Backscatter @ 31.25", 30° | 15 | |
| | 15 | |
| | 15 | |
| | 16 | |
| Backscatter @ 23.75", 45° | 29 | |
| | 26 | |
| | 26 | |
| | 26 | |
| Backscatter @ 9.38", 45° | 274 | |
| | 254 | |
| | 262 | |
| | 276 | |
| Backscatter @ 20.69", 60° | 27 | |
| | 29 | |
| | 29 | |
| | 29 | |

17.1.3.2 Iron

17.1.3.2.1 12" square, 2.50" thick

| LOCATION | TLD READING | |
|---|---|---|
| | SQUARE | ROD |
| Beam collimator exit | 5921000 | |
| | 6044000 | |
| | 6743200 | |
| | 5603200 | |
| | 5559900 | |
| | 5983400 | |
| Backscatterer position | 976400 | |
| | 998400 | |
| | 920800 | |
| | 885100 | |
| | 941100 | |
| | 944700 | |
| Background @ 29.81", 30° | 3 | |
| | 3 | |
| | 4 | |
| | 3 | |
| Background @ 23.94", 45° | 4 | |
| | 4 | |
| | 4 | |
| | 4 | |
| Background @ 21.62", 60° | 4 | |
| | 5 | |
| | 5 | |
| | 4 | |
| Beam collimator exit | 6001300 | |
| | 6251800 | |
| | 5811000 | |
| | 6397600 | |
| | 6302500 | |
| | 6274500 | |

| LOCATION | TLD READING | |
|---|---|---|
| | SQUARE | ROD |
| Backscatter @ 29.81", 30° | 44 | |
| | 44 | |
| | 44 | |
| | 47 | |
| Backscatter @ 23.94", 45° | 60 | |
| | 56 | |
| | 65 | |
| | 54 | |
| Backscatter @ 21.62", 60° | 54 | |
| | 69 | |
| | 59 | |
| | 60 | |
| Beam collimator exit | | 4371100 |
| | | 4654900 |
| | | 4634000 |
| | | 4631400 |
| | | 4890000 |
| | | 4486900 |
| Backscatterer position | | 719000 |
| | | 729000 |
| | | 715100 |
| | | 750300 |
| | | 742900 |
| | | 719700 |
| Background @ 29.06", 30° | | 6 |
| | | 5 |
| | | 5 |
| | | 4 |
| Background @ 23.19", 45° | | 6 |
| | | 6 |
| | | 5 |
| | | 6 |
| Background @ 21.06", 60° | | 5 |
| | | 6 |
| | | 5 |
| | | 5 |

| LOCATION | TLD READING | |
|---|---|---|
| | SQUARE | ROD |
| Beam collimator exit | | 4355700 |
| | | 4945900 |
| | | 3539400 |
| | | 4347700 |
| | | 4577500 |
| | | 4289900 |
| Backscatter @ 29.06", 30° | | 36 |
| | | 41 |
| | | 36 |
| | | 37 |
| Backscatter @ 23.19", 45° | | 41 |
| | | 44 |
| | | 44 |
| | | 48 |
| Backscatter @ 21.06", 60° | | 47 |
| | | 47 |
| | | 50 |
| | | 49 |

17.1.3.2.2 14" square, 2.50" thick

| LOCATION | TLD READING | |
|---|---|---|
| | SQUARE | ROD |
| Beam collimator exit | 6231400 | |
| | 6030300 | |
| | 6646900 | |
| | 5419100 | |
| | 5863700 | |
| | 5731600 | |
| Backscatterer position | 862900 | |
| | 847400 | |
| | 1053700 | |
| | 890200 | |
| | 890600 | |
| | 850000 | |
| Background @ 29.81", 30° | 4 | |
| | 3 | |
| | 3 | |
| | 3 | |
| Background @ 23.94", 45° | 5 | |
| | 6 | |
| | 5 | |
| | 5 | |
| Background @ 21.62", 60° | 6 | |
| | 4 | |
| | 5 | |
| | 5 | |
| Beam collimator exit | 6250400 | |
| | 5622600 | |
| | 6192700 | |
| | 5500100 | |
| | 5324600 | |
| | 5860800 | |
| Backscatter @ 29.81", 30° | 44 | |
| | 39 | |
| | 45 | |
| | 51 | |

| LOCATION | TLD READING | |
|---|---|---|
| | SQUARE | ROD |
| Backscatter @ 23.94", 45° | 55 | |
| | 59 | |
| | 60 | |
| | 51 | |
| Backscatter @ 21.62", 60° | 55 | |
| | 58 | |
| | 62 | |
| | 52 | |
| Beam collimator exit | | 4511300 |
| | | 5059300 |
| | | 4631200 |
| | | 4763700 |
| | | 4406900 |
| | | 4441300 |
| Backscatterer position | | 649200 |
| | | 711600 |
| | | 769800 |
| | | 752000 |
| | | 651700 |
| | | 721300 |
| Background @ 30", 30° | | 2 |
| | | 3 |
| | | 2 |
| | | 2 |
| | | 3 |
| | | 3 |
| Background @ 24.12" 45° | | 3 |
| | | 3 |
| | | 3 |
| | | 3 |
| | | 2 |
| | | 3 |

| LOCATION | TLD READING | |
|---|---|---|
| | SQUARE | ROD |
| Background @ 21.75", 60° | | 3 |
| | | 3 |
| | | 3 |
| | | 3 |
| | | 3 |
| | | 3 |
| Beam collimator exit | | 4418300 |
| | | 4636200 |
| | | 4571700 |
| | | 3514400 |
| | | 4617100 |
| | | 4129800 |
| Backscatter @ 30", 30° | | 31 |
| | | 31 |
| | | 32 |
| | | 34 |
| Backscatter @ 24.12", 45° | | 47 |
| | | 37 |
| | | 46 |
| | | 47 |
| Backscatter @ 21.75", 60° | | 45 |
| | | 43 |
| | | 41 |
| | | 40 |

17.1.3.2.3 12" square, 4.125" thick

| LOCATION | TLD READING | |
|---|---|---|
| | SQUARE | ROD |
| Beam collimator exit | 6789100 | 4239600 |
| | 6265300 | 4514800 |
| | 5710000 | 4660900 |
| | 6600800 | 4692200 |
| | 6163500 | 4731100 |
| | 5774700 | 4257500 |
| Backscatterer position | 884700 | 726300 |
| | 1042700 | 766300 |
| | 937200 | 771500 |
| | 1011600 | 748400 |
| | 916400 | 648500 |
| | 965500 | 721300 |
| Background @ 29.06", 30° | 6 | 3 |
| | 6 | 3 |
| | 6 | 3 |
| | 7 | 3 |
| Background @ 23.19", 45° | 6 | 3 |
| | 6 | 3 |
| | 6 | 3 |
| | 6 | 3 |
| Background @ 21.06", 60° | 6 | 3 |
| | 6 | 3 |
| | 7 | 4 |
| | 7 | 3 |
| Beam collimator exit | 6597300 | 4156200 |
| | 6625100 | 4457600 |
| | 6235700 | 5006200 |
| | 6021100 | 4402900 |
| | 6069700 | 4976000 |
| | 5870100 | 4153200 |
| Backscatter @ 29.06", 30° | 55 | 33 |
| | 50 | 36 |
| | 53 | 39 |
| | 54 | 35 |

| LOCATION | TLD READING | |
|---|---|---|
| | SQUARE | ROD |
| Backscatter @ 23.19", 45° | 63 | 47 |
| | 70 | 41 |
| | 65 | 45 |
| | 71 | 41 |
| Backscatter @ 21.06", 60° | 67 | 46 |
| | 73 | 39 |
| | 76 | 47 |
| | 64 | 47 |

## 17.1.3.3 Concrete

### 17.1.3.3.1 32" square, 8" thick

| LOCATION | TLD READING | |
|---|---|---|
| | SQUARE | ROD |
| Beam collimator exit | 5344300 | |
| | 5936900 | |
| | 5568300 | |
| | 5857700 | |
| | 6239600 | |
| | 6449500 | |
| Backscatterer position | 965900 | |
| | 899800 | |
| | 863800 | |
| | 835200 | |
| | 1004700 | |
| | 778700 | |
| Background @ 28.94", 30° | 4 | |
| | 3 | |
| | 4 | |
| | 4 | |
| Background @ 21.75", 45° | 3 | |
| | 4 | |
| | 5 | |
| | 5 | |
| Background @ 19.50", 60° | 6 | |
| | 5 | |
| | 5 | |
| | 5 | |
| Beam collimator exit | 5941900 | |
| | 5607600 | |
| | 5808100 | |
| | 5559900 | |
| | 5841800 | |
| | 5549200 | |

| LOCATION | TLD READING | |
|---|---|---|
| | SQUARE | ROD |
| Backscatter @ 28.94", 30° | 56 | |
| | 51 | |
| | 48 | |
| | 48 | |
| Backscatter @ 21.75", 45° | 61 | |
| | 76 | |
| | 78 | |
| | 60 | |
| Backscatter @ 19.50", 60° | 67 | |
| | 78 | |
| | 60 | |
| | 78 | |
| Beam collimator exit | | 4596400 |
| | | 4531300 |
| | | 4297800 |
| | | 4185600 |
| | | 4420200 |
| | | 4117400 |
| Backscatterer position | | 703100 |
| | | 675700 |
| | | 621000 |
| | | 630600 |
| | | 635300 |
| | | 686400 |
| Background @ 27.88", 30° | | 3 |
| | | 2 |
| | | 2 |
| | | 3 |
| Background @ 22.75", 45° | | 3 |
| | | 3 |
| | | 3 |
| | | 3 |
| Background @ 19.06", 60° | | 3 |
| | | 3 |
| | | 3 |
| | | 4 |

| LOCATION | TLD READING | |
|---|---|---|
| | SQUARE | ROD |
| Beam collimator exit | | 4640200 |
| | | 4127400 |
| | | 4381200 |
| | | 4009500 |
| | | 4181000 |
| | | 4214400 |
| Backscatter @ 27.88", 30° | | 38 |
| | | 33 |
| | | 37 |
| | | 34 |
| Backscatter @ 22.75", 45° | | 42 |
| | | 28 |
| | | 36 |
| | | 43 |
| Backscatter @ 19.06", 60° | | 32 |
| | | 45 |
| | | 41 |
| | | 42 |

17.1.3.3.2 36" square, 8" thick

| LOCATION | TLD READING | |
|---|---|---|
| | SQUARE | ROD |
| Beam collimator exit | | 4198600 |
| | | 4570500 |
| | | 4442700 |
| | | 4005500 |
| | | 4179900 |
| | | 4521700 |
| Backscatterer position | | 715900 |
| | | 705000 |
| | | 697800 |
| | | 724800 |
| | | 753700 |
| | | 594500 |
| Background @ 27.94", 30° | | 4 |
| | | 4 |
| | | 3 |
| | | 3 |
| Background @ 21.56", 45° | | 3 |
| | | 3 |
| | | 3 |
| | | 3 |
| Background @ 18.0", 60° | | 4 |
| | | 4 |
| | | 3 |
| | | 4 |
| Beam collimator exit | | 4282000 |
| | | 3797100 |
| | | 4208300 |
| | | 3806000 |
| | | 3898800 |
| | | 4334500 |
| Backscatter @ 27.94", 30° | | 37 |
| | | 39 |
| | | 42 |
| | | 35 |

| LOCATION | TLD READING | |
|---|---|---|
| | SQUARE | ROD |
| Backscatter @ 21.56", 45° | | 37 |
| | | 49 |
| | | 42 |
| | | 47 |
| Backscatter @ 18.0", 60° | | 46 |
| | | 53 |
| | | 53 |
| | | 46 |
| Beam collimator exit | 6023700 | |
| | 6046600 | |
| | 5825700 | |
| | 6223000 | |
| | 6057000 | |
| | 6436900 | |
| Backscatter @ 29.12", 30° | 47 | |
| | 52 | |
| | 53 | |
| | 47 | |
| Backscatter @ 21.75", 45° | 60 | |
| | 66 | |
| | 73 | |
| | 50 | |
| Backscatter @ 19.62", 60° | 47 | |
| | 73 | |
| | 66 | |
| | 51 | |

17.1.3.3.3 32" square, 10" thick

| LOCATION | TLD READING | |
|---|---|---|
| | SQUARE | ROD |
| Beam collimator exit | 5540300 | |
| | 5393900 | |
| | 4830500 | |
| | 5329600 | |
| | 5248900 | |
| | 5949500 | |
| Backscatterer position | 752200 | |
| | 880800 | |
| | 927200 | |
| | 819900 | |
| | 943800 | |
| | 884700 | |
| Background @ 27.81", 30° | 4 | |
| | 4 | |
| | 4 | |
| | 5 | |
| Background @ 22.81", 45° | 4 | |
| | 6 | |
| | 5 | |
| | 5 | |
| Background @ 19.19", 60° | 5 | |
| | 5 | |
| | 6 | |
| | 7 | |
| Beam collimator exit | 5922200 | |
| | 5234100 | |
| | 5672000 | |
| | 5804900 | |
| | 5689700 | |
| | 5539400 | |
| Backscatter @ 27.81", 30° | 58 | |
| | 46 | |
| | 54 | |
| | 56 | |

| LOCATION | TLD READING | |
|---|---|---|
| | SQUARE | ROD |
| Backscatter @ 22.81", 45° | 63 | |
| | 48 | |
| | 43 | |
| | 62 | |
| Backscatter @ 19.19", 60° | 67 | |
| | 73 | |
| | 49 | |
| | 45 | |
| Beam collimator exit | | 3848500 |
| | | 4329900 |
| | | 4011600 |
| | | 4748900 |
| | | 3734200 |
| | | 4428000 |
| Backscatter @ 27.88", 30° | | 31 |
| | | 36 |
| | | 33 |
| | | 35 |
| Backscatter @ 22.70", 45° | | 29 |
| | | 46 |
| | | 35 |
| | | 41 |
| Backscatter @ 18.94", 60° | | 41 |
| | | 43 |
| | | 30 |
| | | 35 |

## 17.1.4 Beam divergence

| HORIZONTAL DISPLACEMENT (inches) | TLD READING | |
|---|---|---|
| | Right of Center | Left of Center |
| 17 | 72700 | 74857 |
| | 67600 | 71800 |
| 12 | 78900 | 68500 |
| | 72300 | 60300 |
| 10 | 80300 | 68600 |
| | 74600 | 76500 |
| 8 | 68500 | 69600 |
| | 67700 | 65400 |
| 6 | 83100 | 97300 |
| | 78300 | 81100 |
| 5 | 73000 | 88900 |
| | 80700 | 75900 |
| 4 | 84700 | 88400 |
| | 84600 | 78600 |
| 3 | 73900 | 89800 |
| | 79800 | 77800 |
| 2 | 71600 | 83700 |
| | 81900 | 73600 |
| | 82400 | 76100 |
| | 87300 | 73400 |
| 1 | 87300 | 84200 |
| | 77300 | 59700 |
| | 84400 | 80100 |
| | 78800 | 71000 |
| Center | 85600 | |
| | 85100 | |
| | 78100 | |
| | 74100 | |

| VERTICAL DISPLACEMENT (inches) | TLD READING | |
|---|---|---|
| | Above Center | Below Center |
| 17 | 47500 | 62700 |
| | 66500 | 70900 |
| 12 | 66700 | 74700 |
| | 64100 | 72500 |
| 10 | 70200 | 61500 |
| | 62500 | 76000 |
| 8 | 79800 | 73200 |
| | 77500 | 79800 |
| 6 | 74300 | 84400 |
| | 86000 | 83400 |
| 5 | 89100 | 81500 |
| | 72300 | 89500 |
| 4 | 83100 | 78000 |
| | 79400 | 69100 |
| 3 | 71200 | 91600 |
| | 74500 | 81900 |
| 2 | 74900 | 85900 |
| | 76500 | 74600 |
| | 82800 | 72400 |
| | 86800 | 80300 |
| 1 | 83800 | 86900 |
| | 76800 | 73600 |
| | 77800 | 75200 |
| | 81000 | 87400 |

## 17.2 3.5 MeV

### 17.2.1 Backscatter

#### 17.2.1.1 Lead

| LOCATION | TLD READING | |
|---|---|---|
| | SQUARE | ROD |
| Beam collimator exit | 2110900 | 1964900 |
| | 2495600 | 1755300 |
| | 2536900 | 1706400 |
| | 2320000 | 1719600 |
| | | 1952500 |
| | | 1878500 |
| Backscatterer position | 450300 | 317600 |
| | 455700 | 265100 |
| | 409900 | 288200 |
| | 422300 | 340500 |
| | 440600 | 330900 |
| | 341300 | 324700 |
| Background @ 23.00", 30° 5.625" collimator | | 14 |
| | | 15 |
| | | 14 |
| | | 16 |
| Background @ 20.38", 40° 5.562" collimator | 15 | |
| | 15 | |
| | 17 | |
| | 17 | |
| Background @ 19.00", 50° 6.25" collimator | | 7 |
| | | 8 |
| | | 8 |
| | | 9 |
| Background @ 18.38", 60° 8.00" collimator | 8 | |
| | 9 | |
| | 9 | |
| | 9 | |

| LOCATION | TLD READING | |
|---|---|---|
| | SQUARE | ROD |
| Beam collimator exit | 2452300 | 1775900 |
| | 2298700 | 1558600 |
| | 2381000 | 1633600 |
| | 2372300 | 1636500 |
| | 2328600 | 1923500 |
| | 2611600 | 1754700 |
| Backscatter @ 23.00", 30° 5.625" collimator | | 91 |
| | | 82 |
| | | 87 |
| | | 83 |
| Backscatter @ 20.38", 40° 5.562" collimator | 169 | |
| | 142 | |
| | 145 | |
| | 150 | |
| Backscatter @ 19.00", 50° 6.25" collimator | | 71 |
| | | 76 |
| | | 64 |
| | | 78 |
| Backscatter @ 18.38", 60° 8.00" collimator | 53 | |
| | 52 | |
| | 46 | |
| | 54 | |
| Beam collimator exit | 3976400 | 2914600 |
| | 3649700 | 2657500 |
| | 3854800 | 2797900 |
| | 3818900 | 2551600 |
| | 4013500 | 2677800 |
| | 4185700 | 2890900 |
| Backscatter @ 23.75", 30° 5.562" collimator | 164 | |
| | 168 | |
| | 158 | |
| | 170 | |
| Backscatter @ 20.50", 40° 5.625" collimator | | 147 |
| | | 133 |
| | | 135 |
| | | 122 |

| LOCATION | TLD READING | |
|---|---|---|
| | SQUARE | ROD |
| Backscatter @ 19.50", 50° | 104 | |
| 7.00" collimator | 104 | |
| | 107 | |
| | 102 | |
| Backscatter @ 19.00", 60° | | 47 |
| 7.812" collimator | | 49 |
| | | 46 |
| | | 42 |

17.2.1.2 Iron

| LOCATION | TLD READING | |
|---|---|---|
| | SQUARE | ROD |
| Beam collimator exit | 2234100 | 1585700 |
| | 2491000 | 1539800 |
| | 2422900 | 1767900 |
| | 2414300 | 1775000 |
| | 2302900 | 1720900 |
| | 2144800 | 1721900 |
| Backscatterer position | 456000 | 289300 |
| | 472300 | 330500 |
| | 388100 | 279200 |
| | 392700 | 270700 |
| | 393700 | 309200 |
| | 419700 | 279100 |
| Background @ 23.25", 30° 5.562" collimator | 16 | |
| | 15 | |
| | 14 | |
| | 14 | |
| Background @ 19.94", 40° 5.625" collimator | | 14 |
| | | 12 |
| | | 13 |
| | | 14 |
| Background @ 19.62", 50° 7.00" collimator | 8 | |
| | 7 | |
| | 7 | |
| | 8 | |
| Background @ 18.38", 60° 7.75" collimator | | 6 |
| | | 5 |
| | | 6 |
| | | 5 |
| Beam collimator exit | 2716600 | 1810900 |
| | 2612100 | 1681200 |
| | 2095900 | 1963700 |
| | 2544700 | 1817400 |
| | 2318800 | 1556000 |
| | 2477800 | 2055600 |

| LOCATION | TLD READING | |
|---|---|---|
| | SQUARE | ROD |
| Backscatter @ 23.25", 30° | 78 | |
| 5.562" collimator | 72 | |
| | 72 | |
| | 73 | |
| Backscatter @ 19.94", 40° | | 51 |
| 5.625" collimator | | 53 |
| | | 56 |
| | | 53 |
| Backscatter @ 19.62", 50° | 45 | |
| 7.00" collimator | 45 | |
| | 43 | |
| | 45 | |
| Backscatter @ 18.38", 60° | | 26 |
| 7.75" collimator | | 26 |
| | | 26 |
| | | 25 |
| Beam collimator exit | 4003300 | 2977500 |
| | 4064600 | 3253100 |
| | 4016400 | 3127600 |
| | 4648500 | 3335900 |
| | 4248900 | 3030000 |
| | 4224100 | 2967700 |
| Backscatter @ 23.00", 30° | | 79 |
| 5.625" collimator | | 78 |
| | | 73 |
| | | 72 |
| Backscatter @ 20.50", 40° | 119 | |
| 5.50" collimator | 120 | |
| | 124 | |
| | 115 | |
| Backscatter @ 19.38", 50° | | 63 |
| 6.25" collimator | | 58 |
| | | 65 |
| | | 58 |

| LOCATION | TLD READING | |
|---|---|---|
| | SQUARE | ROD |
| Backscatter @ 18.38", 60° 8.00" collimator | 46 | |
| | 52 | |
| | 43 | |
| | 46 | |

17.2.1.3 Concrete

| LOCATION | TLD READING | |
|---|---|---|
| | SQUARE | ROD |
| Beam collimator exit | 6728400 | |
| | 6899900 | |
| | 5948600 | |
| | 6285400 | |
| | 6052700 | |
| | 6651100 | |
| Backscatterer position | 795200 | |
| | 868500 | |
| | 890300 | |
| | 820300 | |
| | 860800 | |
| | 748800 | |
| Background @ 25.00", 30° 6.25" collimator | 244 | |
| | 236 | |
| | 202 | |
| | 244 | |
| Background @ 23.25", 45° 7.50" collimator | 15 | |
| | 15 | |
| | 14 | |
| | 16 | |
| Background @ 26.00", 60° 9.562" collimator | 16 | |
| | 18 | |
| | 18 | |
| | 18 | |
| Beam collimator exit | 5525800 | |
| | 5793600 | |
| | 5202400 | |
| | 5823000 | |
| | 5923800 | |
| | 5730600 | |

| LOCATION | TLD READING | |
|---|---|---|
| | SQUARE | ROD |
| Backscatter @ 25.00", 30° 6.25" collimator | 343 | |
| | 350 | |
| | 352 | |
| | 292 | |
| Backscatter @ 23.25", 45° 7.50" collimator | 73 | |
| | 65 | |
| | 71 | |
| | 71 | |
| Backscatter @ 26.00", 60° 9.562" collimator | 55 | |
| | 48 | |
| | 51 | |
| | 53 | |

## 17.2.2 Copper absorption in beam

| DEPTH IN COPPER (inches) | TLD READING | |
|---|---|---|
| | SQUARE | ROD |
| 2.50 | | 107 |
| | | 101 |
| | | 97 |
| | | 88 |
| 1.75 | 274 | |
| | 300 | |
| | 267 | |
| | 263 | |
| 1.50 | | 203 |
| | | 315 |
| | | 284 |
| | | 256 |
| 1.25 | 612 | |
| | 600 | |
| | 623 | |
| | 625 | |
| 1.125 | | 507 |
| | | 424 |
| | | 530 |
| | | 579 |
| 1.00 | 1001 | |
| | 1078 | |
| | 1044 | |
| | 1251 | |
| 0.875 | 935 | |
| | 895 | |
| | 1074 | |
| | 782 | |
| 0.75 | | 589 |
| | | 549 |
| | | 397 |
| | | 493 |

| DEPTH IN COPPER (inches) | TLD READING | |
|---|---|---|
| | SQUARE | ROD |
| 0.625 | 1434 | |
| | 1471 | |
| | 1897 | |
| | 1407 | |
| 0.50 | | 1199 |
| | | 1194 |
| | | 843 |
| | | 1187 |
| 0.25 | 2701 | |
| | 2741 | |
| | 3731 | |
| | 2625 | |
| 0.125 | | 2036 |
| | | 1474 |
| | | 1941 |
| | | 1652 |
| 0.0 | 6347 | 3251 |
| | 4788 | 2622 |
| | 6152 | 2951 |
| | 5082 | 3172 |
| 2.50 | | 5372 |
| | | 6499 |
| | | 6325 |
| | | 5872 |
| 1.75 | 9475 | |
| | 8744 | |
| | 9581 | |
| | 9127 | |
| 1.50 | | 5815 |
| | | 5708 |
| | | 5669 |
| | | 5874 |

| DEPTH IN COPPER (inches) | TLD READING | |
|---|---|---|
| | SQUARE | ROD |
| 1.25 | 11787 | |
| | 10808 | |
| | 10718 | |
| | 11374 | |
| 1.125 | | 6606 |
| | | 7570 |
| | | 6818 |
| | | 7053 |
| 1.00 | 12934 | |
| | 13678 | |
| | 11438 | |
| | 13270 | |
| 0.875 | 12772 | |
| | 11719 | |
| | 10241 | |
| | 10210 | |
| 0.75 | | 4724 |
| | | 4300 |
| | | 4540 |
| | | 4544 |
| 0.625 | 12911 | |
| | 12860 | |
| | 13843 | |
| | 12652 | |
| 0.50 | | 6702 |
| | | 7314 |
| | | 6289 |
| | | 6272 |
| 0.25 | 12509 | |
| | 13163 | |
| | 13002 | |
| | 12130 | |

| DEPTH IN COPPER (inches) | TLD READING | |
|---|---|---|
| | SQUARE | ROD |
| 0.125 | | 5468 |
| | | 5118 |
| | | 4862 |
| | | 5981 |
| 0.0 | 14172 | 7555 |
| | 13071 | 7779 |
| | 13162 | 7910 |
| | 12926 | 7123 |

## 17.2.3 Beam divergence

| HORIZONTAL DISPLACEMENT (inches) | TLD READING | |
|---|---|---|
| | RIGHT OF CENTER | LEFT OF CENTER |
| 16 | 7910<br>9001 | 7754<br>9614 |
| 14 | 11405<br>12020 | 11489<br>11738 |
| 12 | 15072<br>16898 | 14919<br>15426 |
| 10 | 23222<br>21290 | 22181<br>24097 |
| 8 | 46807<br>49645 | 49178<br>50300 |
| 6 | 67144<br>66511 | 71202<br>70743 |
| 5 | 67278<br>70701 | 70632<br>75019 |
| 4 | 74633<br>74858 | 75900<br>76889 |
| 3 | 75522<br>72251 | 77582<br>68331 |
| 2 | 75290<br>75878 | 75996<br>77564 |
| 1 | 82713<br>80425 | 81624<br>79453 |
| Center | 79675<br>76865 | |

| VERTICAL DISPLACEMENT (inches) | TLD READING | |
|---|---|---|
| | SQUARE | ROD |
| 18 | 21203 | |
| | 21520 | |
| 16 | 35552 | 44917 |
| | 35577 | 49274 |
| 14 | 52013 | 53497 |
| | 51043 | 50558 |
| 12 | 58143 | 59018 |
| | 58542 | 60972 |
| 10 | 64369 | 63785 |
| | 64483 | 62652 |
| 8 | 69170 | 68468 |
| | 68197 | 69632 |
| 6 | 73174 | 75902 |
| | 72310 | 75904 |
| 5 | 76880 | 73218 |
| | 72636 | 69605 |
| 4 | 75705 | 73732 |
| | 63805 | 69450 |
| 3 | 74771 | 75815 |
| | 77770 | 79808 |
| 2 | 79387 | 78059 |
| | 75922 | 74671 |
| 1 | 75352 | 84514 |
| | 78061 | 78408 |

## 17.3 7.0 MeV

### 17.3.1 Backscatter

#### 17.3.1.1 Lead

| LOCATION | TLD READING | |
|---|---|---|
| | SQUARE | ROD |
| Backscatterer position | 802500 | 543300 |
| | 856600 | 599000 |
| | 872200 | 604700 |
| | 820000 | 581000 |
| | 925400 | 600200 |
| | 832200 | 622200 |
| Background @ 26.94", 30° 5.688" collimator | | 1618 |
| | | 1605 |
| | | 1697 |
| | | 1608 |
| Background @ 26.00", 40° 5.625" collimator | 1211 | |
| | 1338 | |
| | 1387 | |
| | 1473 | |
| Background @ 26.50", 50° 6.50" collimator | | 101 |
| | | 87 |
| | | 95 |
| | | 93 |
| Background @ 30.00", 60° 9.312" collimator | 617 | |
| | 509 | |
| | 613 | |
| | 552 | |
| Backscatter @ 26.75", 30° 5.625" collimator | | 2078 |
| | | 2104 |
| | | 2051 |
| | | 2083 |

| LOCATION | TLD READING | |
|---|---|---|
| | SQUARE | ROD |
| Backscatter @ 25.44", 40° | 2347 | |
| 5.562" collimator | 1919 | |
| | 2036 | |
| | 2359 | |
| Backscatter @ 25.88", 50° | | 401 |
| 6.50" collimator | | 354 |
| | | 413 |
| | | 382 |
| Backscatter @ 29.32", 60° | 205 | |
| 9.312" collimator | 185 | |
| | 188 | |
| | 161 | |
| Backscatterer position | 437400 | 303900 |
| | 433600 | 323300 |
| | 405200 | 308600 |
| | 401600 | 336200 |
| | 440400 | 273900 |
| | 475300 | 306700 |
| Background @ 24.12", 30° | 949 | |
| 5.25" collimator | 942 | |
| | 995 | |
| | 954 | |
| Background @ 23.9", 40° | | 107 |
| 5.688" collimator | | 101 |
| | | 97 |
| | | 119 |
| Background @ 27.50", 50° | 68 | |
| 7.75" collimator | 60 | |
| | 69 | |
| | 63 | |
| Background @ 26.31", 60° | | 107 |
| 8.312" collimator | | 104 |
| | | 94 |
| | | 100 |

| LOCATION | TLD READING | |
|---|---|---|
| | SQUARE | ROD |
| Backscatter @ 24.00", 30° 5.25" collimator | 3679<br>3253<br>3655<br>3139 | |
| Backscatter @ 23.12", 40° 5.625" collimator | | 698<br>780<br>734<br>748 |
| Backscatter @ 27.62", 50° 7.75" collimator | 384<br>401<br>379<br>359 | |
| Backscatter @ 26.50", 60° 8.312" collimator | | 166<br>194<br>175<br>156 |
| Backscatterer position | 428900<br>406000<br>371200<br>424900<br>411800<br>374600 | 303700<br>240900<br>299300<br>284700<br>271500<br>282700 |
| Background @ 26.12", 30° 5.25" collimator | | 3048<br>3272<br>3107<br>2882 |
| Background @ 25.25", 40° 5.75" collimator | 38<br>39<br>37<br>39 | |
| Background @ 31.37", 50° 9.625" collimator | | 96<br>95<br>101<br>88 |

| LOCATION | TLD READING | |
|---|---|---|
| | SQUARE | ROD |
| Background @ 29.31", 60° | 42 | |
| 10.312" collimator | 42 | |
| | 44 | |
| | 50 | |
| Backscatter @ 26.12", 30° | | 5235 |
| 5.25" collimator | | 5233 |
| | | 4791 |
| | | 4833 |
| Backscatter @ 25.25", 40° | 455 | |
| 5.75" collimator | 395 | |
| | 430 | |
| | 446 | |
| Backscatter @ 31.37", 50° | | 104 |
| 9.625" collimator | | 107 |
| | | 102 |
| | | 120 |
| Backscatter @ 29.31", 60° | 95 | |
| 10.312" collimator | 89 | |
| | 89 | |
| | 83 | |

| LOCATION | TLD READING x $10^{-3}$ |
|---|---|
| Beam collimator exit | 3609 |
| | 3610 |
| | 3960 |
| | 3718 |
| | 3793 |
| | 3716 |
| | 3700 |
| | 3527 |
| | 3551 |
| | 3915 |
| Backscatterer position | 870 |
| | 873 |
| | 885 |
| | 838 |
| | 860 |
| | 876 |
| | 887 |
| | 878 |
| | 826 |
| | 880 |
| Beam collimator exit | 4469 |
| | 4196 |
| | 4366 |
| | 4399 |
| | 4366 |
| | 4331 |
| | 4230 |
| | 4225 |
| | 4332 |
| | 4435 |
| Beam collimator exit | 2354 |
| | 2430 |
| | 2183 |
| | 2378 |
| | 2383 |
| | 2331 |
| | 2281 |
| | 2531 |
| | 2426 |
| | 2475 |

| LOCATION | TLD READING x $10^{-3}$ |
|---|---|
| Backscatterer position | 457 |
| | 449 |
| | 450 |
| | 470 |
| | 454 |
| | 470 |
| | 440 |
| | 443 |
| | 461 |
| | 443 |
| Beam collimator exit | 4627 |
| | 4707 |
| | 4402 |
| | 4673 |
| | 4633 |
| | 4402 |
| | 4714 |
| | 4435 |
| | 4501 |
| | 4633 |
| Beam collimator exit | 2340 |
| | 2251 |
| | 2426 |
| | 2281 |
| | 2510 |
| | 2365 |
| | 2417 |
| | 2460 |
| | 2407 |
| | 2448 |
| Backscatterer position | 431 |
| | 434 |
| | 468 |
| | 432 |
| | 422 |
| | 433 |
| | 437 |
| | 478 |
| | 426 |
| | 454 |

| LOCATION | TLD READING x $10^{-3}$ |
|---|---|
| Beam collimator exit | 3335 |
| | 3213 |
| | 3369 |
| | 3285 |
| | 3326 |
| | 3465 |
| | 3197 |
| | 3361 |
| | 3554 |
| | 3333 |

17.3.1.2 Iron

| LOCATION | TLD READING | |
|---|---|---|
| | SQUARE | ROD |
| Backscatterer position | 385700 | 283500 |
| | 382000 | 260300 |
| | 373400 | 289600 |
| | 387700 | 265500 |
| | 373300 | 301800 |
| | 339900 | 262300 |
| Background @ 26.12", 30° 5.25" collimator | | 2162 |
| | | 1012 |
| | | 2115 |
| | | 1868 |
| Background @ 25.25", 40° 5.75" collimator | 34 | |
| | 33 | |
| | 33 | |
| | 32 | |
| Background @ 31.31", 50° 9.562" collimator | | 242 |
| | | 261 |
| | | 256 |
| | | 276 |
| Background @ 29.25", 60° 10.25" collimator | 50 | |
| | 52 | |
| | 44 | |
| | 52 | |
| Backscatter @ 26.13", 30° 5.25" collimator | | 5544 |
| | | 6137 |
| | | 6601 |
| | | 5589 |
| Backscatter @ 25.25", 40° 5.75" collimator | 286 | |
| | 316 | |
| | 274 | |
| | 299 | |

| LOCATION | TLD READING | |
|---|---|---|
| | SQUARE | ROD |
| Backscatter @ 31.38", 50°<br>10.312" collimator | | 56<br>55<br>54<br>58 |
| Backscatter @ 29.31", 60°<br>10.312" collimator | 201<br>196<br>198<br>221 | |
| Backscatter @ 26.94", 30°<br>5.688" collimator | | 3315<br>2720<br>3083<br>2999 |
| Backscatter @ 26.00", 40°<br>5.625" collimator | 1690<br>1514<br>1607<br>1653 | |
| Backscatter @ 26.50", 50°<br>6.50" collimator | | 190<br>214<br>210<br>212 |
| Backscatter @ 30.00", 60°<br>9.312" collimator | 1690<br>1514<br>1607<br>1653 | |
| Backscatterer position | 900400<br>799400<br>844900<br>790600<br>782300<br>699300 | 544700<br>631200<br>545200<br>581500<br>564000<br>549700 |
| Background @ 24.12", 30°<br>5.25" collimator | 2149<br>1996<br>2212<br>2084 | |

| LOCATION | TLD READING | |
|---|---|---|
| | SQUARE | ROD |
| Background @ 23.29", 40° 5.688" collimator | | 220<br>216<br>243<br>234 |
| Background @ 27.50", 50° 7.75" collimator | 142<br>138<br>144<br>141 | |
| Background @ 26.31", 60° 8.312" collimator | | 93<br>78<br>85<br>93 |
| Backscatter @ 24.12", 30° 5.25" collimator | 1823<br>1710<br>1886<br>1681 | |
| Backscatter @ 23.19", 40° 5.688" collimator | | 202<br>245<br>235<br>255 |
| Backscatter @ 27.50", 50° 7.75" collimator | 148<br>146<br>162<br>153 | |
| Backscatter @ 26.31", 60° 8.312" collimator | | 54<br>57<br>48<br>52 |

| LOCATION | TLD READING x $10^{-3}$ |
|---|---|
| Beam collimator exit | 2335 |
| | 2301 |
| | 2153 |
| | 2200 |
| | 2234 |
| | 2350 |
| | 2106 |
| | 2165 |
| | 2304 |
| | 2338 |
| Backscatterer position | 402 |
| | 411 |
| | 394 |
| | 392 |
| | 391 |
| | 413 |
| | 412 |
| | 414 |
| | 405 |
| | 417 |
| Beam collimator exit | 5167 |
| | 4985 |
| | 4607 |
| | 4644 |
| | 4364 |
| | 4736 |
| | 4401 |
| | 4629 |
| | 4955 |
| | 4805 |
| Beam collimator exit | 4203 |
| | 4161 |
| | 4530 |
| | 4399 |
| | 4057 |
| | 4533 |
| | 4255 |
| | 4609 |
| | 4356 |
| | 4468 |

| LOCATION | TLD READING x $10^{-3}$ |
|---|---|
| Beam collimator exit | 3960 |
| | 3985 |
| | 4207 |
| | 4057 |
| | 4200 |
| | 4113 |
| | 4059 |
| | 4061 |
| | 4212 |
| | 3806 |
| Backscatterer position | 859 |
| | 779 |
| | 826 |
| | 811 |
| | 1028 |
| | 778 |
| | 784 |
| | 832 |
| | 839 |
| | 787 |
| Beam collimator exit | 2898 |
| | 2803 |
| | 2898 |
| | 2763 |
| | 2921 |
| | 2831 |
| | 2911 |
| | 2820 |
| | 2862 |
| | 2772 |

17.3.2 Beam divergence

| HORIZONTAL DISPLACEMENT (inches) | TLD READING | |
|---|---|---|
| | RIGHT OF CENTER | LEFT OF CENTER |
| 16 | 480<br>544 | |
| 14 | 842<br>952 | 1849<br>1773 |
| 12 | 2131<br>1670 | 3195<br>2860 |
| 10 | 3975<br>4129 | 4729<br>4416 |
| 8 | 5885<br>5426 | 5262<br>5651 |
| 6 | 6472<br>6127 | 5934<br>6023 |
| 4 | 6751<br>6789 | 6952<br>6709 |
| 2 | 7297<br>7576 | 6676<br>6978 |
| 1 | 7707<br>7498 | 7630<br>7712 |

| VERTICAL DISPLACEMENT (inches) | TLD READING | |
|---|---|---|
| | ABOVE CENTER | BELOW CENTER |
| 16 | 2644 | 3663 |
| | 2380 | 3517 |
| 14 | 3046 | 4425 |
| | 2977 | 4385 |
| 12 | 3719 | 5028 |
| | 4237 | 4629 |
| 10 | 5237 | 5373 |
| | 5031 | 6248 |
| 8 | 5826 | 6521 |
| | 5996 | 6429 |
| 6 | 7137 | 7287 |
| | 7158 | 7209 |
| 4 | 7211 | 7334 |
| | 6917 | 6987 |
| 2 | 7324 | 7248 |
| | 7298 | 7498 |
| Center | 6181 | |
| | 7304 | |

## 17.4 10.5 MeV

### 17.4.1 Backscatter

#### 17.4.1.1 Lead

| LOCATION | TLD READING | |
|---|---|---|
| | SQUARE | ROD |
| Beam collimator exit | 17660000 | 12305100 |
| | 18324100 | 13899600 |
| | 16629900 | 14485700 |
| | 17724400 | 15152800 |
| | 19311000 | 15299200 |
| | 18328100 | 13829100 |
| Backscatterer position | 3030500 | 2165400 |
| | 2789000 | 1935400 |
| | 2906200 | 2182000 |
| | 2665800 | 2084900 |
| | 2932900 | 2093900 |
| | 2680000 | 2360300 |
| Background @ 41.31", 35° | 8804 | |
| 6.687" collimator | 8590 | |
| | 7746 | |
| | 7623 | |
| Background @ 38.06", 40° | | 925 |
| 6.00" collimator | | 865 |
| | | 879 |
| | | 983 |
| Background @ 37.81", 50° | 203 | |
| 11.062" collimator | 190 | |
| | 189 | |
| | 190 | |
| Background @ 36.19", 60° | | 97 |
| 11.938" collimator | | 100 |
| | | 107 |
| | | 102 |

| LOCATION | TLD READING | |
|---|---|---|
| | SQUARE | ROD |
| Beam collimator exit | 29242500 | 22386500 |
| | 30817500 | 20709700 |
| | 29099000 | 20747600 |
| | 31044800 | 20511500 |
| | 29386700 | 23246300 |
| | 30655700 | 21458700 |
| Backscatter @ 41.31", 35° | 10082 | |
| 6.688" collimator | 10426 | |
| | 8100 | |
| | 10262 | |
| Backscatter @ 38.06", 40° | | 2020 |
| 6.00" collimator | | 2038 |
| | | 1987 |
| | | 1973 |
| Backscatter @ 37.81", 50° | 438 | |
| 11.062" collimator | 457 | |
| | 480 | |
| | 494 | |
| Backscatter @ 36.19", 60° | | 373 |
| 11.938" collimator | | 358 |
| | | 345 |
| | | 362 |
| Beam collimator exit | 17920700 | 12099200 |
| | 16397300 | 13602500 |
| | 16555900 | 14372600 |
| | 16775800 | 13228100 |
| | 18253000 | 13852500 |
| | 17377700 | 11729900 |
| Backscatterer position | 5282200 | 3859000 |
| | 4642600 | 3606000 |
| | 4650800 | 3628700 |
| | 4992300 | 3921600 |
| | 4395900 | 3788200 |
| | 5129700 | 3418500 |

| LOCATION | TLD READING | |
|---|---|---|
| | SQUARE | ROD |
| Background @ 41.31", 35° | 7549 | |
| 6.688" collimator | 7152 | |
| | 7197 | |
| | 6599 | |
| Background @ 38.06", 40° | | 1098 |
| 6.00" collimator | | 1185 |
| | | 1205 |
| | | 1019 |
| Background @ 37.81", 50° | 189 | |
| 11.062" collimator | 208 | |
| | 191 | |
| | 199 | |
| Background @ 36.19", 60° | | 36 |
| 11.938" collimator | | 30 |
| | | 38 |
| | | 32 |
| Beam collimator exit | 10244300 | 7354600 |
| | 11017200 | 6690200 |
| | 9046100 | 7605800 |
| | 9347100 | 8084600 |
| | 10427900 | 7375200 |
| | 10059600 | 7196200 |
| Backscatterer position | 1810800 | 1367700 |
| | 1879200 | 1385400 |
| | 1648200 | 1301200 |
| | 1382900 | 1161400 |
| | 1859700 | 1391600 |
| | 1819800 | 1318200 |
| Background @ 60.12", 30° | | 24 |
| 15.938" collimator | | 23 |
| | | 23 |
| | | 20 |
| Background @ 45.88", 40° | | 135 |
| 11.00" collimator | | 144 |
| | | 126 |
| | | 142 |

| LOCATION | TLD READING | |
|---|---|---|
| | SQUARE | ROD |
| Background @ 41.06", 50° | 45 | |
| 11.688" collimator | 44 | |
| | 49 | |
| | 54 | |
| Background @ 38.38", 60° | 16 | |
| 13.75" collimator | 17 | |
| | 18 | |
| | 18 | |
| Beam collimator exit | 7326900 | 4553100 |
| | 6926400 | 4481000 |
| | 6449900 | 5106700 |
| | 6683500 | 4804700 |
| | 6017000 | 5694500 |
| | 6536300 | 4430900 |
| Backscatter @ 60.12", 30° | | 28 |
| 15.938" collimator | | 25 |
| | | 26 |
| | | 29 |
| Backscatter @ 45.88", 40° | | 163 |
| 11.00" collimator | | 147 |
| | | 174 |
| | | 162 |
| Backscatter @ 41.06", 50° | 77 | |
| 11.688" collimator | 74 | |
| | 89 | |
| | 76 | |
| Backscatter @ 38.38", 60° | 44 | |
| 13.75" collimator | 43 | |
| | 46 | |
| | 48 | |
| Beam collimator exit | 8828500 | 1331800 |
| | 7900700 | 1052600 |
| | 9193500 | 1263500 |
| | 9254000 | 1330000 |

| LOCATION | TLD READING | |
|---|---|---|
| | SQUARE | ROD |
| Background @ 60.12", 30° | | 24 |
| 15.938" collimator | | 25 |
| | | 27 |
| | | 25 |
| Background @ 45.38", 40° | | 130 |
| 11.00" collimator | | 156 |
| | | 144 |
| | | 157 |
| Background @ 41.06", 50° | 53 | |
| 11.688" collimator | 53 | |
| | 50 | |
| | 54 | |
| Backscatter @ 38.38", 60° | 22 | |
| 13.75" collimator | 21 | |
| | 21 | |
| | 21 | |
| Beam collimator exit | 5306000 | 3481100 |
| | 4382600 | 3634500 |
| | 5191700 | 3332800 |
| | 5199400 | 3166700 |
| | 4810100 | 3856000 |
| | 5023000 | 3541000 |
| Backscatterer position | 974800 | 718200 |
| | 918000 | 589500 |
| | 781300 | 653700 |
| | 856600 | 637600 |
| | 865100 | 675500 |
| | 982100 | 738000 |
| Background @ 58.69", 30° | 21 | |
| 15.938" collimator | 25 | |
| | 22 | |
| | 24 | |
| Background @ 44.38", 40° | 302 | |
| 11.00" collimator | 294 | |
| | 281 | |
| | 254 | |

| LOCATION | TLD READING | |
|---|---|---|
| | SQUARE | ROD |
| Background @ 39.44", 50° | | 27 |
| 11.625" collimator | | 26 |
| | | 31 |
| | | 31 |
| Background @ 37.53", 60° | | 9 |
| 13.688" collimator | | 10 |
| | | 11 |
| | | 11 |
| Beam collimator exit | 9796700 | 6910700 |
| | 8361800 | 7020400 |
| | 10238200 | 7832300 |
| | 10822300 | 7330200 |
| | 10434000 | 6801200 |
| | 10262400 | 7461200 |
| Backscatter @ 58.69", 30° | 45 | |
| 15.938" collimator | 46 | |
| | 47 | |
| | 44 | |
| Backscatter @ 44.38", 40° | 376 | |
| 11.00" collimator | 375 | |
| | 438 | |
| | 425 | |
| Backscatter @ 39.44", 50° | | 88 |
| 11.625" collimator | | 80 |
| | | 78 |
| | | 75 |
| Backscatter @ 37.53", 60° | | 37 |
| 13.688" collimator | | 38 |
| | | 34 |
| | | 41 |

17.4.1.2 Iron

| LOCATION | TLD READING | |
|---|---|---|
| | SQUARE | ROD |
| Beam collimator exit | 15193900 | 10420400 |
| | 13945000 | 11724800 |
| | 13805700 | 10025500 |
| | 14254600 | 11539300 |
| | 15010900 | 11202900 |
| | 14173100 | 11443100 |
| Backscatterer position | 2381400 | 1700900 |
| | 2067500 | 1845900 |
| | 2241500 | 1651800 |
| | 2080500 | 1809300 |
| | 2167100 | 1732400 |
| | 2090400 | 1471100 |
| Background @ 59.25", 30° 16.00" collimator | 31 | |
| | 30 | |
| | 33 | |
| | 36 | |
| Background @ 44.88", 40° 11.00" collimator | 426 | |
| | 415 | |
| | 432 | |
| | 395 | |
| Background @ 40.06", 50° 11.688" collimator | | 42 |
| | | 37 |
| | | 37 |
| | | 38 |
| Background @ 38.81", 60° 13.75" collimator | | 13 |
| | | 15 |
| | | 13 |
| | | 11 |
| Beam collimator exit | 17877600 | 11242700 |
| | 17426600 | 11109900 |
| | 15207900 | 9996800 |
| | 16488100 | 11811000 |
| | 14324000 | 12960000 |
| | 14944500 | 12037000 |

| LOCATION | TLD READING | |
|---|---|---|
| | SQUARE | ROD |
| Backscatter @ 59.25", 30° | 49 | |
| 16.00" collimator | 52 | |
| | 46 | |
| | 52 | |
| Backscatter @ 44.88", 40° | 267 | |
| 11.00" collimator | 284 | |
| | 281 | |
| | 292 | |
| Backscatter @ 40.06", 50° | | 71 |
| 11.688" collimator | | 67 |
| | | 72 |
| | | 74 |
| Backscatter @ 38.81", 60° | | 37 |
| 13.75" collimator | | 35 |
| | | 37 |
| | | 35 |
| Beam collimator exit | 11921600 | 9126400 |
| | 12547100 | 8095600 |
| | 11545500 | 8823400 |
| | 11739300 | 9610900 |
| Backscatterer position | 1688300 | 1354500 |
| | 1889700 | 1279100 |
| | 1936400 | 1483900 |
| | 2000600 | 1167200 |
| Background @ 59.25", 30° | | 26 |
| 16.00" collimator | | 24 |
| | | 22 |
| | | 24 |
| Background @ 44.88", 40° | | 169 |
| 11.00" collimator | | 175 |
| | | 165 |
| | | 175 |

| LOCATION | TLD READING | |
|---|---|---|
| | SQUARE | ROD |
| Background @ 40.06", 50°<br>11.688" collimator | 53<br>50<br>54<br>58 | |
| Background @ 38.81", 60°<br>13.75" collimator | 20<br>24<br>23<br>21 | |
| Beam collimator exit | 10901600<br>11506000<br>10593300<br>11216100 | 7720800<br>8644400<br>7873800<br>8488500 |
| Backscatter @ 59.25", 30°<br>16.00" collimator | | 26<br>31<br>29<br>33 |
| Backscatter @ 44.88", 40°<br>11.00" collimator | | 159<br>187<br>177<br>183 |
| Backscatter @ 40.06", 50°<br>11.688" collimator | 94<br>82<br>82<br>80 | |
| Backscatter @ 38.81", 60°<br>13.75" collimator | 44<br>35<br>40<br>39 | |

17.4.1.3 Concrete

| LOCATION | TLD READING | |
|---|---|---|
| | SQUARE | ROD |
| Beam collimator exit | 6423700 | 4593000 |
| | 5285100 | 4226300 |
| | 4853600 | 3824800 |
| | 5498400 | 4437100 |
| | 5069700 | 4342800 |
| | 5170800 | 4319900 |
| Backscatterer position | 992800 | 692200 |
| | 1132900 | 703900 |
| | 1064700 | 761400 |
| | 984700 | 788500 |
| | 999100 | 672700 |
| | 936200 | 712400 |
| Background @ 59.25", 30° | 44 | |
| 16.00" collimator | 33 | |
| | 40 | |
| | 38 | |
| Background @ 44.88", 40° | 226 | |
| 11.00" collimator | 249 | |
| | 273 | |
| | 247 | |
| Background @ 40.06", 50° | | 42 |
| 11.688" collimator | | 34 |
| | | 37 |
| | | 34 |
| Background @ 38.81", 60° | | 15 |
| 13.75" collimator | | 15 |
| | | 16 |
| | | 16 |
| Beam collimator exit | 8934300 | 9863300 |
| | 12324300 | 9704200 |
| | 10853500 | 8688500 |
| | 9691200 | 8940000 |
| | 10719600 | 8374400 |
| | 11654700 | 7946300 |

| LOCATION | TLD READING | |
|---|---|---|
| | SQUARE | ROD |
| Backscatter @ 59.25", 30° | 51 | |
| 16.00" collimator | 44 | |
| | 45 | |
| | 45 | |
| Backscatter @ 44.88", 40° | 238 | |
| 11.00" collimator | 212 | |
| | 222 | |
| | 261 | |
| Backscatter @ 40.06", 50° | | 50 |
| 11.688" collimator | | 50 |
| | | 52 |
| | | 50 |
| Backscatter @ 38.81", 60° | | 26 |
| 13.75" collimator | | 21 |
| | | 25 |
| | | 20 |
| Beam collimator exit | 11602600 | 8351900 |
| | 12111600 | 9134900 |
| | 10665400 | 7774800 |
| | 11083900 | 8983500 |
| Backscatterer position | 1741900 | 1502600 |
| | 1848700 | 1236100 |
| | 2054000 | 988800 |
| | 1869600 | 1135400 |
| Background @ 59.25", 30° | 33 | |
| 16.00" collimator | 31 | |
| | 27 | |
| | 28 | |
| Background @ 44.88", 40° | 187 | |
| 11.00" collimator | 217 | |
| | 208 | |
| | 179 | |

| LOCATION | TLD READING | |
|---|---|---|
| | SQUARE | ROD |
| Background @ 40.06", 50° | | 31 |
| 11.688" collimator | | 32 |
| | | 37 |
| | | 34 |
| Background @ 38.81", 60° | | 12 |
| 13.75" collimator | | 11 |
| | | 13 |
| | | 13 |
| Beam collimator exit | 3753900 | 3522100 |
| | 4599500 | 3698000 |
| | 3986600 | 3136500 |
| | 4249600 | 3440100 |
| Background @ 59.25", 30° | 31 | |
| 16.00" collimator | 28 | |
| | 30 | |
| | 30 | |
| Background @ 44.88", 40° | 200 | |
| 11.00" collimator | 191 | |
| | 198 | |
| | 209 | |
| Background @ 40.06", 50° | | 34 |
| 11.688" collimator | | 30 |
| | | 34 |
| | | 34 |
| Background @ 38.81", 60° | | 13 |
| 13.75" collimator | | 11 |
| | | 14 |
| | | 15 |
| Beam collimator exit | 12045300 | 9027100 |
| | 11189100 | 8379400 |
| | 10579900 | 9199000 |
| | 12654900 | 9781500 |

| LOCATION | TLD READING | |
|---|---|---|
| | SQUARE | ROD |
| Backscatter @ 59.25", 30° | 50 | |
| 16.00" collimator | 48 | |
| | 43 | |
| | 46 | |
| Backscatter @ 44.88", 40° | 242 | |
| 11.00" collimator | 225 | |
| | 248 | |
| | 209 | |
| Backscatter @ 40.06", 50° | | 54 |
| 11.688" collimator | | 52 |
| | | 56 |
| | | 48 |
| Backscatter @ 38.81", 60° | | 26 |
| 13.75" collimator | | 22 |
| | | 23 |
| | | 24 |
| Beam collimator exit | 12566400 | 10804100 |
| | 11573200 | 8531400 |
| | 11907500 | 10392200 |
| | 12226000 | 11114200 |
| | 11200700 | 8172900 |
| | 12729700 | 9158500 |
| Backscatterer position | 2123200 | 1512000 |
| | 1914900 | 1790100 |
| | 2210400 | 1519200 |
| | 2098000 | 1564500 |
| | 2036100 | 1721500 |
| | 2008000 | 1625300 |
| Background @ 59.25", 30° | 32 | |
| 16.00" collimator | 29 | |
| | 35 | |
| | 36 | |
| Background @ 44.88", 40° | 230 | |
| 11.00" collimator | 215 | |
| | 249 | |
| | 209 | |

| LOCATION | TLD READING | |
|---|---|---|
| | SQUARE | ROD |
| Background @ 40.06", 50° | | 38 |
| 11.688" collimator | | 37 |
| | | 37 |
| | | 40 |
| Background @ 38.81", 60° | | 15 |
| 13.75" collimator | | 11 |
| | | 12 |
| | | 14 |

## 17.4.2 Copper absorption in beam

| DEPTH IN COPPER (inches) | TLD READING |
|---|---|
| 0.0 | 57100 |
| | 57064 |
| | 59525 |
| | 62146 |
| 0.125 | 38049 |
| | 40497 |
| | 38354 |
| | 44394 |
| 0.25 | 43356 |
| | 42304 |
| | 44106 |
| | 40696 |
| 0.50 | 29291 |
| | 31003 |
| | 30111 |
| | 28917 |
| 0.75 | 22794 |
| | 25503 |
| | 23366 |
| | 24392 |
| 0.875 | 17428 |
| | 16651 |
| | 16749 |
| | 18198 |
| 1.00 | 19569 |
| | 17281 |
| | 19430 |
| | 18427 |
| | 13663 |
| | 13039 |
| | 13980 |
| | 12323 |

| DEPTH IN COPPER (inches) | TLD READING |
|---|---|
| 1.125 | 14407 |
| | 13593 |
| | 14027 |
| | 13796 |
| 1.25 | 16699 |
| | 16483 |
| | 14208 |
| | 14141 |
| 1.50 | 8855 |
| | 9453 |
| | 8994 |
| | 8912 |
| | 11619 |
| | 10575 |
| | 10863 |
| | 11805 |
| 1.75 | 8610 |
| | 7823 |
| | 8369 |
| | 8610 |
| 2.00 | 7462 |
| | 7790 |
| | 8144 |
| | 7935 |
| 2.50 | 5168 |
| | 5215 |
| | 5352 |
| | 5238 |
| 0.0 | 24446 |
| | 27186 |
| | 23500 |
| | 20089 |
| 0.0 | 26688 |
| | 25487 |
| | 25480 |
| | 22365 |

| DEPTH IN COPPER (inches) | TLD READING |
|---|---|
| 0.125 | 19994 |
| | 22068 |
| | 22436 |
| | 23764 |
| 0.25 | 18457 |
| | 18546 |
| | 17033 |
| | 19759 |
| 0.50 | 16021 |
| | 14143 |
| | 15207 |
| | 12508 |
| 0.75 | 10543 |
| | 9202 |
| | 10528 |
| | 9923 |
| 0.75 | 11539 |
| | 11994 |
| | 12978 |
| | 12157 |
| 0.875 | 9313 |
| | 8844 |
| | 8534 |
| | 8795 |
| 0.875 | 12082 |
| | 11747 |
| | 11158 |
| | 13567 |
| 1.00 | 9331 |
| | 9648 |
| | 9725 |
| | 8486 |

| DEPTH IN COPPER (inches) | TLD READING |
|---|---|
| 1.125 | 7633 |
| | 7671 |
| | 8227 |
| | 7161 |
| 1.125 | 10774 |
| | 9553 |
| | 10631 |
| | 11727 |
| 1.25 | 14595 |
| | 15907 |
| | 13587 |
| | 14181 |
| 1.25 | 6506 |
| | 7765 |
| | 6661 |
| | 8304 |
| 1.25 | 5760 |
| | 8183 |
| | 6331 |
| | 8255 |
| 1.50 | 6881 |
| | 6695 |
| | 6646 |
| | 5510 |
| 1.50 | 6293 |
| | 6374 |
| | 6190 |
| | 6084 |
| 1.75 | 5995 |
| | 4947 |
| | 5498 |
| | 4681 |

| DEPTH IN COPPER (inches) | TLD READING |
|---|---|
| 1.75 | 5535 |
| | 4838 |
| | 5655 |
| | 5296 |
| 2.50 | 3798 |
| | 3502 |
| | 4016 |
| | 3280 |
| 3.50 | 2262 |
| | 2163 |
| | 2247 |
| | 2464 |

| BEAM MONITOR | TLD READING |
|---|---|
| 1 | 28363 |
| | 28776 |
| | 19795 |
| | 27964 |
| 2 | 24949 |
| | 24148 |
| | 23413 |
| | 20948 |
| 3 | 18278 |
| | 16864 |
| | 19304 |
| | 18949 |
| 4 | 20926 |
| | 21686 |
| | 22816 |
| | 22054 |
| 5 | 21337 |
| | 21115 |
| | 23820 |
| | 23089 |
| 6 | 32239 |
| | 35034 |
| | 32786 |
| | 33579 |
| 7 | 24403 |
| | 23127 |
| | 22437 |
| | 19047 |

## 17.5 20 MeV

### 17.5.1 Lead Backscatter

| LOCATION | TLD READING |
|---|---|
| Beam collimator exit | 21528 |
| | 21538 |
| Backscatterer position | 2621 |
| | 2866 |
| Background @ 12.0", 22.5° | 43 |
| | 40 |
| Background @ 12.0", 45° | 36 |
| | 38 |
| Background @ 12.0" 67.5° | 37 |
| | 37 |
| Beam collimator exit | 50052 |
| | 51551 |
| Backscatter @ 12.0", 22.5° | 115 |
| | 119 |
| Backscatter @ 12.0", 45° | 96 |
| | 93 |
| Backscatter @ 12.0", 67.5° | 76 |
| | 80 |

## 17.5.2 Lead - infinite size

### 17.5.2.1 12" square, thickness as designated

Background and backscatter measurements @ 10.0", 67.5°

| LOCATION | TLD READING |
|---|---|
| Beam collimator exit | 11255 |
| | 11993 |
| | 11904 |
| Background | 34 |
| | 34 |
| | 34 |
| Beam collimator exit | 18244 |
| | 18919 |
| | 18916 |
| Backscatter, 0.15" thick | 46 |
| | 46 |
| | 48 |
| Beam collimator exit | 16083 |
| | 16796 |
| | 16253 |
| Backscatter, 0.42" thick | 46 |
| | 47 |
| | 45 |
| Beam collimator exit | 16679 |
| | 15381 |
| | 16393 |
| Backscatter, 0.57" thick | 44 |
| | 44 |
| | 45 |
| Beam collimator exit | 15726 |
| | 16307 |
| | 15253 |

| LOCATION | TLD READING |
|---|---|
| Backscatter, 0.86" thick | 45 |
| | 45 |
| | 43 |
| Beam collimator exit | 13061 |
| | 12146 |
| | 14174 |
| Backscatter, 1.15" thick | 42 |
| | 43 |
| | 44 |
| Beam collimator exit | 15806 |
| | 16941 |
| | 15639 |
| Backscatter, 1.42" thick | 45 |
| | 46 |
| | 47 |
| Beam collimator exit | 16442 |
| | 16881 |
| | 16488 |
| Backscatter, 1.72" thick | 47 |
| | 45 |
| | 46 |
| Beam collimator exit | 17258 |
| | 17147 |
| | 15385 |
| Backscatter, 1.81" thick | 47 |
| | 47 |
| | 48 |
| Beam collimator | 17469 |
| | 15879 |
| | 16803 |
| Backscatter, 2.50" thick | 47 |
| | 47 |
| | 50 |

| LOCATION | TLD READING |
|---|---|
| Beam collimator exit | 22031 |
| | 20962 |
| | 23097 |
| Background | 34 |
| | 33 |
| | 35 |

17.5.2.2 4.0" thick, area as designated

Background and backscatter measurements @ 10.0", 67.5°

| LOCATION | TLD READING |
|---|---|
| Beam collimator exit | 10130 |
| | 10864 |
| | 10480 |
| Background | 38 |
| | 34 |
| | 32 |
| Beam collimator exit | 24819 |
| | 24206 |
| | 24368 |
| Backscatter, 4.0" square | 54 |
| | 55 |
| | 54 |
| Beam collimator exit | 13787 |
| | 14275 |
| | 13989 |
| Background | 60 |
| | 57 |
| | 59 |
| Beam collimator exit | 32048 |
| | 35767 |
| | 35383 |
| Backscatter, 6.0" square | 87 |
| | 86 |
| | 84 |
| Beam collimator exit | 24843 |
| | 27299 |
| | 25039 |
| Background | 39 |
| | 41 |
| | 44 |

| LOCATION | TLD READING |
|---|---|
| Beam collimator exit | 39737 |
| | 38883 |
| | 39883 |
| Backscatter, 8.0" square | 70 |
| | 73 |
| | 74 |
| Beam collimator exit | 18959 |
| | 16176 |
| | 18726 |
| Background | 25 |
| | 30 |
| | 28 |
| Beam collimator exit | 37433 |
| | 43698 |
| | 41218 |
| Backscatter, 10.0" square | 63 |
| | 63 |
| | 66 |
| Beam collimator exit | 13087 |
| | 13609 |
| | 12722 |
| Background | 34 |
| | 33 |
| | 34 |
| Beam collimator exit | 31428 |
| | 34260 |
| | 31282 |
| Backscatter, 12.0" square | 59 |
| | 67 |
| Beam collimator exit | 23593 |
| | 23720 |
| | 22409 |

| LOCATION | TLD READING |
|---|---|
| Background | 37 |
| | 38 |
| | 38 |
| Beam collimator exit | 40587 |
| | 37074 |
| | 41238 |
| Backscatter, 14" square | 69 |
| | 65 |
| | 72 |

## 17.6 30 MeV

### 17.6.1 Lead - infinite size

#### 17.6.1.1 4.0" thick, area as designated

Background and backscatter measurements @ 10.0", 67.5°

| LOCATION | TLD READING |
|---|---|
| Beam collimator exit | 40519 |
| | 39086 |
| | 40072 |
| Background | 556 |
| | 548 |
| | 544 |
| Beam collimator exit | 88644 |
| | 78352 |
| | 74421 |
| Backscatter, 4.0" square | 825 |
| | 754 |
| | 733 |
| Beam collimator exit | 48000 |
| | 48000 |
| | 47973 |
| Background | 20 |
| | 17 |
| | 18 |
| Beam collimator exit | 90399 |
| | 82734 |
| | 82429 |
| Backscatter, 6.0" square | 86 |
| | 70 |
| | 77 |

| LOCATION | TLD READING |
|---|---|
| Beam collimator exit | 25908 |
| | 33677 |
| | 32829 |
| Background | 557 |
| | 585 |
| | 586 |
| Beam collimator exit | 74749 |
| | 76408 |
| | 82676 |
| Backscatter, 8.0" square | 704 |
| | 680 |
| | 696 |
| Beam collimator exit | 30201 |
| | 32691 |
| | 35421 |
| Background | 652 |
| | 644 |
| | 631 |
| Beam collimator exit | 64450 |
| | 62447 |
| | 68474 |
| Backscatter, 10" square | 676 |
| | 663 |
| | 663 |
| Beam collimator exit | 37594 |
| | 37548 |
| | 40205 |
| Background | 594 |
| | 603 |
| | 608 |
| Beam collimator exit | 51130 |
| | 57250 |
| | 55916 |

| LOCATION | TLD READING |
|---|---|
| Backscatter, 12" square | 685 |
| | 678 |
| | 668 |
| Beam collimator exit | 30192 |
| | 27610 |
| | 28660 |
| Background | 872 |
| | 699 |
| | 716 |
| Beam collimator exit | 45095 |
| | 51497 |
| | 48551 |
| Backscatter, 14" square | 358 |
| | 1062 |
| | 1063 |

17.6.2 Beam cross-section

| HORIZONTAL DISPLACEMENT (inches) | TLD READING | |
|---|---|---|
| | LEFT OF CENTER | RIGHT OF CENTER |
| 2.00 | 549 | |
| 1.50 | | 502 |
| 1.19 | 2924 | |
| 0.75 | | 1296 |
| 0.38 | 3921 | |
| 0.19 | | 3160 |
| Center | 3386 | |

| VERTICAL DISPLACEMENT (inches) | ABOVE CENTER | BELOW CENTER |
|---|---|---|
| 2.00 | | 574 |
| 1.50 | 585 | |
| 1.19 | | 1180 |
| 0.56 | 2635 | |
| 0.75 | | 3239 |
| 0.44 | 3628 | |

## 17.7 40 MeV

### 17.7.1 Lead backscatter

| LOCATION | TLD READING |
|---|---|
| Beam collimator exit | 55982 |
| | 51498 |
| Backscatterer position | 6506 |
| | 6362 |
| Background @ 12.0", 22.5° | 43 |
| | 44 |
| Background @ 12.0", 45° | 40 |
| | 43 |
| Background @ 12.0", 67.5° | 41 |
| | 45 |
| Beam collimator exit | 89616 |
| | 93046 |
| Backscatter @ 12.0", 22.5° | 153 |
| | 158 |
| Backscatter @ 12.0", 45° | 113 |
| | 120 |
| Backscatter @ 12.0", 67.5° | 86 |
| | 82 |

## 17.7.2 Lead - infinite size

### 17.7.2.1 12.0" square, thickness as designated

Background and backscatter measurements @ 10.0", 67.5°

| LOCATION | TLD READING |
|---|---|
| Beam collimator exit | 31741 |
| | 35690 |
| | 30545 |
| Background | 22 |
| | 21 |
| | 23 |
| Beam collimator exit | 39941 |
| | 39604 |
| | 39835 |
| Backscatter, 0.15" thick | 42 |
| | 44 |
| | 42 |
| Beam collimator exit | 46973 |
| | 45341 |
| | 51020 |
| Backscatter, 0.36" thick | 54 |
| | 57 |
| | 59 |
| Beam collimator exit | 49006 |
| | 48373 |
| | 49690 |
| Backscatter, 0.57" thick | 59 |
| | 59 |
| | 61 |
| Beam collimator exit | 43699 |
| | 43817 |
| | 39169 |

| LOCATION | TLD READING |
|---|---|
| Backscatter, 0.86" thick | 59 |
| | 54 |
| | 56 |
| Beam collimator exit | 43810 |
| | 40618 |
| | 39892 |
| Backscatter, 1.15" thick | 49 |
| | 54 |
| | 55 |
| Beam collimator exit | 46309 |
| | 43357 |
| | 47239 |
| Backscatter, 1.42" thick | 57 |
| | 58 |
| | 56 |
| Beam collimator exit | 51367 |
| | 56323 |
| | 52752 |
| Backscatter, 1.72" thick | 64 |
| | 62 |
| | 61 |
| Beam collimator exit | 55867 |
| | 55275 |
| | 53278 |
| Backscatter, 2.08" thick | 61 |
| | 60 |
| | 60 |
| Beam collimator exit | 48948 |
| | 47355 |
| | 50388 |
| Backscatter, 2.57" thick | 60 |
| | 59 |
| | 58 |

| LOCATION | TLD READING |
|---|---|
| Beam collimator exit | 50150 |
| | 49913 |
| | 51811 |
| Background | 23 |
| | 23 |
| | 24 |

17.7.2.2 4.0" thick, area as indicated

| LOCATION | TLD READING |
|---|---|
| Beam collimator exit | 163105 |
| | 153437 |
| | 161074 |
| Background | 51 |
| | 51 |
| | 55 |
| Beam collimator exit | 163129 |
| | 157548 |
| | 172490 |
| Background | 53 |
| | 53 |
| | 55 |
| Beam collimator exit | 183929 |
| | 155932 |
| | 160574 |
| Backscatter, 4.0" square | 178 |
| | 166 |
| | 167 |
| Beam collimator exit | 183124 |
| | 192225 |
| | 173896 |
| Background | 61 |
| | 59 |
| | 56 |
| Beam collimator exit | 190277 |
| | 182371 |
| | 175496 |
| Backscatter, 6.0" square | 220 |
| | 218 |
| | 235 |

| LOCATION | TLD READING |
|---|---|
| Beam collimator exit | 44997 |
| | 37150 |
| | 45530 |
| Background | 28 |
| | 34 |
| | 29 |
| Beam collimator exit | 75728 |
| | 89594 |
| | 88461 |
| Backscatter, 8.0" square | 93 |
| | 94 |
| | 98 |
| Beam collimator exit | 60961 |
| | 54860 |
| | 56489 |
| Background | 559 |
| | 447 |
| | 33 |
| Beam collimator exit | 172964 |
| | 192693 |
| | 175334 |
| Backscatter, 10.0" square | 224 |
| | 212 |
| | 236 |
| Beam collimator exit | 39309 |
| | 39917 |
| | 36748 |
| Background | 19 |
| | 20 |
| | 20 |
| Beam collimator exit | 190843 |
| | 157822 |
| | 178053 |

| LOCATION | TLD READING |
|---|---|
| Backscatter, 12.0" square | 130 |
| | 136 |
| | 157 |
| Beam collimator exit | 62502 |
| | 57142 |
| | 70865 |
| Background | 19 |
| | 22 |
| | 26 |
| Beam collimator exit | 172333 |
| | 187764 |
| | 203856 |
| Backscatter, 14.0" square | 178 |
| | 171 |
| | 188 |

17.7.3 Beam cross-section

| HORIZONTAL DISPLACEMENT (inches) | TLD READING | |
|---|---|---|
| | LEFT OF CENTER | RIGHT OF CENTER |
| 2.00 | 310 | |
| 1.56 | 722 | 773 |
| 1.19 | 7525 | |
| 0.75 | | 1150 |
| 0.38 | 9435 | 8409 |
| 0.19 | | 9184 |
| Center | 9291<br>9091 | |

| VERTICAL DISPLACEMENT (inches) | | |
|---|---|---|
| | ABOVE CENTER | BELOW CENTER |
| 2.38 | 282 | |
| 1.56 | | 703 |
| 1.19 | 1054 | |
| 0.81 | 4119 | |
| 0.75 | | 5058 |
| 0.38 | 8262 | 8550 |
| 0.19 | | 9268 |

## 17.8 60 MeV

### 17.8.1 Lead backscatter

| LOCATION | TLD READING |
|---|---|
| Beam collimator exit | 111316 |
| | 110444 |
| Backscatterer position | 9025 |
| | 8136 |
| Background @ 12.0", 22.5° | 48 |
| | 55 |
| Background @ 12.0", 45° | 44 |
| | 43 |
| Background @ 12.0", 67.5° | 40 |
| | 47 |
| Beam collimator exit | 275054 |
| | 272831 |
| Backscatter @ 12.0", 22.5° | 382 |
| | 360 |
| Backscatter @ 12.0", 45° | 304 |
| | 270 |
| Backscatter @ 12.0", 67.5° | 166 |
| | 160 |

## 17.8.2 Lead - infinite size

### 17.8.2.1 12.0" square, thickness as designated

Background and backscatter measurements
@ 10.0", 67.5°

| LOCATION | TLD READING |
|---|---|
| Beam collimator exit | 30646 |
| | 29827 |
| | 28822 |
| Background | 38 |
| | 37 |
| | 36 |
| Beam collimator exit | 65507 |
| | 67690 |
| | 70239 |
| Backscatter, 0.15" thick | 71 |
| | 77 |
| | 76 |
| Beam collimator exit | 98671 |
| | 98107 |
| | 101194 |
| Backscatter, 0.36" thick | 102 |
| | 102 |
| | 104 |
| Beam collimator exit | 100049 |
| | 95412 |
| | 105191 |
| Backscatter, 0.57" thick | 110 |
| | 109 |
| | 104 |
| Beam collimator exit | 86741 |
| | 75480 |
| | 91520 |

| LOCATION | TLD READING |
|---|---|
| Backscatter, 0.79" thick | 97 |
| | 101 |
| | 92 |
| Beam collimator exit | 65329 |
| | 60036 |
| | 66151 |
| Backscatter, 1.15" thick | 89 |
| | 90 |
| | 81 |
| Beam collimator exit | 69499 |
| | 64865 |
| | 66368 |
| Backscatter, 1.42" thick | 88 |
| | 88 |
| | 91 |
| Beam collimator exit | 76791 |
| | 80212 |
| | 76251 |
| Backscatter, 1.72" thick | 99 |
| | 104 |
| | 98 |
| Beam collimator exit | 77287 |
| | 72870 |
| | 73558 |
| Backscatter, 2.10" thick | 96 |
| | 99 |
| | 93 |
| Beam collimator exit | 81958 |
| | 79575 |
| | 81459 |
| Backscatter, 2.57" thick | 92 |
| | 90 |
| | 94 |

| LOCATION | TLD READING |
|---|---|
| Beam collimator exit | 73017 |
| | 71364 |
| | 69466 |
| Background | 42 |
| | 43 |
| | 42 |

17.8.2.2 4.0" thick, area as designated

| LOCATION | TLD READING |
|---|---|
| Beam collimator exit | 97084 |
| | 85156 |
| | 90687 |
| Background | 107 |
| | 109 |
| | 108 |
| Beam collimator exit | 186002 |
| | 163199 |
| | 188759 |
| Backscatter, 4.0" square | 236 |
| | 224 |
| | 221 |
| Beam collimator exit | 19536 |
| | 20349 |
| | 13676 |
| Background | 314 |
| | 313 |
| | 330 |
| Beam collimator exit | 184787 |
| | 179372 |
| | 179721 |
| Backscatter, 6.0" square | 434 |
| | 419 |
| | 422 |
| Beam collimator exit | 133378 |
| | 137203 |
| | 128563 |
| Background | 107 |
| | 105 |
| | 104 |

| LOCATION | TLD READING |
|---|---|
| Beam collimator exit | 181783 |
| | 177818 |
| | 192393 |
| Backscatter, 8.0" square | 214 |
| | 220 |
| | 231 |
| Beam collimator exit | 9220 |
| | 7260 |
| | 2693 |
| Background | 520 |
| | 469 |
| | 583 |
| Beam collimator exit | 225300 |
| | 208864 |
| | 219958 |
| Backscatter, 10.0" square | 674 |
| | 571 |
| | 540 |
| Beam collimator exit | 76575 |
| | 79163 |
| | 82820 |
| Background | 108 |
| | 112 |
| Beam collimator exit | 149123 |
| | 176767 |
| | 181433 |
| Backscatter, 12.0" square | 239 |
| | 242 |
| | 221 |
| Beam collimator exit | 85081 |
| | 80621 |
| | 76680 |

| LOCATION | TLD READING |
|---|---|
| Background | 283 |
| | 290 |
| | 332 |
| Beam collimator exit | 200714 |
| | 180116 |
| | 181880 |
| Backscatter, 14.0" square | 155 |
| | 144 |
| | 137 |

17.8.3 Beam cross-section

| HORIZONTAL DISPLACEMENT (inches) | TLD READING | |
|---|---|---|
| | LEFT OF CENTER | RIGHT OF CENTER |
| 2.00 | | 1925 |
| 1.56 | 17252 | 2999 |
| 1.19 | 22287 | |
| 0.75 | | 4097 |
| 0.38 | 24288 | 5562 |
| 0.19 | | 19073 |
| Center | 22667<br>20145 | |

| VERTICAL DISPLACEMENT (inches) | | |
|---|---|---|
| | ABOVE CENTER | BELOW CENTER |
| 2.38 | 971 | |
| 1.56 | 3071 | 3239 |
| 1.19 | 4372 | |
| 0.81 | 18735 | 16972 |
| 0.38 | 19736 | 20443 |
| 0.19 | | 21388 |

## 17.9 TLD annealing procedures

### 17.9.1 Annealing cycle

| | | TLD READING |
|---|---|---|
| Pre-anneal: | 1 hour @ 400° C | 678 |
| | 2 hours @ 100° C | 729 |
| Post-anneal: | 10 min. @ 100° C | 727 |
| Pre-heat: | None | 701 |
| Read-out: | 15 sec. @ 250° C | 749 |
| | | 744 |
| | | 713 |
| | | 689 |
| | | 753 |
| | | 732 |
| | | 729 |
| | | 724 |
| | | 689 |
| | | 728 |
| | | 745 |
| | | 730 |
| | | 742 |
| | | 663 |
| | | 703 |
| | | 719 |
| | | 705 |
| | | 739 |
| | | 677 |
| | | 724 |
| | | 690 |

## 17.9.2 Annealing cycle

| | | TLD READING |
|---|---|---|
| Pre-anneal: | 1 hour @ 400°C | 709 |
| | 2 hours @ 100°C | 678 |
| Post-anneal: | 10 min. 100°C | 733 |
| Pre-heat: | 7 sec. @ 165°C | 744 |
| Read-out: | 15 sec. @ 250°C | 693 |
| | | 737 |
| | | 691 |
| | | 697 |
| | | 718 |
| | | 587 |
| | | 752 |
| | | 733 |
| | | 722 |
| | | 670 |
| | | 704 |
| | | 698 |
| | | 712 |
| | | 716 |
| | | 715 |
| | | 709 |
| | | 592 |
| | | 708 |
| | | 716 |
| | | 584 |
| | | 702 |

17.9.3 Annealing cycle

| | | TLD READING |
|---|---|---|
| Pre-anneal: | 1 hour @ 400°C | 727 |
| | 2 hours @ 100°C | 723 |
| Post anneal: | None | 742 |
| Pre-heat: | 7 sec. @ 165°C | 700 |
| Read-out: | 15 sec. @ 250°C | 700 |
| | | 705 |
| | | 698 |
| | | 729 |
| | | 756 |
| | | 672 |
| | | 741 |
| | | 748 |
| | | 703 |
| | | 701 |
| | | 721 |
| | | 687 |
| | | 662 |
| | | 737 |
| | | 724 |
| | | 676 |
| | | 704 |
| | | 699 |
| | | 706 |
| | | 705 |

## 17.9.4 Annealing cycle

| | | TLD READING |
|---|---|---|
| Pre-anneal: | 1 hour @ 400°C | 712 |
| | 24 hours @ 80°C | 703 |
| Post-anneal: | None | 722 |
| Pre-heat: | None | 677 |
| Read-out: | 15 sec. @ 250°C | 703 |
| | | 711 |
| | | 717 |
| | | 684 |
| | | 721 |
| | | 716 |
| | | 675 |
| | | 707 |
| | | 726 |
| | | 727 |
| | | 691 |
| | | 717 |
| | | 683 |
| | | 668 |
| | | 704 |
| | | 737 |
| | | 704 |
| | | 721 |
| | | 673 |
| | | 738 |
| | | 673 |

17.9.5 Annealing cycle

| | | TLD READING |
|---|---|---|
| Pre-anneal: | 1 hour @ 400°C | 723 |
| | 24 hours @ 80°C | 744 |
| Post-anneal: | None | 750 |
| Pre-heat: | 7 sec. @ 165°C | 713 |
| Read-out: | 15 sec. @ 250°C | 703 |
| | | 702 |
| | | 740 |
| | | 689 |
| | | 680 |
| | | 707 |
| | | 683 |
| | | 718 |
| | | 699 |
| | | 696 |
| | | 705 |
| | | 698 |
| | | 715 |
| | | 703 |
| | | 720 |
| | | 662 |
| | | 713 |
| | | 711 |
| | | 684 |

17.9.6 Annealing cycle

| | | TLD READING |
|---|---|---|
| Pre-anneal: | 1 hour @ 400°C | 715 |
| | 24 hours @ 80°C | 694 |
| Post-anneal: | 10 min. @ 100°C | 671 |
| Pre-heat: | None | 733 |
| Read-out: | 15 sec. @ 250°C | 697 |
| | | 700 |
| | | 688 |
| | | 669 |
| | | 707 |
| | | 692 |
| | | 698 |
| | | 721 |
| | | 670 |
| | | 698 |
| | | 713 |
| | | 638 |
| | | 702 |
| | | 680 |
| | | 714 |
| | | 681 |
| | | 706 |
| | | 693 |
| | | 719 |
| | | 681 |
| | | 705 |

## 17.9.7 Annealing cycle

| | | TLD READING |
|---|---|---|
| Pre-anneal: | 1 hour @ 400°C | 682 |
| | 24 hours @ 80°C | 700 |
| Post-anneal: | 10 min. @ 100°C | 713 |
| Pre-heat: | 7 sec. @ 165°C | 654 |
| Read-out: | 15 sec @ 250°C | 716 |
| | | 694 |
| | | 716 |
| | | 585 |
| | | 698 |
| | | 592 |
| | | 677 |
| | | 665 |
| | | 677 |
| | | 684 |
| | | 705 |
| | | 690 |
| | | 652 |
| | | 633 |
| | | 689 |
| | | 672 |
| | | 675 |
| | | 656 |
| | | 727 |
| | | 685 |
| | | 668 |

## 17.9.8 Annealing cycle

| | | TLD READING |
|---|---|---|
| Pre-anneal: | 1 hour @ 400°C | 723 |
| | 24 hours @ 80°C | 744 |
| Post-anneal: | None | 750 |
| Pre-heat: | 7 sec. @ 165°C | 713 |
| Read-out: | 15 sec. @ 250°C | 703 |
| | | 702 |
| | | 740 |
| | | 689 |
| | | 680 |
| | | 707 |
| | | 683 |
| | | 718 |
| | | 699 |
| | | 696 |
| | | 705 |
| | | 698 |
| | | 715 |
| | | 703 |
| | | 720 |
| | | 662 |
| | | 713 |
| | | 711 |
| | | 684 |

## 17.9.9 Annealing cycle

| | | TLD READING |
|---|---|---|
| Pre-anneal: | 1 hour @ 400°C | 983 |
| Post-anneal: | 10 min. @ 100°C | 944 |
| Pre-heat: | None | 967 |
| Read-out: | 15 sec. @ 250°C | 960 |
| | | 960 |
| | | 929 |
| | | 967 |
| | | 928 |
| | | 957 |
| | | 950 |
| | | 894 |
| | | 990 |
| | | 962 |
| | | 1003 |
| | | 962 |
| | | 999 |
| | | 956 |
| | | 967 |
| | | 974 |
| | | 985 |
| | | 920 |
| | | 1004 |
| | | 962 |
| | | 965 |
| | | 1015 |

17.9.10 Annealing cycle

| | | TLD READING |
|---|---|---|
| Pre-anneal: | 1 hour @ 400°C | 965 |
| Post-anneal: | 10 min. @ 100°C | 918 |
| Pre-heat: | 7 sec. @ 165°C | 912 |
| Read-out: | 15 sec. @ 250°C | 959 |
| | | 935 |
| | | 947 |
| | | 898 |
| | | 1008 |
| | | 954 |
| | | 975 |
| | | 967 |
| | | 982 |
| | | 862 |
| | | 931 |
| | | 924 |
| | | 947 |
| | | 977 |
| | | 909 |
| | | 829 |
| | | 952 |
| | | 938 |
| | | 882 |
| | | 923 |
| | | 897 |
| | | 926 |

17.9.11 Annealing cycle

| | | TLD READING |
|---|---|---|
| Pre-anneal: | 1 hour @ 400°C | 992 |
| Post-anneal: | None | 936 |
| Pre-heat: | 7 sec. @ 165°C | 973 |
| Read-out: | 15 sec. @ 250°C | 918 |
| | | 928 |
| | | 910 |
| | | 931 |
| | | 959 |
| | | 934 |
| | | 944 |
| | | 921 |
| | | 958 |
| | | 914 |
| | | 817 |
| | | 905 |
| | | 865 |
| | | 942 |
| | | 924 |
| | | 941 |
| | | 939 |
| | | 978 |
| | | 978 |
| | | 972 |
| | | 924 |
| | | 888 |

17.9.12 Annealing cycle

| | | TLD READING |
|---|---|---|
| Pre-anneal: | 1 hour @ 400°C | 939 |
| Post-anneal: | None | 961 |
| Pre-heat: | 7 sec. @ 165°C | 951 |
| Read-out: | 15 sec. @ 250°C | 1026 |
| | | 962 |
| | | 972 |
| | | 926 |
| | | 970 |
| | | 895 |
| | | 1005 |
| | | 1011 |
| | | 956 |
| | | 1018 |
| | | 980 |
| | | 966 |
| | | 962 |
| | | 983 |
| | | 913 |
| | | 972 |
| | | 933 |
| | | 880 |
| | | 947 |
| | | 909 |
| | | 972 |
| | | 980 |

In any set of experimentally obtained data, there exist points sufficiently far from the mean to be suspect. The discarding of suspect values without some firm and repeatable criteria might lead to loss of real information. The small number of measurements (four to eight) taken at each point during any one run, preclude the use of standard deviation or chi square testing for the rejection of extreme values.

Chauvenet's Criterion (128), which states: "any reading of a series of 'n' readings shall be rejected when the magnitude of its deviation from the mean of the series is such that the probability of occurrence of all deviations that large, or larger, does not exceed $\frac{1}{2n}$ ", was used in this dissertation. Chauvenet's Criterion for rejection (or more precisely, Chauvenet's Ratio) was applied to each set of TLD readings obtained and to final albedo calculations before using or reporting an average value. This procedure allows for the checking of values which appear to differ greatly from the average.

# J. ERROR ANALYSIS

## J.1 STATISTICAL VARIATION OF THERMOLUMINESCENT DOSIMETERS

A number of LiF crystals exposed to the same radiation dose do not emit the same amount of light upon read-out. The degree of this variance and its dependence upon the crystal's prior history are discussed in Appendix F. The error limits discussed there apply to a rather larger number of crystals exposed in each setting than was possible in the experiments conducted (Section 5). Also those limits apply to a given set of readings and the data gained by experiment required the subtraction of background, beam normalization, etc., thus possibly combining errors. Through standard techniques (reviewed below) and the method of data reduction discussed in Section 6, total variance may be calculated.

$$\left[\sigma(N_1 \pm N_2 \pm \ldots)\right]^2 = \left[\sigma(N_1)\right]^2 + \left[\sigma(N_2)\right]^2 + \ldots\ldots$$

Eq. J.1

$$\left[\frac{\sigma\left(\frac{N_1}{N_2}\right)}{\left(\frac{N_1}{N_2}\right)}\right]^2 = \left[\frac{\sigma(N_1N_2)}{N_1N_2}\right]^2$$

$$\approx \left[\frac{\sigma(N_1)}{N_1}\right]^2 + \left[\frac{\sigma(N_2)}{N_2}\right]^2 \qquad \text{Eq. J.2}$$

$$\sigma_{\bar{x}} = \frac{\sigma}{\sqrt{n}} \qquad \text{Eq. J.3}$$

Putting Eq. 6.7 in symbols more convenient for this appendix, and leaving the energy absorption coefficient corrections for discussion in Section J.3

$$\alpha_D \propto \frac{DR - (DBG)\left(\frac{BCS}{BCG}\right)}{DI\left(\frac{BCS}{BCG}\right)\Omega} \qquad \text{Eq. J.4}$$

where:

$\alpha_D$ = the differential albedo

DR = measured reflected dose

DBG = measured background dose

BCS = measured dose at beam collimator exit during backscatter run

BCG = measured dose at beam collimator exit during background run

DI = measured dose at backscatterer position

$\Omega$ = the effective solid angle viewed

In each case the measured dose is the average of some number of readings and has associated with it some variance. The variance of $\alpha_D$ may then be calculated.

Rearranging Eq. J.4 and leaving the error associated with $\Omega$ for discussion in Section J.2:

$$\alpha_D \propto \frac{DR\left(\frac{BCG}{BCS}\right) - DBG}{DI} \qquad \text{Eq. J.5}$$

and adopting, for this development, the notation:

$$\frac{\sigma(N)}{N} = f\,\sigma(N) \qquad \text{Eq. J.6}$$

then

$$\left[f\sigma(\alpha_D)\right]^2 = \left[f\sigma\left(DR\left[\frac{BCG}{BCS}\right] - DBG\right)\right]^2 + \left[f\sigma(DI)\right]^2 \qquad \text{Eq. J.7}$$

$$\left[\sigma\left(DR\left[\frac{BCG}{BCS}\right] - DBG\right)\right]^2 = \left[\sigma\left(DR\left[\frac{BCG}{BCS}\right]\right)\right]^2 + \left[\sigma(DBG)\right]^2$$

Eq. J.8

$$\left[f\,\sigma\left(DR\left[\frac{BCG}{BCS}\right]\right)\right]^2 = \left[f\,\sigma(DR)\right]^2 + \left[f\,\sigma\left(\frac{BCG}{BCS}\right)\right]^2$$

Eq. J.9

$$\left[f\,\sigma\left(\frac{BCG}{BCS}\right)\right]^2 = \left[f\,\sigma(BCG)\right]^2 + \left[f\,\sigma(BCS)\right]^2$$

Eq. J.10

$$\sigma(\alpha_D) = \alpha_D \left\{ \left[\frac{\sigma(DI)}{DI}\right]^2 + \frac{\left[\sigma(DBG)\right]^2}{\left[DR\left(\frac{BCG}{BCS}\right) - DBG\right]^2} + \frac{\left[DR\left(\frac{BCG}{BCS}\right)\right]^2 \left[\left\{\frac{(DR)}{DR}\right\}^2 + \left\{\frac{(BCG)}{BCG}\right\}^2 + \left\{\frac{(BCS)}{BCS}\right\}^2\right]}{\left[DR\left(\frac{BCG}{BCS}\right) - DBG\right]^2} \right\}^{\frac{1}{2}}$$

Eq. J.11

This would be the standard deviation of one measurement of the differential albedo due to variation in TLD readings. As each albedo was measured at least twice and generally several times, Eq. J.3 was used to obtain the standard

deviation of the average albedo due to dosimeter variation. The percent of this deviation ran from 3.8% for iron @ 2.0 MeV to 17.6% for lead @ 7.0 MeV.

## J.2 PHYSICAL MEASUREMENTS

Measurement of collimator length and detector to slab distance determines the effective solid angle and viewed area used in the albedo calculation. The collimators used in this work were milled to the nearest thousandth of an inch. Variation of even five thousandths compared to the collimator dimensions would still introduce far smaller error than discussed in Section J.1. The detector to scattering center distance was made with a standard steel tape measure and checked against a second tape. The author feels an error of 0.25" in 25.0" (1.0%) would be difficult to pass unnoticed. An error of this magnitude in the measurement of dosimeter to scatter surface would cause an error of ±2.0% in the resulting calculated albedo.

An error in measuring the angular relationship of the collimator axis to the scattering slab would result in a changed area relationship and the measurement of a slightly different albedo than intended. The angles reported in this dissertation were measured from a protractor of 12.0" radius which had been checked against an engineering compass. At

12.0" the linear separation of $10^{o}$ is approximately 1.094" or 0.109" per degree. The author feels alignment to be well within 10% or one degree. Neither albedo nor the trigonometric relationships are rapidly varying between 30 and 60 degrees (the range of interest in this dissertation). The error in measured albedo due to ±10% alignment is considerably smaller than that due to ±1.0% distance measurement (±0.2%).

J.3 ANALYTICAL

Considered here are errors due to false assumptions, theoretical approximations and calculational mistakes. The major assumptions employed are that of semi-infinite slab area, uniform irradiation of the slab surface, and the energy absorption coefficient corrections to the dose measurements made. Extreme care has been taken to verify the required slab size by reference to previous works on this subject (Section 5.1) and experimental verification of a number of points (Appendix G). Uniform irradiation of the viewed area is demonstrated for nearly every case (Appendix H) and the one case in which uniform irradiation of the entire slab is questionable (i.e. concrete) is discussed in Appendix H.

Theoretical approximations made in the handling of the

data are discussed in Appendix B and Appendix C and Section 6. The error involved in the point detector approximation is shown to be much below others of this section. The validity of applying computer generated spectra for a collimator penetration effect correction may be debated. A comparison of the spectral data given in Appendix D and of the generated spectra to the literature cited in Section 2 indicate the computer spectra certainly to be reasonable. To apply no correction would be to knowingly over-estimate the real collimator length. The corrections made decrease the albedos by 2.0% (lead @ 2.0 MeV) to 11.0% (iron @ 2.0 MeV). These values would certainly exceed the error made by performing the correction.

The mass energy-absorption coefficient correction to the absorbed dose used in Section 6 is based on both the input and reflected spectra. The coefficients of LiF and water follow very closely throughout the energy range of interest in this dissertation and are essentially identical above a few hundred KeV (Appendix E). Even with the wide variation of input spectra discussed in Appendix D the ratio of mass energy-absorption coefficients,

$\left[\frac{\left(\frac{\mu_{en}}{\rho}\right)_{H_2O}}{\left(\frac{\mu_{en}}{\rho}\right)_{LiF}}\right]$ varies only on the order of ±6% for any given bremsstrahlung maximum energy spectra. However, the $\left[\frac{\left(\frac{\mu_{en}}{\rho}\right)_{Slab}}{\left(\frac{\mu_{en}}{\rho}\right)_{LiF}}\right]$ ratio varies greatly with the low energy portion of the energy spectra, as a glance at plots of the mass energy-absorption coefficients for the various reflecting materials would indicate. This variance is far too great to include with the measurements to which it is applied and leave any meaning in the result. Therefore, until more reliable information becomes available as to the low energy make-up of flash x-ray bremsstrahlung spectra, no error limits can realistically be assigned those measurements plotted in Figures 17 through 27.

It is also assumed that the doses measured at each point are comparable (since they are manipulated algebraically together). The TLD packaging used (~0.14 gm/cm$^2$) is not thick enough to create charged particle equilibrium

(CPE) to high (>1 MeV) energy photons. At the backscatter energies, the thickness of packaging is adequate. At 2.0, 3.5, and 10.5 MeV, the incident beam contains such a large number of low energy photons that a true charged particle equilibrium cannot be achieved. The absorption of low energy photons predominates the electron build-up. The packaging chosen, therefore, is desirable as the surface dose most nearly approximates the "equilibrium dose". However, the more heavily filtered 7.0 MeV incident beam does indeed show a build-up with increasing depth. Work at Kirtland (Figure 87) by EG&G indicates an "equilibrium dose" is reached at about 1.0 $gm/cm^2$. The measured dose is at about 0.965 of that and has been corrected accordingly, resulting in a 3.5% lowering of the albedo at that energy.

Any time a large number of computations are made, the very real possibility of human error exists. Each calculation made was repeated at a separate time and any suspect resultant values (as pointed up by the Chauvenet ratio test) were again checked. Due to the check made for extreme values (Appendix I) the author believes any prejudicing of reported values due to computational errors has been kept to a minimum.

Variance of the bremsstrahlung peak energy is

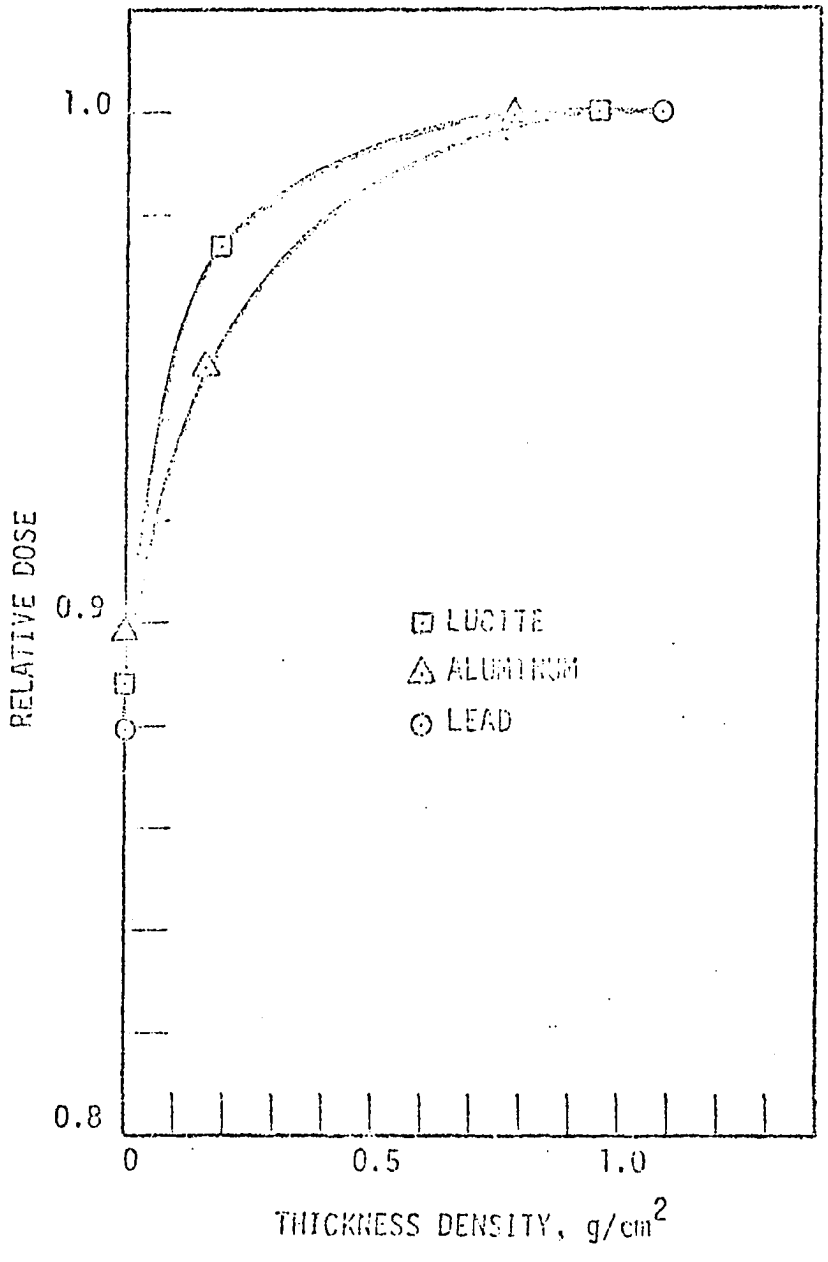


Figure 87 Charged particle equilibrium

discussed in Section 5 and results of that variance shown in Section 6.

The error bars reported in Section 6 are a statistical combination of the limits discussed in this appendix.

## K. MONTE CARLO PROGRAM

The program used in this dissertation is based on a Monte Carlo adaptation of Adams and Mehl (106) used for calculating the deposition of energy by photons. The original program includes fluorescence and Compton scattering, but neglects pair production interactions. Since, at the energies of interest in this dissertation, pair production interactions are quite important, it was necessary to add a sub-routine to handle this item. Mr. K. G. Adams of Sandia Corporation was extremely helpful in adding this feature to the existing Monte Carlo program.

The program, in its updated form, is somewhat limited as to material inputs, and requires certain material data to be included in the update patch not regularly part of the input. Otherwise input is as specified in (106), allowing a wide choice of input energy (or number) spectra and various output forms.

The update to the original program (106) is included here and is for the CDC 6600 computer.

```
*IDENT KOP
*INSERT,SLAB.1191
      SIGMT(MAT+1,J) = 1.E+10
*INSERT,SLAB.31
      COMMON/PAIR/AA(3,20),ELOSS,NPAIR,IPP,IPPFL,
     1SIGPP(20),PAIRA(20),NANNIH
*DELETE,SLAB.37
     1,PALOG,IMPINT,IMP,IPP
*INSERT,SLAB.259
      NPAIR=0
      NANNIH=0
      ELOSS=0.
*INSERT,SLAB.297
      IF(IPP.NE.1) WRITE(3,7000) (SIGPP(I),I=1,NMAT)
 7000 FORMAT(/(7H SIGPP=E12.4))
      ELOSS=ELOSS*511.906
      IF(IPP.NE.3) WRITE(3,7001) NPAIR,ELOSS,NANNIH
 7001 FORMAT(/' NUMBER PAIR PRODUCTION'I10,5X'TOTAL ENERGY LOSS'
     1,F15.3,5X'ANNIHILATION PHOTONS',I10)
      ELOSS=ELOSS/511.906
*INSERT,SLAB.389
      IF(IPP.NE.0) CALL PAIRCA(I)
*INSERT,SLAB.735
      IF(IPP.NE.0) CALL PAIRCA(M)
*INSERT,SLAB.781
      COMMON/PAIR/AA(3,20),ELOSS,NPAIR,IPP,IPPFL,
     1SIGPP(20),PAIRA(20),NANNIH
      DIMENSION XARRAY(1)
      EQUIVALENCE(X2,XARRAY(1))
*INSERT,SLAB.799
      E0=E1
      IF(E1-2.) 218,219,224
  224 IF(IPP) 219,219,220
  220 CALL SPELL1
      IF(SIGPP(M)/SIGT(M)-RAN1) 218,221,221
  221 E1=1.
      IF(E0-E1) 223,23,23
  223 IPPFL=2
      DO 222 I=1,16
  222 PAIRA(I)=XARRAY(I)
      PAIRA(17)=M
      CALL SPELL1
      GAM2=1.-2.*RAN1
      ELOSS=ELOSS+(E0-E1*2)
      NANNIH=NANNIH+1
      NPAIR=NPAIR+1
      RETURN
  218 CONTINUE
*INSERT,SLAB.946
      COMMON/PAIR/AA(3,20),ELOSS,NPAIR,IPP,IPPFL,
     1SIGPP(20),PAIRA(20),NANNIH
*DELETE,SLAB.954
      IF(IPPFL-1) 8,8,9
    9 IPPFL=IPPFL-1
      PAIRA(16)=-GAM2
    8 RETURN
```

```
      *INSERT,CLAB.967
            COMMON/PAIR/AA(8,20),ELOSS,NPAIR,IPP,IPPFL,
           1SIGPP(20),PAIRA(20),NANNIH
            DIMENSION XARRAY(1)
            EQUIVALENCE(X2,XARRAY(1))
            IF(IPPFL) 5003,5003,5002
       5002 DO 5004 I=1,16
       5004 XARRAY(I)=PAIRA(I)
            M=PAIRA(17)
            NANNIH=NANNIH+1
            IPPFL=IPPFL-1
            E1=1.
            RETURN
       5003 CONTINUE
      *INSERT,CLAB.969
            IF(IPP.NE.0) CALL PAIPCA(I)
      *INSERT,CLAB.123
            COMMON/PAIR/AA(8,20),ELOSS,NPAIR,IPP
      *INSERT,CLAB.1697
            IF(IPP.NE.0) CALL PAIPRO(NOMAT)
      *INSERT,SLAB.1764
            SUBROUTINE PAIPRO(NOMAT)
            COMMON/TEMPCO/TEMP(4114),AMT(30,20),NOAT(30)
      C THIS SUBROUTINE CALCULATES PAIR PRODUCTION CROSS SECTIONS FROM      PAI   2
      C COEFFICIENTS STORED ON CROSS SECTION DATA TAPE                      PAI   3
            COMMON/TRANS/UMU,UMUPE,UMUAB,EP,NL
            COMMON/A/B(8,20)
            COMMON/PAIR/AA(8,20),ELOSS,NPAIR,IPP,IPPFL,
           1SIGPP(20),PAIRA(20),NANNIH
      C READ COEFFICIENTS FROM DATA TAPE                                    PAI   6
            DATA(NAME1=8HPAIR PRO)                                        PAI   7
            REWIND 4                                                      PAI   8
        1   READ (4,2) NAME                                               PAI   9
        2   FORMAT (A4)                                                   PAI  10
            IF (NAME.NE.NAME1) GO TO 1                                    PAI  11
            DO 7 J=1,NL
        3   READ(4,4) NO,(B(I,J),I=1,7)
        4   FORMAT (I3,7E11.3)                                            PAI  14
            READ(4,5) B(8,J)
        5   FORMAT (E10.3)                                                PAI  16
            IF (NO-NOAT(J)) 3,7,6                                         PAI  17
        6   REWIND 4                                                      PAI  18
            GO TO 1                                                       PAI  19
        7   CONTINUE                                                      PAI  20
            DO 20 I=1,8
            DO 20 J=1,20
       20   AA(I,J)=0
            DO 25 I=1,NL
            DO 25 J=1,NOMAT
            DO 25 K=1,8
       25   AA(I,K)=AA(I,K)+AMT(J,I)*B(K,J)
            RETURN                                                        PAI  21
      C CALCULATE PAIR PRODUCTION CROSS SECTION                           PAI  22
            ENTRY PAIPCA                                                  PAI  23
            FAC=(EP-1022.012)                                             PAI  24
            IF (FAC) 8,10,10                                              PAI  25
```

```
      A     UPP=0                                                    PAI  26
          9 SIGPP(NL)=UPP
            RETURN
         10   IF (SP-1500.) 11,11,12                                 PAI  28
         11 UPP = AA(NL,8)*FAC**2
            GO TO 9                                                 PAI  30
         12   UPP=0                                                 PAI  31
            FAC=SQRT(FAC)                                           PAI  32
            DO 13 I=1,7                                             PAI  33
         13 UPP = UPP + AA(NL,I)*FAC**I
            UPP=UPP/(1.+1.7E-13*FAC**6)                             PAI  35
            GO TO 9                                                 PAI  36
            END                                                     PAI  37-
*COMPILE SLAB
```

```
SLAB          COMMON/PAIR/AA(8,20),ELOSS,NPAIR,IPP,IPPFL,                KOR     00001   ACTIVATED
SLAB         1SIGPP(20),PAIRA(20),NANNIH                                 KOR     00002   ACTIVATED
SLAB         1,HALOG,IPPINT,IMP                                          SLAB    00037   DEACTIVATED
SLAB         1,HALOG,IPPINT,IMP,IPP                                      KOR     00003   ACTIVATED
SLAB          NPAIR=0                                                    KOR     00004   ACTIVATED
SLAB          NANNIH=0                                                   KOR     00005   ACTIVATED
SLAB          ELOSS=0.                                                   KOR     00006   ACTIVATED
SLAB          IF(IPP.NE.0) CALL PAIRCA(I)                                KOR     00007   ACTIVATED
SLAB          IF(IPP.NE.0) WRITE(7,7000) (SIGPP(I),I=1,NMAT)             KOR     00008   ACTIVATED
SLAB     7000 FORMAT(//(/H SIGPP=E12.4))                                 KOR     00009   ACTIVATED
SLAB          ELOSS=ELOSS*511.006                                        KOR     00010   ACTIVATED
SLAB          IF(IPP.NE.0) WRITE(7,7001) NPAIR,ELOSS,NANNIH              KOR     00011   ACTIVATED
SLAB     7001 FORMAT(/* NUMBER PAIR PRODUCTION*I10,5X*TOTAL ENERGY LOSS* KOR     00012   ACTIVATED
SLAB    1,E12.3,5X*ANNIHILATION PHOTONS*,I10)                            KOR     00013   ACTIVATED
SLAB          ELOSS=ELOSS/511.006                                        KOR     00014   ACTIVATED
SLAB          IF(IPP.NE.0) CALL PAIRCA(M)                                KOR     00015   ACTIVATED
SLAB          COMMON/PAIR/AA(8,20),ELOSS,NPAIR,IPP,IPPFL,                KOR     00016   ACTIVATED
SLAB         1SIGPP(20),PAIRA(20),NANNIH                                 KOR     00017   ACTIVATED
SLAB          DIMENSION XARRAY(1)                                        KOR     00018   ACTIVATED
SLAB          EQUIVALENCE(X2,XARRAY(1))                                  KOR     00019   ACTIVATED
SLAB          E2=E1                                                      KOR     00020   ACTIVATED
SLAB          IF(E1-2.) 219,218,224                                      KOR     00021   ACTIVATED
SLAB      224 IF(IPP) 218,218,220                                        KOR     00022   ACTIVATED
SLAB      220 CALL SPELL1                                                KOR     00023   ACTIVATED
SLAB          IF(SIGPP(M)/SIGT(M)-RAN1) 218,221,221                      KOR     00024   ACTIVATED
SLAB      221 E1=1.                                                      KOR     00025   ACTIVATED
SLAB          IF(E2-E1) 223,23,23                                        KOR     00026   ACTIVATED
SLAB      223 IPPFL=2                                                    KOR     00027   ACTIVATED
SLAB          DO 222 I=1,16                                              KOR     00028   ACTIVATED
SLAB      222 PAIRA(I)=XARRAY(I)                                         KOR     00029   ACTIVATED
SLAB          PAIRA(17)=M                                                KOR     00030   ACTIVATED
SLAB          CALL SPELL1                                                KOR     00031   ACTIVATED
SLAB          SCANG=1.-2.*RAN1                                           KOR     00032   ACTIVATED
SLAB          ELOSS=ELOSS+(E2-E1*2)                                      KOR     00033   ACTIVATED
SLAB          NANNIH=NANNIH+1                                            KOR     00034   ACTIVATED
SLAB          NPAIR=NPAIR+1                                              KOR     00035   ACTIVATED
SLAB          RETURN                                                     KOR     00036   ACTIVATED
SLAB      218 CONTINUE                                                   KOR     00037   ACTIVATED
SLAB          COMMON/PAIR/AA(8,20),ELOSS,NPAIR,IPP,IPPFL,                KOR     00038   ACTIVATED
SLAB         1SIGPP(20),PAIRA(20),NANNIH                                 KOR     00039   ACTIVATED
SLAB          RETURN                                                     SLAB    00054   DEACTIVATED
SLAB          IF(IPPFL-1) 8,8,9                                          KOR     00040   ACTIVATED
SLAB        9 IPPFL=IPPFL-1                                              KOR     00041   ACTIVATED
SLAB          PAIRA(16)=-GAM2                                            KOR     00042   ACTIVATED
SLAB        8 RETURN                                                     KOR     00043   ACTIVATED
SLAB          COMMON/PAIR/AA(8,20),ELOSS,NPAIR,IPP,IPPFL,                KOR     00044   ACTIVATED
SLAB         1SIGPP(20),PAIRA(20),NANNIH                                 KOR     00045   ACTIVATED
SLAB          DIMENSION XARRAY(1)                                        KOR     00046   ACTIVATED
SLAB          EQUIVALENCE(X2,XARRAY(1))                                  KOR     00047   ACTIVATED
SLAB          IF(IPPFL) 5003,5003,5002                                   KOR     00048   ACTIVATED
SLAB     5002 DO 5004 I=1,16                                             KOR     00049   ACTIVATED
SLAB     5004 XARRAY(I)=PAIRA(I)                                         KOR     00050   ACTIVATED
SLAB          M=PAIRA(17)                                                KOR     00051   ACTIVATED
SLAB          NANNIH=NANNIH+1                                            KOR     00052   ACTIVATED
SLAB          IPPFL=IPPFL-1                                              KOR     00053   ACTIVATED
```

```
SLAB          E1=1.                                                    KOR     00054    ACTIVATED
SLAB          RETURN                                                   KOR     00055    ACTIVATED
SLAB       5003 CONTINUE                                               KOR     00056    ACTIVATED
SLAB          IF(IPP.NE.0) CALL PAIPCA(I)                              KOR     00057    ACTIVATED
SLAB          COMMON/PAIP/AA(8,20),ELOSS,NPAIR,IPP                     KOR     00058    ACTIVATED
SLAB          IF(IPP.NE.0) CALL PAIPPD(NOMAT)                          KOR     00059    ACTIVATED
SLAB          STAPMT(MM+1,J) = 1.E+10                                  KOR     00060    ACTIVATED
SLAB          SUBROUTINE PAIPPD(NOMAT)                                 KOR     00061    ACTIVATED
SLAB          COMMON/TEMPCC/TEMP(4114),AMT(30,20),NCAT(30)             KOR     00062    ACTIVATED
SLAB      C THIS SUBROUTINE CALCULATES PAIR PRODUCTION CROSS SECTIONS FROM KOR     00063    ACTIVATED
SLAB      C COEFFICIENTS STORED ON CROSS SECTION DATA TAPE             KOR     00064    ACTIVATED
SLAB          COMMON/TRANC/UMU,UMUPE,UMUAB,EP,NL                       KOR     00065    ACTIVATED
SLAB          COMMON/1/B(8,20)                                         KOR     00066    ACTIVATED
SLAB          COMMON/PAIP/AA(8,20),ELOSS,NPAIR,IPP,IPPFL,              KOR     00067    ACTIVATED
SLAB         1SIGPP(20),PAIPA(20),NANRTH                               KOR     00068    ACTIVATED
SLAB      C READ COEFFICIENTS FROM DATA TAPE                           KOR     00069    ACTIVATED
SLAB          DATA(NAME1=8HPAIR PRO)                                   KOR     00070    ACTIVATED
SLAB          REWIND 4                                                 KOR     00071    ACTIVATED
SLAB      1   READ (4,2) NAME                                          KOR     00072    ACTIVATED
SLAB      2   FORMAT (A8)                                              KOR     00073    ACTIVATED
SLAB          IF (NAME.NE.NAME1) GO TO 1                               KOR     00074    ACTIVATED
SLAB          DO 7 J=1,NL                                              KOR     00075    ACTIVATED
SLAB        3 READ(4,4) NO,(B(I,J),I=1,7)                              KOR     00076    ACTIVATED
SLAB      4   FORMAT (I3,7E11.3)                                       KOR     00077    ACTIVATED
SLAB          READ(4,5) B(8,J)                                         KOR     00078    ACTIVATED
SLAB      5   FORMAT (E10.3)                                           KOR     00079    ACTIVATED
SLAB          IF (NO-NCAT(J)) 3,7,6                                    KOR     00080    ACTIVATED
SLAB      6   BKSPD 4                                                  KOR     00081    ACTIVATED
SLAB          GO TO 1                                                  KOR     00082    ACTIVATED
SLAB      7   CONTINUE                                                 KOR     00083    ACTIVATED
SLAB          DO 20 I=1,8                                              KOR     00084    ACTIVATED
SLAB          DO 20 J=1,20                                             KOR     00085    ACTIVATED
SLAB       20 AA(I,J)=0                                                KOR     00086    ACTIVATED
SLAB          DO 25 I=1,NL                                             KOR     00087    ACTIVATED
SLAB          DO 25 J=1,NOMAT                                          KOR     00088    ACTIVATED
SLAB          DO 25 K=1,8                                              KOR     00089    ACTIVATED
SLAB       25 AA(I,J)=AA(I,K)+AMT(J,I)*B(K,J)                          KOR     00090    ACTIVATED
SLAB          RETURN                                                   KOR     00091    ACTIVATED
SLAB      C-CALCULATE PAIR PRODUCTION CROSS-SECTION                    KOR     00092    ACTIVATED
SLAB          ENTRY PAIPCA                                             KOR     00093    ACTIVATED
SLAB          FAC=(EP-1022.012)                                        KOR     00094    ACTIVATED
SLAB          IF (FAC) 8,10,10                                         KOR     00095    ACTIVATED
SLAB      8   UPP=0                                                    KOR     00096    ACTIVATED
SLAB        9 SIGPP(NL)=UPP                                            KOR     00097    ACTIVATED
SLAB          RETURN                                                   KOR     00098    ACTIVATED
SLAB      10  IF (EP-1500.) 11,11,12                                   KOR     00099    ACTIVATED
SLAB       11 UPP = AA(NL,8)*FAC**2                                    KOR     00100    ACTIVATED
SLAB          GO TO 9                                                  KOR     00101    ACTIVATED
SLAB      12  UPP=0                                                    KOR     00102    ACTIVATED
SLAB          FAC=SQRTF(FAC)                                           KOR     00103    ACTIVATED
SLAB          DO 13 I=1,7                                              KOR     00104    ACTIVATED
SLAB       13 UPP = UPP + AA(NL,I)*FAC**I                              KOR     00105    ACTIVATED
SLAB          UPP=UPP/(1.+1.7E-13*FAC**6)                              KOR     00106    ACTIVATED
SLAB          GO TO 9                                                  KOR     00107    ACTIVATED
SLAB          END                                                      KOR     00108    ACTIVATED
SLAB      *NEOR                                                        SLAB    01365
```

## L. DTF PROGRAM

The discrete ordinates program used in this dissertation (called DTF-69) is based on work by J. H. Renken and K. G. Adams (63) of Sandia Corporation. The program, as written, is actually two programs, a cross-section generating program (GAMLEG 69) and the photon transport program (DTF-69). The program allows a very wide range of inputs, covering any Z material and various spectra to 15 MeV, but is one dimension limited. Fluorescence, Compton scattering, and pair-production are each calculated.

The program was designed primarily for use in energy deposition and energy passage calculation. Differentiation into energy spectra and emergent angle is somewhat more complicated. DTF results in this mode often show a disturbing tendency to oscillate.

Due to the wealth of output available from DTF, transfer from the energy given to the dose desired for comparison to TLD data was unwieldy. The author is much indebted to Joann H. Flinchum of Sandia Corporation for an

update to the DTF program which calculates dose in addition to the energy outputs.

The update to the DTF program (63) used in this work follows and puts DTF in a form much more useful to the health physicist interested in shielding calculations. From an input consisting primarily of the shielding material and source to be shielded, one may obtain the dose transmitted or reflected through any thickness.

The major advantage DTF holds over Monte Carlo programs is a great computer time saving. A half-hour program in Monte Carlo takes less than five minutes with DTF.

The following program is written for the CDC 6600 computer.

```
*IDENT KOR
*DELETE,DTF.542
      SFLUX1,A(JJXCO),A(JFLIN),A(JGK),JMM,JMM1,A(JIQB),A(JIQM1),A(JJ_))
*DELETE,DTF.556
      SUBROUTINE(GO,JMM,JMM1,ANGFLU,ANGFTU,GB)
*DELETE,DTF.579
      COMMON/ALL/NTAPE,NTAPE
*INSERT,DTF.583
      1,GB(1),TEMP(50),AA3B(200),S(75,50),SNU(2_),SES(21)
*INSERT,DTF.598
      IF(IGO.EQ.0)READ(NTAPE,125)(AAMB(IW),IW=1,IGM)
  125 FORMAT(6E12.4)
      DO 126 IV = 1,IP
      DO 126 IW = 1,MM
  126 S(IV,IW)=0.
*INSERT,DTF.644
      S1=S2=0.
      IF(IGO.EQ.0) GO TO 131
      GO TO 132
  131 DO 130 IW = 1,MM
  130 SNU(IW)=SES(IW)=0.
  132 CONTINUE
*DELETE,DTF.820
      I=IP
*INSERT,DTF.824
      TGO=(GB(IG)+GB(IG+1))/2.
      WRITE(NTAPE,110)
  110 FORMAT(1H0,11HENERGY FLUX)
      DO 111 I = 1,MM
      SNU(I)=SNU(I) + XNU(IP,I)
      TEMP(I)=XNU(IP,I) * TGO
  111 SES(I)=SES(I) + TEMP(I)
      WRITE(NTAPE,112)(TEMP(I),I=1,MM)
  112 FORMAT(3E19.6)
      S2=S2+TEMP(I)
      DO 114 I = 1,IP
      DO 113 M = 1,MM
      XNU(I,M)=XNU(I,M)*TGO*AA3B(IG)
  115   S(I,M) = S(I,M) + XNU(I,M)
  114 CONTINUE
      WRITE(NTAPE,116)
  116 FORMAT(1H0,4HHOUSE//)
      DO 117 I = 1,IP
  117 WRITE(NTAPE,60)I,NA(I),(XNU(I,M),M=1,MM)
  118 FORMAT(1H0,12H NUMBER SUMS)
  120 FORMAT(1H0,12H ENERGY SUMS)
*DELETE,DTF.955
   60   WRITE(NTAPE,116)
        WRITE(NTAPE,112)(SNU(IW),IW=1,MM)
        WRITE(NTAPE,121)
        WRITE(NTAPE,112)(SES(IW),IW=1,MM)
        WRITE(NTAPE,127)
  127   FORMAT(*   DOSE SUMS*/)
        DO 128 IV = 1,IP
  128    WRITE(NTAPE,60)IV,NA(IV),(S(IV,IW),IW=1,MM)
        WRITE(NTAPE,119)
```

```
  119  FORMAT(1H0,2H G,22H  INCIDENT ENERGY FLUX,9X,20HINCIDENT ENERGY DO
      1SE/)
       S1=S2=0.
       DO 120 I = 1,164
       TGH=(GB(I)+GB(I+1))/2.
       T1=FLUX(I)*TGH
       T2=T1 * AA3(I)
       S1 = S1 + T1
       S2 = S2 + T2
  120  WRITE(MTAPE,121)I,T1,T2
  121  FORMAT(I3,E18.6,E25.6)
       WRITE(MTAPE,122) S1,S2
  122  FORMAT(1H0,2X,E18.6,E25.6)
       IF(JHM-IHM)01,02,01
      *COMPILE OIF
```

```
      SUBROUTINE FLUX(A,A(JFLUX),A(JFLUX),A(JSK),JMM,JMM1,A(JEGB),A(JEGB1))
      SUBROUTINE FLUX(A,A(JFLUX),A(JFLUX),A(JSK),JMM,JMM1,A(JEGB),A(JEGB1),A(JVL))
      SUBROUTINE FLUX(A,SS,JMM,JMM1,A,GPLU,A,GPTU)
      SUBROUTINE FLUX(A,SS,JMM,JMM1,A,GPLU,A,GPTU,G1)
      COMMON/ALL/MTAPE
      COMMON/ALL/MTAPE,MTAPE
      DIMENSION(I),TEMP(99),AA99(100),S(99,99),SNU(21),SES(21)
      IF(IGM.EQ.1)READ(MTAPE,125)(AA99(IW),IW=1,IGM)
  125 FORMAT(6E12.4)
      DO 126 IW = 1,IP
      DO 126 IW = 1,MM
  126 S(IW,IW)=0.
      S1=SE=0.
      IF(IGM.EQ.0) GO TO 131
      GO TO 132
  131 DO 133 IW = 1,MM
  133 SNU(IW)=SES(IW)=0.
  132 CONTINUE
   60 IF (J-M-1+M) 61,62,61
   61 WRITE(MTAPE,113)
      WRITE(MTAPE,112)(SNU(IW),IW=1,MM)
      WRITE(MTAPE,135)
      WRITE(MTAPE,112)(SES(IW),IW=1,MM)
      WRITE(MTAPE,127)
  127 FORMAT(*   GOSE SUMS*/)
      DO 128 IV = 1,IP
  128  WRITE(MTAPE,60)IV,NA(IV),(S(IV,IW),IW=1,MM)
      WRITE(MTAPE,113)
  113 FORMAT(1H0,2H G,22H  INCIDENT ENERGY FLUX,9X,20HINCIDENT ENERGY GO
     1ES/)
      S1=SE=0.
      DO 120 I = 1,IGM
      TGB=(GB(I)+GB(I+1))/2.
      T1=FLUX(I)*TGB
      T2=T1 * AA99(I)
      S1 = S1 + T1
      S2 = S2 + T2
  120 WRITE(MTAPE,121)I,T1,T2
  121 FORMAT(I3,E16.6,E25.6)
      WRITE(MTAPE,122) S1,S2
  122 FORMAT(1H0,2X,E16.6,E25.6)
      IF(JMM-IMM)61,62,61
      DO 7 I=1,IP
      I=IP
      TGB=(GB(IG)+GB(IG+1))/2.
      WRITE(MTAPE,110)
  110 FORMAT(1H0,11HENERGY FLUX)
      DO 111 I = 1,MM
      SNU(I)=SNU(I) + XNU(IP,I)
      TEMP(I)=XNU(IP,I) * TGB
  111 SES(I)=SES(I) + TEMP(I)
      WRITE(MTAPE,112)(TEMP(I),I=1,MM)
  112 FORMAT(6E15.6)
      S2=S2+TEMP(1)
      DO 114 I = 1,IP
```

```
OTF             DO 115 M = 1,MM                                          KOR   00051   ACTIVATED
OTF             XNJ(I,M)=XNJ(I,M)*TGB*AASB(IG)                           KOR   00052   ACTIVATED
OTF      115     S(I,M) = S(I,M) + XNJ(I,M)                               KOR   00053   ACTIVATED
OTF      114    CONTINUE                                                  KOR   00054   ACTIVATED
OTF             WRITE(MTAPE,116)                                         KOR   00055   ACTIVATED
OTF      116    FORMAT(1H0,4H00SL//)                                      KOR   00056   ACTIVATED
OTF             DO 117 I = 1,IP                                          KOR   00057   ACTIVATED
OTF      117    WRITE(MTAPE,60)I,RA(I),(XNJ(I,M),M=1,MM)                 KOR   00058   ACTIVATED
OTF      110    FORMAT(1H0,12H NUMBER SUMS)                              KOR   00059   ACTIVATED
OTF      130    FORMAT(1H0,12H ENERGY SUMS)                              KOR   00060   ACTIVATED
```

## M. A COMPARISON OF MONTE CARLO AND DTF TO PREVIOUSLY PUBLISHED EXPERIMENTAL RESULTS

Due to the less than perfect fit of the experimental data of this dissertation to the computer runs, a few runs were made to examine the closeness of fit with experimental data of other researchers.

Figures 88 and 89 are plots of DTF and Monte Carlo results compared to results of two experimenters who used NaI scintillators in their albedo measurements. Figure 88 shows the results for an incident energy of 0.662 MeV and a lead reflector. Figure 89 is for 1.33 and 1.17 MeV reflected from iron. The experimental design of the two experimenters differs somewhat and is discussed in detail in Section 2. The design of Steyn closely resembles that of the present research.

Figure 88 $\alpha_{E1}$ vs Angle for Cs-137 lead scatterer

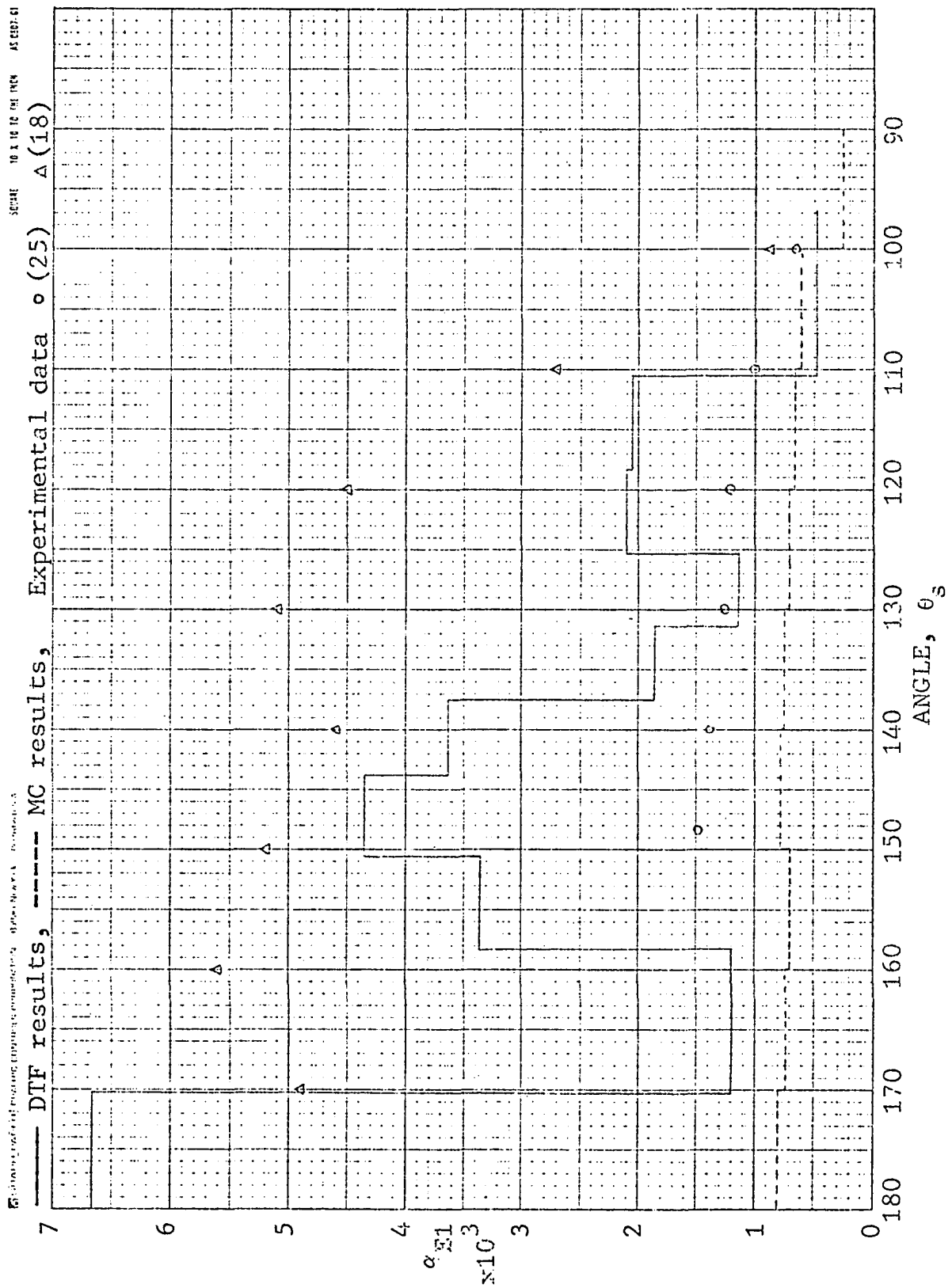

Figure 89 $\alpha_{E1}$ vs Angle for Co-60, iron scatterer

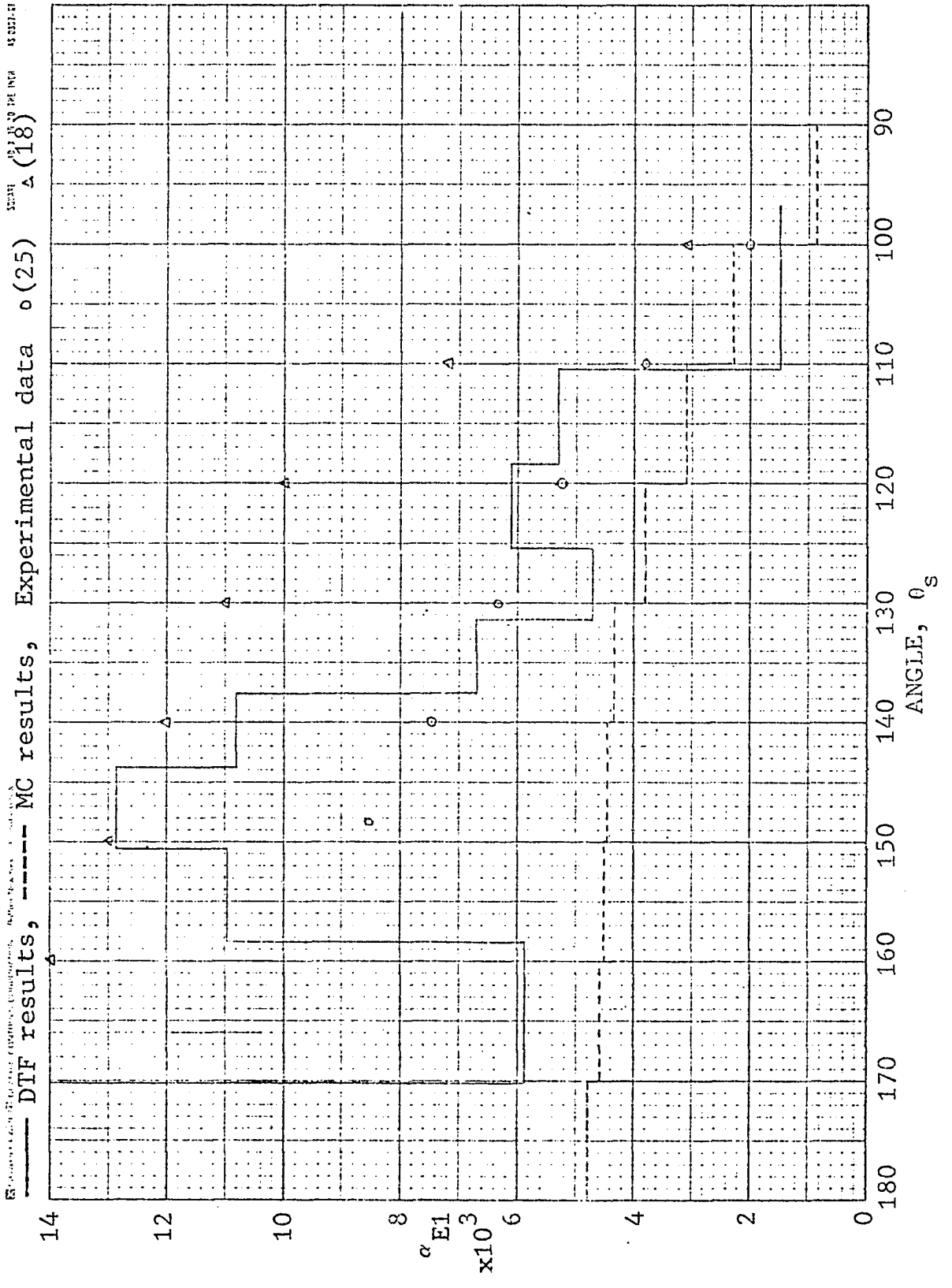

## N. RESULTS OF THE CHILTON-HUDDLESTON EQUATIONS APPLIED TO THE "EFFECTIVE" ENERGIES OF THE PRESENT WORK

The Chilton-Huddleston formulation is discussed in Section 4. The formula, as given there, is:

$$a_D = \frac{C\ K(\theta_s)\ 10^{26} + C'}{1 + \cos\theta_o \sec\theta} \qquad \text{Eq. N.1}$$

Values for C and C' have been published for 0.2, 0.66, 1.0, 2.5, and 6.13 MeV. To obtain values for the energies of this work, Figures 90, 91, and 92 were made. Table 18 notes the values of C and C' used for the calculations made in this appendix. $K(\theta_s)\ 10^{26}$ was calculated as indicated in reference 11 and values are tabulated in Table 19. Results of Eq. N.1 are tabulated in Table 20 and plotted with the experimental and computer results in Section 6.

Figure 90 Lead C and C' vs Energy

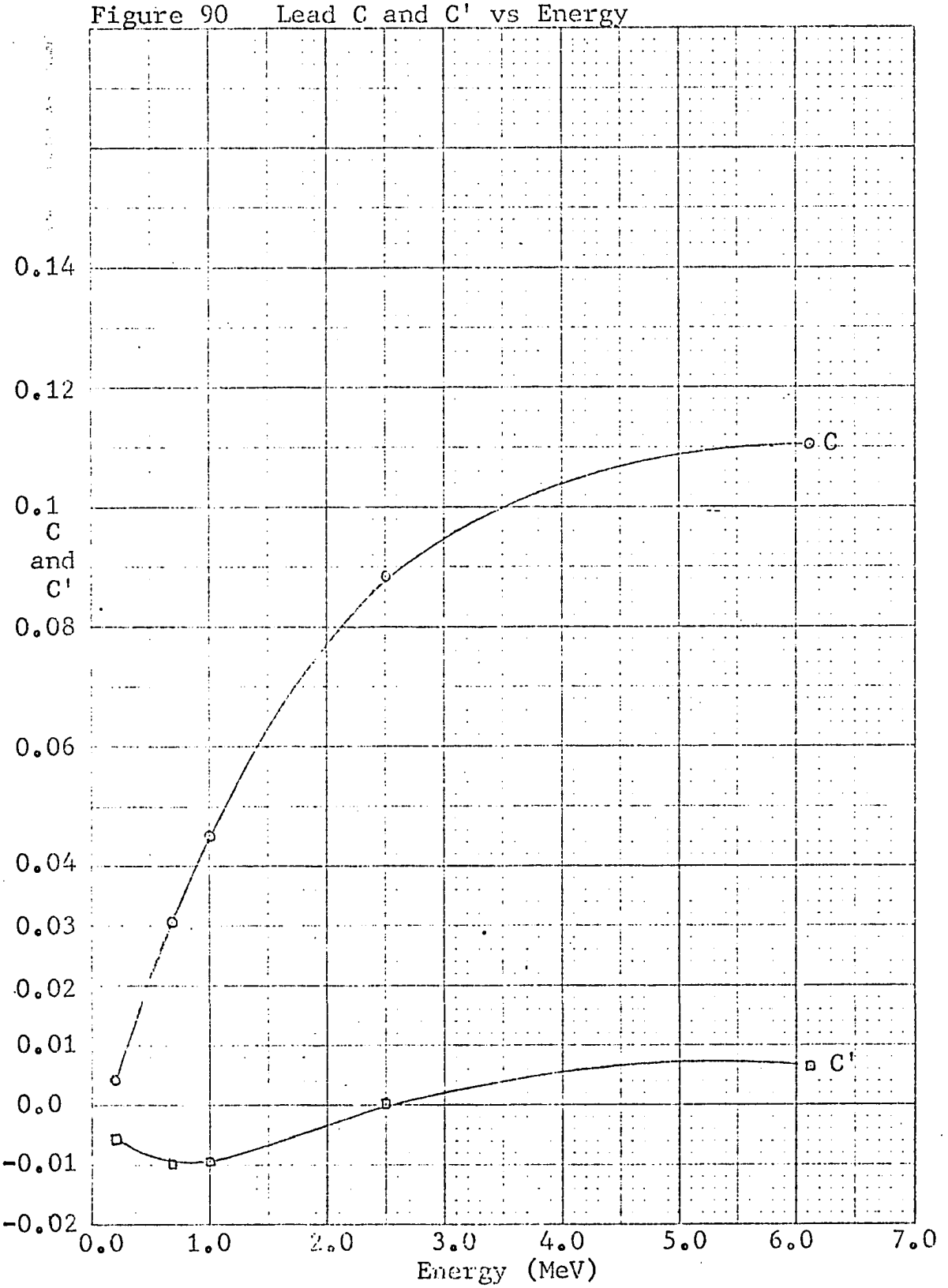

Figure 91 Iron C and C' vs Energy

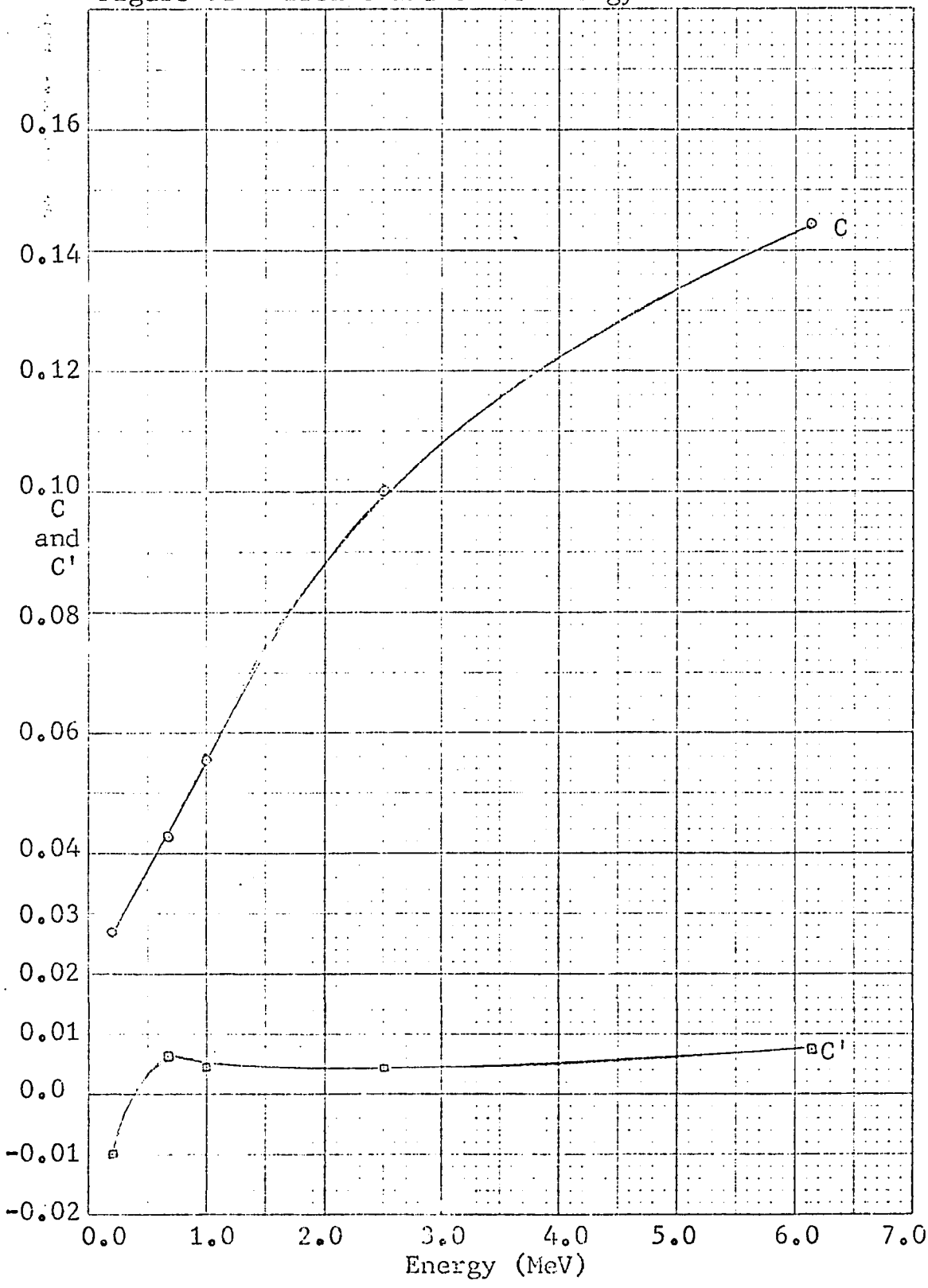

Figure 92 Concrete C and C' vs Energy

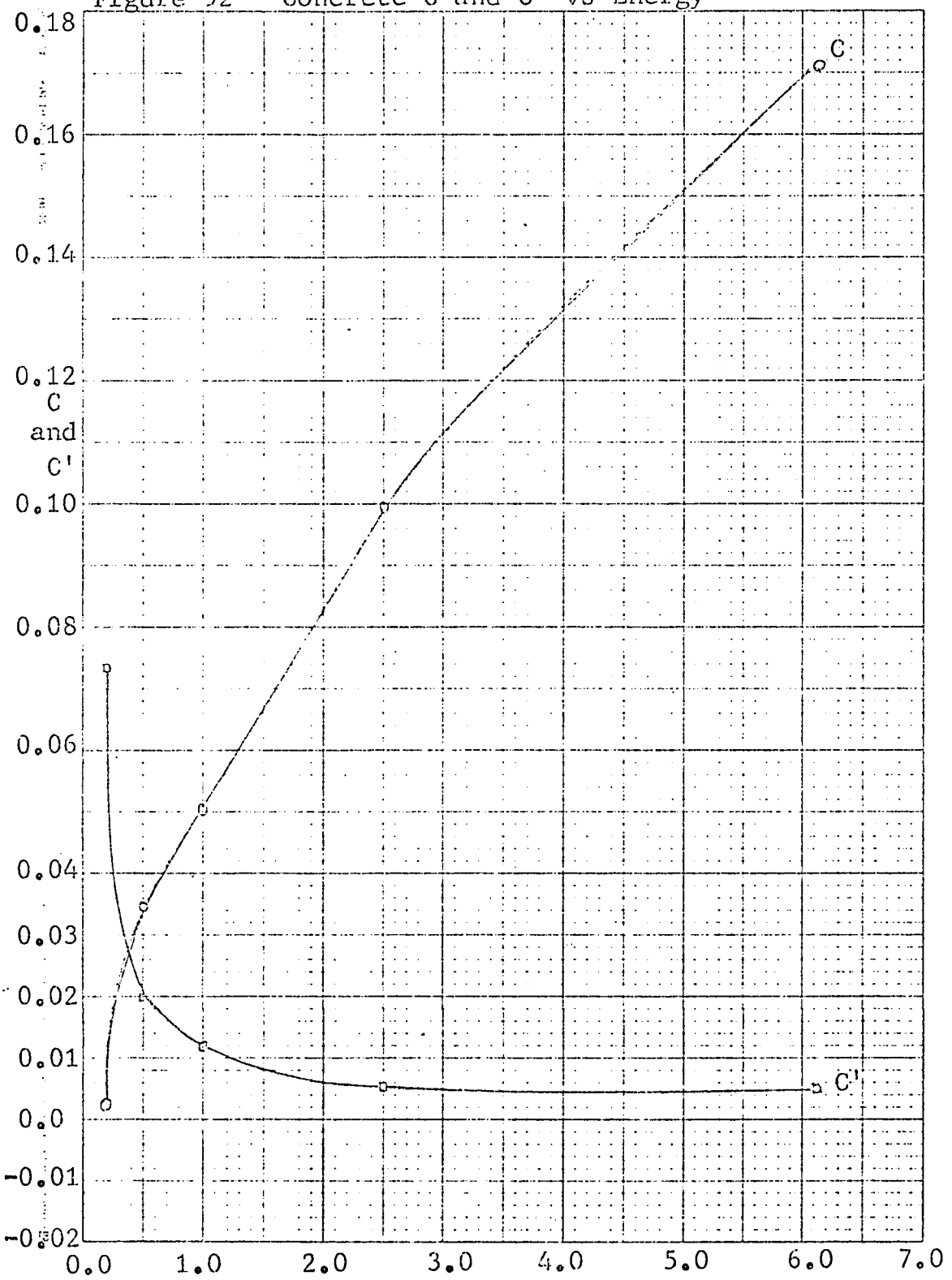

TABLE 18

CHILTON-HUDDLESTON PARAMETERS

| EFFECTIVE ENERGY (MeV) | BACKSCATTER MATERIAL | C | C' |
|---|---|---|---|
| 0.24 | Lead | 0.0062 | -0.0055 |
| | Iron | 0.0281 | -0.008 |
| | Concrete | 0.016 | 0.051 |
| 0.28 | Lead | 0.010 | -0.0061 |
| | Iron | 0.0298 | -0.006 |
| | Concrete | 0.020 | 0.038 |
| 0.85 | Lead | 0.039 | -0.0095 |
| | Iron | 0.050 | 0.0052 |
| | Concrete | 0.0453 | 0.0137 |
| 1.34 | Lead | 0.0563 | -0.0074 |
| | Iron | 0.0666 | 0.004 |
| | Concrete | 0.0612 | 0.009 |
| 4.1 | Lead | 0.1059 | 0.005 |
| | Iron | 0.1302 | 0.0059 |
| | Concrete | 0.132 | 0.0051 |

TABLE 19

KLEIN-NISHINA CROSS-SECTIONS

| EFFECTIVE ENERGY (MeV) | SCATTERING ANGLE | $\frac{K(\theta_s)\ 10^{26}}{d\Omega}$ |
|---|---|---|
| 0.24 | $120^{\circ}$ | 1.2977 |
| | $135^{\circ}$ | 1.2604 |
| | $150^{\circ}$ | 1.2357 |
| 0.28 | $120^{\circ}$ | 1.0880 |
| | $135^{\circ}$ | 1.0692 |
| | $150^{\circ}$ | 1.0641 |
| 0.85 | $120^{\circ}$ | 0.2819 |
| | $135^{\circ}$ | 0.2525 |
| | $150^{\circ}$ | 0.2354 |
| 1.34 | $120^{\circ}$ | 0.14339 |
| | $135^{\circ}$ | 0.1232 |
| | $150^{\circ}$ | 0.1114 |
| 4.1 | $120^{\circ}$ | 0.02216 |
| | $135^{\circ}$ | 0.01784 |
| | $150^{\circ}$ | 0.01538 |

TABLE 20

CHILTON-HUDDLESTON ALBEDO VALUES

| EFFECTIVE ENERGY (MeV) | BACKSCATTER MATERIAL | SCATTERING ANGLE | $a_D \times 10^3$ |
|---|---|---|---|
| 0.24 | Lead | 120° | 1.18 |
| | | 135° | 0.959 |
| | | 150° | 0.720 |
| | Iron | 120° | 13.21 |
| | | 135° | 11.36 |
| | | 150° | 8.91 |
| | Concrete | 120° | 33.31 |
| | | 135° | 29.48 |
| | | 150° | 23.59 |
| 0.28 | Lead | 120° | 2.22 |
| | | 135° | 1.90 |
| | | 150° | 1.51 |
| | Iron | 120° | 12.26 |
| | | 135° | 10.71 |
| | | 150° | 8.57 |
| | Concrete | 120° | 27.73 |
| | | 135° | 24.60 |
| | | 150° | 19.76 |
| 0.85 | Lead | 120° | 0.693 |
| | | 135° | 0.144 |
| | | 150° | Negative |
| | Iron | 120° | 8.95 |
| | | 135° | 7.38 |
| | | 150° | 5.66 |
| | Concrete | 120° | 12.28 |
| | | 135° | 10.41 |
| | | 150° | 8.12 |

TABLE 20 (cont'd)

| EFFECTIVE ENERGY (MeV) | BACKSCATTER MATERIAL | SCATTERING ANGLE | $a_D \times 10^3$ |
|---|---|---|---|
| 1.34 | Lead | $120^o$ | 0.312 |
| | | $135^o$ | Negative |
| | | $150^o$ | Negative |
| | Iron | $120^o$ | 6.29 |
| | | $135^o$ | 5.06 |
| | | $150^o$ | 3.81 |
| | Concrete | $120^o$ | 8.25 |
| | | $135^o$ | 6.85 |
| | | $150^o$ | 5.27 |
| 4.1 | Lead | $120^o$ | 3.72 |
| | | $135^o$ | 3.09 |
| | | $150^o$ | 2.38 |
| | Iron | $120^o$ | 4.00 |
| | | $135^o$ | 3.41 |
| | | $150^o$ | 2.42 |

## O. 20 - 60 MeV BACKSCATTER

A few preliminary measurements were made with a medical Synchrotron unit. The maximum bremsstrahlung edge was adjustable from 20 to 60 MeV. A thick target, thin window arrangement was used with standard Schiff spectra expected.

The experimental set-up was similar to that discussed in Section 5, but the detectors were essentially uncollimated and the incident beam restricted to four square inches at the backscatter slab. Slabs of lead and concrete were used. The concrete was built up of light weight cinder block and thus those results are not comparable to the rest of this dissertation. That data is not presented. Results with lead at 20, 40, and 60 MeV follow.

Due to the experimental configuration chosen, backgrounds were much higher, resulting in greater error limits for the data. One standard deviation for the data presented here varies from 10 to 20% on the TLD measurements. Results presented here are not directly comparable to other results of the dissertation due to the narrow beam arrangement used,

but are presented here for possible comparison elsewhere. Because of the nature of Schiff spectra at low (<250 KeV) energies, no dose absorption corrections are made for $^{a}(slab)$ calculations. The results presented in Table 21 are differential dose flux albedo, $^{a}D3(H_2O)$ as discussed in Section 6, for the specific experimental configuration considered here.

The results appear to be a bit lower than those of Table 3, but are similarly grouped, despite the change in $E_{max}$.

TABLE 21

DIFFERENTIAL DOSE FLUX ALBEDO

BACKSCATTER ANGLE — LEAD SCATTERER

20.0 MeV Incident Spectra Bremsstrahlung Maximum

| $\theta_s$ | $a_{D3(H_2O)} \times 10^3$ |
|---|---|
| 157.5° | 9.56 |
| 135.0° | 7.70 |
| 112.5° | 5.12 |

40.0 MeV Incident Spectra Bremsstrahlung Maximum

| $\theta_s$ | $a_{D3(H_2O)} \times 10^3$ |
|---|---|
| 157.5° | 9.44 |
| 135.0° | 6.17 |
| 112.5° | 3.00 |

60.0 MeV Incident Spectra Bremsstrahlung Maximum

| $\theta_s$ | $a_{D3(H_2O)} \times 10^3$ |
|---|---|
| 157.5° | 13.84 |
| 135.0° | 10.80 |
| 112.5° | 4.93 |